Defining roles of the yeast lysine acetyltransferase NuA4 in metabolism

Elizabeth Walden

A thesis submitted in partial fulfillment of the requirements for the
Doctorate in Philosophy degree in Biochemistry

Department of Biochemistry, Molecular Biology, and Immunology
Faculty of Medicine
University of Ottawa

Authorizations

Manuscript #1:

Walden EA, Fong RY, Pham TT, Knill H, Laframboise SJ, Huard S, Harper M-E, Baetz K. Phenomic screen identifies a role for the yeast lysine acetyltransferase NuA4 in the control of Bcy1 subcellular localization, glycogen biosynthesis, and mitochondrial morphology Copenhaver GP, editor. *PLOS Genetics*. 2020;16(11): e1009220. http://dx.doi.org/10.1371/journal.pgen.1009220. doi: 10.1371/journal.pgen.1009220

Manuscript #2:

Walden EA, Knill, H, Sproule, A, Overy, D, Baetz, K. The lysine acetyltransferase NuA4 in regulation of ergosterol dynamics in *Saccharomyces cerevisiae*.

Submitted to G3 on October 16, 2022.

Manuscript #3 (Co-Author Appendix A):

Pham T, **Walden EA**, Huard S, Pezacki J, Fullerton MD, Baetz K. Fine tuning Acetyl-CoA Carboxylase 1 activity through localization: Functional genomics reveal a role for the lysine acetyltransferase NuA4 and sphingolipid metabolism in regulating Acc1 activity and localization. *Genetics*. 2022;(May). doi:10.1093/genetics/iyac086

Abstract

The yeast lysine acetyltransferase complex NuA4 was initially described to target histone H4 for acetylation but since then many non-histone targets of NuA4 have been identified, a surprising number of which have been implicated in metabolic control. Here we use functional genomics, chemogenetics, high content microscopy and phenotype analysis combined with secondary analysis to discover and investigate novel roles of NuA4 in metabolic control in the *Saccharomyces cerevisiae* model system. In my first study, I screened 368 GFP-tagged metabolic proteins and identified 23 as high confidence hits for a change in localization or abundance upon deletion of *EAF1,* a key scaffolding member of the NuA4 complex. Top hits from the screen identified changes in the localization/abundance of glycogen synthesis and mitochondrial proteins in the *eaf1Δ* yeast. Targeted investigation of these phenotypes led to us characterize a NuA4 dependent regulation of the localization of Bcy1, the regulatory subunit of yeast PKA. The proposed acetylation of Bcy1 affected PKA activity downstream regulating mitochondrial dynamics and glycogen synthesis. The second study stemmed from our identification of a change in the localization of Acc1, the enzyme catalyzing the first step in *de novo* lipid synthesis, upon deletion of *EAF1*. The modulation of a protein in lipid synthesis prompted an investigation into NuA4 dependent lipid regulation, specifically investigating a role for NuA4 in regulating ergosterol dynamics. The *eaf1Δ* yeast are more sensitive to drugs targeting ergosterol and ergosterol biosynthesis, have increased staining with filipin, contain more ergosterol biosynthesis intermediates, and have more lipid droplets than WT yeast cells, suggesting an increase in both ergosteryl esters and free ergosterol in *eaf1*Δ cells. A chemical genomic screen identified *ERG3, POT1, GAL83, GIP3,* and *AFR1* as gene deletions which reverse the *eaf1Δ* dependent increase in ergosterol. As NuA4 and its catalytic subunit Esa1 are highly conserved to Tip60, a lysine acetyltransferase commonly deregulated in human disease, our research showing metabolic control in yeast may have implications in understanding metabolic deregulation in association with alterations in Tip60 activity in disease.

Contents

List of Figures

List of Tables

List of Abbreviations

ACC1	acetyl-CoA carboxylase 1
AcK	acetyl-lysine
AFU	arbitrary fluorescence units
AICD	APP intracellular domain
AKAP	a-kinase anchoring proteins
AMPK	AMP activated kinase
ANOVA	analysis of variance
APP	amyloid precursor protein
AR	androgen receptor
ATP	adenosine triphosphate
BCY1	bypass of cyclic-AMP requirement 1/yeast PKA R subunit
cAMP	cyclic amp
CBP	CREB-binding protein
CIT1	citrate synthase 1/mitochondrial marker
CRISPR	clustered regularly interspaced short palindromic repeats
CYCLoPs	collection of yeast cells localization patterns
DAG	diacylglycerol
DAPI	4′,6-diamidino-2-phenylindole
DMA	deletion mutant array
DNA	deoxyribonucleic acid
EAF1	Esa1p-associated factor
ECAR	extracellular acidification rate
EE	ergosteryl ester
ER	endoplasmic reticulum
Erg	ergosterol biosynthesis
FAA4	fatty acid activation 4 protein/lipid droplet marker
FU	arbitrary fluorescence units
GC-MS	gas chromatography–mass spectrometry
GCN5	general control nonderepressible 5/ yeast KAT
GDB1	glycogen debranching 1
GFP	green fluorescent protein
GNAT	GCN5-related N-acetyltransferases
GO	gene ontology
GSY1	glycogen synthase 1
GSY2	glycogen synthase 2
HAT	histone acetyltransferase (see KAT)
HDAC	histone deacetylase (see KDAC)
K	lysine
KAT	lysine acetyltransferase
KDAC	lysine deacetylase
LD	lipid droplet
LRP	lipoprotein receptor

MSN2	multicopy suppressor of SNF1 mutation/ stress responsive transcription factor
MSN4	multicopy suppressor of SNF1 mutation/ stress responsive transcription factor
MSTFA	N-Methyl-N-trimethylsilyl-trifluoroacetamide
MYST	MOZ, Ybf2, Sas2, and Tip60
NAD+	nicotinamide adenine dinucleotide
NPC	Niemann-Pick Type C
NuA4	nucleosomal acetyltransferase of histone H4
OCR	oxygen consumption rate
OD	optical density
OD600	optical density at 600 nm
PA	Phosphatidic acid
PAM	protospacer adjacent motif
PC	phosphatidylcholine
PCA	protein-fragment complementation assay
PCR	polymerase chain reaction
PE	phosphatidylethanolamine
PHD	plant homeodomains
PI	phosphatidylinositol
PKA	protein kinase A
PS	phosphatidylserine
PTM	post translational modification
Q	glutamine
R	arginine
RNA	ribonucleic acid
ROI	region of interest
RPD3	reduced potassium dependency 3/yeast KDAC
SE	sterol esters
SGA	synthetic genetic array
SGD	saccharomyces genome database
SNF1	sucrose non-fermenting 1/ AMPK in yeast
STRE	stress response elements
TAG	triacylglycerol
TAG	triacylglycerol
Tip60	tat interactive protein 60 kDa/KAT5/human NuA4
TPK1/2/3	Takashi's Protein Kinase/PKA catalytic subunits
WT	wild type
XF	seahorse extracellular flux analyzer
YEATS	Yaf9, ENL, AF9, Taf14 and Sas5
YP	yeast extract peptone media
YPD	yeast extract peptone dextrose media
YPE	yeast extract peptone ethanol media
YPG	yeast extract peptone glycerol media

Acknowledgements

I have been extremely privileged during the course of my doctoral studies to have been supported from every angle. I therefore have a long list of people to acknowledge.

First, I would like to thank my supervisor Dr. Kristin Baetz for her guidance and support in my development as a scientist through this degree. Not only has she been a supervisor who pushed me to investigate complex scientific problems, but she has also been an amazing role model and mentor in her successful career in science, with a specific focus on the importance of equity, diversity, and inclusion and promoting science-policy interactions. I look forward to hearing about her continued work on these topics as the Dean of Science at the University of Calgary.

Additionally, I would like to thank Drs Michael Downey, Mary-Ellen Harper, Mireille Ouimet, and Julie St-Pierre for their input into my work through service on my Thesis Advisory Committee and as collaborators on research topics. Additionally, I would like to thank Amanda Sproule and Dr. David Overy at Agriculture Canada for their help with our mass spectrometry analysis. The diverse expertise and technical advice provided by all of these collaborators was key not only to the development of data for this thesis but also for my development as a critically thinking scientist.

My 5 years in the Baetz lab have seen the coming and going of many excellent scientists both in the Baetz lab and in the surrounding OISB community. All of you have played a role in my PhD journey. Thank you to Sylvain Huard for being a constant sounding board for ideas and solving mechanical/tech support issues. Thank you to Trang Pham for her foundational work toward the work done in this thesis and for introducing me to the fundamentals of yeast research. Thank you to Roger Fong and Hana Knill for pouring countless plates for screens and being amazing mentees. To Jessica Gosse and Lauren Deneault, thanks for everything you did in your short time in the Baetz lab, not the least of which was coordinating the exit from UOttawa. Thank you to Kevin Mercurio, Amanda Bentley-De Sousa, Eugene Fletcher, Sangavi Sivananthan, Garrett Fairman, and Sarah Laframboise for being there through science successes, commiserating about fails/complications, discussing possible solutions, and for being great friends through it all. I will forever appreciate that we made the final 5 years of the Baetz Lab at UOttawa a memorable one. #YeastBeasts.

To my parents and brother, thank you for your unwavering support in everything I do. You have modelled the importance of learning throughout my life. You have given me the tools to critically think and problem solve, which have and will continue to be the skills I treasure most. With this being the 4th university degree, I think I will stop formal education, but I will never stop learning.

To my in-laws, thank you for instilling a love for learning and education in Graham and for defending me to everyone for still being a student.

To my partner Graham, while I may have been able to get a PhD without you, I sure would not want to go back and do it that way. Thank you for everything you have done. From being a champion of my success, to listening to my complaints, and even to troubleshooting my code, your love and support has made these last 5 years significantly better. You always remind me that a PhD is a marathon not a sprint, and I am so glad that you are here at the finish line with me.

Finally, I must acknowledge my pandemic dog Casper, for making me take breaks, enjoy the outdoors, and making me smile everyday.

Chapter 1: Introduction

1.1 Lysine acetylation, an integral post translational modification in the cell

Post-translational modifications (PTMs) are important for the regulation of proteins in the cell. They are ubiquitous across species and errors in modification are associated with numerous diseases[1–3]. One of the most prevalent post-translational modifications is protein acetylation, where an acetyl group is covalently added to specific sites on the protein [4]. There are two prominent classes of protein acetylation [5]. The first is N-terminal acetylation and the second is Nε lysine acetylation (henceforth referred to as lysine acetylation) [5]. N-terminal acetylation is a common modification which occurs across protein classes and is an irreversible modification that occurs either co- or post-translationally [5–7]. The other major class of protein acetylation is lysine acetylation which differs as it occurs on the side chain of lysine residues on proteins (Figure 1.1) [8]. Lysine acetylation is a highly regulated and reversible process which was originally characterized as a post-translational modification on histones [8,9], but increasingly non-histone targets of lysine acetylation are being identified [10]. The process of acetylation is catalyzed by an enzyme class called lysine acetyltransferases (KATs) which were initially named histone acetyltransferases (HATs) [11,12]. KATs transfer the acetyl group from a donor acetyl-CoA to the nitrogen atom of the lysine sidechain [5]. This covalent alteration can then be reversed by the opposing class of enzymes, lysine deacetylases (KDACs) also known as histone deacetylases (HDACs) [13].

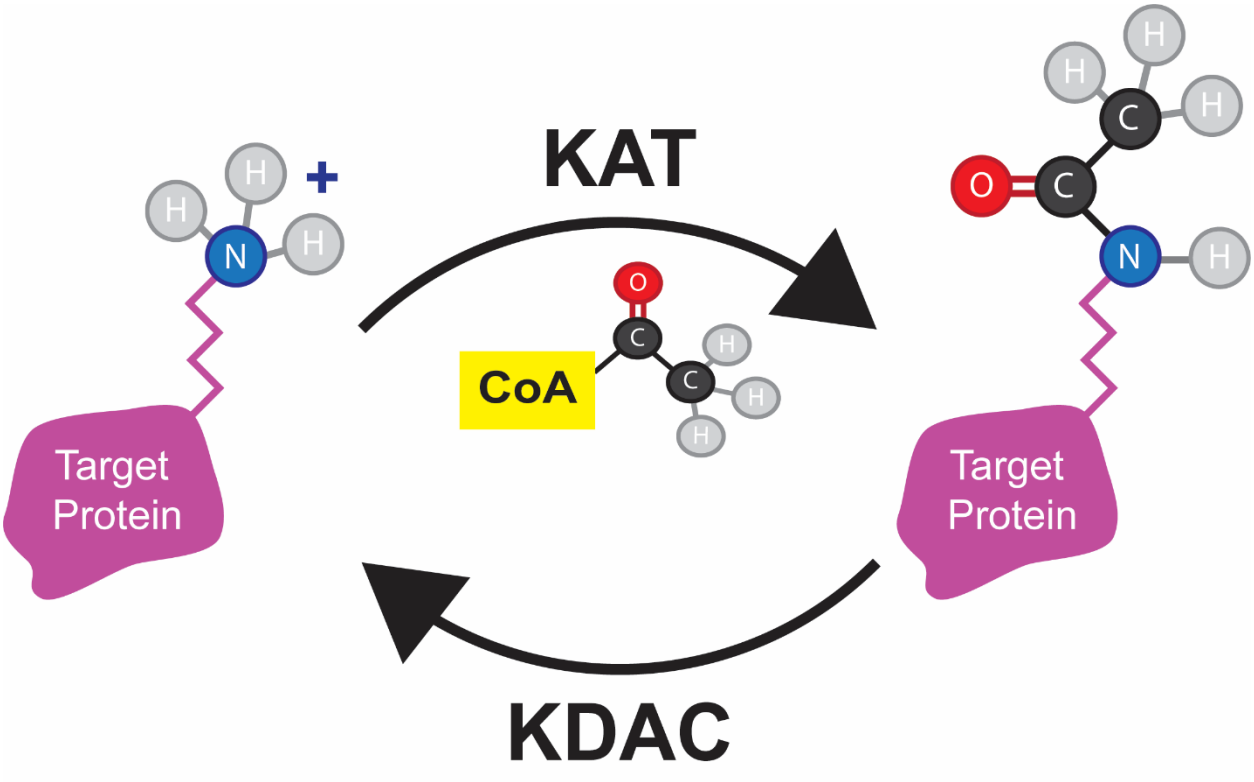

Figure 1.1 Schematic of catalytic lysine acetylation. Lysine acetylation occurs on lysine residues within target proteins. Lysine acetyltransferase (KAT) enzymes use acetyl-CoA to add acetyl groups onto the nitrogen atom of lysine residues causing a change in the local structure and charge of the residue. The covalent lysine acetylation modification can be reversed by lysine deacetylase (KDAC) enzymes.

Non-catalyzed lysine acetylation is also possible under favourable conditions which include a high pH and an abundance of acetyl-CoA [14]. Such conditions are present in the mitochondria and may be responsible for the abundance of acetylated proteins found in this cellular compartment. Non-catalyzed lysine acetylation in the mitochondria is supported by the fact that while mammalian Sirtuin 3 has been identified as the prominent mitochondrial KDAC, and Gcn5L1 and Acat1 [15,16] acetylate some mitochondrial proteins, a KAT responsible for broad spectrum mitochondrial acetylation has not been identified [17–19].

1.2 Protein targets of lysine acetylation

The first classification of lysine acetylation was on histone proteins [8]. Histone acetylation destabilizes the nucleosome by neutralizing the positive charged lysine side chain thereby altering the electrostatic interaction with the negatively charged DNA, leading to an opening of the DNA secondary structure and promoting transcription [20]. In addition to altering the interaction of the histone with DNA, the change in the local charge of the lysine by acetylation can also alter protein-protein interactions, in the case of histones the change in charge on the lysine can affect the structure of the core nucleosome [21,22]. Lysine acetylation of histones is also involved in the recruitment of other proteins, specifically proteins which have acetylation reader abilities through domains including bromodomains, YEATS (Yaf9, ENL, AF9, Taf14 and Sas5) domains, and PHDs (plant homeodomains) [23–26]. After the initial characterization of histone acetylation as a PTM, tubulin and p53 were some of the next major proteins to be identified as being acetylated [27,28]. Since then, regulation of transcription by lysine acetylation was identified through the acetylation of transcription factors and transcriptional co- regulators as well as autoacetylation of KATs and their associated complex members [9,27,29–31]. The identified pool of acetylated proteins quickly grew beyond the initial histone targets [10,11,32].

There are three families of KATs: 1) the GCN5-related N-acetyltransferases (GNAT) family, 2) the p300/CREB-binding protein (p300/CBP) family, and 3) the MOZ, Ybf2, Sas2, and Tip60 (MYST) family [5,32,33]. Across these classes of KATs the central acetyl-CoA binding site is well conserved while they differ in the flanking regions which may aid in target selectivity and the slight differences in chemical mechanism of acetylation [32,34,35]. Conversely, there are 4 classes of KDACs which are sorted based on homology and sub-cellular localization. Class I, II, and IV are zinc dependent, while class III is comprised of the Sirtuins which use NAD+ as a co-substrate [5,36]. Histone acetylations and deacetylations are in equilibrium in the cell, and they play a key role in the regulation of diverse cellular processes. Therefore, the acetylation state of a cell is a complex and highly regulated system.

1.3 Yeast as a model organism to study lysine acetylation

Lysine acetylation is found across classes of organisms, including in baker's yeast, *Saccharomyces cerevisiae*, which has long been an excellent model organism for genetic study. In fact, it was the first organism to have its entire genome sequenced [37]. Yeast is relatively simple to culture, easy to genetically manipulate, and has a high conservation to human cells which has led it to be a foundational platform for scientific discovery [37–41]. In recent years, the ability to perform genome wide screens in yeast has expanded our knowledge of cellular processes. Genome wide screening began with the creation of collections of yeast strains including the deletion mutant array (DMA), the overexpression collection, and the green fluorescent protein (GFP) -tagged collection [42–45]. These collections of mutant yeast strains allowed for the large scale study of the functions of individual genes/proteins but by combining the collections with synthetic genetic array technology (SGA), thereby creating multi-mutant collections, the amount of interaction information which can be probed within the cell increased exponentially [41,46,47]. For example, SGA technology was combined with the GFP-tagged collection for an assessment of not only the localization of all the GFP-tagged proteins under a variety of conditions but also the effects of deletion of the KDAC gene *RPD3* on the localization of all the tagged proteins in the GFP collection [41]. This was the first large scale analysis of the effects of a mutation on the *in vivo* proteome of a cell and demonstrated an important role of lysine deacetylation in protein localization and abundance.

Yeast are also an excellent model for lysine acetylation research because it has been shown that lysine residues in yeast that are acetylated are conserved to lysine sites in human proteins at a higher rate than non-acetylated lysine residues, suggesting that the important roles for lysine acetylation are also conserved [48]. Indeed, there are many examples of the conservation of acetylation of lysine residues ranging from acetylation on histones [49–51] to non-histone acetylation [52,53]. Additionally, many of the known KATs and KDACs in the human system have conserved partner enzymes in the *S. cerevisiae* system [51,54–56]. One conserved pair of interest in the Baetz lab is Tip60 (KAT5) in humans which is homologous to Esa1 the catalytic member of the NuA4 complex in yeast [51].

1.4 NuA4, a yeast acetyltransferase

NuA4 or the Nucleosomal Acetyltransferase of Histone H4 is a KAT complex whose long form name describes its initial characterization as a complex having specificity for the acetylation of histone H4 in the nucleosome [57,58]. Since then, many other targets of NuA4 regulation have been identified but the original name has remained [59,60].

NuA4 is the yeast lysine acetyltransferase homolog of Tip60 (KAT5), a mammalian KAT which has been associated with many diseases including cancer, developmental issues, and neurodegenerative disease [51,61–65]. Given the exceptional conservation of KAT function across eukaryotes, the study of the homologous NuA4 complex in the genetically amenable *Saccharomyces cerevisiae* may provide insight into further understanding the biological roles of Tip60 and the cellular consequences of its deregulation in disease [51].

NuA4 is part of the MYST class of lysine acetyltransferases and is a 13 subunit complex [51,58]. Of these 13 subunits, 6 are essential genes for viability, including the gene for the catalytic subunit *ESA1*, which is the only essential KAT in yeast (Figure 1.2)(Table 1.1) [58,66–69]. The NuA4 complex can be divided into 4 submodules: 1) The catalytic submodule, also known as the piccolo complex, is made up of Esa1, Yng2, Eaf6, and Epl1 and is responsible for the catalytic acetylation function of the complex [68,70]. The piccolo sub module is enzymatically active but lacks targeting to specific locations through interactions with transcription factors [71,72]. 2) The TINTIN functions both within and independently of the holo NuA4 [73]. The TINTIN subcomplex is comprised of Eaf3, Eaf5, and Eaf7 and is important for the interaction of NuA4 with the nucleosome, specifically through an interaction with methylated histone H3 [73,74]. 3) Tra1 is the largest member of the complex and is a common subunit between NuA4 and SAGA, another yeast KAT complex. In both the NuA4 and the SAGA complexes it forms a platform for the interaction with transcriptional activators [75]. 4) Finally, the core module connects the other three modules and is made up of Eaf1, Swc4, Yaf9, Arp4 and, Act1 (Table 1.1) [70]. These 4 submodules come together to form the holo NuA4 complex however the structure of the holo complex is an ongoing area of research.

In the last year, multiple groups have made progress on the characterization of the structure of the NuA4 complex. Cryo-EM structure determination suggested that the core module was made up of the previously characterized Eaf1, Swc4, Arp4 and, Act1 but that the Epl1 tail also is found within the core module [76]. This work and another further showed that Eaf1 and the Epl1 tail form an important entangled interface between Tra1 and the rest of the core module as well as a bridge to the catalytic module [76,77]. It was additionally found that Eaf1 binding to Tra1 occupies an important surface essentially outcompeting and excluding SAGA subunits, explaining how Tra1 functions distinctly within the SAGA and NuA4 complexes [77]. Similar recent research also using Cryo-EM was able to further characterize this Eaf1 interface with the addition of the catalytic subunit in contact with the nucleosome [78]. However, this work chose to classify the complex into 2 major modules: the HAT (KAT) module and the TRA module linked by a disordered bridge region [78]. This classification also relates to the proposed functions with the HAT module interacting with and acetylating the nucleosome while proposing the TRA module as more of an activator binding surface[78]. To date, the structures that have been solved show a large L-shaped complex which has numerous interactions underlying the above listed sub modules and their interactions (Protein Data Bank 5Y81) [68,70]. In the future it will be interesting to elucidate the structure of the complex in association with acetylation of non-histone targets and compare it to the structures elucidated in association with the nucleosome.

Table 1.1: A summary of the components of the NuA4 and Tip60 complexes. Information derived from the Alliance of Genome Resources V 5.2.1. * Denotes essential protein in *S. cerevisiae*.

Components of NuA4/Tip60

***S. Cerevisiae* Protein**	**Role in yeast**	**Tip60 complex members (Human Orthologs)**
Esa1*	NuA4 Catalytic subunit	TIP60
Yng2	NuA4 Catalytic module	ING3
Eaf6	NuA4 Catalytic module	MEAF6
Epl1*	NuA4 Catalytic module	Epc1/2
Eaf3	NuA4 TINTIN	MORF4L1/2
Eaf5	NuA4 TINTIN	
Eaf7	NuA4 TINTIN	MRGBP
Tra1*	NuA4 Tra1	TRRAP
Eaf1	NuA4 Core module	(similarities to EP400)
Swc4*	NuA4 Core module	DMAP1
Yaf9	NuA4 Core module	YEATS4
Arp4*	NuA4 Core module	ACTL6A/B
Act1*	NuA4 Core module	Actin (many)
		EP400
Vps72	Swr1 Complex	VPS72
		BRD8
		MSL3(P1)
Sas5 and Taf14	SAS complex, INO80, SWI/SNF, and NuA3 complexes	YEATS2
Rvb1/2*	Ino80 and Swr1 complexes	RUVBL1/2
		MBTD1
Sas5 and Taf14	SAS complex, INO80, SWI/SNF, and NuA3 complexes	MLLT1/3

An important structural protein of NuA4 complex is Eaf1, which is found in the core module and is the primary scaffolding factor [66,76,79]. Eaf1 binds tightly to Tra1, and the interaction creates the platform for interaction of the piccolo module [70]. Yeast cells deficient for Eaf1 are viable but lose much of the targeting of the enzymatic activity of catalytic Esa1 subunit (Figure 1.2), making the *eaf1Δ* an excellent system to study possible protein targets of Esa1 acetylation [66,67,79,80]. Additionally, Eaf1 is the only member that has exclusively been associated with the NuA4 complex [66,79]. Alternatively, while *ESA1* is essential and therefore cannot be deleted, NuA4 function can be probed using the temperature sensitive mutation, *esa1-ts* (*esa1-L254P*), which reduces the acetylation activity of Esa1 at increased temperatures

[58,81,82]. These mutations are fundamental to discovering functions of the NuA4 lysine acetyltransferase complex.

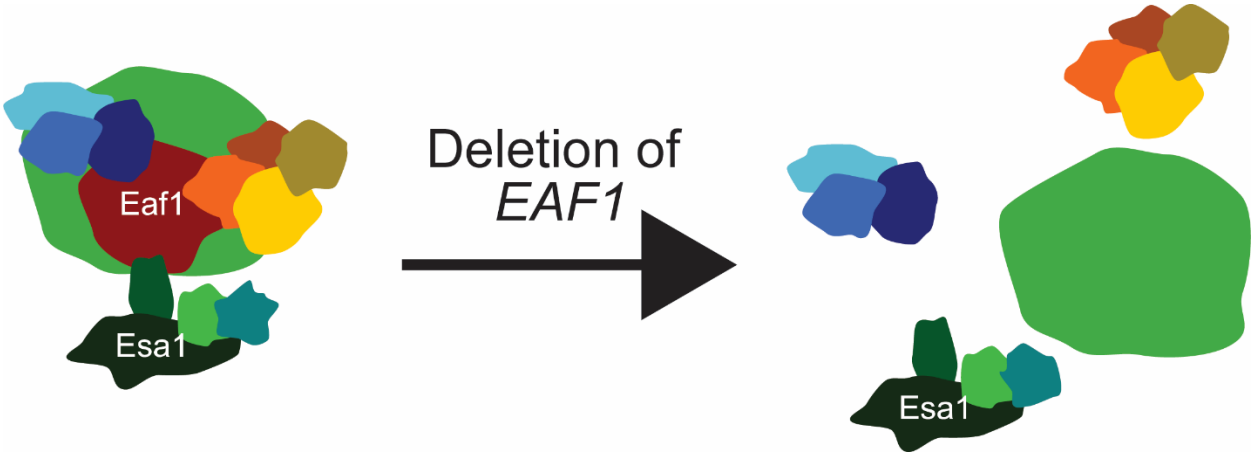

Figure 1.2: The NuA4 complex is a multi subunit lysine acetyltransferase complex in yeast. The gene for the catalytic subunit, *ESA1*, is an essential gene in yeast. *ESA1* cannot be deleted but the deletion of the gene for the core scaffolding complex member *EAF1* causes dissociation of the complex and a reduction in targeting of Esa1 activity and therefore a reduction in acetylation of NuA4 targets.

1.5 Tip60 a human lysine acetyltransferase implicated in disease

Esa1/NuA4 in yeast and Tip60 (aka KAT5) in mammalian cells were discovered and characterized independently around the same time at the end of the 20th century [81,83]. These two different KATs were characterized to have similar specificities for histone acetylations in different species and have since been characterized as homologs between the species [51,58]. Tip60 and Esa1 share a common MYST domain for catalytic function and have 2 large areas of sequence homology (Uniprot Reference numbers: Esa1 Q08649 and Tip60 Q92993). The Esa1 protein has 47-48 % sequence identity to the four different Tip60 isoforms (Figure 1.3). The name Tip60 came from the initial isolation of the protein as a HIV-tat interactive protein of 60 kDa size and while the name is still commonly used it has more recently also been denoted as KAT5 [84,85]. Similar to how Esa1 functions as the catalytic member of the NuA4 complex, Tip60 is a catalytic lysine acetyltransferase protein which functions within the larger Tip60

complex in humans, much of which has orthologous genes found within the yeast NuA4 complex (Table 1.1) [62]. The primary Tip60 encoded protein is one of 4 splice isoforms of the gene and will be the focus of this discussion [86]. Tip60 is also highly regulated itself by post translational modifications including acetylation, phosphorylation, and SUMOylation [87–90].

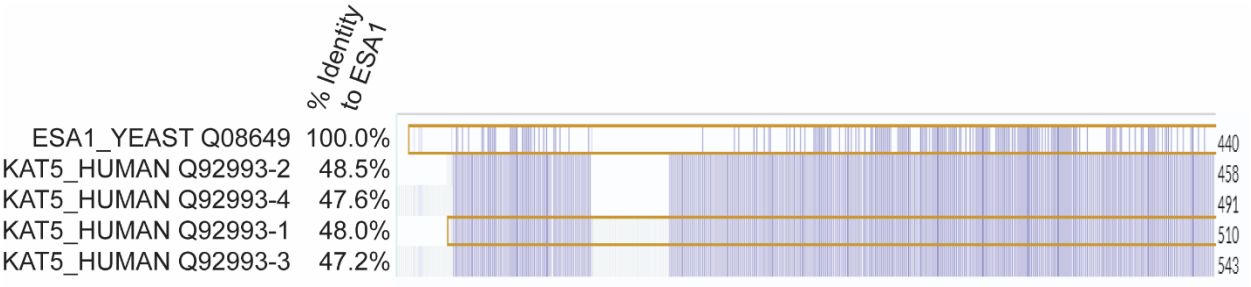

Figure 1.3: Sequence alignment of Saccharomyces cerevisiae Esa1 protein with the 4 isoforms of the human Tip60 (KAT5) proteins. The percent identity to the Esa1 protein is listed followed by an alignment figure showing homology at the amino acid level using purple lines. Sequence alignment was performed using UniProt.

Esa1 is an essential gene in yeast [69] , and similarly Tip60 is an essential gene in mammals. The knockout of Tip60 in mice is embryonic lethal following the blastocyst stage of development [91]. Meanwhile, heterozygous mice have apparently normal development and mating [69,92], however these mice have an increased susceptibility to Myc-induced B-cell lymphomas [92], one of the many ways Tip60 deregulation has been linked to cancer. In their work, Gorrini and colleagues demonstrated a haplo-insufficient tumor suppressor function of Tip60 in the early stages of Myc-induced cancers [92]. They additionally found that a reduction in Tip60 expression was a common event in human cancers ranging from breast to head and neck squamous cell carcinoma and noted a deregulation in the localization of Tip60 in these cancer cells [92]. Similarly, an analysis of Tip60 localization and abundance in breast cancer cells and tissue found that Tip60 staining patterns are associated with cancer sub-type and tumour grade [93]. Specifically, low Tip60 expression was identified as a risk factor for cancer recurrence and poorer

survival [93,94]. In most recorded cases, Tip60 acts as a tumor suppressor which has been interrupted in association with the cancer. However, in contrast to its role in the above-described cancers, Tip60 acts as an oncogene in prostate cancer and results in an increase in androgen receptor signalling [20,95]. In the prostate, Tip60 interacts with androgen receptor (AR) and acetylation of AR is important for activation [95,96]. Therefore, Tip60 has become a target of interest for drug inhibitors in prostate cancer [20]. Similarly, Tip60 activity has been linked to Cisplatin resistance during cancer treatment [97]. Accordingly, in Cisplatin resistant cancers and in prostate cancers inhibition of Tip60 may be an important therapeutic avenue to explore.

The mechanisms for Tip60 in cancer progression are thought to be related to its complex roles in the regulation of gene expression, apoptosis, and perhaps most well explored is its role in regulating DNA damage repair [55,62,88]. Tip60 regulates the DNA damage response and repair through a number of mechanisms including acetylation of ATM and p53 [98]. P53 is one of the most well characterized and prevalent dysregulations in cancer [99]. These mechanisms also link Tip60 activity to apoptosis in the case of severe damage [98].

In addition to cancer, a number of other human diseases have been linked to Tip60 deregulation. Work in Drosophila has implicated Tip60 as neuroprotective for neurodegeneration [100]. In fly models of Parkinson's Disease, Huntington's Disease, and Amyotrophic Lateral Sclerosis disruption of Tip60 is a early occurring and common event which affect neural epigenetics [101]. Additionally, in humans, regulation of p53 by Tip60 also has potential implications in Alzheimer's Disease through p53 phosphorylation of Tau [86,102]. On the opposing side to neurodegeneration, Tip60 is also implicated in neurodevelopment. Tip60 acetylation of MARCKs, a protein involved in neurulation, is induced in conditions of maternal diabetes and primes MARCKs for phosphorylation leading to neural tube defects [65]. Additionally, missense variants in Tip60 (KAT5) which affect its activity have been found in a rare neurodevelopmental syndrome [103]. Tip60 association with neurodevelopment along with embryonic

lethality of Tip60 null mice, emphasizes the importance of Tip60 in development. Finally, Tip60 has been associated with diabetes through work on mice [53]. Mice expressing a mutant non-phosphorylatable Tip60 exhibited increase insulin sensitivity, greater glucose tolerance, and reduced body weight [53]. While transcriptional and histone-based regulation by Tip60 may underpin the deregulation in many of these diseases, non-histone regulation of cellular pathways by Tip60 can also play an important independent or parallel role.

While there has been large efforts to use KDAC inhibitors in clinical treatment [36], inhibition of Tip60 has been less explored. One inhibitor in particular, NU9056, has been shown to specifically inhibit Tip60 with at least a 16 fold better inhibition of Tip60 over other related KATs but clinical exploration into the use of NU9056 has been limited [20,104,105]. Tip60 is an essential gene and therefore dysregulation has impacts across the body. It is commonly deregulated in cancer and other human diseases, but its roles are complex. For example, Tip60 has been identified to function as a tumor suppressor in some cancer conditions and as an oncogene in others. Continued research into functions of Tip60 and the homologous yeast NuA4 complex in the cell may provide important insights for human disease and future therapeutic interventions.

1.6 Additional targets and functions of the NuA4 complex

In addition to its initial well characterized role in the acetylation of histones and therefore regulating gene expression, NuA4 has now been linked to the regulation of many other cellular processes. Intriguingly, many of the non-histone target regulations by NuA4 are involved in metabolism [52,59,60,106]. Indeed, even a early microarray experiment highlighted the enrichment of metabolic pathway enzymes and effectors in a list of possible NuA4 non-histone targets [59]. This section will outline characterized roles for NuA4 outside of histone acetylation which are also summarized in Figure 1.4.

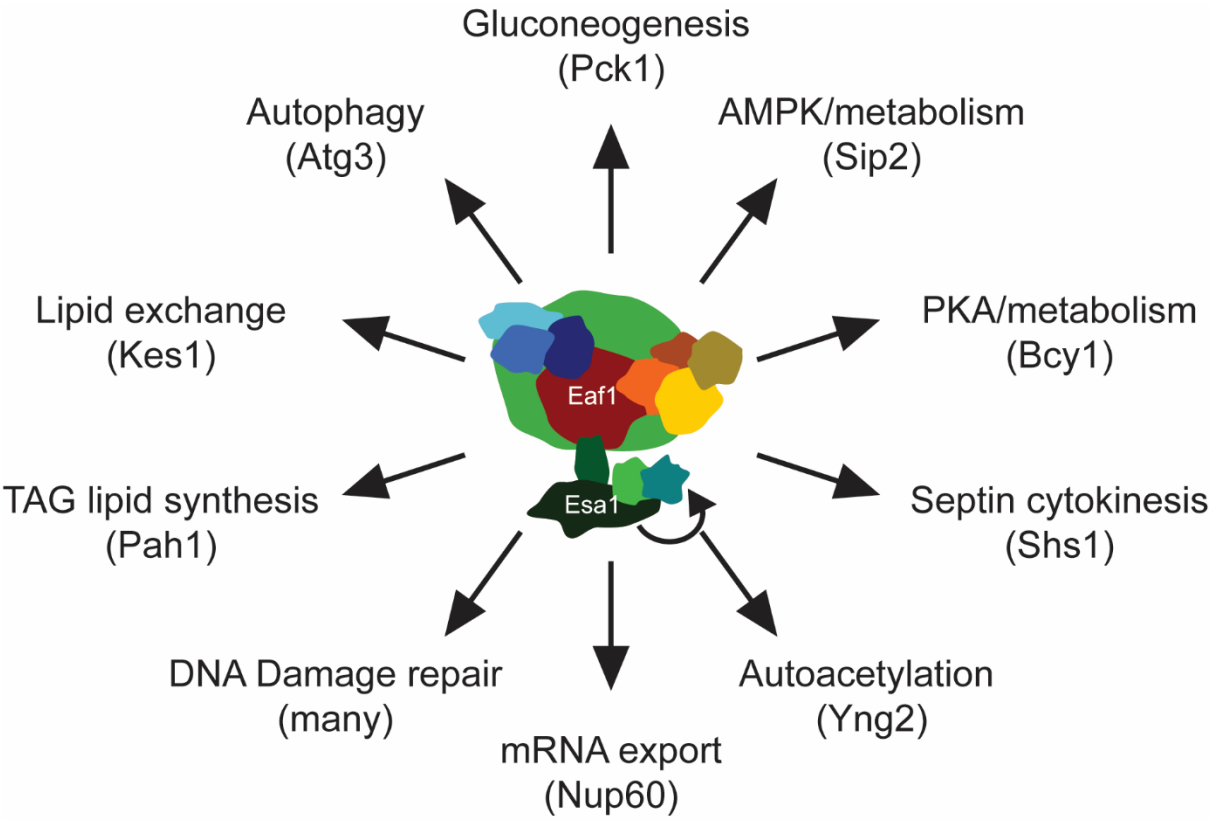

Figure 1.4: Pictorial representation of additional targets and functions of the NuA4 complex discussed in this thesis. Arrows point to the pathways regulated and the specific regulated protein target identified in each pathway is listed below in brackets.

1.6.1: NuA4 complex auto-acetylation

Self regulation by post-translational modification enzymes, including KATs, is common [107,108]. Indeed, auto-acetylation sites have been identified on Esa1 [109] and Tip60 [107]. In Tip60 these auto-acetylations are important for regulating structure and enzymatic activity as well as affecting Tip60 interactions with substrates [107,110]. In an *in vitro* KAT assay, the NuA4 complex acetylates many of its component members [111], but more directly, Esa1 has been implicated in the acetylation of NuA4 complex member Yng2 [112]. The acetylation of Yng2 is important for both the stability and function of the Yng2 protein and therefore of the activity of the NuA4 Piccolo enzymatic submodule [112].

1.6.2: NuA4 regulation of DNA damage repair and response

In the early 2000s, novel work showed that acetylation of the H4 histone tail by NuA4 was not only important for regulating the nucleosome for transcriptional purposes but was also important for DNA double strand break repair [113]. Since then, a large body of research has been developed showing links between NuA4/Tip60 acetyltransferase activity and the different modes of DNA damage repair. Major roles in the DNA damage repair pathway for Tip60 include regulation of ATM kinase, an apex regulator of DNA damage repair, and p53 which responds to DNA damage and arrests cells or in case of prolonged damage activates apoptosis [55,84,98]. There have also been many other important links of NuA4 to the DNA damage response and repair pathways. In yeast, the incorporation of the H2A.Z histone variant into nucleosomes is stimulated by NuA4 acetylation of H4 and H2A in the DNA damage response [114]. Additionally, NuA4 dependent acetylation of the DNA damage marker histone H2AX is involved in H2AX removal following DNA damage repair [115]. Outside of histone alterations, NuA4 is also important for the recruitment of other chromatin remodelers as well as for repair pathway choice. NuA4 acetylation of Nej1 and Ku80 at DNA breaks inhibits non-homologous end joining (NHEJ) in promotion of DNA end resection and homologous repair [116,117]. NuA4 activity has also been associated with other mechanisms of DNA repair. The deletion of *YNG2* and depletion of Esa1 both reduce the level of nucleotide excision repair by half relative to WT yeast following UV induced damage [118]. Similarly, treatment of NuA4 yeast mutants with methyl methanesulfonate (MMS) to create lesions in the DNA demonstrated that NuA4 activity promotes translesion synthesis [119]. Finally, outside of specific DNA damage but in the field of regulating DNA structure, NuA4 has recently been shown to acetylate Pif1, a DNA helicase which is important for unwinding G-quadruplexes and R-loops, altering its helicase activity [120]. Overall, the association of NuA4 with histones and DNA has made it an excellent candidate for the cell to use in regulating DNA repair.

1.6.3: NuA4 regulation of gluconeogenesis protein Pck1

In yeast, the phosphoenolpyruvate carboxykinase (Pck1) was one of the first identified non-histone targets of NuA4 using protein microarray screening [59]. Pck1 catalyzes the rate limiting step of gluconeogenesis and its acetylation by NuA4 at the K514 site was deemed crucial for maximal enzymatic activity of Pck1[59,121]. Based on this work, mutants which decrease the activity of NuA4, such as the *eaf1Δ*, have a reduction in Pck1 activity and therefore also reduced gluconeogenic activity. Of importance for motivating future experimentation, this work was found to be conserved to humans with Tip60 acetylation of Pck1 also being associated with human cell gluconeogenesis activity [59].

1.6.4: NuA4 regulation of Snf1 (AMPK)

NuA4 yeast mutants have long been classified as having replicative lifespan defects [122]. The microarray work which identified Pck1 discussed above also identified Sip2 as a potential target for NuA4 dependent acetylation [59]. Sip2 acetylation was confirmed in follow up work which also showed that the replicative lifetime defects in NuA4 mutants are due to impairments in Sip2 acetylation [59,60]. Sip2 is one of the three inhibitory β subunits of Snf1. The Snf1 kinase complex is responsible for responding to cellular AMP levels and signalling changes in metabolism and is the homolog to human AMP activated kinase (AMPK) [60,122]. Snf1 kinase activity is well characterized to be activated in response to glucose limitation, however, Snf1 activity is also important for the cellular response to numerous other external stressors including pH, temperature, and oxidative stress [123]. The activation of Snf1 is dependent upon a balance phosphorylation by upstream kinases Sak1, Elm1, and Tos3 and dephosphorylation by Glc7 [123]. While Snf1 is homologous to human AMPK, unlike AMPK, Snf1 has not been demonstrated to be allosterically activated by AMP but the AMP:ATP ratio is correlated with Snf1 activity [123,124]. The activity of Snf1 kinase is required for the cell to adapt to use alternative carbon sources and has numerous effects on cellular metabolic activity[123].

Acetylation of Sip2 by NuA4 increases its interaction with Snf1 thereby inhibiting Snf1 kinase activity, and preventing activation of glucose repressed gene transcription [60,123]. The acetylation of Sip2

and the associated inhibition of Snf1 activity extended replicative lifespan and made yeast more resistant to oxidative stress [60]. Based on this work, mutants with decreased NuA4 activity have increased Snf1 activity, increased downstream phosphorylation of Snf1 targets, and expression of glucose repressed genes.

1.6.5: NuA4 regulation of PKA and Msn2/4 stress response

NuA4 has also been associated with the activity of another set of partially redundant yeast kinases, Tpk1, 2, and 3 [52]. These proteins are the cyclic AMP sensors of yeast, homologous to human PKA, and are a key stress response signalling pathway [125,126]. In the yeast PKA system, the three Tpks act as the catalytic kinase which is regulated by their interactions with the repressor subunit, Bcy1 [127]. There are numerous direct ways in which the activity of PKA is regulated including: phosphorylation, cAMP binding, and spatially by subcellular separation of its subunits [128–130]. Recently, Filteau and colleagues identified that acetylation is also a key regulator of PKA [52]. Specifically, Filteau and colleagues propose that NuA4 acetylates Bcy1 at lysine (K) 313 resulting in decreased association of Bcy1 with the Tpks, and therefore increased PKA activity. However, while they show that Tip60 overexpression leads to decreased association of the regulatory subunit to the catalytic subunit in mammals, the acetylation of Bcy1 by NuA4, and the downstream effects on the Tpks and signalling are not assessed in this paper [52]. Based on this work, NuA4 deficient mutants may have a reduction in PKA activity.

Downstream of PKA activity is the regulation of the functionally redundant stress response transcription factors Msn2 and Msn4 (Msn2/4) [131]. PKA phosphorylation plays a role in maintaining Msn2/4 as cytoplasmic [131]. Under stress conditions, Msn2/4 enter the nucleus and bind to stress-response elements (STREs) [132]. Relocalization of Msn2/4 to the nucleus causes the transcription of stress response genes including Hsp12 (Heat shock response) and Gsy1/2 (glycogen synthesis) [132,133]. NuA4 has been demonstrated to co-immunoprecipitate with Msn2 and Msn4 and in the absence of NuA4 activity, Msn2/4-dependent transcription is de-repressed [79].

1.6.6: Links of NuA4 to the Sec14/Kes1 signalling axis

On the lipid side of metabolism, NuA4 has been linked to lipid exchange and fatty acid biosynthesis through a genetic interaction with *SEC14* [80,134] as well as through regulation of Kes1 [108,13]. Sec14 is a phosphatidylinositol/phosphatidylcholine transfer protein which is negatively regulated by Kes1 (Osh4), a yeast oxysterol binding related protein [135]. When nutrients are limited, Kes1 functions as a negative regulator of cell cycle progression [134]. Kes1 overexpression results in decreased viability or lethality in NuA4 mutants and Kes1 activity was demonstrated to be regulated by NuA4 dependent acetylation of Kes1 on K109 [111,134]. Acetylation of Kes1 at K109 is associated with a decrease in Kes1 activity and therefore regulation of cell cycle progression and lipid exchange [134]. Additionally, PKA signalling and Msn2/4 activity, which are disrupted in NuA4 mutants, are altered in Kes1 mutants [134].

1.6.7: NuA4 dependent acetylation of Pah1

Also, on the topic of lipid regulation, the NuA4 catalytic enzyme Esa1 and Tip60 have both been proposed to target Pah1 (human lipin 1) for acetylation. Pah1 is the enzyme which dephosphorylates PA to diacylglycerol (DAG) in the triacylglycerol (TAG) synthesis pathway and *PAH1* has genetic interaction with 2 genes for NuA4 subunits (*EAF7* and *YNG2*) [112,136]. The acetylation of Pah1 is associated with the translocation of Pah1 from the cytoplasm to the ER which promotes triacylglycerol (TAG) synthesis [53]. Deficiencies in TAG synthesis because of the lack of Pah1/Lipin 1 acetylation may explain why Tip60 mutant mice are lean and produce milk which has less TAG than their WT counterparts [53].

1.6.8: NuA4 in the regulation of septin dynamics

Previous work by Mitchell and colleagues in the Baetz lab using a synthetic dosage lethal screen identified NuA4 dependent regulation of septin proteins in yeast [111]. Septins are a group of filament proteins which were discovered in yeast and whose primary role is in cytokinesis [137]. Septin proteins have

many acetylation sites that can be acetylated *in vitro* by NuA4, but specific Esa1-dependent acetylation of Shs1 was characterized by Mitchell and colleagues using *in vitro* and *in vivo* analysis of specific targets of acetylation [111]. The acetylation of Shs1 is important for bud morphology as both NuA4 mutants and Shs1 mutant yeast have a portion of budded cells with elongated buds [111]. The elongated bud phenotype was associated with a mislocalization of septins in NuA4 mutants suggesting that acetylation may be important for the ring to collar reorganization during mitosis [111].

1.6.9: NuA4 in the regulation of autophagy

A targeted screen identified Esa1 as a KAT which is necessary for autophagy in yeast [138]. The acetylation of the autophagy protein Atg3 is induced upon starvation, dependent on Esa1 activity [138]. Acetylation of Atg3 affects the activity of Atg3 and its interaction with Atg8 [138]. While equivalent modification of Atg3 in mammalian cells has not been proven, Tip60 has also been linked to autophagy [86]. When growth factors are depleted or the ER is stressed, Tip60 is phosphorylated by GSK3 increasing Tip60 interaction with and acetylation of Ulk1 (yeast Atg1), effecting an increase in Ulk1 kinase activity in autophagy [139,140]. In a similar pathway, Tip60 was found to interact with and acetylate Pacer, a regulator of autophagy, *in vitro*, which was also dependent on phosphorylation of Tip60 by GSK3 [89]. Pacer acetylation increases the association of Pacer with HOPS and Stx17 and is important for regulating autophagy through autophagosome maturation and lipid catabolism [89,141].

1.6.10: NuA4 acetylation of the nuclear pore complex

NuA4 has recently been demonstrated to acetylate Nup60, a component of the nuclear pore complex [142]. Nup60 acetylation by NuA4 regulates the export of mRNA from the nucleus as well as impacting the G1/S transition with Esa1 activity promoting mRNA export and the Start transition [142]. The acetylation of Nup60 and therefore regulation of mRNA export is opposed by the Hos3 KDAC and can be compensated for by the Gcn5 KAT in the case of loss of Esa1 [142].

1.7 Lysine acetylation is tightly linked to metabolism

In addition to the above-described mechanisms of NuA4 dependent regulation of a few metabolic pathways, lysine acetylation more broadly is tightly intertwined with cellular metabolism on many fronts.

A major connecting compound of these processes is acetyl-CoA. Acetyl-CoA is the molecular source of the acetyl group which is added onto proteins in lysine acetylation [4]. It is also a central molecule in the metabolic landscape. Acetyl-CoA is used in lipid, cholesterol/ergosterol, and amino acid synthesis as well as being the main source of cellular ATP production under aerobic respiration [1,4]. Therefore, acetyl-CoA intrinsically links acetylation and metabolism through regulation of acetyl-CoA abundance thereby providing an excellent feedback mechanism [143]. Indeed, an increase in acetyl-CoA, which occurs in glucose rich conditions, is associated with an increase in acetylation within yeast and mammalian cells, and correspondingly, caloric restriction is associated with reduced mitochondrial acetylation [144,145]. Similarly, recent work showed that starvation of yeast was associated with a reorganization of the histone acetylome through KATs and KDACs to promote transcription of gluconeogenic and fat metabolism genes in order to generate acetyl-CoA [146]. Another molecule which links acetylation state and metabolism is NAD+ which is used as a cofactor by the sirtuin class of KDACs and is also a central coenzyme in cellular metabolism [147].

As a reversible post-translational modification, lysine acetylation can act quickly as a switch to regulate metabolism. Lysine acetylation is extremely common on metabolic proteins and sites of acetylation on metabolic proteins in yeast are largely conserved to mammalian cells [48]. More specifically, lysine acetylation is an abundant PTM in the mitochondria [148]. In fact, it has been proposed that it is a more abundant PTM than phosphorylation in the compartment [148]. Deacetylation in the mitochondria is managed by KDACs such as Sirtuin 3 while much of the acetylation in the mitochondria may be non-enzymatic [14]. However, some associations of Tip60 with the mitochondria have been made. First Tip60 has been implicated in the regulation of mitochondrial elongation through the acetylation and destabilisation of MFN1, a protein involved in outer membrane fusion of the mitochondria [149].

Additionally, the previously discussed Tip60 acetylation of MARCKS, a protein required for neural tube closure in development, leads to increased phosphorylation of MARCKS and its dissociation from the mitochondria.

Overall, it is clear that metabolism and lysine acetylation are woven together and there is continually growing evidence that lysine acetylation is not only impacted by metabolism but can also affect cellular metabolism through various modes of regulation.

1.8 Hypothesis

Given that NuA4 has previously been implicated in the regulation of metabolic processes including gluconeogenesis and AMPK signalling [59,60], that acetylation has many ties to metabolism [147], and that regulation of non-histone pathways by NuA4 are increasingly being identified:

I hypothesized that the yeast lysine acetyltransferase complex, NuA4, has additional yet to be characterized roles in the regulation of yeast cellular metabolism. Discovery of these roles may have important implications for understanding functions of the homologous Tip60 complex in human disease.

1.9 Aims and Motivations

1.9.1 Aim 1A:

Identify metabolic proteins whose localization or abundance are dependent on NuA4 activity.

Aim 1A was motivated by three main facts: 1. Many early non-histone targets of NuA4 were associated with metabolic control. 2. Rpd3, a KDAC which often opposes NuA4 activity affects the localization and abundance of numerous proteins [60,120,138]. 3. Parallel work in the Baetz lab found that the localization of Acc1, a key metabolic protein, is remodelled upon disruption of the NuA4 complex (Appendix A). In order to identify metabolic proteins whose localization or abundance are dependent on NuA4 activity, a screen comparing the observed distribution of GFP-tagged metabolic proteins in a WT and *eaf1Δ* background was performed.

Aim 1A was addressed in the first manuscript "Phenomic screen identifies a role for the yeast lysine acetyltransferase NuA4 in the control of Bcy1 subcellular localization, glycogen biosynthesis, and mitochondrial morphology" (Chapter 2) as well as in the supplemental co-authored paper "Fine tuning

Acetyl-CoA Carboxylase 1 activity through localization: Functional genomics reveal a role for the lysine acetyltransferase NuA4 and sphingolipid metabolism in regulating Acc1 activity and localization" (Appendix A).

1.9.2 Aim 1B:

Characterize the role of NuA4 in Bcy1/PKA dependent regulation of mitochondrial morphology and glycogen synthesis.

Aim 1B was motivated by the results of the screen performed in Aim 1A. The GFP screen identified 23 metabolic proteins which changed localization or abundance upon deletion of *EAF1* with high confidence. First, three of the GFP-tagged proteins that changed localization/abundance upon deletion of *EAF1* were associated with glycogen biosynthesis (Gdb1, Gsy1, and Gsy2). Second, more than half (14 of 23) of the identified protein changes in the *eaf1Δ* were mitochondrial associated proteins which were categorized into a mitochondrial elongation phenotype. Third Bcy1, the regulator subunit of yeast PKA, was identified by our screen to change localization upon deletion of *EAF1*. Therefore, we were motivated to characterize the role of NuA4 in Bcy1/PKA dependent regulation of mitochondrial morphology and glycogen synthesis.

Aim 1B was addressed in the first manuscript "Phenomic screen identifies a role for the yeast lysine acetyltransferase NuA4 in the control of Bcy1 subcellular localization, glycogen biosynthesis, and mitochondrial morphology" (Chapter 2).

1.9.3 Aim 2:

Identify and describe changes in lipid composition dependent on NuA4 activity, specifically detailing a change in ergosterol and ergosteryl ester dynamics in the *eaf1Δ* yeast cell.

Aim 2 was motivated by the identification of NuA4 in the metabolic control of lipids through Pah1 (Lipin) signalling [53] and parallel work that I co-authored which demonstrates that NuA4 regulates Acetyl-CoA carboxylase 1 (Acc1) activity and localization (Appendix A). Acetyl-CoA carboxylase (Acc1) converts acetyl-CoA into malonyl-CoA creating the committed precursor for fatty acid synthetase to produce long chain fatty acids [150]. Phenotypic changes in Acc1 localization were identified in NuA4 mutants and were also found in mutants affecting sphingolipid and very long chain fatty acid metabolism [151]. These links of the NuA4 complex to lipid metabolism motivated us to assess lipid composition of WT and *eaf1Δ* yeast and found two key changes. First there was an overall reduction in lipid chain lengths in cells deficient for *EAF1* [151]. Second, there was a significant increase in the relative abundance of ergosteryl esters in the *eaf1Δ* cells. The change in Acc1 and lipid composition of the *eaf1Δ* cell prompted us to identify and describe changes in lipid composition dependent on NuA4 activity, specifically detailing a change in ergosterol and ergosteryl ester dynamics in the *eaf1Δ* cell.

Aim 2 was addressed in the second manuscript "The lysine acetyltransferase NuA4 in regulation of ergosterol dynamics in *Saccharomyces cerevisiae*" (Chapter 3) as well as in the supplemental co-authored paper "Fine tuning Acetyl-CoA Carboxylase 1 activity through localization: Functional genomics reveal a role for the lysine acetyltransferase NuA4 and sphingolipid metabolism in regulating Acc1 activity and localization" (Appendix A).

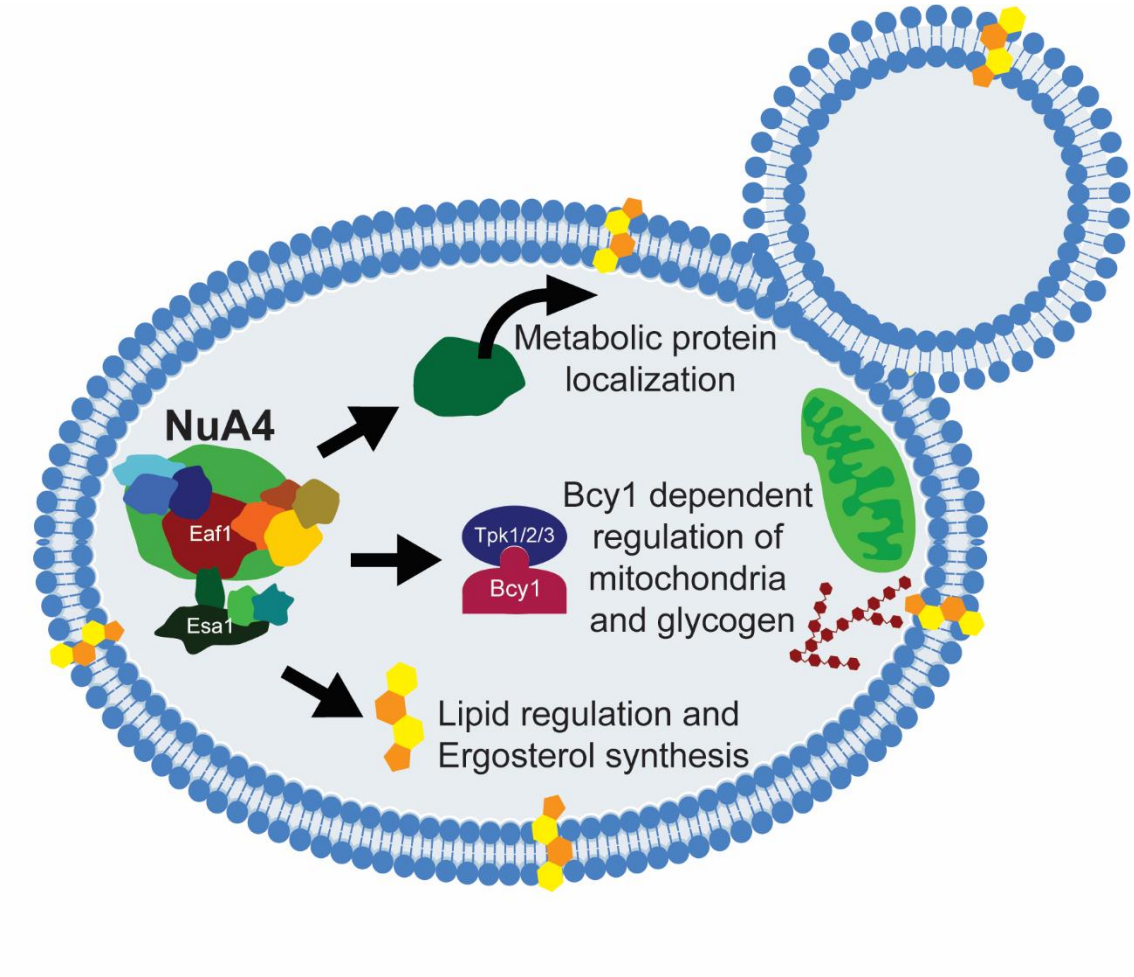

Figure 1.5: Pictorial summary of the aims of the thesis. Aim 1A) Identify metabolic proteins whose localization or abundance are dependent on NuA4 activity. Aim 1B) Characterize the role of NuA4 in Bcy1/PKA dependent regulation of mitochondrial morphology and glycogen synthesis. Aim 2) Identify and describe changes in lipid composition dependent on NuA4 activity, specifically detailing a change in ergosterol and ergosteryl ester dynamics in the *eaf1Δ* cell.

Chapter 2: Manuscript #1

Publication Information:

Walden EA, Fong RY, Pham TT, Knill H, Laframboise SJ, Huard S, Harper M-E, Baetz K. Phenomic screen identifies a role for the yeast lysine acetyltransferase NuA4 in the control of Bcy1 subcellular localization, glycogen biosynthesis, and mitochondrial morphology Copenhaver GP, editor. *PLOS Genetics*. 2020;16(11): e1009220. http://dx.doi.org/10.1371/journal.pgen.1009220. doi: 10.1371/journal.pgen.1009220

Phenomic screen identifies a role for the yeast lysine acetyltransferase NuA4 in the control of Bcy1 subcellular localization, glycogen biosynthesis, and mitochondrial morphology.

Elizabeth A. Walden [1,2], Roger Y. Fong [1,2], Trang T. Pham [1,2], Hana Knill [1,2], Sarah Jane Laframboise [1,2], Sylvain Huard [1,2], Mary-Ellen Harper [1,2], Kristin Baetz [1,2]*

[1] Department of Biochemistry, Microbiology and Immunology, Faculty of Medicine, University of Ottawa, Ottawa, Canada

[2] Ottawa Institute of Systems Biology, Ottawa, Canada

2.1 Abstract

Cellular metabolism is tightly regulated by many signaling pathways and processes, including lysine acetylation of proteins. While lysine acetylation of metabolic enzymes can directly influence enzyme activity, there is growing evidence that lysine acetylation can also impact protein localization. As the *Saccharomyces cerevisiae* lysine acetyltransferase complex NuA4 has been implicated in a variety of metabolic processes, we have explored whether NuA4 controls the localization and/or protein levels of metabolic proteins. We performed a high-throughput microscopy screen of over 360 GFP-tagged metabolic proteins and identified 23 proteins whose localization and/or abundance changed upon deletion of the NuA4 scaffolding subunit, *EAF1*. Of the identified proteins, three proteins were required for glycogen synthesis and 14 proteins were associated with the mitochondria. We determined that in *eaf1*Δ cells the transcription of glycogen biosynthesis genes is upregulated resulting in increased proteins and glycogen production. Further, in the absence of *EAF1*, mitochondria are highly fused, increasing in volume 3-fold, and are chaotically distributed but remain functional. Both the increased glycogen synthesis and mitochondrial elongation in *eaf1*Δ cells are dependent on Bcy1, the yeast regulatory subunit of PKA. Surprisingly, in the absence of *EAF1*, Bcy1 localization changes from being nuclear to cytoplasmic and PKA activity is altered. We found that NuA4-dependent localization of Bcy1 is dependent on a lysine residue at position 313 of Bcy1. However, the glycogen accumulation and mitochondrial elongation phenotypes of *eaf1Δ,* while dependent on Bcy1, were not fully dependent on Bcy1-K313 acetylation state and subcellular localization of Bcy1. As NuA4 is highly conserved with the human Tip60 complex, our work may inform human disease biology, revealing new avenues to investigate the role of Tip60 in metabolic diseases.

2.2 Author Summary

Metabolism, how cells process nutrients and energy substrates, is dramatically altered in many diseases. For example, during tumorigenesis, changes in cellular metabolism allow for the rapid cellular growth and division. One way to control metabolism is by moving the proteins involved in metabolism to different parts of the cell. Similar to an assembly line, when all the "parts" (metabolic proteins) are brought together, efficiency can be increased. In contrast, if one or more parts are shipped to the wrong place (mislocalized), production is decreased, and an alternative production process may even be necessary to meet demands. Here we ask whether Tip60, a protein complex implicated in many diseases, affects the location of metabolic proteins in the cell. We use budding yeast as a model system to assess the effect of disrupting yeast Tip60 on the location of over 360 metabolic proteins. We found that Tip60 controls the location of many metabolic proteins and in the absence of Tip60 there is an increase in the mitochondria and in cellular carbohydrate storage (the metabolic 'hubs' of the cell). This work suggests that yeast Tip60 functions as a "brake" on cellular metabolism and provides novel potential roles of Tip60 in metabolic diseases.

2.3 Introduction

Lysine acetylation is one of the most common post-translational modifications (PTM) in the cell. Lysine acetylation has been historically characterized as a PTM occurring on histones, however, in the last 10 years, thousands of non-histone acetylation sites have been identified through global screens for protein acetylation, establishing lysine acetylation as a conserved and dynamic PTM [48,82,152–155]. It is therefore not surprising that lysine acetylation plays diverse roles in the regulation of cellular processes and that it is deregulated in many human diseases [61,156–158].

Lysine acetylation is catalytically controlled by two opposing classes of enzymes: Lysine acetyltransferases (KATs) and lysine deacetylases (KDACs). Our work focuses on the *Saccharomyces cerevisiae* KAT complex NuA4, the yeast homolog of the human Tip60 complex, which has been associated with many diseases including cancer, developmental issues, and neurodegenerative disease [51,61–65]. Given the exceptional conservation of KAT function across eukaryotes, the study of the homologous NuA4 complex may provide insight into further understanding the biological roles of Tip60 and the cellular consequences of its deregulation in disease [51].

NuA4 contains 13 subunits, six of which are essential genes for viability, including the gene for the catalytic subunit *ESA1* [58,66–68]. Though non-essential, the *EAF1* subunit is a critical scaffolding protein required to maintain the complete NuA4 complex [66,68]. Yeast cells deficient for Eaf1 are viable but lose much of the targeting of the catalytic Esa1 subunit, making the *eaf1Δ* mutant an excellent genetic model system to identify the biological roles and protein targets of NuA4 [66,67,79,80]. Alternatively, NuA4 function can be probed using the temperature sensitive mutation, *esa1-ts* (*esa1-L245P*), which reduces the acetylation activity of Esa1 at increased temperatures [58,81,82].

Given its essential role, it is not surprising that NuA4 has been implicated in a myriad of biological processes, including metabolism. Indeed, lysine acetylation, which neutralizes the positive lysine side chain charge, has been suggested to be an ideal "switch" to turn off and on enzymes. For example, NuA4 dependent acetylation of phosphoenolpyruvate carboxykinase (Pck1) is important for activating its function in the rate controlling step of gluconeogenesis [59,112,121]. Acetylation has also been implicated in controlling protein-protein interactions. NuA4 yeast mutants have replicative lifespan defects caused by impairments in the NuA4-dependent acetylation of Sip2 [60]. Sip2 acetylation increases its interaction with Snf1 decreasing Snf1 activity [60]. Sip2 is one of the three inhibitory β subunits of the Snf1 complex (AMPK in humans) [122,123]. The Snf1 kinase responds to changes in cellular AMP levels and plays an important role in the adaptation of yeast cells to glucose limiting conditions as its kinase activity leads to the derepression of many glucose repressed genes [60,122,123,159,160]. Similarly, work by Filteau and colleagues suggests that the protein-protein interactions which control the activity of the Protein Kinase A (PKA), also referred to as cAMP-dependent protein kinase, are regulated through NuA4-dependent acetylation of the PKA regulatory subunit Bcy1 [52]. PKA is a central metabolic kinase and has been extensively linked to many cellular processes including stress response and mitochondrial processes [161–164]. In yeast, the PKA complex is a heterotetrameric complex containing two Bcy1 regulatory subunits bound to two catalytic subunits, of the three partially redundant Tpk1, Tpk2, and Tpk3 [125,127,165,166]. The study by Filteau and colleagues suggests that the unacetylated form of Bcy1 can interact with and inhibit the catalytic PKA subunits Tpk1/2/3, but when Bcy1 is acetylated the Bcy1-Tpk interaction is disrupted leading to PKA activation [52]. In humans, PKA activity can be regulated through being anchored to different parts of the cell including the mitochondria by A-Kinase Anchoring Proteins (AKAPs) [167]. While AKAPs have not been identified in yeast, the localization of the Tpks and Bcy1 are regulated in response to environmental factors which is likely also associated with changes in activity or substrates [163,168,169]. One key downstream effect of Tpk activity is the regulation of the localization of the functionally redundant Msn2 and Msn4 (Msn2/4) stress response transcription factors which are phosphorylated and sequestered in the cytoplasm [131,170]. Upon stress or inhibition of PKA activity,

Msn2/Msn4 phosphorylation decreases allowing for translocation into the nucleus where they bind to stress response elements (STREs) and activate transcription of genes related to β oxidation of fatty acids, glycolysis, and stress response [132,171,172]. Interestingly, Msn2/4-dependent transcription is de-repressed in NuA4 mutants [79]. While this transcriptional de-repression may be associated with PKA activity, it is also possible that there is direct regulation as NuA4 can co-IP with Msn2 and Msn4 [79,131]. Finally, PKA activity and transcriptional activation of Msn2/4 targets have also been linked to another target of NuA4, the oxysterol binding protein Kes1 [134]. Kes1 functions as a lipid exchange protein in the cell and its acetylation has been demonstrated to regulate cell cycle arrest in response to nutrient stress [134]. Yeast with impaired NuA4 activity showed increased Kes1 activity with an associated increase in Msn2/4 transcriptional activity in addition to the metabolic characteristics of quiescence [134]. Overall, many preliminary links of NuA4 to metabolism have begun to be uncovered.

In addition to regulating enzyme activities and protein-protein interactions directly, lysine acetylation has also been associated with contributing to protein subcellular localization. For example, in mammalian cells, Tip60 acetylation of lipin drives its localization to the endoplasmic reticulum [53]. Indeed, the role of acetylation in regulating protein subcellular localization may be far reaching. Chong and colleagues used synthetic genetic array (SGA) technology coupled with high content screening to assess the impact of the deletion of the KDAC *RPD3* on over 4000 GFP fusions [41]. *RPD3* deletion led to a large number of proteins that increased in abundance but more intriguingly, the subcellular localization of more than 30 proteins were altered upon deletion of *RPD3* [41].

Given that NuA4 is implicated in the regulation of a variety of metabolic proteins [59,173], and the global impact of Rpd3 on protein abundance and localization [41], here we ask if NuA4 impacts the subcellular localization or abundance of metabolic proteins. We identified 23 proteins that displayed altered localization or abundance upon deletion of *EAF1* and of these, 14 were associated with mitochondria and three were associated with glycogen synthesis. We determined that the mitochondrial

elongation and increased glycogen detected in *eaf1Δ* cells are partially due to the yeast PKA regulatory subunit, Bcy1, and that NuA4 is regulating the subcellular localization of Bcy1.

2.4 Results

***EAF1* dependent remodeling of the metabolic proteome**

To identify metabolic protein localization and abundance changes between wild type (WT) and the NuA4 mutant *eaf1Δ* we performed a focused phenomic screen. Using synthetic genetic array technology [174,175], both WT and *eaf1Δ* strains were crossed to 407 C-terminal GFP-fusion proteins from the GFP collection [42] with known or implicated roles in metabolism. Due to attrition of strains during mating, this resulted in a pair matched single (X-GFP) and double (X-GFP *eaf1Δ*) mutant set consisting of 368 genes (Screen outlined in S2.1 Fig).

The localization and protein abundance of the 368 GFP-tagged metabolic proteins was assessed in the WT and *eaf1Δ* background by high-throughput microscopy. In total, manual classification identified 70 proteins whose protein level and/or localization is impacted by deletion of *EAF1*. Additionally, the GFP intensity between WT and *eaf1Δ* cells for each strain was compared using ImageJ to assess changes in protein abundance, many of which corresponded with the manual classifications (S2.1 Table and S2.2 Fig). Of the approximately 70 potential changes identified (manually and by Image J), we selected 23 GFP fusions that had dramatic observable changes in localization upon deletion of *EAF1* to reassess. The identity of the selected GFP fusions were confirmed by PCR in both WT and *eaf1Δ* backgrounds and secondary microscopy was performed (Figure 2.1, S2.3 Fig, and S2,1 Table). The 23 confirmed changes were categorized into six categories: mitochondrial elongation, cytoplasm to punctate, nucleus to cytoplasm, cytoplasm to nucleus, cell periphery to cytoplasm, and increased abundance (Figure 2.1A, S2.3 Fig, and S2.2 Table). Two categories of localization changes particularly stood out, the

cytoplasm to punctate phenotype and the mitochondrial elongation phenotype. The cytoplasm to increased punctate phenotype (represented by Gsy2-GFP in Figure 2.1B) was of interest because all three proteins within this category are part of the glycogen regulation pathway. The second striking feature of this screen were the 14 GFP-tagged mitochondrial proteins, which displayed elongated mitochondrial phenotype (represented by Aco2-GFP in Figure 2.1B). Our screen shows that deletion of *EAF1* results in remodeling of a subset of the yeast metabolic proteome.

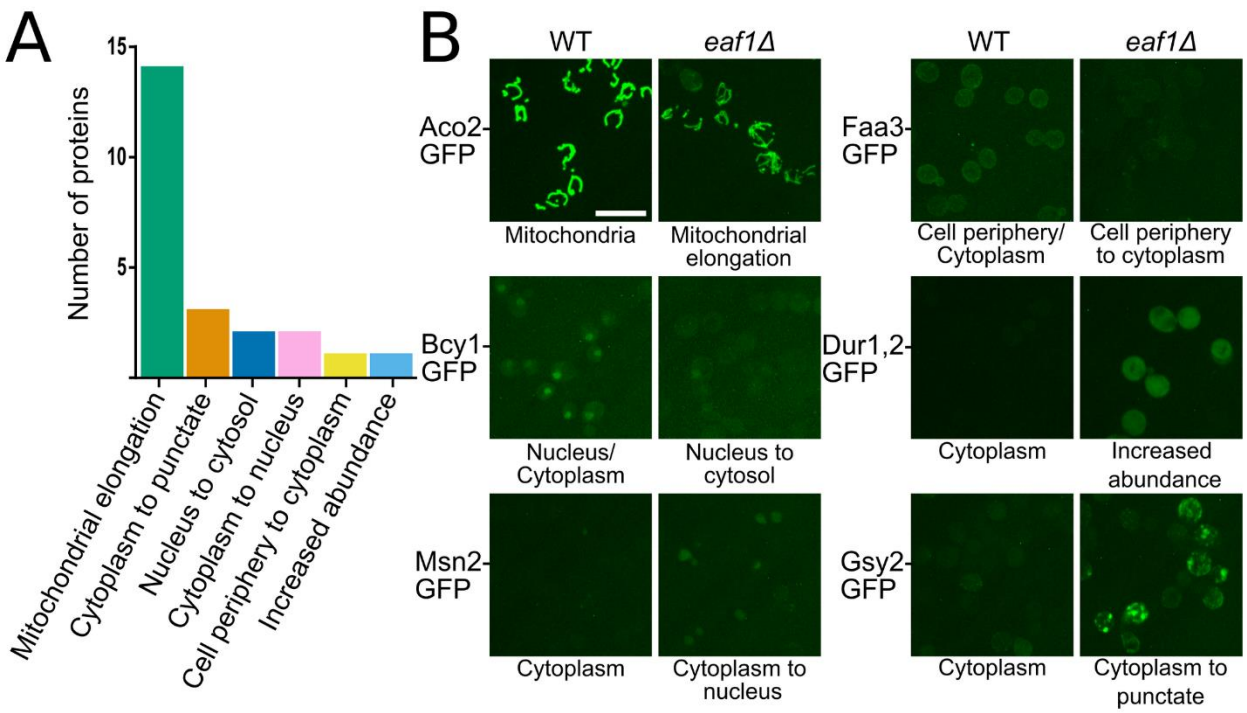

Figure 2.1. Summary of impact of *EAF1* deletion on metabolic protein localization and signal. (A) A phenomic screen for changes in protein localization and abundance between WT and *eaf1Δ* yeast was performed using SGA technology and high throughput microscopy. 23 confirmed changes in GFP signal localization or abundance were identified and categorized (S2.2 Table). (B) Six representative images of the change in GFP-fusion proteins identified in the phenomic screen (images of all confirmed changes available in S2.3 Fig). WT localization of proteins as previously reported at https://thecellvision.org/cyclops/ are listed under the WT image and the change category is listed under the *eaf1Δ* image. Some of these proteins also had changes in abundance in the *eaf1Δ* relative to WT. Fold changes outside our cut-off were: Aco2=0.51, Dur1, 2 = 3.77, and Gsy2 = 1.65. Scale bar = 10 μm.

NuA4 regulation of glycogen biosynthesis is dependent on PKA and Msn2/Msn4

Our screen identified three GFP-tagged glycogen biosynthesis proteins (Gdb1, Gsy1, and Gsy2) that in *eaf1Δ* cells increased in GFP signal and were concentrated into punctate structures (Figure 2.1B, S2.3 and S2.4A Figs). These proteins are responsible for glycogen synthesis (Gsy1 and Gsy2) and glycogen debranching (Gdb1) [176]. Glycogen is a large polysaccharide molecule made of repeating and branching glucose molecules [176] (Figure 2.2A). It is an important energy storage molecule for mammals and yeast [176–178]. Iodine staining to assess glycogen content confirmed that *eaf1Δ* cells have a higher level of glycogen (darker staining) than WT cells [179] (Figure 2.2B). Additionally, at the semi-restrictive temperature of 30^{o}C the temperature sensitive *ESA1* mutant *esa1*^{L254P} *(esa1-ts*) also demonstrated an increase in iodine staining (S2.4 Fig).

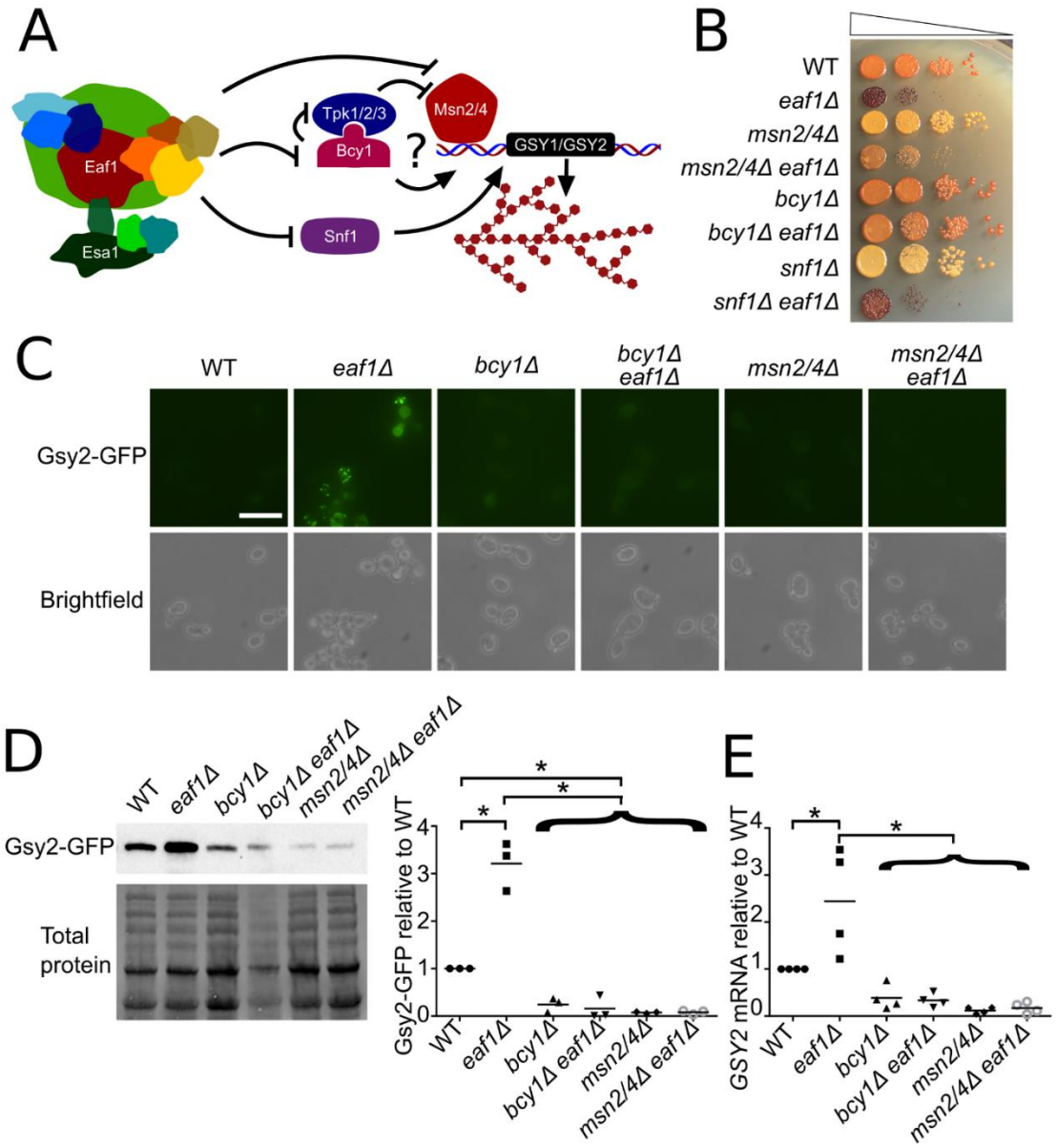

Figure 2.2. NuA4 regulation of glycogen biosynthesis proteins is mediated by PKA-Msn2/4 pathway. (A) Schematic model of NuA4 regulation of glycogen biosynthesis genes. (B) Increased glycogen levels in *eaf1Δ* cells is suppressed by *bcy1Δ* and *msn2Δ msn4Δ*. The indicated strains were serially diluted on to YPD plates, grown at 30ºC for 24 hours prior to exposure to iodine crystal vapours. Darker color corresponds to more glycogen storage. (C) Gsy2-GFP expression and localization were assessed in the indicated strain backgrounds by microscopy. Images are representative of three independent biological replicates. Scale bar = 10 μm. (D) Gsy2-GFP protein levels were assessed by quantitative western blot analysis using whole cell extracts from the indicated strains expressing Gsy2-GFP. Panel to the left is representative anti-GFP western and total protein blot; panel to the right is the quantification of western blots for three independent biological replicates where the Gsy2-GFP band intensity was normalized to total protein. (E) *GSY2* mRNA was measured using RT-qPCR relative to the *TDH3* gene for indicated yeast strains using four biological replicates. For D and E, ANOVA analysis was performed with a Tukey's multiple comparison test comparing pairs of means. *= $p < 0.05$, relevant significance bars shown. Horizontal bar in data represents the mean.

We next sought to determine mechanistically how deletion of *EAF1* causes an increase in glycogen biosynthesis proteins. Given the similar induction in protein levels observed by microscopy and western blot (Figure 2.2C and 2.2D and S2.4 Fig) and that *GDB1*, *GSY1*, and *GSY2* genes are all associated with stress response element (STRE) activated transcription [172,180–182], we performed further characterization using only Gsy2, the predominant glycogen synthase in yeast [183]. As both the PKA-Msn2/Msn4 axis and Snf1 have been implicated in the transcriptional regulation of glycogen biosynthesis genes [180,181,184,185] (Figure 2.2A) we asked if the increased glycogen level seen in *eaf1Δ* cells is dependent on *MSN2/MSN4, BCY1*, or *SNF1* (Figure 2.2B). We found that *eaf1Δ* cells have a much darker iodine staining than WT cells, suggesting an accumulation of glycogen (Figure 2.2B). While *snf1*Δ cells displayed less iodine staining than WT cells, suggesting less glycogen accumulation, *snf1Δeafδ* cells displayed iodine staining similar to *eaf1Δ* cells. In contrast, deletion of both *MSN2* and *MSN4* (*msn2/4Δ)* or deletion of *BCY1* (*bcy1Δ)* suppressed glycogen accumulation in *eaf1Δ* cells when analyzed by iodine staining (Figure 2.2B). This suggests that NuA4-dependent regulation of the PKA-Msn2/4 pathway contributes to the control of glycogenesis, while NuA4-dependent regulation of AMPK/Snf1 does not. Further, we were surprised to see that deletion of *BCY1* suppressed the slow growth defects of *eaf1Δ* cells, where *msn2Δmsn4Δ* did not (Figure 2.2B). The *bcy1Δ* suppression of *eaf1Δ* slow growth was confirmed by OD-based growth curve analysis and calculation of doubling time for each strain (S2.5 Fig). This suggests that derepression of Msn2/Msn4-dependent transcription is not contributing to slow growth of *eaf1Δ*, rather other targets of PKA are likely contributing to its slow growth. The dependence of the glycogen content on Msn2/4 signalling was of additional interest to us as our screen also identified Msn2 to move from the cytoplasm to the nucleus upon deletion of *EAF1* (Figure 2.1B). Parallel analysis of the Gsy2-GFP signal by microscopy and quantitative western blot confirmed that Gsy2-GFP protein expression is induced upon deletion of *EAF1* and demonstrated that this is dependent on Msn2/Msn4 and Bcy1 (Figure 2.2C and 2.2D). qRT-PCR determined that the increase in Gsy2 protein was at least partially due to a significant increase in *GSY2* mRNA expression in *eaf1Δ* cells relative to WT (Figure 2.2E). Finally, the increase in protein abundance of Gsy2-GFP and mRNA levels of *GSY2* seen in *eaf1*Δ

cells were suppressed upon deletion with *msn2Δmsn4*Δ or *bcy1Δ (*Figure 2.2C, 2.2D, and 2.2E). Together this work is consistent with the conclusion that the increase in glycogen biosynthetic proteins identified in our screen are at least partially due to NuA4 regulation of PKA and Msn2/Msn4 activity.

Mitochondrial volume increases in the absence of NuA4

Our screen identified 14 mitochondrial proteins that had a change in GFP signal between WT and *eaf1Δ* (Figure 2.1A and S2.3 Fig.). As all of the 14 proteins are resident mitochondrial proteins, rather than proteins that are relocalizing to the mitochondria, it suggests that mitochondrial elongation is occurring in *eaf1Δ* cells. To confirm this hypothesis we assessed 3 common markers of the mitochondria in both WT and *eaf1Δ* cells: Cit1-GFP, Aco2-GFP and MitoLoc [186], a plasmid expressing a mitochondrial localized GFP peptide (Figure 2.3 and S2.6 Fig.). In each case, we detected hyperelongated mitochondria with increased branching in *eaf1Δ* cells. Despite the fact that *eaf1Δ* cells are almost 2x larger than WT cells (Figure 2.3 and S2.7 Fig.), when the change in the mitochondrial volume is normalized to the increased cell size of the *eaf1Δ*, there is still a significant 1.7-fold increase in the mitochondrial volume relative to cell size (mitochondrial fraction) (Figure 2.3). When cell size is not accounted for, the mitochondrial volume of the *eaf1Δ* strain was found to be approximately three times larger than WT (S2.8 Fig). The mitochondrial morphology of the *esa1-ts* was also assessed after 2 hours at a semi-permissive temperature of 33^{o}C and there was a slight change in mitochondrial morphology and but no significant change in mitochondrial fraction was identified (S2.9 Fig). The difference in the penetrance of the mitochondrial phenotype between the *eaf1Δ* and the *esa1-ts* may be explained by the difference in the mutation type. The *esa1-ts* is functional when grown at 25^{o}C and the short 2-hour incubation at 33^{o}C decreases NuA4 catalytic activity however extended temperature shift dramatically decreases viability. In contrast, deletion of *EAF1* disrupts the NuA4 complex, including substrate targeting, but the catalytic activity remains intact. It is also possible that Eaf1 plays a role outside of the NuA4 complex and Esa1 targeting, but that remains as a speculation, and the small effect of the *esa1-ts* on mitochondrial morphology seen in our experiments would suggest that this is not the case. Altogether, this indicates that

a reduction in NuA4 activity results in altered mitochondrial morphology (a fused phenotype) and increased mitochondrial content per cell (mitochondriogenesis).

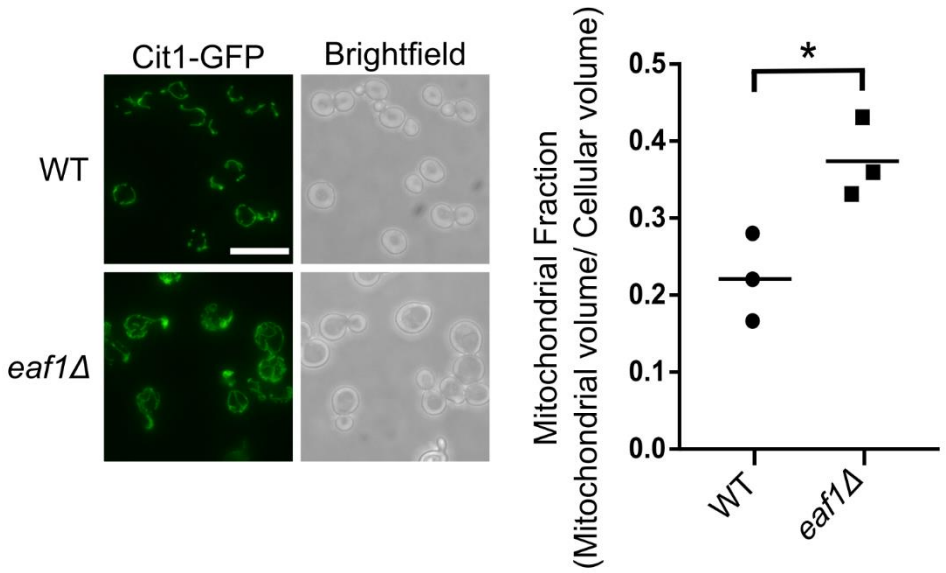

Figure 2.3. Mitochondrial morphology and volume are altered in NuA4 mutants. Cit1-GFP was used as a marker of the mitochondria to compare WT and *eaf1Δ* mitochondrial morphology by fluorescent microscopy. The mitochondrial volume was quantified based on the Cit1-GFP fluorescence using the MitoMap plugin for ImageJ which was then divided by the average total cellular volume of the strain to give the Mitochondrial Fraction (Raw cellular and mitochondrial volume measurements can be found in S2.7 and S2.8 Figs). Images are representative of 3 independent biological replicates and at least 50 cells per replicate were analyzed for quantification Scale bar = 10 μm. An unpaired T-test was run. *= $p < 0.05$. Horizontal bar in data represents the mean.

While chaotic and elongated, the mitochondria in *eaf1Δ* cells are functional

The structure of the mitochondria is important to its function [187]. Therefore, we sought to test if mitochondrial function was intact in *eaf1Δ* cells using three different assays. First, a Seahorse Extracellular Flux Analyzer (XF; Agilent) was used to measure mitochondrial bioenergetics. WT and *eaf1Δ* yeast were prepared overnight in YPD and then diluted in the morning into YPD or YPE (Ethanol), a non-fermentable carbon source that forces mitochondrial oxidative reactions over glycolysis. The oxygen consumption rate (OCR) of the mutant was compared to the control in YPD and YPE media and in both cases the *eaf1Δ* consumed significantly more oxygen than the WT yeast (Figure 2.4A and 2.4B).

The oxygen consumption was confirmed to be mitochondrial dependent as the addition of sodium azide, an electron transport chain inhibitor, significantly reduced the OCR in both cases. As a second measure of mitochondrial activity, we compared the viability of WT and *eaf1Δ* cells to treatment with a mitochondrial inhibitor. We anticipated that if *eaf1Δ* cells had increased functional mitochondria, they would be less sensitive to antimycin A, an inhibitor of the electron transport chain complex III. As expected, through dot assay analysis we found that both WT and *eaf1Δ* cells are able to survive antimycin A treatments in the presence of glucose (YPD) when cells do not require mitochondrial function to survive. However, when grown on a non-fermentable carbon source such as glycerol (YPG) mitochondrial function is essential and WT cells were hyper-sensitive to antimycin A treatment compared to *eaf1Δ* cells (Figure 2.4C). Together with the mitochondrial bioenergetics assays, this suggests that not only do *eaf1Δ* cells have more mitochondria but that the mitochondria are functional. Finally, as the elongated mitochondria seen in *eaf1Δ* cells could reflect excessive mitochondrial fusion, or alternatively increased biogenesis, we next performed biogenesis and fragmentation assays. We first assessed the mitochondrial fission response upon exposure to hydrogen peroxide. Similar to WT cells, the mitochondria of *eaf1Δ* cells were able to fragment under hydrogen peroxide stress, indicating that mitochondrial fission is intact in *eaf1Δ* cells (Figure 2.4D). We then tested the ability of the *eaf1Δ* cells to undergo mitochondriogenesis in the non-fermentable condition of ethanol, where the mitochondria are required for ATP production and cell growth [188]. Both WT and *eaf1Δ* cells increased mitochondrial content upon ethanol treatment to a similar extent suggesting mitochondrial biogenesis is intact in *eaf1Δ* cells (Figure 2.4D). Consistent with this observation we determined that the increased mitochondrial volume of *eaf1Δ* cells is not reversed upon deletion of *HAP4*, the activator member of the Hap complex important for mitochondrial biogenesis (S2.10 Fig) [189]. Together our work shows that *eaf1Δ* cells not only have increased mitochondrial volume and are more fused and elongated, but that their mitochondria are functional and can respond to environmental stresses.

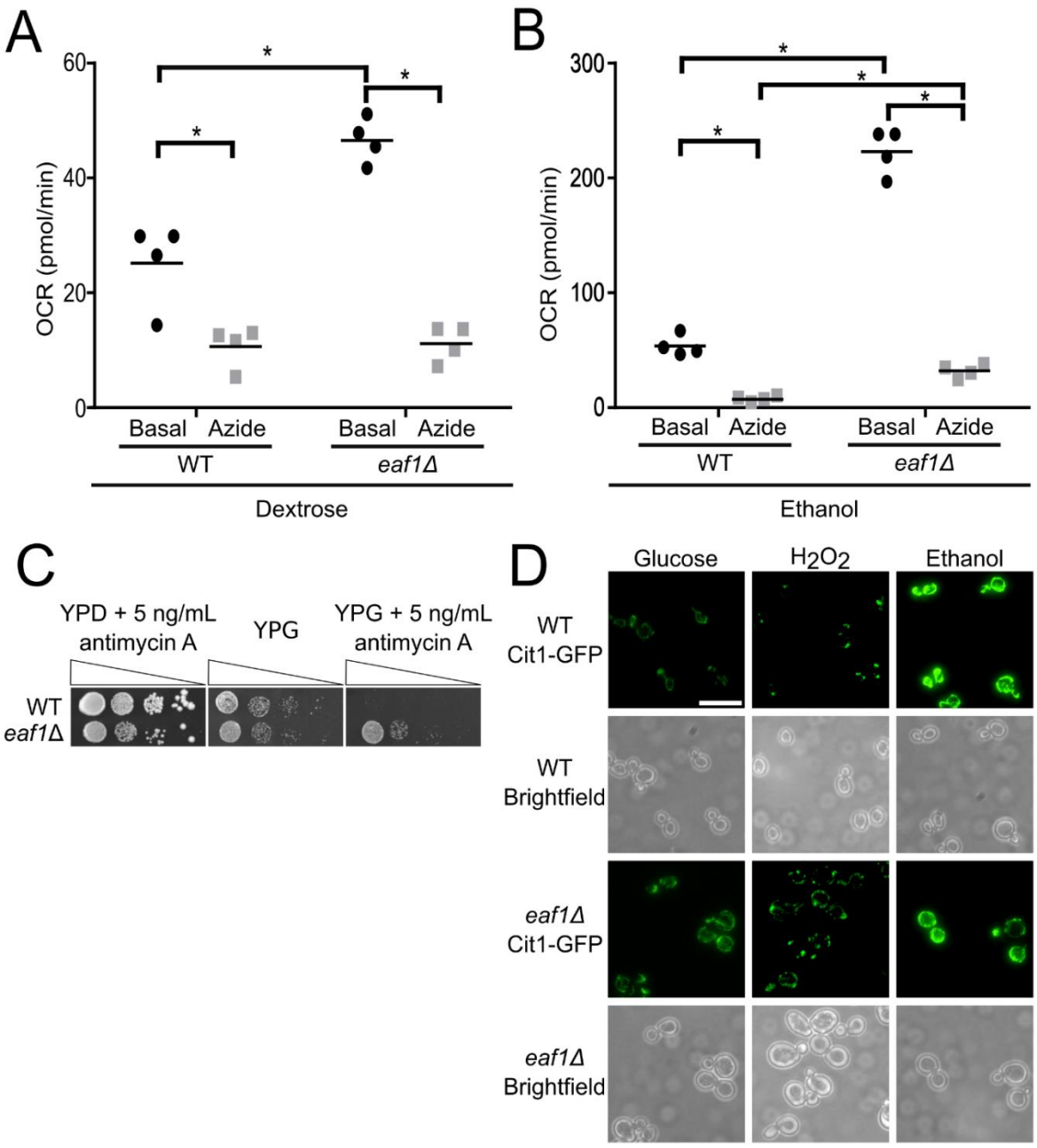

Figure 2.4. *eaf1Δ* mutants have functional mitochondria and are able to respond to biogenesis and fission signals. The oxygen consumption rate (OCR) of either WT or *eaf1Δ* cells was measured using the Seahorse Extracellular Flux Analyzer. After basal measurements, sodium azide was injected into the wells to shut off mitochondrial oxygen consumption and an additional set of measurements were taken. This was performed for (A) cells grown in dextrose media and (B) for cells grown in ethanol media for four biological replicates. ANOVA analysis was performed with a Tukey's multiple comparison test comparing pairs of means. *= $p < 0.05$. Horizontal bars in the data represents the mean. (C) WT and *eaf1Δ* cells were serially diluted onto YP plates containing glucose (YPD) or the nonfermentable glycerol (YPG) in the presence of the mitochondrial complex III inhibitor antimycin A. (D) Mitochondrial responsiveness to environmental stressors was assessed by growing WT and *eaf1Δ* cells in the presence of ethanol to assess biogenesis or H_2O_2 to assess stress induced fission. Scale bar = 10 μm.

Mitochondrial elongation in *eaf1Δ* cells can be partially reversed upon deletion of *BCY1*

We next sought to determine a mechanism by which NuA4 may regulate mitochondrial morphology and volume. We first focused our attention on the AMPK/Snf1 and PKA-Msn2/Msn4 axis as they have both been implicated in mitochondrial dynamics [161,190–193]. Snf1 is a key kinase in yeast metabolic signalling [123]. In response to stress or low availability of glucose, and therefore high AMP, Snf1 kinase is activated and phosphorylates transcription factors leading to the transcription of glucose repressed genes[123]. Snf1 has also been more directly associated with mitochondria by regulating fission, mitophagy, and mitochondrial biogenesis [60,122,194]. The transcription factors Msn2 and Msn4 are activators of glycolysis [172], and they have also been linked to autophagy and mitochondrial respiration [191,195]. Finally, PKA activity has been closely linked to the control of mitochondrial processes through multiple targets [196–202]. Therefore, we assessed the structure of the mitochondria using Cit1-GFP in WT and *eaf1Δ* backgrounds in combination with *snf1Δ*, *msn2msn4Δ*, and *bcy1Δ* (hyperactive PKA) (Figure 2.5). Though the morphology or mitochondrial fraction (mitochondrial volume divided by cellular volume) were not significantly changed in *snf1Δ* or *msn2Δmsn4Δ* cells, there was a slight increase in mitochondrial fraction in *bcy1Δ* cells, however the morphology of the mitochondria was similar to WT (Figure 2.5A). The elongated and branched structure and increased mitochondrial fraction in *eaf1Δ* cells was not impacted by the deletion of *SNF1* or *MSN2/4*. In contrast, mitochondrial structure in *bcy1Δ eaf1Δ* cells did not appear different from *bcy1Δ* cells (Figure 2.5A). Similarly, there was no significant increase in the mitochondrial fraction in *bcy1Δ eaf1Δ* cells compared to *bcy1Δ* cells (Figure 2.5B and S2.8 Fig.). Our work suggests that NuA4 regulates mitochondrial morphology and volume through a mechanism dependent on the regulatory subunit of PKA, Bcy1, which is independent of Msn2/Msn4.

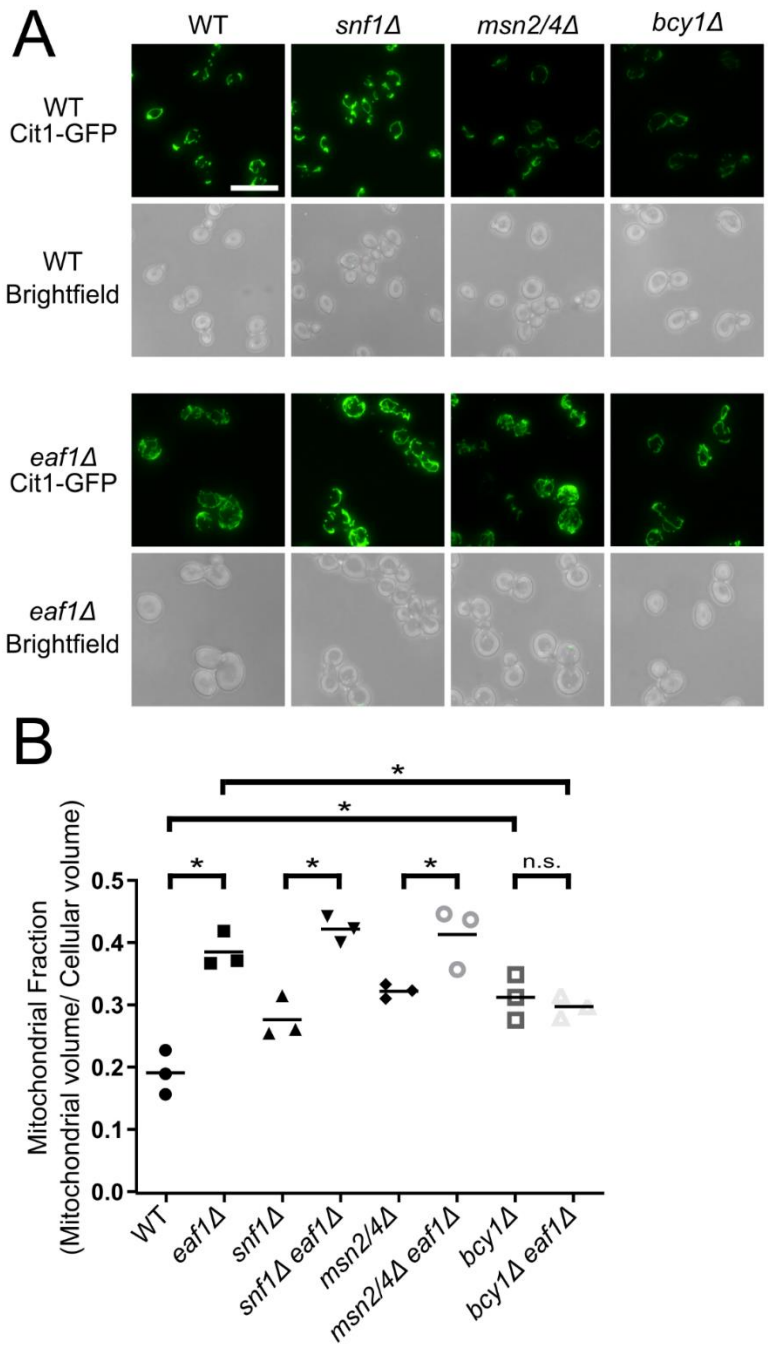

Figure 2.5. The increase in mitochondrial volume in an *eaf1Δ* is partially dependent on Bcy1. (A) Mitochondrial morphology was assessed in the indicated strains expressing the mitochondrial marker Cit1-GFP. Images are representative of three independent biological replicates. Scale bar = 10 μm. (B) The mitochondrial volume was quantified based on the Cit1-GFP fluorescence using the MitoMap plugin for ImageJ which was then divided by the average total cellular volume of the strain to give the Mitochondrial Fraction (Raw cellular and mitochondrial volume measurements can be found in S2.7 and S2.8 Figs). Images are representative of 3 independent biological replicates and at least 50 cells were quantitated per each biological replicate. ANOVA analysis was performed with a Tukey's multiple comparison test comparing pairs of means. *= $p<0.05$, n.s. = $p> 0.05$, select relevant significance bars shown. Horizontal bars in the data represent the mean.

Bcy1-GFP localization to the nucleus is dependent on NuA4

The glycogen synthesis and mitochondrial content phenotypes identified in the screen are partially, if not fully, dependent on Bcy1, the regulatory subunit of yeast PKA (catalytic subunits are Tpk1/2/3). Additionally, the deletion of *BCY1* appears to reverse the growth defect of an *eaf1Δ* (Figure 2.2B). Interestingly, Bcy1 was also one of the 23 hits from our phenomic screen. While our screen and other studies [163,168] have determined that Bcy1-GFP is enriched in the nucleus in log phase WT cells grown in glucose, upon the deletion of *EAF1* in the same conditions, Bcy1-GFP nuclear signal decreases with an increase in cytoplasmic localization (Figs 2.1B, 2.6A, and 2.6B). Fluorescent intensity profile plots of Bcy1-GFP signal across the whole cell centred on the nucleus indicate that within the population there is an accumulation of Bcy1-GFP in the nucleus of WT cells, however this signal is spread more evenly across *eaf1Δ* cells indicative of dispersion of Bcy1-GFP throughout the cell (Figure 2.6A). The proportion of cells with prominent nuclear localization of Bcy1-GFP was also quantified demonstrating that nuclear localization of Bcy1-GFP is reduced in an *eaf1Δ* (Figure 2.6B). While the localization of at least Tpk1 has been suggested to be associated with Bcy1 localization [163,168], we did not find any associated changes in the localization of Tpk1, 2, or 3 upon deletion of *EAF1* in our screen or in follow up analysis (S2.11 Fig).

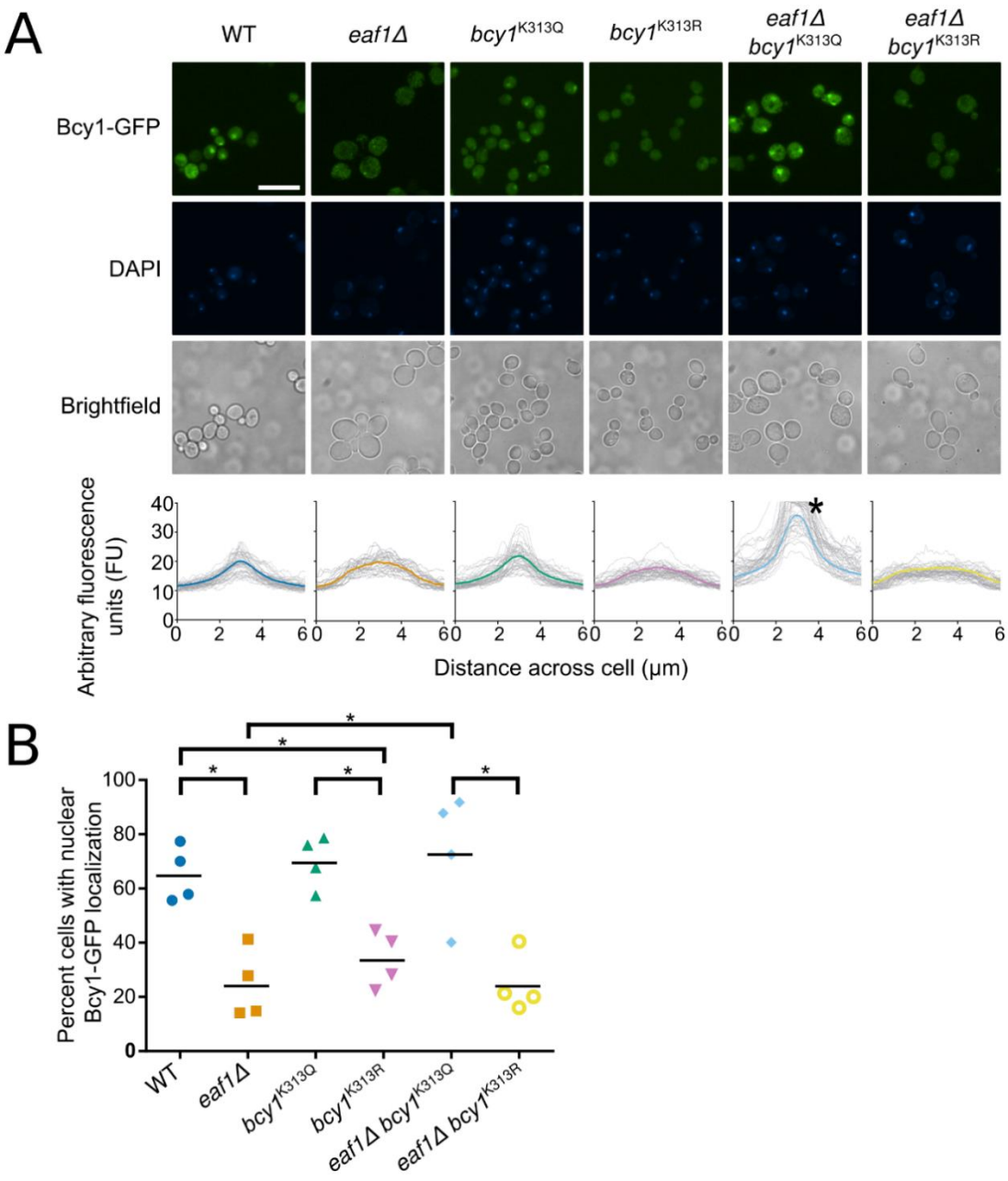

Figure 2.6. Bcy1 nuclear localization is dependent on NuA4 and the acetylation state of Bcy1-K313. (A) The localization of Bcy1-GFP, Bcy1^{K313Q}-GFP and Bcy1^{K313R}-GFP was assessed in WT and *eaf1Δ* yeast. Scale bar = 10 μm. Fluorescent intensity plots of Bcy1-GFP were derived by measuring the fluorescent intensity value of pixels across a nucleus-centered line using Plot Profile in ImageJ Software (Lower panel). The coloured line is the mean of three biological replicates for each strain, and profiles for 50 cells are shown in dotted lines. * For *eaf1Δ bcy1*^{K313Q} the y-axis has been cropped at 40 for comparison. The height of the peak corresponds with the pixel intensity maximum of the nucleus and therefore approximates the abundance of Bcy1-GFP in the nucleus. (B) The percentage of cells with nuclear localization of Bcy1-GFP was calculated for each strain indicated. A minimum of 50 cells were counted for each of the four biological replicates. ANOVA analysis was performed with a Tukey's multiple

comparison test comparing pairs of means. *= $p<0.05$, relevant significance bars shown. Horizontal bars in the data represent the mean.

Previous work has suggested that Bcy1 binding to the catalytic subunits of PKA may be regulated through NuA4-dependent acetylation of lysine K313 [52]. It has been proposed that the unacetylated form of Bcy1 can interact with and inhibit PKA subunits, Tpk1/2/3, but when Bcy1 is acetylated by NuA4 the Bcy1-TPK interaction is disrupted leading to activation of PKA. Our work suggests that NuA4 is also regulating Bcy1 localization. Hence, we sought to establish if the acetylation state of Bcy1-K313 affects its localization. We used CRISPR-Cas9 to create the $Bcy1^{K313Q}$-GFP and $Bcy1^{K313R}$-GFP mutations in the yeast genome to assess the impact of K313 lysine acetylation on the localization of Bcy1. The structure and electron distribution of arginine (R) is a good resemblance for a lysine residue in the unacetylated state while glutamine (Q) resembles the acetylated form of lysine [203]. We first assessed the nuclear localization of these mutations using DAPI stain as a marker for the nucleus and quantified cells with an enrichment of Bcy1-GFP in the nucleus. The nuclear enrichment is maintained in the $Bcy1^{K313Q}$-GFP acetylated mimic mutant but not in the $Bcy1^{K313R}$-GFP unacetylated mimic (Figure 2.6). This suggests that mislocalization of Bcy1-GFP in *eaf1Δ* cells is potentially due to a lack of acetylation on Bcy1-K313. If this hypothesis is correct, we would anticipate that $Bcy1^{K313Q}$-GFP expressed in *eaf1Δ* cells would restore localization to the nucleus. As expected, the $Bcy1^{K313Q}$-GFP expressed in *eaf1Δ* background is enriched in the nucleus while the non-acetylatable lysine mimic $Bcy1^{K313R}$-GFP expressed in *eaf1Δ* is dispersed across the cell (Figure 2.6A and 2.6B). Together our results suggest that the Eaf1-dependent localization of Bcy1 is regulated by the acetylation state of K313.

Bcy1-K313 mutation affects mitochondrial morphology and glycogen content

We next asked whether the Bcy1-K313 dependent change in localization of Bcy1 in *eaf1Δ* cells is contributing to either the increase in glycogen or mitochondrial content. We first assessed mitochondrial morphology and determined that there is slight but not significant increase in the mitochondrial fraction and mitochondrial elongation in both the *bcy1*^{K313R} and *bcy1*^{K313Q} mutants similar to that of *bcy1*Δ mitochondria (Figure 2.7A and 2.7B, and S2.8 Fig.). Further, both the *bcy1*^{K313Q} and *bcy1*^{K313R} could both slightly suppress the increase in the mitochondrial fraction and the mitochondrial elongation in *eaf1Δ* cells (Figure 2.7A and 2.7B, and S2.8 Fig.) a phenotype similar to the mitochondria of the *bcy1Δ eaf1Δ* (Figs 2.5 and 2.7). As mitochondrial morphology is not significantly different in *bcy1*^{K313R} and *bcy1*^{K313Q} mutants, it suggests that K313 is important for Bcy1 function and is not necessarily acetylation state specific. Therefore, there may also be an additional level of Bcy1 regulation by NuA4 outside of direct K313 acetylation.

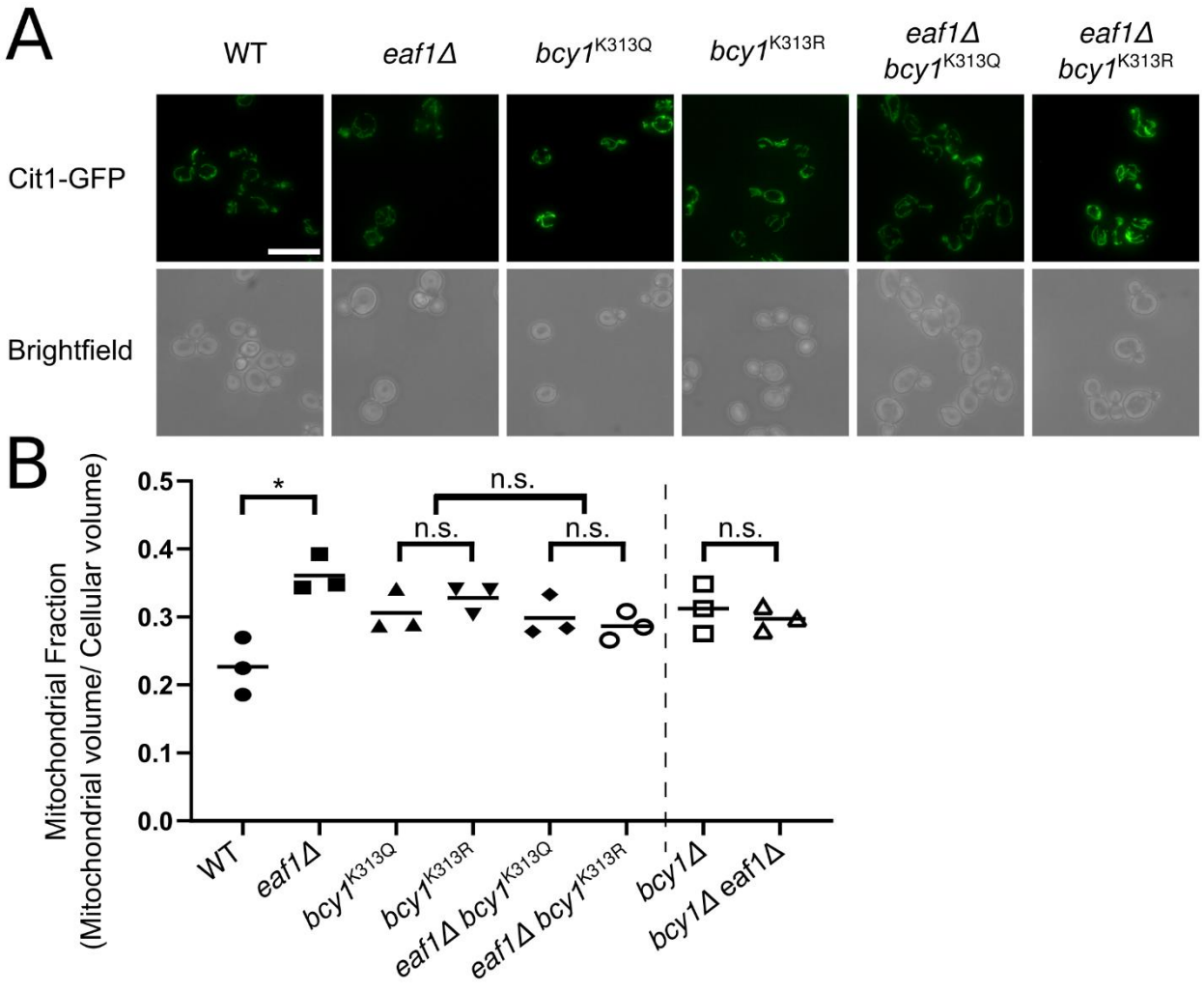

Figure 2.7. Assessment of mitochondrial volume in Bcy1-K313Q/R mutants. (A) The mitochondrial structure and volume were assessed in the indicated strains expressing the mitochondrial marker Cit1-GFP. Scale bar = 10 μm. (B) The mitochondrial volume was quantified based on the Cit1-GFP fluorescence using the MitoMap plugin for ImageJ which was then divided by the average total cellular volume of the strain to give the Mitochondrial Fraction (Raw cellular and mitochondrial volume measurements can be found in S2.7 and S2.8 Figs). Images are representative of 3 independent biological replicates and at least 50 cells per replicate were analyzed for quantification. This volume was compared to previously calculated *bcy1Δ* and *bcy1Δ eaf1Δ* mitochondrial volume measurements (x-axis break represents experiments previously shown in Figure 2.5). ANOVA analysis was performed with a Tukey's multiple comparison test comparing pairs of means. *= $p<0.05$, n.s. = $p>0.05$, relevant significance bars shown. Horizontal bars in the data represent the mean.

To assess the impact of the *bcy1* mutants on glycogen, we performed both iodine staining of cells and measured glucose released from the hydrolyzed cellular glycogen [185,204]. As expected, the *bcy1*^{K313R} cells displayed higher glycogen levels (darker iodine staining) than WT, *bcy1*^{K313Q}, and *bcy1Δ* cells, yet lower than the *eaf1Δ* cells (Figure 2.8A). However, *bcy1*^{K313Q} cells were also stained darker compared to WT cells, suggesting glycogen levels are increased in both mutants. This may be the result of the inability of a glutamine residue to perform all functionality of an acetylated lysine. The intermediate effects of the *bcy1* mutants were also seen in the suppression of glycogen accumulation in *eaf1Δ* cells. The *bcy1*^{K313Q} *eaf1*Δ appeared consistently slightly lighter in iodine staining that *bcy1*^{K313R} *eaf1*Δ, however the *bcy1*^{K313Q} mutant does not fully suppress glycogen accumulation in *eaf1*Δ cells (Figure 2.8A) [52]. Similar trends were detected by hydrolyzation of cellular glycogen. There was approximately a 15-fold increase in glucose released from *eaf1Δ* cells relative to WT cells (Figure 2.8B). This increase was suppressed by the deletion of *BCY1* in the *eaf1Δ* strain. Consistent with the iodine staining, the glucose released from all of the Bcy1-K313 mutants was closer to the WT cells than the *eaf1Δ* cells. However, while not significant there was a small increase in the glucose released by hydrolyzation in *bcy1*^{K313R} cells compared to the *bcy1*^{K313Q} cells and the *eaf1Δ bcy1*^{K313R} cells did show a significant increase in glucose release relative to the *eaf1Δ bcy1*^{K313Q} cells. This suggests that the accumulation of glycogen in *eaf1*Δ cells is only partially due to decreased acetylation on K313 and mislocalization of Bcy1. Together this suggests that while acetylation state of Bcy1-K313 may regulate its subcellular localization, the acetylation of this target site alone is not fully responsible for NuA4-dependent regulation of mitochondrial morphology or PKA-regulation of glycogen biosynthesis.

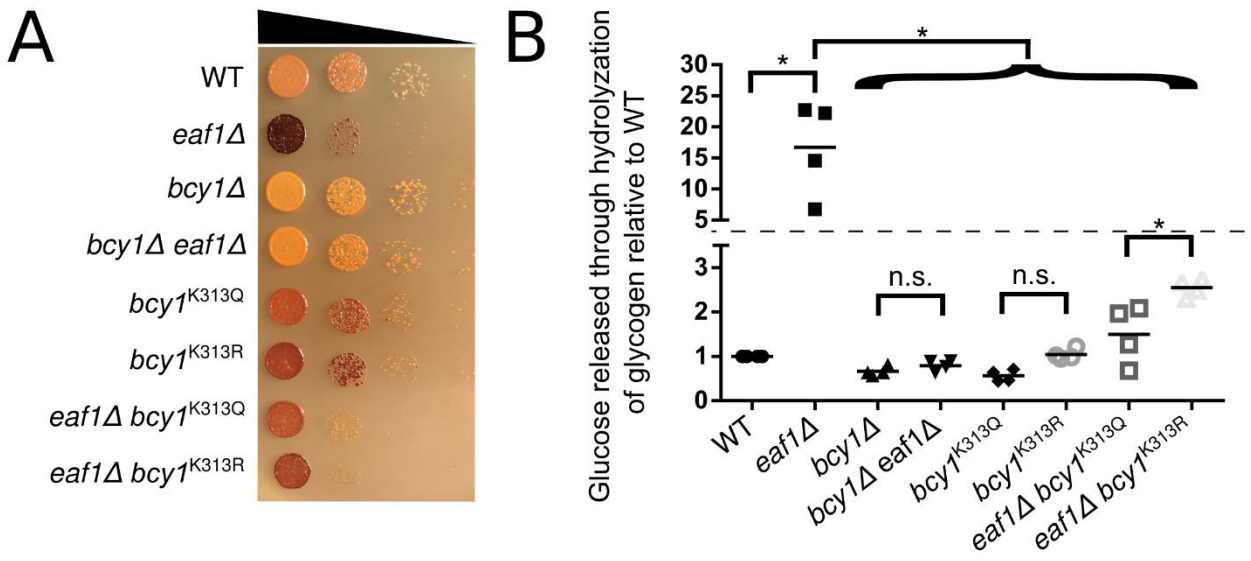

Figure 2.8. Bcy1-K313Q/R mutants partially suppress glycogen accumulation of *eaf1Δ* cells **(**A) Cellular glycogen levels was assessed using iodine staining. The indicated strains were serially diluted on to YPD plates, grown at 30°C for 24 hours prior to exposure to iodine crystals. Darker staining represents more glycogen within the cell. Image is representative of three independent dot assays. (B) Cellular glycogen content was assessed by measuring glucose released from hydrolyzation of glycogen. Cellular glycogen was extracted and treated with amyloglucosidase to break down glycogen into glucose. Glucose was then measured directly using the Glucose Colorimetric/Fluorometric assay kit (Biovision, K606). The amount of glucose released through the hydrolyzation of glycogen in each replicate was normalized to that of the WT strain. The Y-axis is broken (horizontal dotted line) in order to best show the data. ANOVA analysis was performed with a Tukey's multiple comparison test comparing pairs of means. *= $p<0.05$, n.s. = $p>0.05$, relevant significance bars shown. Horizontal bars in the data represents the mean.

PKA phosphorylation substrates are impacted by deletion of *EAF1*

Though mutations that mimic the acetylated and un-acetylated state of Bcy1-K313 impact its interaction with Tpk1/2/3 [52] and its subcellular distribution (Figure 2.6), our work suggests NuA4-regulation of PKA activity maybe more complex then simply acting as an on or off switch through Bcy1 acetylation. Therefore, we next asked if deletion of *EAF1* affects global PKA activity or if only a subset of PKA substrates are impacted. Overall activity of the yeast PKA catalytic subunits (Tpks) was assessed by blotting whole cell extracts from WT and *eaf1Δ* cells with a Phospho-PKA Substrate (RRXS*/T*) antibody, which is commonly used to assess PKA activity [205–207]. Interestingly, in glucose-rich conditions there was no significant difference in total phosphorylation between WT and *eaf1Δ* cells, but there are reproducible distinct changes in substrates detected by the anti-phospho-PKA antibody (Figure 2.9A).

One protein at approximately 100 kDa reproducibly appeared as an increased phosphorylation target in the *eaf1Δ* strains while a protein at 25 kDa appeared to have slightly reduced phosphorylation (Figure 2.9A). As PKA activity is affected by glucose abundance, we also assessed phosphorylation of PKA targets in the WT and *eaf1Δ* cells after 1 hour of glucose starvation. Under glucose starvation the *eaf1Δ* cells had approximately a 30% reduction in total phosphorylation compared to WT cells, including complete loss of some phospho-PKA substrates (Figure 2.9B). These results suggest that NuA4 is not simply turning on or off PKA activity but is playing a potential role in regulating PKA substrates.

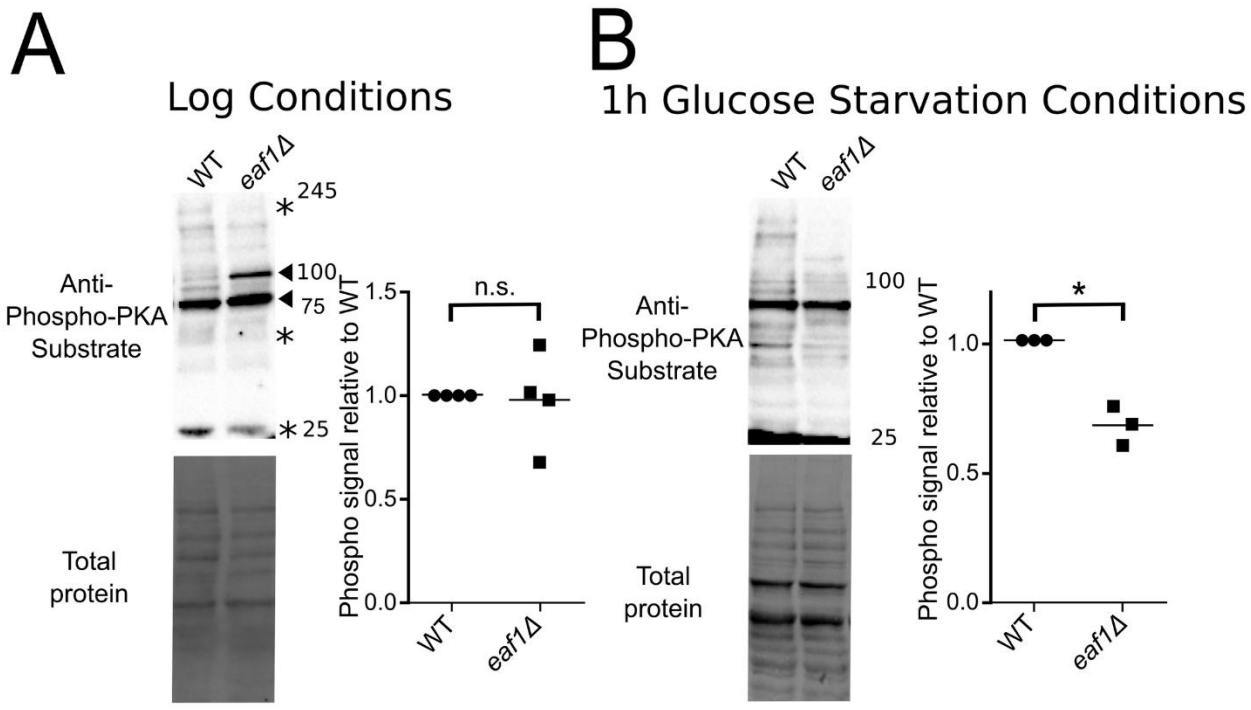

Figure 2.9. PKA activity is altered in an *eaf1Δ.* (A) PKA substrate phosphorylation under glucose rich conditions was assessed by quantitative western blot analysis using whole cell extracts from WT and *eaf1Δ* strains. Panel to the left is a representative of a total phosphorylation and a total protein blot (Stars highlight bands that decreased, and arrows highlight bands that increase in *eaf1Δ* extracts); panel to the right is the quantification of western blots for four independent biological replicates where the total phosphorylation signal intensity was normalized to total protein. (B) PKA substrate phosphorylation under glucose starvation conditions was assessed by quantitative western blot analysis using whole cell extracts from WT and *eaf1Δ* strains that were starved for glucose for 1 hour. Panel to the left is a representative total phosphorylation and total protein blot; panel to the right is the quantification of western blots for three independent biological replicates where the total phosphorylation signal intensity was normalized to total protein.

2.5 Discussion

We found that 23 metabolic proteins change localization and/or abundance upon disruption of the NuA4 complex (Figure 2.1 and S2.3 Fig.). Remarkably, we determined that the majority of the detected changes, including induction of the glycogen biosynthesis pathway and mitochondrial elongation, were at least partially dependent on NuA4-target Bcy1 (Figs 2.2 and 2.5). Given the well-established role of Bcy1 in regulating the PKA catalytic subunits (Tpk1/2/3), this suggests that many of the cellular impacts of NuA4 on metabolism are likely mediated through regulation of PKA.

How is NuA4 impacting PKA activity? Contrary to many other metabolic enzymes where acetylation is acting as an "on" or "off" switch, our work suggests that NuA4-dependent regulation of PKA is more subtle. Our work suggest a model that in the absence of *EAF1* or NuA4 activity, acetylation of Bcy1-K313 is decreased allowing for Bcy1 to translocate to the cytoplasm altering the inhibition of some or all of the yeast PKA enzymes, Tpk1/2/3 (Figure 2.10). Indeed, upon deletion of *EAF1*, under glucose rich and replete conditions, we demonstrated that substrates detected by the phospho-PKA substrate antibody are not simply globally decreased, but rather altered.

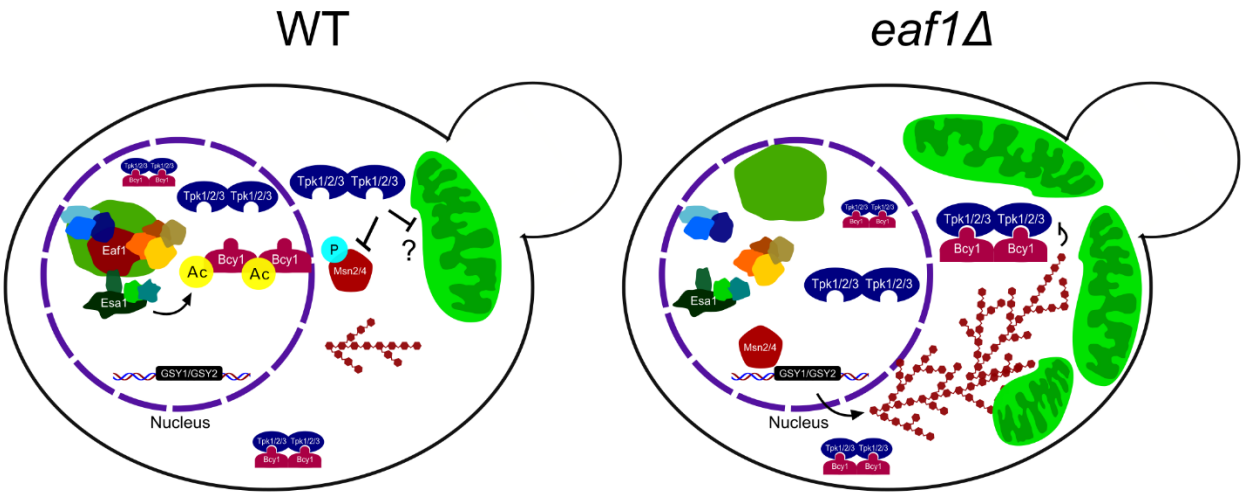

Figure 2.10. Model for regulation of mitochondrial morphology and glycogen synthesis by NuA4. We propose that NuA4 regulates Bcy1 acetylation and subcellular distribution leading to a change in Tpk activity downstream, thereby affecting regulation of mitochondrial volume and glycogen synthesis gene transcription.

NuA4 regulation of glycogen synthesis

Our screen determined that glycogen synthesis pathway proteins are increased in *eaf1Δ cells*, leading to increased glycogen content (Figs 2.2B and 2.8). The small differences between the glycogen content results of the iodine staining and hydrolyzation by amyloglucosidase may be accounted for by difference in the chemistry of these methods [204]. Iodine binds to endogenous glycogen to produce the red/brown colour in the cell while glycogen must be extracted for hydrolyzation then glycogen is indirectly measured through the amount of glucose released [204]. Each have limitations, but together they strongly support that *eaf1Δ* cells have significantly more glycogen than WT. This fits well with the literature demonstrating that *GSY1*, *GSY2*, and *GDB1* are established transcriptional targets of Msn2/Msn4 [172,180,181] and that other Msn2/Msn4-dependent genes are derepressed in NuA4 mutants [79,208]. As the deletion of *EAF1* results in the reduction of nuclear Bcy1-GFP, enriched nuclear Msn2-GFP, and an induction of Gsy2-GFP, a simple explanation is that NuA4 is regulating PKA activity simply through regulation of Bcy1 localization. However, this is not the case as *bcy1*^{K313R} cells do not accumulate glycogen to similar levels of *eaf1Δ* cells (Figure 2.8), despite the fact that Bcy1^{K313R}-GFP has a similar decrease in nuclear enrichment as Bcy1-GFP in *eaf1Δ* cells (Figure 2.6). Even more surprisingly, although the *eaf1Δ bcy1*^{K313R} cells have more glycogen than the *eaf1Δ bcy1*^{K313Q} cells, both have far less glycogen accumulation than the *eaf1Δ* alone. This suggests that NuA4 may also regulate the PKA-Msn2/Msn4 axis through additional mechanisms outside of Bcy1-K313 acetylation.

NuA4 regulation of mitochondrial morphology

How is deletion of *EAF1* resulting in elongation of the mitochondria? A simple explanation could have been that NuA4 regulates transcription of genes required for mitochondrial biogenesis and fusion. However, we determined that Eaf1-dependent mitochondrial changes are not mediated by Msn2/4 (Figure 2.5) or Hap4 (S2.10 Fig). Indeed, transcriptome studies do not indicate any up-regulation of genes

involved in mitochondrial biogenesis, fusion, or fission upon deletion of *EAF1* [67], suggesting NuA4's impact on mitochondrial morphology is not due to transcriptional defects.

We found that the mitochondrial defects in *eaf1*Δ cells can be partially rescued by deletion of *BCY1* (Figure 2.5), which suggests that altered PKA activity in NuA4 mutants contributes to mitochondrial elongation. However, deletion of *BCY1* or mutation of Bcy1-K313 to either R or Q resulted in increases in the mitochondrial fraction per cell, albeit not as high as seen in *eaf1Δ* cells (Figs 2.5 and 2.7). This suggests that both K313 mutants have compromised Bcy1 function that results in increased mitochondrial function.

At first, this seems counter intuitive. How could *bcy1*Δ cells with increased PKA activity and *eaf1Δ* cells that we show have altered PKA activity and many hallmarks of decreased PKA activity, both lead to increased mitochondrial content? Our work suggests that NuA4 and acetylation of Bcy1 is not simply acting as an on or off switch for PKA activity. Rather, we show that under glucose rich conditions, deletion of *EAF1*, and presumably the collapse of NuA4, alters the PKA-substrate profile, with some phospho-PKA substrates increasing while others decreasing (Figure 2.9). Though one can not rule out the possibility that deletion of *EAF1* is impacting the protein levels of PKA substrates, indeed our high content screen does detect changes in protein levels (Figure 2.1 and S2.2 Fig), overall the impact of *EAF1* on global transcription is minor [67]. Future studies will be needed to identify the extent by which NuA4 impacts PKA activity and substrate selection, including through acetylation of Bcy1 or other mechanisms.

Interestingly, PKA has been extensively linked to various aspects of mitochondrial regulation, including biogenesis and disassembly. PKA activity has been generally demonstrated to promote mitochondrial fusion and function, explaining why the deletion of *BCY1* alone may result in slightly more mitochondria than in WT cells [164]. Studies have shown that PKA phosphorylates Drp1, a key mitochondrial fission protein, inhibiting its function and promoting fusion [209,210]. Similarly, PKA phosphorylates MIC60 reducing PINK1 presence at the mitochondria, preventing mitochondrial degradation [211]. Additionally, deleting *BCY1* and high cAMP conditions, both of which should increase PKA activity, each led to an

increase in mitochondrial content in yeast, while deletion of *TPK3* (one of the yeast PKA catalytic subunits) was associated with a decrease in cytochrome C content [161,212]. Outside of overall mitochondrial structure and content regulation PKA also directly phosphorylates members of the electron transport chain as well as translocase of the outer membrane (TOM) proteins responsible for mitochondrial protein import [199–201]. Finally, PKA activity has been associated with mitochondriogenesis through phosphorylation and activation of CREB leading to transcription of PGC1α, a key cotranslational activator of mitochondriogenesis [167,213].

Given this research, it is clear that NuA4 is regulating mitochondrial elongation through PKA, but the mechanism(s) remain to be established. There are complex nuances associated with PKA signalling, and perhaps it is not as cut and dry as increased versus decreased PKA activity affecting mitochondrial regulation. For example, PKA dependent phosphorylation of two different apoptotic proteins Bad and Bim has opposite functions, preventing and promoting apoptosis respectively [214–216]. While we did not see large scale changes in the localization of any of the Tpk subunits in an *eaf1Δ* when compared to WT (S2.11 Fig), we cannot rule out that NuA4 is modulating distinct pools of PKA (e.g., Tpk1 vs Tpk2, or different compartmentalized groups) that have different effects on mitochondrial biology. Indeed, due to functional redundancies, the biological roles of individual PKA subunits in yeast have yet to be discerned in detail.

NuA4 dependent regulation of Bcy1 subcellular localization

Previous high throughput protein-fragment complementation assay (PCA) studies identified a role for NuA4 in regulating PKA [52]. In particular, this study determined that upon deletion of *EAF1* or *EAF7* the Tpk1-Bcy1 (PKA1) interaction is increased under both glucose and galactose conditions, however Tpk2-Bcy1 (PKA2) was not impacted, supporting the idea that NuA4 may differentially regulate the individual PKA subunits. Further, through PCA-based assay in mammalian cells they showed that

increasing acetylation through either overexpression of KATs or inhibition of KDACs results in a reduction of PKA type II interactions. Though not directly tested, it was proposed that acetylation of Bcy1-K313 reduced its interaction with Tpk1, hence relieving inhibition of PKA. While this may be the case, our work shows that Eaf1 (and presumably NuA4) and acetylation are regulating the subcellular localization of Bcy1. Bcy1-GFP is predominantly nuclear in glucose grown cells [163] while in the absence of *EAF1*, Bcy1-GFP is present in both nuclear and cytoplasmic compartments (Figs 2.1 and 2.6). Further, $Bcy1^{K313R}$-GFP, which mimics the unacetylated state, displays a similar disperse cellular signal as seen for Bcy1-GFP in *eaf1Δ* cells, and the $Bcy1^{K313Q}$ -GFP mutant maintains a nuclear localization even when *EAF1* is deleted (Figure 2.6).

The subcellular localization of Bcy1 is extremely important as the compartmentalization of PKA components plays a role in regulating its activity [169]. For example, in the mammalian system, specific A-Kinase anchor proteins (AKAPs) have evolved to localize PKA to different areas of the cell [169,217]. While mammalian AKAP homologs have not been identified in yeast, the localization of yeast PKA members is dependent on carbon source availability and environmental stresses and many interacting proteins have been identified [163,169,218]. In glucose, Bcy1 is predominantly nuclear [163,169], however upon glucose starvation or when grown in non-fermentable Ethanol or Glycerol media, Bcy1 has a nucleo-cytoplasmic distribution [163,169]. In contrast, each TPK subunit has distinct subcellular distribution, while Tpk2 is predominantly nuclear, Tpk1 and Tpk3 are evenly distributed between nucleus and cytoplasm under logarithmic growth in glucose. Interestingly, when cells enter stationary phase, while Tpk1 and Bcy1 are distributed across the cytoplasm and nucleus, Tpk2 and Tpk3 are enriched in P-bodies that are largely devoid of Bcy1 [169]. In the absence of nuclear localized Bcy1, others have shown that nuclear Tpk1 is also reduced, suggesting Bcy1 may not only regulate PKA activity but sequester PKA catalytic subunits to specific locations [163]. Interestingly, while we determined that upon deletion of *EAF1*, Bcy1-GFP nuclear localization is reduced (Figs 2.1 and 2.6), we did not see a change in Tpk1-GFP subcellular distribution (S2.11 Fig). The fact that Tpk1 localization is not dramatically altered in an *eaf1Δ* cell suggests that

enough Bcy1 remains in the nucleus to maintain pools of Tpk1 in the nucleus. Alternatively, while our screen and direct analysis did not detect any dramatic changes in the localization or abundance of the Tpks, we cannot rule out if subtle changes in Tpk1, Tpk2, and Tpk3 subcellular localization are regulated by NuA4 through Bcy1-K313 acetylation or other means. Further exploration will require detailed temporal and spatial analysis of subcellular localization and activity of individual PKA subunits upon modulation of NuA4 activity.

As the disperse localization of Bcy1-GFP in *eaf1Δ* cells grown in glucose conditions (Figure 2.6) looks similar to localization of Bcy1-GFP upon glucose deprivation [163,168], one simple explanation is that *eaf1Δ* cells are defective for glucose sensing resulting in the mislocalization of Bcy1-GFP indirectly. However, our work suggests that subcellular localization is dependent on the acetylation state of Bcy1-K313 (Figure 2.6), which suggests NuA4 is directly regulating Bcy1 localization through acetylation. Presently it is not known if NuA4 activity changes upon starvation or glucose deprivation, however NuA4 is implicated in regulating stress granule formation upon glucose deprivation [173] and glucose-starvation apoptosis in cancer cells [88]. Therefore, it will be interesting to determine if the acetylation state of Bcy1 changes upon glucose deprivation and if so, if this is dependent on NuA4.

Regulation of Bcy1 localization by post-translational modification is not new. The Yak1-dependent phosphorylation of the N-terminal domain of Bcy1 drives its localization to the cytoplasm where it is retained by Zds1 [163,168]. Interestingly the Bcy1-K313 site is not within the established N-terminal clusters required for interaction with Zds1 and cytoplasmic localization of Bcy1. This suggest that other proteins may be interacting with the acetylated or unacetylated versions of Bcy1 aiding in changing its subcellular distributions. Though we or others have yet to establish if acetylation of Bcy1 is also impacting the physical interaction with TPKs, what is clear is that deleting *EAF1* decreases Bcy1 nuclear localization and results in phenotypes that suggest PKA activity is decreased, including increased glycogen production, Msn2 relocalization to the nucleus, and mitochondriogenesis (Figs 2.1, 2.2, and 2.7). However, localization of Bcy1 is clearly not the only contributor of NuA4-dependent regulation of

PKA activity, as *bcy1*^{K313R} and *bcy1*^{K313Q} mutants, despite having strong separation of Bcy1 localization (Figure 2.6), have similar impacts on mitochondria morphology and only small differential impacts on glycogen accumulation (Figs 2.7 and 2.8). One possibility that should be considered is that while K to R and K to Q are used as mimics for acetylation states *in vivo*, these are in fact not ideal. For example, NuA4 has been shown to regulate the oxysterol binding protein Kes1 *in vivo*, but the Kes1 acetylated and unacetylated mimics proteins do not fully replicate Kes1 acetylated and unacetylated proteins *in vitro* biochemical assays [134]. The limitation of these acetylation state mimics may explain why the *bcy1*^{K313R} and *bcy1*^{K313Q} mutants appear to act similarly to each other in some cases. However, their additional similarity to *bcy1*Δ and differences from WT and *eaf1Δ* in terms of mitochondrial morphology and glycogen content does support an important function of the K3l3 position of Bcy1, although how NuA4 dependent acetylation of this residue is involved awaits further study.

2.6 Conclusions

Our results clearly demonstrate that NuA4 is regulating the localization of a master regulator of cellular metabolism, Bcy1, the regulatory subunit PKA. Additionally, both the increased glycogen synthesis proteins and mitochondrial elongation of *eaf1*Δ cells identified in our screen are dependent on Bcy1, and PKA activity is altered upon deletion of *EAF1*, supporting our proposed PKA regulation. Finally, our screen suggests that NuA4 may be regulating multiple metabolic pathways through the localization of proteins. Taken together, our work indicates that human homolog of NuA4, Tip60, may play a key role in controlling cellular metabolism, perhaps explaining how aberrant Tip60 function may be important in the development of human disease.

2.7 Materials and Methods

Strains and culturing conditions

The BY4741 (S288C) strain was used throughout this work. A list of yeast strains used in this study can be found in S2.3 Table. The GFP collection was used for the phenomic screening [42]. Additional GFP-tag and deletion mutants were taken from the GFP collection [42] or deletion mutant array (DMA) (GE, CAT# YSC1053) or were made by PCR-mediated insertion/deletion [219]. All strains listed (S2.3 Table) were confirmed by PCR. Yeast were cultured at 30^{o}C in YPD, unless otherwise specified. Yeast cultures were grown by shaking in YPD (1% yeast extract, 2% peptone, 2% dextrose) at 30^{o}C unless otherwise stated. In preparation for experiments, yeast were grown overnight in YPD before being diluted to an OD600 of 0.1 (or 0.15 for *eaf1Δ*) in the morning and grown to mid log (OD600 = 0.5-0.8).

High content screen

A focused mini array of 407 metabolic-associated GFP-tagged genes were extracted from the GFP library (*MATa* ORF-GFP::HIS) [42]. The genes were selected based on literature review and the Saccharomyces Genome Database (SGD) (List of Genes in S2.1 Table) and fell into categories relating to metabolic processes, gluconeogenesis, changes in regulation dependent on glucose, glucose import, cAMP, and AMPK. Using synthetic genetic array technology [175] and the Singer HTP robotic platform, the GFP fusion metabolic strain mini array was mated to a WT (*ura3Δ:*:NAT) or *eaf1Δ* (*eaf1Δ*::NAT) query strains to create both WT and *eaf1*Δ GFP fusion arrays as previously described [41].

Strains generated for the focused high throughput microscopy screen were grown overnight and diluted to 0.1 in the morning. Once they had reached log-phase (OD600 =0.4-0.7), the cells were collected and diluted in SC media before being plated onto concavalin A-treated 96-well imaging plates. Plated cells were centrifuged and washed twice with SC media. Fluorescent images were taken using a CellVoyager CV1000 disk confocal microscope (Yokogawa Electric Corporation, Musashino Tokyo,

Japan). All images were initially captured at a 300 ms exposure for the GFP channel, 30 z-stacked images were taken using the GFP signal with 30 corresponding brightfield images. Two fields of view with at least 35 cells each were captured for each strain (most fields had in the range of 75-200 cells). Images were manually compared for differences in GFP signal between the WT and *eaf1Δ* backgrounds of each GFP-tagged protein by three independent researchers. Each WT- *eaf1Δ* pair was assessed for changes in where the GFP signal was localized and for obvious abundance differences based on GFP intensity in the cell. Additionally, the overall intensity of the WT and *eaf1Δ* images were compared using an in house macro-based batch analysis in ImageJ comparing mean grey value per cell. Two fields of view were analyzed for each strain. Cells were highlighted as regions of interest (ROIs) using the brightfield image to define the cell limits and those ROIs were used to measure the GFP signal intensity per cell. The mean grey value per cell was measured as it removed issues with differences in cell size between the WT and *eaf1Δ* strains. The mean grey value of the measured cells was then averaged for each image and the average mean cell intensity of the *eaf1Δ* image was divided by the average mean cell intensity of a paired WT image. This gave a measurement of the change in the intensity of the GFP signal of each protein in an *eaf1Δ* cell relative to WT cell. Changes in intensity were ranked and primary hits were selected as strains having a greater than 1.3-fold increase or 0.7-fold decrease in intensity in the *eaf1Δ* relative to WT. The top 70 ranked images from the manual analysis were also reanalyzed a second time using the same batch analysis comparison of the mean GFP intensity per cell. If changes were detected through the manual scoring or the intensity measurements, they were reconfirmed in another round of microscopy, and top consistent changes were selected resulting in the confirmed set. Localization of the proteins and their associated changes were categorized based on the well characterized WT localization of GFP-tagged proteins in the CYCLoPs database and literature review [41,220].

Microscopy

All additional microscopy was done using a Leica fluorescent microscope (DMI6000; Leica Microsystems) equipped with a high-performance camera (Hamamatsu), DG4 light source (Sutter Instruments) and Volocity 4.3.2 software (PerkinElmer). Strains were grown to mid log, spun down to collect live cell pellet and resuspended in SC media containing glucose for live GFP and brightfield imaging. As indicated, cells were stained with DAPI (Sigma) prior to spinning down culture. DAPI was added to the liquid culture at a concentration of 1 μg/mL plus 0.1% Triton X-100 (CSH protocols).

Mitochondrial volume was assessed using the MitoMap plugin for ImageJ [186]. Images were corrected to scale dimensions using SetScale. Individual cells were selected and analyzed with the MitoMap plugin [186]. This plugin identifies pixels highlighted with the Cit1-GFP signal and quantifies the volume and surface area of the input mitochondria, for our analysis volume was used. For all quantifications, a minimum of 50 cells were analyzed per replicate.

To test mitochondrial response to ethanol, yeast were grown overnight, diluted to OD600 of 0.1 in Yeast Peptone media supplemented with 3% ethanol, a non-fermentable carbon source, and grown to mid log phase before imaging by microscopy. For the fragmentation assay, Hydrogen peroxide was added to mid log day cultures at a final concentration of 4 μM and the cultures were returned to the incubator for 30 minutes before analysis by fluorescent microscopy as described above.

Bcy1-GFP fluorescence was first quantified manually by percent cells with prominent nuclear localization. Additionally, a profile of Bcy1-GFP intensity was measured using ImageJ Software and compressed z-stack images [221]. A 60 unit (6.23 μm) long line was placed across the nucleus of the cell (centred on the nucleus), and Plot Profile analysis was performed to give the fluorescent intensity value of pixels along the line. This was repeated for three biological replicates of 25 cells for each sample. The mean of all replicates was plotted on a representative graph for sample comparison.

Serial dilution spot assays

Cultures were grown to mid log in YPD before being diluted to an OD600 of 0.1 and three 10-fold serial dilutions (0.01, 0.001, 0.0001). 5 μL of the serial dilutions were spotted onto the indicated plates. To make drug plates, a stock solution of antimycin A (Sigma) was created in 95% Ethanol and was used to create final plates with a concentration of 5 ng/mL. Iodine staining was performed after dot assay growth as described below.

Glycogen Assays

For analysis by iodine staining, spot assays were prepared as above and iodine glycogen assays were performed as previously described [222]. After 24 hours of growth on plain YPD, plates were inverted over iodine crystals for 3-5 minutes, exposing the yeast to the vapours and causing them to stain relative to the abundance of glycogen.

Quantitative measurements of glycogen were assessed by extracting glycogen from cells and treating extracts with amyloglucosidase. This enzyme breaks down glycogen into glucose which can then be measured directly. Cultures of yeast were grown in 100 mL to mid log and a volume of yeast equivalent to 25 ODs was spun down to collect a yeast pellet. Pellets were washed twice in water prior to being flash frozen in liquid nitrogen and stored at -80^{o}C. Pellets were thawed in 500 uL of 0.25 M Na_2CO_3, vortexed, and boiled at 95oC for 4h. Glycogen (Sigma) was used as a control. The pH of the samples was adjusted by adding 300ul of 1M acetic acid and 1200 ul 0.2M NaOAc pH 5.2. Half of the sample was kept as the no enzyme control and to the other half 20 ul of 20mg/ml amyloglucosidase (Sigma, 10115, 70U/mg protein) was added prior to an overnight incubation at 57^{o}C overnight.
The digested samples were centrifuged, and supernatants were collected. The glucose released by digestion in each sample was diluted and analyzed using the Glucose Colorimetric/Fluorometric assay kit (Biovision, K606) according to the manufacturer's protocol.

Growth curve analysis

Cultures were grown to mid log in YPD before being diluted to an OD600 of 0.1 in YPD. 200uL of this dilution was plated into a BioScreen C honeycomb plate. The plate was incubated at 30^{o}c for 48h in a BioScreen C plate reader which collected OD600 readings every 15 minutes. Growth curve data was averaged for 3 technical replicates then 3 biological replicates and plotted for the first 24 hours. The doubling time for each strain was calculated based on the slope of the log (OD600) curve during log growth of the strain (between 3 and 7.5 hours). Doubling time = Δt*Log (2)/ (Log (OD600@t2/OD600@t1)).

Quantitative Western blot

Yeast strains were grown overnight in YPD and diluted into 50 mL cultures in the morning to an OD600 of 0.1. Cells were harvested at mid log and whole cell extracts were collected as previously described [79]. Briefly, cells were collected by centrifugation and pellets were flash frozen in liquid nitrogen and stored at -80^{o}C. The cell pellets were thawed in 3x the pellet volume of lysis buffer (20 mM HEPES, pH 7.4, 0.1% Tween 20, 2 mM $MgCl_2$, 300 mM NaCl, protease inhibitor cocktail [P-8215; Sigma]) and lysed using bead beating 6 times for 1 minute with an equal volume of glass beads (Fisher 35-5350). Whole cell extracts were collected by centrifugation and quantified using a Bradford assay. In the case of glucose starvation, cultures were grown to mid log, spun down and washed 2x in YP (glucose free) media and resuspended in YP for 1 hour of growth at 30^{o}C before collecting pellets and freezing as above.

A standard curve for each protein was performed to determine the optimal amount of protein to be loaded on TGX quantitative gels for western blot [223]. For Gsy2-GFP, 40 µg of protein was found to be optimal, so this was loaded onto TGX gels, run, and a standard western blot protocol for TGX gels was followed. Following electrophoresis, the gel was activated and visualized by UV before being transferred onto nitrocellulose (Bio-Rad 1620112). Total protein was imaged using UV. For GFP blots, the blots were blocked in 5% skim milk in PBS-T (phosphate buffered saline + 1% Tween 20) before incubation

overnight with a 1: 500 dilution of anti-GFP primary antibody (Sigma-Aldrich 11874460000) in 5% milk PBS-T. Next blots were washed 3X in PBS-T, incubated for 1h with goat-anti-mouse secondary antibody (BioRad; cat. # 170–6516) at 1: 2500 in 5% milk PBS-T and washed 3 times. A similar procedure was followed for the PKA assay but blocking and antibodies were done in 3% Bovine Serum Albumin (BSA Sigma-Aldrich A7906). For PKA activity 80 µg of protein was run and the Phospho-PKA Substrate (RRXS*/T*) (Cell Signaling 100G7E) primary was used followed by a goat-anti-rabbit secondary antibody (BioRad; cat. # 170-6515). Finally, blots were incubated with Clarity Western ECL substrate (Bio-Rad 170-5061) and imaged using the Bio-Rad ChemiDoc imaging system. Relative protein abundance of our proteins of interest was quantified using the Image Lab software (Bio-Rad) and each band was normalized to the total protein signal of the lane then calculated relative to the WT signal of the protein.

qPCR

Yeast were prepared in YPD, and 30 mL of OD600 = 0.5 cells were pelleted and washed with water before flash freezing in liquid nitrogen. Cell pellets were thawed in an equal volume of lyticase reaction solution (1.2 M sorbitol + 1 mg/mL lyticase (Sigma)) then incubated at 30^{o}C for 30 min. Cell lysis and RNA purification were then performed using the Ambion PureLink RNA Mini Kit according to manufacturer's instructions. Briefly, cells were lysed by vortexing in lysis buffer with 2-mercaptoethanol and extracts collected following centrifugation. Ethanol was added to disrupt enzymatic function and RNA was purified and collected using a spin cartridge. RNA extracts were then treated with DNase I for 1 h at 37oC before performing a phenol/chloroform/isoamyl extraction and measuring RNA concentration by nanodrop. At this point the quality of the RNA was assessed by agarose gel. 2 µg of the mRNA was reverse transcribed using the High-Capacity cDNA Reverse Transcription Kit (Applied Biosystems). Serial dilutions of the cDNA product were performed and a pooled standard curve to determine optimal dilution for each transcript type. mRNA transcript levels were measured using the SsoFast EvaGreen

Supermix for qPCR (Bio-Rad) with the appropriate primer pairs (S2.4 Table). The data for each experiment was normalized to the chosen internal control (*TDH3* mRNA) and then compared to WT using the ΔΔCt method.

Seahorse Assays

Seahorse assays were performed as previously described [224]**.** Briefly**,** Yeast cultures were grown overnight in YPD and in the morning they were split and diluted to an OD600 of 0.1 in YPD or 0.25 in YPE (Yeast Peptone Ethanol 3%), grown to mid log (OD600 of 0.5- 0.7) prior to cells being pelleted (3000 RPM for 3 min) and resuspended into yeast seahorse assay media (0.167% yeast nitrogen base, 0.5% ammonium sulfate, and 3% ethanol or 2% dextrose respectively). Cells were counted and diluted to a concentration of 2.8 x 10^6 cells/mL in yeast seahorse media. 180 µL of the cell dilutions were used to seed the wells of a Seahorse XF96 cell culture microplate (Agilent) that had been pre-treated with poly-l-lysine to enable cell adhesion (MilliporeSigma). A minimum of 8 technical replicates were performed for each experiment. The seeded plate was centrifuged at 500 RPM for 3 min to promote yeast adhesion and the plate was rested for 30 min at 30^{o}C. A soaked and calibrated Seahorse XF96 Sensor Cartridge was prepared with 0.5% sodium azide (Sigma) injection in chamber A before loading into the Seahorse XF96 analyzer (Agilent) and measurement of oxygen consumption rate (OCR) of the yeast in the cell culture microplate. Measurements were performed at 30^{o}C. Three basal OCR measurements were taken for 3 minutes each with 1.5 minutes of mixing between measurements. Sodium azide was then programmed to be injected and three additional OCR measurements were performed for 3 min with 1.5 minutes of mixing between.

Acetylation mimics/CRISPR-Cas9

Point mutations on Bcy1 at the lysine 313 (K313) site were performed by targeting with CRISPR-Cas9 to cut the DNA and introducing a homologous strand of DNA with the mutation of interest. The lysine 313 site of Bcy1 was mutated to a Glutamine (Q) or Arginine (R) to represent an unacetylated and an acetylated form of Bcy1 (K313Q and K313R).

The general DiCarlo *et. al*. protocol was followed with minor adjustments. Briefly, the Cas9 plasmid, p414-TEF1p-Cas9-CYC1t [225], was transformed using lithium acetate into the Bcy1-GFP, Bcy1-GFP *eaf1Δ*, Cit1-GFP, and cit1-GFP *eaf1Δ* strains and maintained by growth on SC-LEU. In parallel to account for problems with off target effects, two different PAM sequences targeting the Bcy1-K313 area were cloned into the guide RNA plasmid, p426-SNR52p-NotI (gRNA)-SUP4t by PCR amplification. These sequences were selected from DiCarlo and colleague's list [225]. Following PCR, the resulting plasmid was treated with DPN1, transformed into DH5α *E. coli* for amplification, and sent for sequencing at the TCAG facility (SickKids) to confirm guide RNA incorporation. Double stranded DNA homologous to the area to be cleaved but containing the mutations to the K313 and the NGG PAM site was prepared by ordering single stranded oligos and annealing them at 100^{o}C and slowly ramping down the temperature. The dsDNA for homologous repair and the corresponding guide RNA plasmid were transformed using lithium acetate into the strains pre-prepared with the Cas9 expression plasmid. Transformed cells were selected on SC-LEU-URA and positive colonies were collected, genomic DNA extracted, and a PCR of the area of interest was performed, which was then sent for sequencing at the TCAG Facility (SickKids, Toronto) to confirm the mutation in the genome.

Statistical Analyses information

Statistical analyses were performed using GraphPad Prism. When comparing two groups a student's t-test was performed. In the case of more than two groups a 2-way ANOVA was performed, and individual pairs were compared by a Tukey's multiple comparison test comparing each mean to the mean of every other group. For all analyses, a $p < 0.05$ to define significance was used.

Acknowledgements

We thank Brenda Andrews and Christian Landry for providing strains and plasmids.

Chapter 3: Manuscript #2

Walden EA, Knill, H, Sproule, A, Overy, D, Baetz, K. The lysine acetyltransferase NuA4 in regulation of ergosterol dynamics in *Saccharomyces cerevisiae*.

Submitted to G3 on October 16, 2022.

The lysine acetyltransferase NuA4 in regulation of ergosterol dynamics in Saccharomyces cerevisiae

Elizabeth Walden [1,2], Hana Knill [1,2], Amanda Sproule [3], David Overy [3], Kristin Baetz [1,2,4]*

Author Affiliations:

[1] Ottawa Institute of Systems Biology, uOttawa, Ottawa, K1H 8M5 Canada

[2] Department of Biochemistry, Microbiology and Immunology, Faculty of Medicine, uOttawa, Ottawa, K1H 8M5 Canada

[3] Agriculture and Agri-food Canada, Ottawa Research and Development Centre, Ottawa, ON K1A 0C6, Canada

[4] Department of Biological Sciences, Faculty of Science, University of Calgary, Calgary T2N 1N4, Canada

[*] Corresponding author: Department of Biological Sciences, Faculty of Science, University of Calgary, Calgary T2N 1N4, Canada. E-mail: kristin.baetz@ucalgary.ca

Running head: NuA4 in regulation of ergosterol

Keywords: NuA4, Eaf1, Lysine acetylation, Ergosterol, Ergosteryl esters, Tip60, *Saccharomyces cerevisiae*, Amphotericin B.

3.1 Abstract

Recently, we determined that mutants of the *Saccharomyces cerevisiae* lysine acetyltransferase NuA4 have increased ergosteryl ester content. Ergosteryl esters are the storage form of ergosterol, the yeast equivalent of cholesterol. Here we use genetic manipulation, chemical sensitivity, GC-MS, and microscopy to characterize changes in ergosteryl esters and ergosterol upon deletion of Eaf1, a key scaffolding member of the NuA4 complex. Compared to WT cells, *eaf1Δ* yeast cells are more sensitive to drugs targeting ergosterol and ergosterol biosynthesis, including amphotericin B, have increased staining with filipin, contain more ergosterol biosynthesis intermediates, and have more lipid droplets suggesting an increase in both ergosteryl esters and free ergosterol in *eaf1*Δ cells. However, the observed differences in *eaf1*Δ cells was not associated with changes in the localization or abundance of ergosterol biosynthesis enzymes nor dependent on changes in Acc1 or Snf1 activity. To gain insight into the molecular mechanism contributing to increased ergosteryl ester levels in *eaf1*Δ cells, we performed a chemical genomic screen to identify non-essential gene deletions which reverse the sensitivity of the *eaf1Δ* cells to amphotericin B. Sixty-one double deletion strains had larger than expected colony growth on amphotericin B, of which the 5 top hits were *ERG3, POT1, GAL83, GIP3,* and *AFR1*. These deletions reduced the sensitivity of *eaf1Δ* yeast to multiple drugs which target ergosterol indicating that these genes likely reverse the *eaf1Δ* dependent increase in ergosterol. This work demonstrates that NuA4 regulates ergosterol dynamics in the cell.

3.2 Introduction

The NuA4 complex is a lysine acetyltransferase (KAT) in *Saccharomyces cerevisiae* which is well characterized for its regulation of gene expression through acetylation of histones [68,72]. However, the biological role of NuA4 is not limited to transcription as a number of non-histone targets have been identified, including the regulation of various aspects of lipid metabolism [52,59,60,106,134]. Both histone and non-histone targets of NuA4 in yeast are of interest as the human homolog of NuA4, Tip60, has been found to be deregulated in a number of human diseases, the most common of which is cancer [51,61–64,93,158,226]. Importantly, many of the enzymatic functions of NuA4 are conserved in Tip60, hence, yeast is an outstanding surrogate model organism for Tip60 research [52,53]. NuA4 is a 13 subunit complex of which Esa1 is the catalytic component [61,70,81]. The *ESA1* gene encodes for the only essential KAT in *S. cerevisiae* and a temperature sensitive mutation, *esa1-L254P* (*esa1-ts*) is commonly used to explore NuA4 cellular function [69,81]. Alternatively, *eaf1*Δ cells are also a used a model for NuA4 dysfunction. *EAF1* encodes a key structural subunit that is required to maintain integrity of the NuA4 complex [66,68] where *EAF1* deletion leads to disassembly of the NuA4 complex and a reduction in the ability of Esa1 to acetylate protein targets, making the *eaf1Δ* mutant an excellent model for NuA4 dysfunction [66–68,79,106].

Intriguingly, many of the non-histone targets regulated by NuA4 are involved in metabolism [52,59,60,106]. Specifically, NuA4 has been associated with the acetylation of Pck1 which catalyzes the rate limiting step of gluconeogenesis [59] and Sip2, one of the three regulatory β subunits of Snf1 (human AMP activated kinase, AMPK) [60,123]. NuA4 has also been found to regulate Bcy1, the regulator subunit of yeast Protein Kinase A (PKA) through acetylation of K313 and regulation of cytoplasmic localization which has downstream effects modulating glycogen synthesis and mitochondrial morphology [52,106]. In lipid metabolism, NuA4 has been linked to lipid exchange and fatty acid biosynthesis through a genetic interaction with *SEC14* [80,134], the gene encoding for the Phosphatidylinositol/phosphatidylcholine transfer protein (Sec14), and acetylation of a yeast oxysterol binding protein Kes1 [134]. Kes1 acetylation at K109 is associated with a decrease in Kes1 activity and regulation of cell cycle progression and lipid exchange [134].

Finally, both Esa1 and Tip60 have both been shown to target Pah1 (lipin 1 in humans) for acetylation which results in the translocation of Pah1 from the cytoplasm to the ER allowing triacylglycerol (TAG) synthesis [53]. In addition to these previously identified non-histone modes of NuA4 regulation of metabolism, our lab recently identified a NuA4 dependent regulation in *de novo* lipid synthesis through Acc1 localization and activity [151,173]. Lipidomic analysis of the NuA4 mutant, *eaf1Δ,* indicate a reduction of chain length across lipid classes, along with a small but significant increase in the abundance of ergosteryl esters as compared to WT cells [151].

In yeast, ergosteryl esters are the storage form of free ergosterol and are localized in the cytosol in lipid droplets. These lipid droplets are composed of a single phospholipid layer which encases neutral lipids, mainly TAG and sterol esters (SE), which are found in approximately equal abundances under glucose growth [227,228]. These non-polar lipid stores provide a readily available pool of ergosterol, which is vital for stress adaptation in yeast [229]. The unesterified (free) form of ergosterol is a polar molecule and like its human counterpart cholesterol, is an integral component of cellular membranes [229].

In yeast cells, ergosterol plays an important role in the response to stress, and the biosynthesis of ergosterol is therefore highly regulated. Ergosterol biosynthesis begins much the same as cholesterol synthesis, with the conversion of acetyl-CoA to mevalonate, followed by the production of farnesyl pyrophosphate, after which ergosterol biosynthesis begins to differentiate from cholesterol synthesis in series of reactions through squalene, lanosterol, zymosterol, episterol, and the final production of ergosterol make up the third module (Figure 1A) [229–231]. The importance of the ergosterol pathway and associated products in yeast is underlined by the fact members of the first two modules are mediated by proteins products of gene which are essential for yeast viability [229,232]. The proteins responsible for ergosterol biosynthesis (Erg proteins) are found spread across the cytoplasm and endoplasmic reticulum (ER) and ergosterol biosynthesis is performed primarily in the endoplasmic reticulum [42,229,232]. Ergosterol is then transported to the cell membrane through non vesicular transport or esterified by Are1 or Are2 for storage in lipid droplets [229,233]. While the storage of esterified ergosterol within lipid droplets is the

primary method that yeast cells employ to protect themselves from the toxic accumulation of excess ergosterol, ergosterol levels are also modulated via secretion into the environment following acylation [232]. Conversely, during anaerobic conditions where ergosterol is not synthesized, yeast cells will uptake externally provided sterols from the growth medium [234]. Cellular ergosterol concentrations are also controlled through the abundance of Erg proteins, which are regulated by transcription (through Upc2 and Ecm22) and by ubiquitin dependent degradation [235–238]. Variation in environmental growth conditions have a large effect on the cellular synthesis of ergosterol with carbon source, oxygen abundance, heme availability, ethanol concentration, osmotic pressure, sterol abundance, and pH all being important factors [239–241]. While WT Erg proteins predominantly localize to the ER, some alternatively localize to lipid droplets or the cytoplasm and the site of localization is associated with differences in Erg protein activity [41,42,229,242].

While our lab recently identified a novel change in ergosteryl esters in NuA4 mutants [151], two other studies have made less direct associations between NuA4/Tip60 and pathways associated with ergosterol or cholesterol [243,244]. First, in studying amyloid precursor protein (APP) and lipoprotein receptor (LRP), Liu and colleagues found that Tip60 interacts with the cleaved APP intracellular domain (AICD) of APP and these act together to suppress transcription of the LRP1 promoter [243]. The transcription of LRP1 in turn is associated with an increase in cholesterol and a LRP1 forebrain knockout mouse model had significantly less cholesterol observed in the brain compared to their WT littermates, thereby indirectly linking Tip60 to cholesterol accumulation in the brain [244]. A second study was interested in the rare cholesterol transport disease Niemann-Pick C (NPC) where the homolog in yeast (Ncr1) was used to identify genes that had a negative genetic interaction with the deletion of *NCR1* so that the reverse processes could be identified as potential therapeutic targets [244]. In their screen, the yeast strains were grown in anaerobic conditions where ergosterol biosynthesis is absent thereby emphasizing the role of transport. Two members of the NuA4 complex, Eaf1 and Yaf9, were identified as hits in the screen, and follow up work demonstrated the importance of acetylation in NPC as HDAC inhibitors were

effective at reversing some of the phenotypes of NPC in human cells [244,245]. Once again tangentially implicating NuA4 in ergosterol regulation.

Given the change in ergosteryl esters identified by lipidomic analysis, the disease relevance of cholesterol/ergosterol, and previous links between NuA4 and metabolism, our research aimed to elucidate the mechanism(s) through which NuA4 regulates ergosterol and ergosteryl esters. Here, we show that the previously characterized change in ergosteryl esters is accompanied by an increase in free ergosterol and ergosterol precursors dependent on the key ergosterol biosynthesis gene *ERG3*. Additionally, the increase in ergosteryl esters found in the *eaf1Δ* mutant is also associated with an increase in the number of lipid droplets per cell but not a change in lipid droplet size. The change in ergosterol concentration did not appear to be dependent on Acc1, previously documented mRNA expression or acetylation, or protein abundance and localization. However, the *eaf1Δ* yeast were sensitive to a number of chemical inhibitors allowing for the screening for pathways which could be involved in the regulation. This screen confirmed a dependence on ergosterol biosynthesis and additionally pointed to the involvement of Glc7, Snf1, and Pot1 in NuA4 regulation of ergosterol dynamics.

3.3 Methods

Strains and culturing conditions

Yeast were grown at 30 ^{o}C with rotation in YPD (1% yeast extract, 2% peptone, 2% dextrose) or on YPD agar plates unless otherwise stated. In preparation for experiments performed on mid-log phase cells (OD_{600} = 0.5-0.8), overnight cultures of yeast were grown in YPD before being diluted into day cultures to an OD_{600} of 0.1 (or 0.15 for *eaf1Δ*) and grown for several hours until mid-log phase was reached. The BY4741 (S288C) is the WT background strain in this work. All strains used in this study are listed in S3.1 Table. GFP-tag and deletion mutants were taken from the GFP collection [42] or deletion

mutant array (DMA) (GE, CAT# YSC1053) respectively or were made by PCR-mediated insertion/deletion as previously described [219]. All strains listed (S3.1 Table) were confirmed by PCR.

Serial dilution spot assays:

Yeast cultures grown to mid-log phase were diluted in YPD to an OD600 of 0.1 and three 10-fold serial dilutions (0.01, 0.001, 0.0001) in a 96 well plate. A 5 µL aliquot of the serial dilutions were spotted onto the indicated plates and allowed to grow at 30 ^{o}C for 48 hours unless otherwise indicated. For drug sensitivity testing, the following inhibitors were added to YPD agar plates just prior to pouring: 50 µg/mL Terbinafine (Cedarlane 10011619), 250 µg/mL Lovastatin (Cedarlane 10010338), 250 ng/mL Amphotericin B (Millipore Sigma A2942), 50 µg/mL Fluconazole (Fisher Scientific 86386-73-4), and 5 µg/mL Nystatin (Bio Basic NB0390).

Bligh and Dyer lipid extracts:

Lipid extracts were collected from mid log phase cells using a Bligh and Dyer style extraction on 25 OD_{600} units of frozen yeast pellets [246]. Briefly, frozen pellets were resuspended in a 2:1 (v: v) methanol: chloroform mixture with an equivalent volume of glass beads. This mixture was vortexed for 6, one-minute intervals alternating with one-minute ice interval. Cholestane was spiked in as a standard control for each sample by adding 50 µL of 10 µg/mL cholestane dissolved in chloroform. This was followed by an additional 250 µL of chloroform and 250 µL of water and a 1.5 min vortex. All liquid was moved to a new tube which was centrifuged to separate the aqueous and organic phases. The organic phase was removed to a glass vial and evaporated with nitrogen gas. The dried samples were stored at -80 °C until analysis.

Sample derivatization and GC-MS analysis:

Samples were reconstituted in 100 µL N-methyl-N-trimethylsilyl-trifluoroacetamide (MSTFA) with 1% TMCS (Restek, Bellefonte PA, USA) and vortexed for 10 s before incubating at 37 °C for 30 min at 500 rpm (Eppendorf ThermoMixer C). The samples were transferred to glass vial inserts and analyzed using a Trace 1310 GC equipped with a TriPlus RSH autosampler coupled to an ISQ 7000 single quadrupole mass spectrometer (Thermo Scientific, Waltham MA, USA). The GC-MS method was adapted from previously published work [247]. A 1 µL aliquot of each sample was injected and vaporized in the injector at 250 °C with a split flow of 30 mL/min and a purge flow of 5 mL/min helium. Sterols were separated using a ZB-5ms column (30 m + 10 m guard with 0.25 mm diameter and film thickness of 0.25 µm, Phenomenex, Torrance CA, USA). The column oven was maintained at 50 °C for 1 min, increased by 50 °C/min until 260 °C, followed by an incremental increase by 4 °C/min until 310 °C and held for 5 min at 310 °C before returning to starting conditions. The MS transfer line was 270 °C and samples were ionized using EI with an ion source temperature of 230 °C and scanning a range of 50-600 amu.

GC-MS data analysis:

Ergosterol, lanosterol, and squalene peaks were confirmed by database matches in the NIST 2017 MS Library. Peak areas were integrated for relative quantification using the Chromeleon 7 Chromatography Data System software (Thermo Scientific, version 7.2.9) and normalized by dividing by the peak area of the cholestane internal standard. GC-MS *.raw* data files were also processed using MZmine2 (V2.53) [248]. The data was filtered to process only the scans in the sterol region of the chromatogram, 10-21 min. The mass detection threshold was set at 1E3 and the ADAP module was used to construct chromatograms with a minimum group size of 5 scans and group intensity threshold and minimum highest intensity of 1E4 [249]. Chromatogram deconvolution was performed using the ADAP wavelets algorithm with a S/N threshold of 2 and coefficient threshold of 85. Spectral deconvolution was used to select a single model peak based on the highest intensity for each cluster of chromatograms with a minimum distance of 0.05 min, edge-to-height ratio of 0.3, delta-to-height ratio of 0.2 and minimum

sharpness of 10. The shape-similarity tolerance was set at 80. The data was aligned with a minimum confidence interval of 0.1, retention time tolerance of 0.05, m/z tolerance of 0.2 and score weight of 0.1. The aligned feature list was gap-filled and exported to Excel where the data was normalized by dividing the peak area of each feature by the peak area of the cholestane internal standard in the respective sample, and background peaks were manually removed before processing in RStudio (V1.2.1335).

Microscopy:

Microscopy was performed using a Leica fluorescence microscope (DMI600; Leica Microsystems) with a high-performance camera (Hamamatsu), DG4 light source (Sutter Instruments) or an Excelitas X-Cite 120 LEDMini Light Source and Volocity 4.3.2 software (PerkinElmer). Yeast were grown to mid log phase in YPD then for integrated GFP imaging, yeast cells were centrifuged (1000 rpm for 1 min) and resuspended in Synthetic Complete (SC) medium for live imaging. For Bodipy staining, Bodipy (ThermoFisher D-3922) was added to 1-2 mL of log phase YPD culture to a final concentration of 1 µg/mL. Cultures were then incubated for 20 min at 30^{o}C, centrifuged (1000 rpm for 1 min), washed in SC, and resuspended in 20 µL of SC medium for imaging. Filipin (Millipore Sigma F9765) staining was performed by spinning down 2 mL of culture resuspending in 20 µL of SC media and adding 2 µL of 5 mg/mL stock filipin solution, and immediately (within 1-3 min) imaged. Image stacks of 35 images over 7 µm were captured for each channel. Brightfield control images were taken. The number of lipid droplets per cell (by Bodipy and Faa4-GFP) were manually assessed based on compressed z-stack images and a minimum of 100 cells per replicate were counted. Quantification of lipid droplet size was performed using Imaris software, specifically with dot analysis on z stacked images.

Amphotericin B Colony Growth Screen:

Synthetic genetic array (SGA) technology and robotic manipulation of the Deletion Mutant Array (DMA) (GE, CAT# YSC1053) using a Singer RoToR HAD (Singer Instruments) was used to incorporate *eaf1Δ* into the DMA collection as previously described [79]. The DMA was condensed onto 7 solid YPD plates with 1536 yeast strains spotted on each and 2 replicates of each deletion mutant and then the DMA was crossed with the *eaf1Δ*::NAT query strain by co-pinning onto YPD. Mated diploids were selected for using G418 and NAT and then sporulation was induced on SPO media over 10 days at 25 ^{o}C in the dark. Sequential selection through SC-HIS- ARG +CAN (for Mating type A), SC-HIS- ARG +CAN + G418 (for DMA mutants), and SC-His- ARG +CAN + G418 + NAT (for *eaf1Δ*) plates allowed for a final collection with the DMA collection of mutants in an *eaf1Δ* mutant background. The WT DMA and the *eaf1Δ* DMA collections were then pinned on 1.5 µg/µL amphotericin B YPD agar and grown at 25 ^{o}C for 48 h. Two biological and two technical replicates were performed. Plates were imaged using a Biorad ChemiDoc system and were analyzed using SGA tools [47] comparing growth on YPD and the growth on YPD with amphotericin B generating two SGA scores for each mutant (one per biological replicate) for the WT and the *eaf1Δ* screens. Scores were mapped to genes, averaged over technical replicates, and compared between biological replicates using in house Python analysis. An SGA score cut-off >0.6 was selected for analysis. Scores above this cut-off represent those strains that grew better than expected and therefore reduced the sensitivity of the yeast to amphotericin B. The hits from the WT screen were then compared to those of the *eaf1Δ* generating a list of gene deletions that specifically decrease the sensitivity of the *eaf1Δ* mutant to amphotericin B. Top hits were confirmed by dot assays and the identify of the knock-out confirmed by PCR validation generating a final list of high confidence hits. GO analysis using Panther [250] and BiNGO [251] in Cytoscape were performed. Network figures were generated using Cytoscape and adapted in Illustrator [252].

Statistical analysis

Statistical analysis was performed with GraphPad Prism 9 software as indicated in the figure legends. For graphs, mean was plotted with standard deviation as the error bars.

3.4 Results

Ergosterol biosynthesis is increased in a NuA4 mutant:

Given that our lipidomic study identified an increase in ergosteryl esters in an *eaf1Δ* mutant [151], we sought to determine if this change was specific to ergosteryl esters or if there was a correlated change in ergosterol biosynthesis and free ergosterol. As mammalian cells do not contain or synthesize ergosterol, the presence and synthesis of ergosterol are validated targets for fungicides [232,247]. In fact, amphotericin B is one of the gold standard treatments for fungal/yeast infections [253,254]. Statins, which were developed to target cholesterol synthesis, are also useful inhibitors of the yeast Hmg1/2 proteins as the first modules of ergosterol biosynthesis are extremely similar to cholesterol synthesis [230,255]. Inhibitors of ergosterol biosynthesis and free ergosterol in the membrane can be useful tools in the study of ergosterol dynamics in the cell [230,255–260] (Figure 3.1A). As a means of assessing changes in ergosterol biosynthesis and free ergosterol in the membrane, the growth sensitivity of *eaf1Δ* cells to a series of ergosterol biosynthesis inhibitors and fungicides was compared to WT and *erg3Δ* cells. The *eaf1Δ* yeast displayed similar sensitivity to lovastatin and terbinafine as compared to WT cells, drugs that target the first half of ergosterol biosynthesis pathway (Figure 3.1B). However, *eaf1Δ* cells were more sensitive than WT to fluconazole, a drug which inhibits Erg11, indicating that the NuA4 mutant may have a reduction in Erg11 activity or a greater requirement for the late ergosterol biosynthesis pathway than WT cells. Finally, *eaf1Δ* cells were more sensitive to both amphotericin B and nystatin which function as ionophores, binding to membrane ergosterol and creating pores [261,262]. The sensitivity of a yeast strain to drugs such as amphotericin B is correlated to cellular ergosterol abundance [230,263], as was observed for the

erg3Δ mutant, which interrupts ergosterol biosynthesis decreasing free ergosterol, as being less sensitive than the WT to amphotericin B and nystatin (Figure 3.1B). The increased sensitivity of *eaf1Δ* cells to amphotericin B and Nystatin suggest that *eaf1Δ* mutants may have increased levels of membrane ergosterol. In agreement, *eaf1Δ* cells display a small increase in filipin staining, a dye which binds to free ergosterol in the membrane (Figure 3.1C)[264]. We next assessed changes in ergosterol biosynthesis directly by performing GC-MS analysis of lipid extracts. Blight and dyer lipid extracts were collected from WT, *eaf1Δ*, *erg3Δ*, and the double *erg3Δ eaf1Δ* yeast cells prior to derivatization and analysis by GC-MS. Ergosterol quantification showed a small but not significant increase in ergosterol in an *eaf1Δ* mutants relative to WT which was completely reduced in both the *erg3Δ* and *erg3Δ eaf1Δ* mutants (Figure 3.1D). However, there is a significant increase in the abundance of the ergosterol biosynthesis intermediates lanosterol and squalene in the *eaf1Δ* mutant (Figure 3.1D). The observed increases in lanosterol and squalene were abolished in *eaf1Δ erg3Δ* mutant cells suggesting that the increase in ergosterol and intermediates in an *eaf1Δ* cells is dependent on ergosterol biosynthesis.

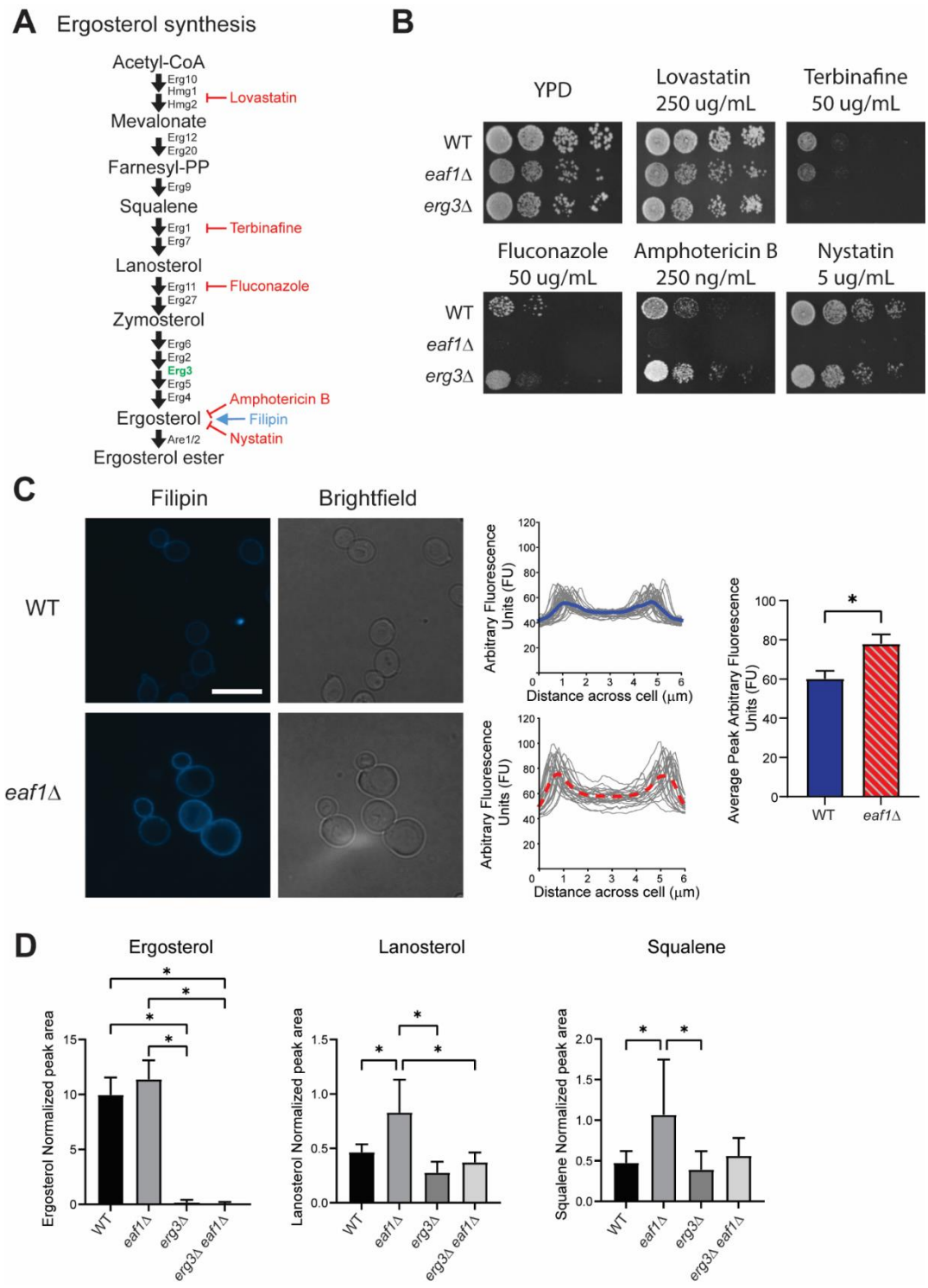

Figure 3.1: Deletion of *EAF1* increases free ergosterol and ergosterol precursors in yeast. A) A simplified schematic of the ergosterol biosynthesis pathway highlighting the key proteins, intermediates, and drugs that target the pathway. Derived from Bhattacharya et al. 2018. B) *eaf1Δ* cells are more sensitive to drugs which target ergosterol biosynthesis and ergosterol in the membrane. WT, *eaf1Δ*, and *erg3Δ* cells were grown to mid log in liquid YPD before being spotted onto solid YPD with or without a series of

ergosterol targeting compounds. The strains were spotted in serial dilutions beginning at 0.1 and three 10-fold dilutions from there onto the plates. These spots were then allowed to grow for 48 h at 30°C and images were taken. Images are representative of three replicates. C) *eaf1Δ* cells have increased Filipin staining. Live cell imaging was performed on WT and *eaf1Δ* cells immediately after staining with Filipin, which binds to free ergosterol. Images are representative of three replicates. Scale bar = 10 μm (Left panel). Quantification was done using the plot profile function along a 60-unit (6.23 μm) line across 25 cells per replicate of 3 replicates. All measurements from one replicate are shown in thin grey lines and the average of those measurements is overlayed in solid blue for WT or dotted red for the *eaf1Δ* (Middle graphs). The maximum peak height was also calculated for the three replicates of the WT and the *eaf1Δ* measurements. These values are plotted (Right panel) and a t-test was performed. * Denotes $p < 0.05$. D) GC-MS analysis was performed on Bligh and Dyer lipid extracts from WT, *eaf1Δ, erg3Δ*, and *erg3Δ eaf1Δ* yeast. Samples were reconstituted and injected and vaporized into the GC-MS where they were separated using a ZB-5ms column. Peaks corresponding to ergosterol, lanosterol and squalene peaks were identified and confirmed by database matches in the NIST 2017. The peak area were then quantified and normalized to the spiked in cholestane internal standard. Normalized peak area for each compound was plotted. ANOVA analysis with a Tukey's multiple comparisons test was used to compare the means of the WT and mutants. * Denotes $p < 0.05$. n=8.

NuA4 mutants affect ergosteryl esters and lipid droplet abundance:

Our work here suggests that ergosterol biosynthesis is increased in *eaf1Δ* cells, but the GS-MS data did not reflect significant increase in the levels of free ergosterol in *eaf1Δ* cells. A potential reason may be the esterification of excess ergosterol for storage in lipid droplets to protect cells from ergosterol toxicity. To determine if this is the case, the size and abundance of lipid droplets in WT and *eaf1Δ* strains was assessed using microscopic analysis with two fluorescent markers, Bodipy a stain of neutral lipids [265] and Faa4-GFP, a tagged protein which is commonly used to mark Lipid droplets [227,228,266]. Both Faa4-GFP and Bodipy analysis demonstrated that *eaf1Δ* cells have approximately 2 times more lipid droplets per cell than WT cells (Figure 3.2A and B), while there is no significant difference in the size of lipid droplets between the two strains (Figure 3.2C). This observation was consistent with our previous data suggesting that the *eaf1Δ* mutant has an increased relative abundance of ergosteryl esters relative to WT [151]. In addition to previous lipidomic analysis of ergosteryl esters in the *eaf1Δ* mutant, complementary lipidomic analysis of temperature shifted WT and *esa1-ts* yeast also demonstrated a small but significant increase in ergosteryl esters thereby implicating the catalytic subunit of NuA4, Esa1, in this regulation (S3.1 Fig. and S3.3 Table).

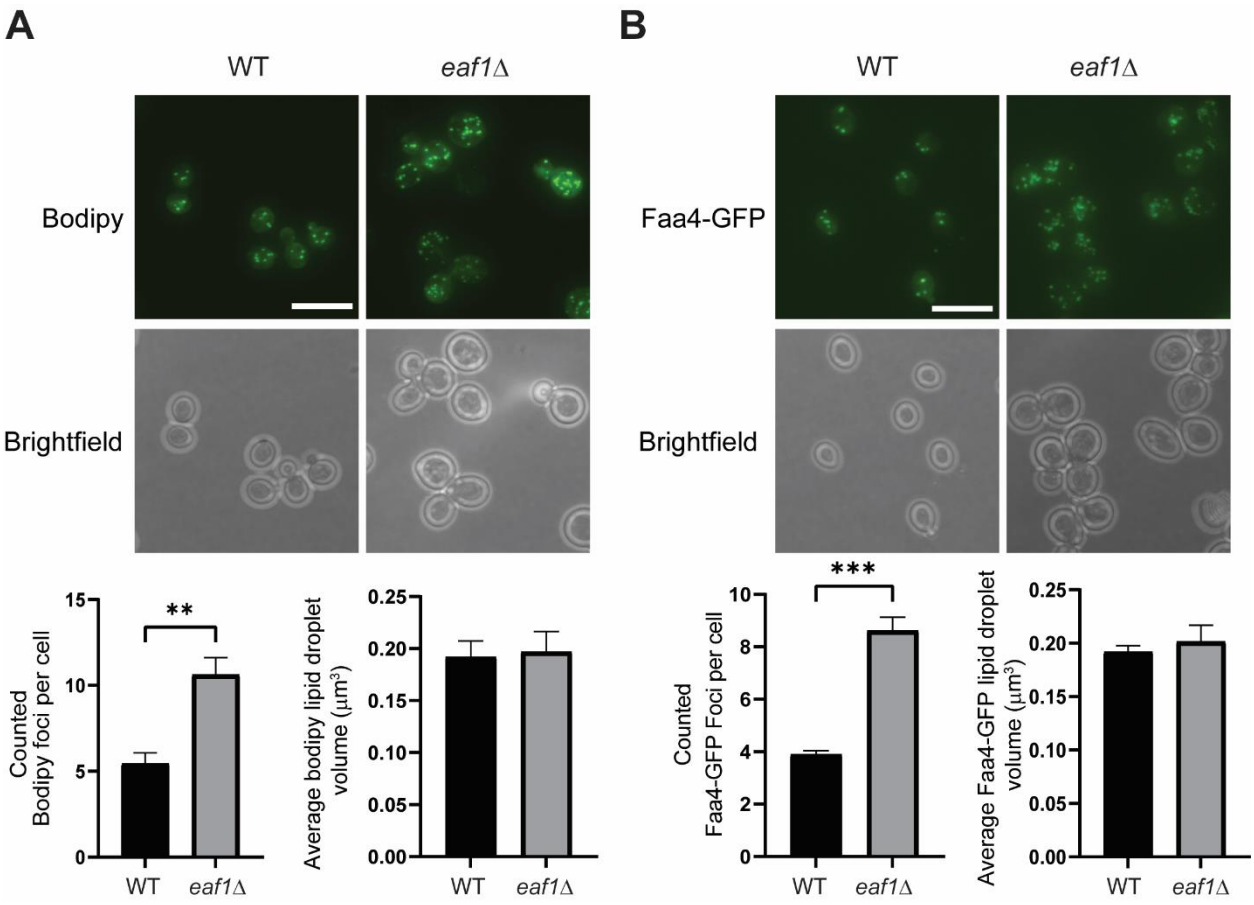

Figure 3.2: Deletion of *EAF1* results in an increase in the number of lipid droplets per cell. Lipid droplets are composed of neutral lipids, mainly ergosteryl esters and triacylglycerols. Live cell imaging of lipid droplets was performed using Bodipy, a stain which binds to neutral lipids (A) and Faa4-GFP, a protein marker of the lipid droplet (B) (Top panel). Scale bar = 10 μm. The number of lipid droplets per cell was counted for at least 100 cells per replicate for both lipid droplet markers (n=3) (Bottom left panel). The size of the lipid droplets was quantified using Imaris dot identification and measurement for both lipid droplet markers (Bottom right panel). * Denotes statistical significance at a p-value < 0.05 determined using a t-test. The same cells used for counting number of lipid droplets per cell were used to quantify lipid droplet size (n=3).

NuA4 dependent regulation of ergosterol is independent of ergosterol biosynthesis protein localization or abundance and Acc1 activity.

Given the change in the abundance of ergosterol, ergosterol precursors, and ergosteryl esters, we next sought to determine how NuA4 may be affecting this pathway. As ergosterol, lanosterol, and squalene accumulation in an *eaf1Δ* is dependent on *ERG3*, a key enzyme in the ergosterol biosynthesis pathway, we postulated that NuA4 may be regulating some aspect of ergosterol biosynthesis. Hence, we first assessed if deletion of *EAF1* impacted the abundance or subcellular localization of key Erg proteins. Surprisingly, we did not detect any significant changes in ergosterol biosynthesis pathway proteins in *eaf1Δ* cells (Figure 3.3 and S3.2 Fig) or in a previous screen done in our lab [106]. The lack of change in Erg proteins is also in agreement with previous microarray data which did not identify changes in the mRNA expression of *ERG* genes dependent on NuA4 [67]. Additionally, while many studies have identified acetylation sites on Erg proteins, to date none have been determined to be dependent on NuA4/Esa1 [153]. Another option could be that ergosterol biosynthesis is upregulated in the NuA4 mutants because of an increased abundance of acetyl-CoA associated with a decreased activity of acetyl-CoA carboxylase 1 (Acc1), the committed step of *de novo* fatty acid synthesis [151,173]. However, the *acc1*^{S1157A} hyperactive mutant, which lowers acetyl-CoA abundance [151,267] was unable to reverse the sensitivity of the *eaf1Δ* mutant to amphotericin B and nystatin (Figure 3.3) suggesting that the regulation is independent of Acc1 and acetyl-CoA accumulation.

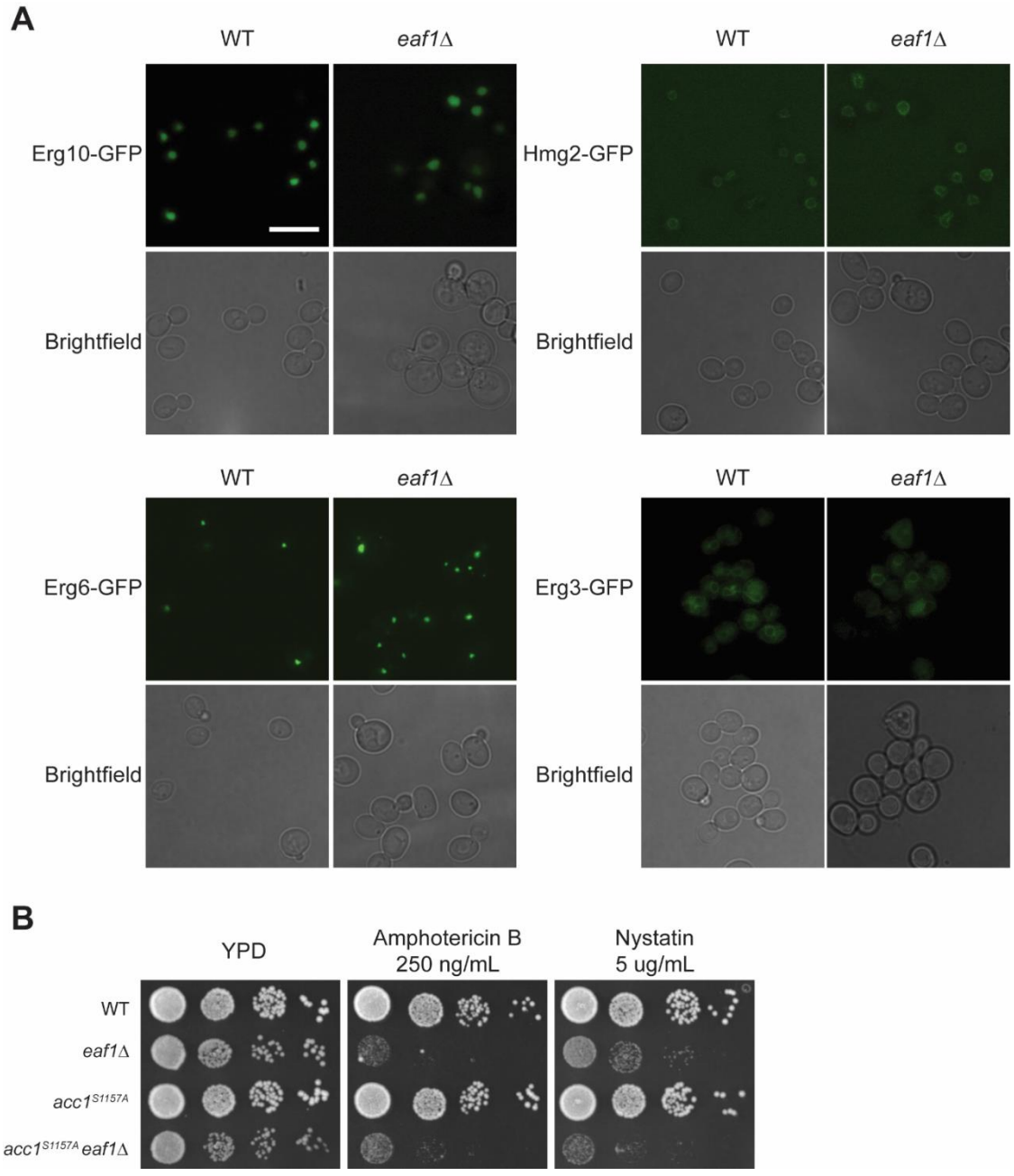

Figure 3.3: NuA4 dependent regulation of ergosterol is independent of ergosterol biosynthesis protein localization or abundance and Acc1 activity. A) The localization and abundance of members of the ergosterol biosynthesis pathway was assessed by comparing GFP-tagged proteins in the WT and *eaf1Δ* background. Images were taken in mid-log growth in YPD media. Figures are representative of n=3. Scale bar = 10 μm. Four representative ergosterol biosynthesis GFP-tagged strains with various localizations are shown here, and additional strain images can be seen in S3.2 Fig. B) A hyperactive Acc1 mutant, $acc1^{S1157A}$ was unable to reverse the sensitivity of the *eaf1Δ* to amphotericin B or nystatin. WT, *eaf1Δ*, $acc1^{S1157A}$ and $acc1^{S1157A}$ *eaf1Δ* yeast were grown to mid log in liquid YPD before being spotted onto solid YPD with or without amphotericin B and nystatin. The strains were spotted in serial dilutions beginning at 0.1 and three 10-fold dilutions from there onto the plates. These spots were then allowed to grow for 48h, and images were taken. Images are representative of three replicates.

A chemogenomic screen identifies candidate genes for NuA4 dependent regulation of ergosterol.

As our directed approach to identify potential pathways through which NuA4 regulates ergosterol biosynthesis was unsuccessful, we next opted to perform a chemogenomic screen. The dependence of ergosterol and precursor compound accumulation in an *eaf1Δ* on *ERG3* seen by GC-MS (Figure 3.1D) also translated to reversal of amphotericin B sensitivity. Specifically, the growth defect of the *eaf1Δ* on amphotericin B was reversed in the double *erg3Δ eaf1Δ* mutant (Figure 3.4A). Therefore, we performed a screen to identify other mutants that reversed the sensitivity of the *eaf1Δ* mutant to amphotericin B with the overall goal that amphotericin B sensitivity suppressors may provide insight into the mechanism by which NuA4 may regulate ergosterol dynamics. Synthetic genetic array (SGA) technology [174] was used to generate a double mutant collection of *eaf1Δ* combined with the approximately 4000 yeast deletion mutants to create the *eaf1Δ* DMA collection. This was done in duplicate to prepare two biological replicates. The *eaf1Δ* DMA collection was plated onto YPD alone and YPD containing amphotericin B in parallel, and the growth rate of each colony assessed and compared using SGA tools to generate a score (Figure 3.4C). The SGA tools analysis gave a measurement of the ratio of growth on amphotericin B to the growth on YPD for each mutant in our *eaf1Δ* DMA. The distributions of scores for the *eaf1Δ* collection demonstrates a normal distribution where high scores have the best growth on amphotericin B and the lowest scores had the lowest growth (Figure 3.4C and S3.4 Fig.). Any strain that had an average score of 0.6 and above was considered a top hit (S3.2 Table). At a 0.6 cut-off, we identified 61 *eaf1Δ* double deletion hits that grew better than expected on amphotericin B, suggesting that they may be involved in NuA4's regulation of ergosterol. As expected within the top hits was *erg3Δ* (score =0.801) indicating the screen was successful. GO analysis was performed using PANTHER [250] and BiNGO [251] and no pathways or processes were found to be significantly enriched with the list of top hits. The same screen was performed comparing the growth of the WT DMA on YPD and YPD + amphotericin B as an additional control to remove gene hits that were not specific to the deletion of *EAF1*. We selected 1.5 µg/µL amphotericin B for our screening concentration. At this concentration, the majority of WT strains

grew very well while the majority of *eaf1Δ* strains grew poorly. Therefore, at a cut-off of 0.6, no common hits were found between the WT and *eaf1Δ* screens, suggesting that all gene hits specifically improved growth of the *eaf1Δ* background and not the WT background (S3.3 Fig.).

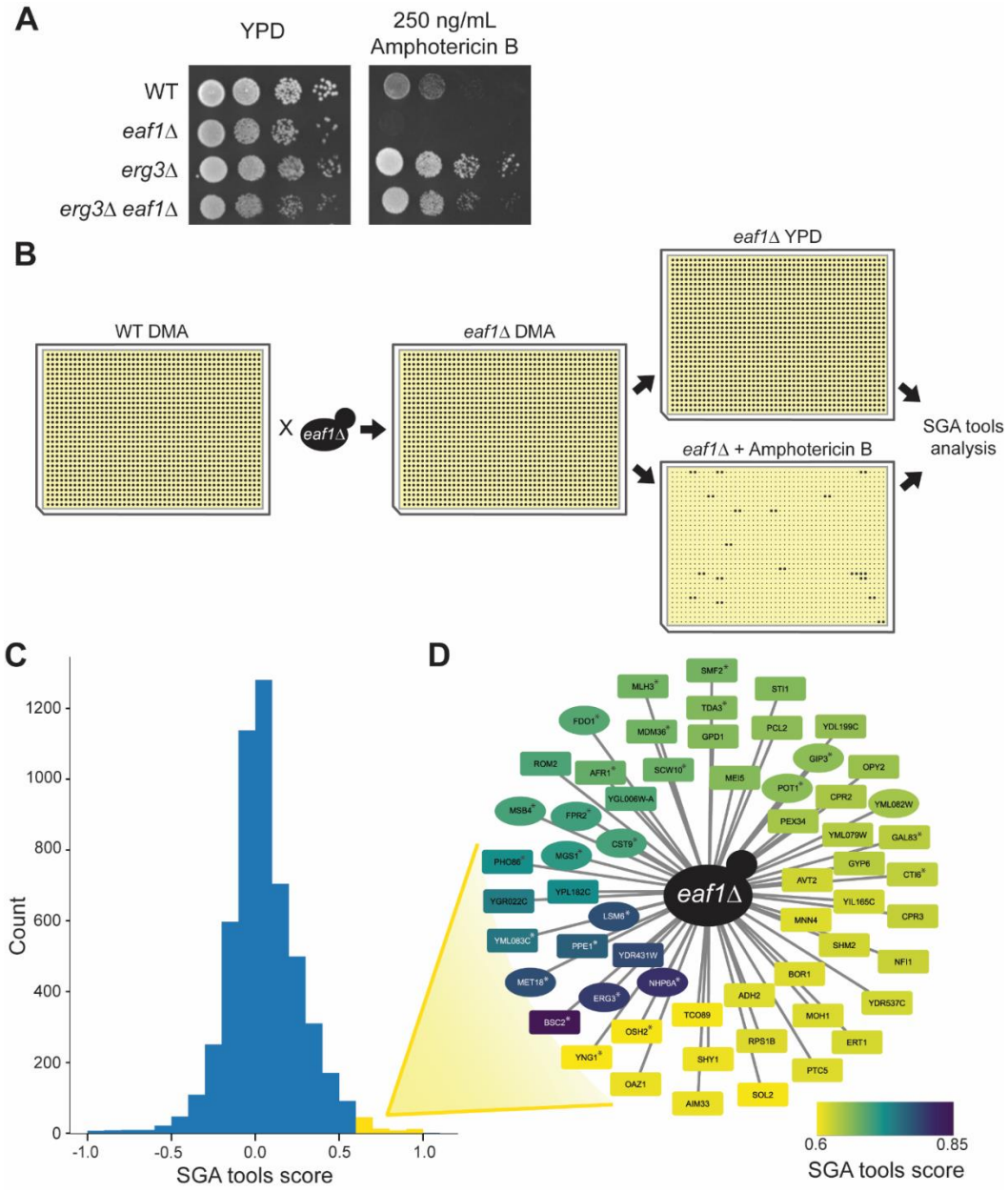

Figure 3.4: Yeast chemogenomic screen for genes which reverse the sensitivity of the *eaf1Δ* to amphotericin B. A) The *erg3Δ eaf1Δ* double mutant reverses the sensitivity of *eaf1Δ* yeast to amphotericin B. WT, *eaf1Δ, erg3Δ*, and *erg3Δ eaf1Δ* yeast were grown to mid-log in liquid YPD before being spotted onto solid YPD with or without a series of ergosterol targeting compounds. The strains were spotted in serial dilutions beginning at 0.1 and three 10-fold dilutions from there onto the plates. These spots were then allowed to grow for 48h. Images are representative of three replicates. B)

Schematic of the creation of the *eaf1Δ* collection, screening on amphotericin B, and SGA tools analysis. The screen was performed for 2 biological replicates with 2 side by side technical replicates per plate. C) A histogram of the SGA tools scores generated from the *eaf1Δ* screen. A score of zero represents a strain that grows the same as the background *eaf1Δ* single mutant. Positive scores represent a better growth on amphotericin B than the *eaf1Δ* single mutant and negative scores represent worse growth than the *eaf1Δ* single mutant. Any score above 0.6 was deemed as a top score and a gene deletion that may reverse the sensitivity of the *eaf1Δ* mutant to amphotericin B. These top hits are highlighted in yellow on the histogram and are zoomed in and listed in the network diagram in D) Network diagram of top hits which reversed the sensitivity of the *eaf1Δ* mutant to amphotericin B. Hits are colour coded on a heat map style scale for the SGA tools score of 0.6 to 0.85. Twenty-five of the top hits were selected for follow-up study, these are denoted by *. Hits in oval shapes were top identified hits after confirmation by PCR and dot assay on amphotericin B.

Following our initial screen, 25 of the top hits of interest were confirmed through secondary dot assays on amphotericin B and the identity of the deletion mutant was confirmed by PCR (Figure 3.4D and S3.4 Fig). These 25 hits were selected as they were either the hits with the highest score or hits of interest selected based on their previous association to NuA4 or cellular lipids. For the dot assays, the growth of the double mutant (*eaf1Δ genexΔ*) was compared to the growth of the single DMA mutant (*genexΔ*), the single *eaf1Δ*, and to the WT BY4741 strain. Twelve of the top hits were confirmed by PCR and both replicates had a strong reversal of sensitivity to amphotericin B. An additional six strains had a weak reversal in amphotericin B sensitivity and the final seven either did not reverse the sensitivity of the *eaf1Δ* mutant in the dot assays or failed to be confirmed by PCR (S3.4 Fig. and S3.2 Table). Of the strongest hits, we selected *ERG3*, *POT1*, *GAL83*, *GIP3*, and *AFR1* for further assessment. *ERG3* was selected as it had one of the highest SGA scores. *GAL83*, *GIP3*, and *AFR1* were selected as they are all associated somehow with Snf1, which has previous associations with NuA4 regulation through Sip2 [60]. Gal83 is a direct regulator of Snf1 [268]. Gip3 and Afr1 are regulators of Glc7, which dephosphorylates and inactivates Snf1 kinase [269]. Finally, Pot1, a 3-ketoacyl-CoA thiolase, was selected as its activity produces acetyl-CoA, linking Pot1 to potential acetylation activity. All of the selected double mutants were able to reverse the sensitivity of the *eaf1Δ* to fluconazole, nystatin, and amphotericin B while not affecting the sensitivity of the other inhibitors (Figure 3.5). As many of the hits showed links to Snf1, and regulation by NuA4 through Sip2 acetylation has been previously demonstrated, we tested whether deletion of Snf1 could

reverse the sensitivity of the *eaf1Δ* mutant to amphotericin B. We found that the *snf1Δ eaf1Δ* grew similarly to the *eaf1Δ* alone and worse than the *snf1Δ* alone suggesting that the regulation of ergosterol by NuA4 may be independent of Snf1 signalling (Figure 3.6).

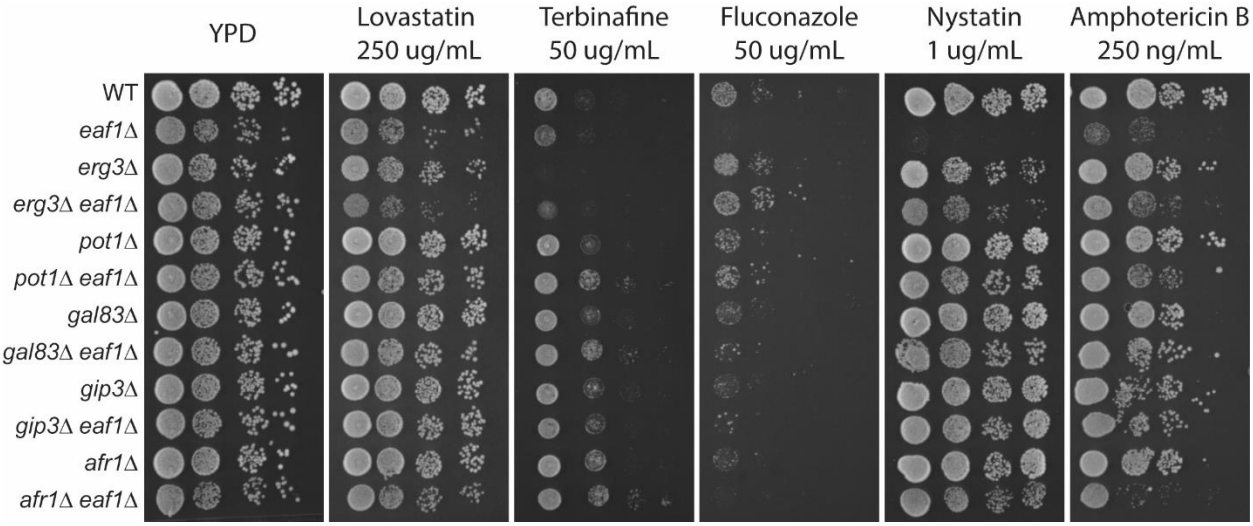

Figure 3.5: Top suppressors of *eaf1Δ* sensitivity to amphotericin B also reverse the sensitivity of the *eaf1Δ* to other ergosterol pathway targeting drugs. Indicated yeast strains were grown to mid log in liquid YPD before being spotted onto solid YPD with or without a series of ergosterol targeting compounds. The strains were spotted in serial dilutions beginning at 0.1 and three 10-fold dilutions from there onto the plates. These spots were then allowed to grow for 48 h and images were taken. Images are representative of three replicates.

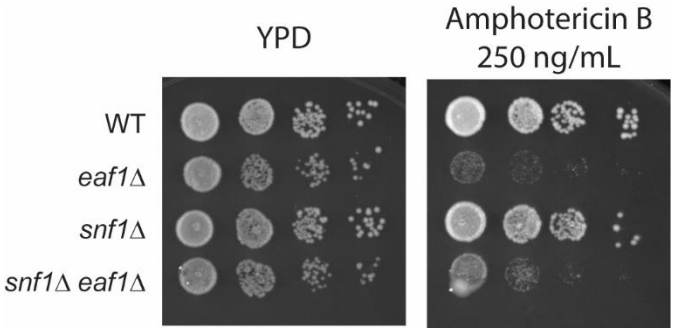

Figure 3.6: The *snf1Δ eaf1Δ* double mutant was unable to restore growth on amphotericin B. WT, *eaf1Δ, snf1Δ*, and *snf1Δ eaf1Δ* yeast were grown to mid log in liquid YPD before being spotted onto solid YPD with or without amphotericin B. The strains were spotted in serial dilutions beginning at 0.1 and three 10-fold dilutions from there onto the plates. These spots were then allowed to grow for 48 h and images were taken. Images are representative of three replicates.

3.5 Discussion

The presented research confirms that NuA4 plays a role in the regulation of ergosteryl esters as well as providing evidence that free ergosterol is also regulated through this KAT complex. Deletion of *EAF1* was associated with an altered sensitivity to drugs which target ergosterol and ergosterol biosynthesis and *eaf1Δ* cells display an increased filipin staining of free ergosterol at the membrane. Gas Chromatography coupled with mass spectrometry analysis found a small change in ergosterol content in *eaf1Δ* cells but an even more prominent increase in ergosterol biosynthesis intermediates (Figure 3.1). The change in cellular ergosterol is further confirmed by the fact that deleting *ERG3*, which reduces ergosterol biosynthesis, was able to reverse the sensitivity of the *eaf1Δ* yeast to amphotericin B and nystatin (Figure 3.4 and 3.5).

Interestingly, Munkacsi and colleagues first implicated NuA4 and lysine acetylation in ergosterol regulation through assessment of gene deletions which affected the sterol auxotrophy lethality in combination with deletion of the Niemann-pick type c related gene deletion, *ncr1Δ* [244]. In the Munkacsi study, the *ncr1Δ eaf1Δ* double mutant had a phenotype of anaerobic inviability and an altered sterol profile. The observed phenotype was also observed for another NuA4 component gene *yaf9Δ.* The

conditions of the double mutant lethality were consistent with NuA4 compensating for the accumulation of toxic metabolites in the *ncr1Δ.* Our work additionally indicates that the deletion of *EAF1* alone causes a disruption in the sterol profile of yeast which may exacerbate problems of the *ncr1Δ.* While the work from Munkacsi and colleagues did not identify changes in either of the single mutants, they observed changes in the sterol profile of the *ncr1Δ eaf1Δ* double mutant, specifically an increased abundance of squalene, lanosterol, zymosterol, and fecosterol. Our work suggests that an altered sterol profile may be driven by the disruption of NuA4, as we identified changes in ergosterol biosynthesis intermediates in the *eaf1Δ* alone. Perhaps the observed alteration of sterol composition in the *eaf1Δ* single mutant was observed due to the more targeted lipid extraction methodology used our study.

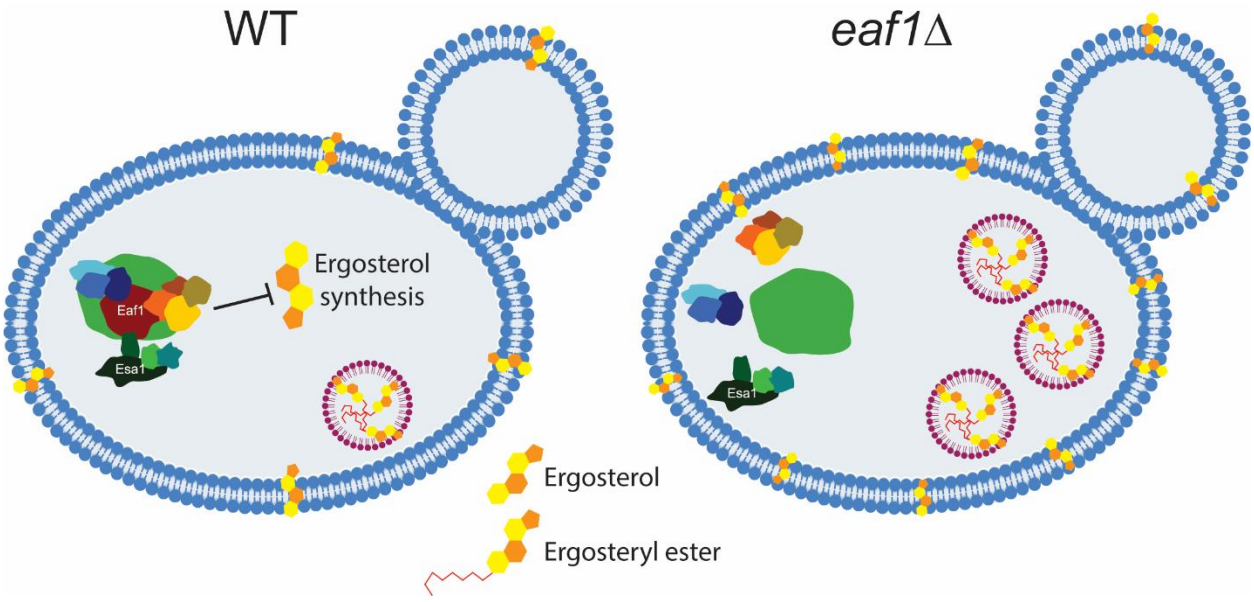

Figure 3.7: Model of NuA4 regulation of ergosterol dynamics in the cell.

How could NuA4 be regulating ergosterol?

Since ergosterol biosynthesis is partially transcriptionally regulated it might be assumed that the change in ergosterol abundance was due to NuA4's known role in gene transcription. While we have not directly excluded this hypothesis, we did not observe a difference in the abundance of ergosterol

biosynthesis proteins by microscopy (Figure 3.3 and S3.2 Fig.) and previous microarray analysis found no change in the transcription of most of the ergosterol biosynthesis genes, although *ERG3* and *ERG6* did have a modest approximately 1.5 fold increase in gene expression in an *eaf1Δ* [67]. Though NuA4 has been implicated in the regulation of subcellular localization of numerous metabolic enzymes [106], we did not detect any changes in the subcellular localization of ergosterol biosynthesis proteins in *eaf1Δ* cells. An alternative possibility is that NuA4 is impacting ergosterol through Acc1 and elevated acetyl-CoA levels [151,173]. Intriguingly a screen for mutant genes which altered the sensitivity of yeast to amphotericin B also identified Acc1 [270]. However, we found that the hyperactive mutant of Acc1 which decreases acetyl-CoA levels was unable to restore the amphotericin B sensitivity of the *eaf1Δ* mutant, suggesting that the increase in ergosterol biosynthesis in *eaf1Δ* yeast is not due to a decrease in acetyl-CoA, allowing for a flux of acetyl-CoA into the ergosterol biosynthesis pathway.

Our initial screen identified 61 genes deletions which were able to improve the growth of the *eaf1Δ* cells on amphotericin B. The reversal of the growth defect suggests that these genes were able to reduce the accumulation of free ergosterol or its precursors in an *eaf1Δ* background. The validity of the screen was highlighted by *ERG3* being one of the predominant hits. Indeed, previous screens in *S. cerevisiae* and drug resistance work in *Candida* species identified deletion or downregulation of *ERG3* as a mechanisms of resistance to amphotericin B [263,271,272].

In secondary assays we confirmed 18 deletion mutants reversed *eaf1Δ* sensitivity to amphotericin B and further confirmed that 5 deletion mutants, *ERG3, POT1, GAL83, AFR1* and *GIP3*, were able to reverse the sensitivity to Nystatin and Fluconazole. The observed reversal suggests that these gene deletions were able to either compensate for or reverse the accumulation of ergosterol upon deletion of *EAF1*. *POT1* encodes one of the two yeast thiolases, the other of which is Erg10 [273]. Pot1 functions in the beta-oxidation of fatty acids to cleave 3-ketoacyl-CoA into acyl-CoA and acetyl-CoA [274]. Theoretically by deleting *POT1*, the pool of acetyl-CoA could be reduced, which could in turn reduce the substrate abundance for ergosterol biosynthesis. Another hit was *GAL83* which encodes one of the three alternate

beta-subunits of the Snf1 (AMPK) kinase in yeast. This is intriguing as Gal83 is a paralog of Sip2 [275,276], and Sip2 was one of the first identified non-histone targets of NuA4 acetylation [60]. While Sip2 is important for inhibiting Snf1 activity, Gal83 is important for modulating Snf1 activity and nuclear localization [277]. Sip2 and Gal83 may have some overlapping functions but they have been demonstrated to have differential relocalization and functions of Snf1 upon glucose depletion [278]. Indeed, of the three B-subunits, deletion of Gal83 has been associated with the largest changes in cellular gene expression [279]. Therefore, the proposed alteration in Snf1 activity an *eaf1Δ* may be alleviated by deletion of *GAL83* [279]. Additionally, the deletion of Snf1 beta subunits is associated with an increase in the expression of a larger number of ergosterol biosynthesis genes [279]. Zhang and colleagues suggest that Snf1 represses ergosterol biosynthesis under glucose limiting [279]. Consistent with our identification of Gal83 but not Sip2 in the screen, Zhang and colleagues also found that Gal83 was more important than Sip2 in regulation of ergosterol biosynthesis genes.

Further, we were intrigued to find *AFR1* and *GIP3*, both of which are involved in the regulation of Glc7, as some of our top hits. Glc7, dephosphorylates and inactivates Snf1 kinase in glucose rich conditions [269]. While *GLC7* itself was not in our screen because it is essential, previous work has shown that *GLC7* is also synthetic dosage lethal with the *eaf1Δ* [111]. While many of these hits are associated with Snf1, we found that deleting *SNF1* itself was unable to restore the sensitivity of the *eaf1Δ* mutant to amphotericin B to a level of WT cells (Figure 3.6). This suggests that the previously characterized increase in Snf1 activity in an *eaf1Δ* mutant is not the cause of the increased ergosterol content of these cells but does not fully eliminate altered Snf1 activity as having an impact.

Through our screen we aimed to determine the mechanism by which NuA4 regulates ergosterol dynamics. Interestingly, there were a number of possible avenues of ergosterol regulation in an *eaf1Δ* which our screen did not identify as important. First, ergosterol storage and transport. In terms of storage, Tip60 (also known as KAT5 and the human homolog of NuA4) was recently identified to play a role in the lipolysis of lipid droplets in humans through

acetylation of the choline kinase, CHKα2[280]. Liu and colleagues did not directly assess how this Tip60 dependent lipolysis affects cellular stores of cholesteryl esters, but their work creates an interesting link between Tip60 and cholesteryl/ergosteryl ester storage in humans. While our work does not specifically address whether NuA4 plays a similar role in the regulation of lipolysis, we do see an accumulation of lipid droplets in the *eaf1Δ*. However, the deletion mutants of the yeast homologs of CHKα2, Cki1 and Eki1, were in our screen and were unable to reverse the sensitivity of the *eaf1Δ* to amphotericin B (Supplemental Table 2). In terms of ergosterol transport, only *OSH2*, a gene expressing one of the oxysterol binding proteins [281,282], was identified as a potential hit but in follow up assays it was not one of the strongest candidates with inconsistent phenotype reversal. In terms of ergosterol biosynthesis, while *ERG3* was identified as one of the strongest hits of the screen, there was no general enrichment of ergosterol biosynthesis genes. This is likely because of redundancy and flexibility within the non-essential genes in the pathway as well as a large number of ergosterol biosynthesis genes being essential and therefore excluded from our screen [229–231]. Finally, the high sensitivity of the *eaf1Δ* to amphotericin B meant that most of the *eaf1Δ* DMA double mutants had very little growth on the screening plates. Therefore, our screen focused on genes which reversed the sensitivity of the *eaf1Δ* to amphotericin B not those which increased the sensitivity of the *eaf1Δ* to amphotericin B.

An additional potential avenue of future assessment is the role of ergosterol in the stress response in NuA4 mutants. NuA4 mutants have many phenotypes which are also associated with a stressed state of the cell [59,80,106] and ergosterol is a very important molecule in maintaining cell integrity in the stress

response of cells [229,239–241]. It could therefore be interesting to study the role of NuA4 dependent regulation of ergosterol in stress conditions.

3.6 Conclusions

The presented research study implicates NuA4 in the regulation of ergosteryl esters and free ergosterol. This regulation is dependent on ergosterol biosynthesis as deletion of *ERG3* reduced the accumulation of ergosterol and ergosterol biosynthesis intermediates in *eaf1Δ* yeast and reversed the sensitivity of the *eaf1Δ* to ergosterol targeting compounds. As other NuA4 dependent regulations have been found to be conserved to Tip60 in the human system [52,53], NuA4 dependent regulation of ergosterol dynamics may have an important translational impact to the regulation of cholesterol. Indeed, research by Munkasci and colleagues found that treating NPC-26 fibroblasts with an HDAC/KDAC inhibitor was associated with a reduction in filipin staining [244], consistent with the inhibition of the opposing process that we assessed here with NuA4 mutants. Therefore, as HDAC/KDAC inhibitors continue to be tested in the clinic [36,283], perhaps a more specific role for NuA4/Tip60 acetylation in cholesterol regulation and overall metabolic control should be assessed.

3.7 Data Availability Statement

Relevant data are within the manuscript and its Supporting Information files. Full raw data of the Screen is in the Supplemental tables, anything else is available upon request.

3.8 Funding

This work was supported by a grant from the Canadian Institutes of Health Research (CIHR; http://www.cihr-irsc.gc.ca/e/193.html) to KB (MOP-142403). EW was supported by the Natural Sciences

and Engineering Research Council (NSERC) Postgraduate Scholarships-Doctoral program and an Ontario Graduate Scholarship.

3.9 Conflict of Interest

The authors have no conflicts of interest to declare.

Chapter 4: General Discussion

4.1 Overview of the Thesis work

Our understanding of the functions of NuA4 and Tip60 in the cell has progressed significantly since their initial characterization at the end of the 20th century [58,81,83]. The early characterized role of histone acetylation has been massively expanded upon and roles for these protein complexes have now been found in diverse pathways across the cell ranging from additional roles in chromatin organization including in DNA damage repair, to novel non-histone regulation including regulation of gluconeogenesis and aging [59,60]. The research in this thesis specifically characterizes novel roles for the lysine acetyltransferase complex NuA4 in the regulation of metabolic pathways in *Saccharomyces cerevisiae*.

The first aim of this thesis was to identify metabolic proteins whose localization or abundance are dependent on NuA4 activity. To complete this aim, we screened 368 GFP-tagged metabolic proteins and identified 23 as high confidence hits for change in localization or abundance upon deletion of *EAF1* and therefore disruption of the NuA4 complex (Chapter 2). Follow up from the screen addressed key hits identified through characterizing changes in the localization/abundance of glycogen synthesis and mitochondrial proteins upon deletion of *EAF1*. This led us to characterize a NuA4 dependent regulation of the localization of Bcy1, the regulatory subunit of yeast PKA, and by extension the regulation of PKA activity which downstream regulates the mitochondria and glycogen synthesis in Aim 1B (Chapter 2). Aim 2 was motivated by parallel work in our lab in which we identified a change in the localization of Acc1, the first step in *de novo* lipid synthesis, upon deletion of *EAF1* (Appendix A). This prompted an investigation into NuA4 dependent lipid regulation, specifically this thesis explored a role in ergosterol dynamics, and our data supports a flux through the ergosterol biosynthesis pathway as well as an associated storage of ergosteryl esters.

4.1.1 NuA4 regulation of metabolic protein localization and abundance

Through the combination of the GFP-screen performed in Chapter 2 and the work on Acc1 performed in Appendix A, the Baetz lab has identified 24 new metabolic proteins which change localization or abundance with high confidence upon deletion of *EAF1*, as well as almost 50 proteins with possible yet to be confirmed changes. Additionally, the localization and abundance of ergosterol biosynthesis (ERG) proteins upon deletion of *EAF1* was assessed in Chapter 3 but no significant changes were identified. This group of work supports that NuA4 plays a role in the regulation of metabolic processes including mitochondrial structure and glycogen synthesis through impacting protein localization and abundance. While changes in transcriptional regulation by NuA4 [67] had been previously assessed, the ability to screen *in vivo* changes in protein localization as impacted by mutations is a relatively new procedure [41]. So called phenomic screening for protein localization is made possible by the ease of genetic manipulation of yeast and the existence of GFP-tagged protein collections, and was first published as a high throughput analysis by Chong and colleagues in 2015 [41]. Chong *et. al.* investigated the effect of two chemical inhibitors, as well as deletion of the yeast KDAC *RPD3,* on proteome wide protein localization. Deletion of *RPD3* affected the abundance of a large portion of proteins, while a change in subcellular localization in the *rpd3Δ* mutant background was characterized for only approximately 30 proteins [41]. Our targeted screen of 368 selected metabolic proteins identified 23 protein changes upon deletion of *EAF1*, a number on par with the whole proteome screen performed on the *rpd3Δ* collection. Intriguingly, although in many recorded cases Rpd3 and NuA4 function in opposition [60,120,138], with the exception of Acs2-GFP, there was little overlap in the changes in localization identified in the two screens [41,106]. It is possible that a proteome wide screen using the *eaf1Δ* may increase the number of common proteins identified between the *rpd3Δ* and *eaf1Δ* screens. In terms of comparison, both proteome wide and mini targeted screens have benefits and drawbacks [284]. An automated proteome wide screen has the obvious benefit of coverage, there are simply more proteins to explore. For that reason, and since we did identify changes in our targeted mini screen, it would be interesting in the future to perform a genome wide screen to assess effect of the deletion of *EAF1* on the proteome beyond our selected 368 metabolic

proteins. However, there are also merits to our targeted mini screen. In fact, it is likely that we were only able to identify the mitochondrial elongation and nuclear elongation phenotypes in our screen because all changes were assessed both computationally for abundance and manually for abundance and localization changes. The structural changes in the mitochondria and nucleus may have been missed in a high-throughput genome-wide screen with machine learning classification as the machine learning algorithm previously used was trained only on canonical structures of these compartments [41]. Therefore, the classification algorithm likely lacks the ability to classify a change in the structure of the mitochondria or nucleus as these structures were not represented in the training data. It is therefore likely that the high throughput machine learning algorithm would have either missed these structural changes or would have misclassified the localization of the GFP protein to another cellular compartment.

A role for NuA4 in the relocalization of proteins may have important implications for our understanding of Tip60 cellular roles, especially as Tip60 activity has been associated with the relocalization of proteins. Early research associated Tip60 with a relocalization of p53 from the nucleus to promyelocytic leukemia (PML) bodies [285]. There is also work in prostate cancer research suggesting that Tip60 regulates androgen receptor (AR) localization as Tip60 knockdown led to cytoplasmic AR localization and acetylation mimics on the AR nuclear localization signal led to nuclear AR localization [96]. Finally, more recently, Tip60 dependent acetylation of lipin 1 (Pah1 in yeast) was determined to regulate TAG synthesis by regulating lipin1 relocalization to the ER [53]. This relocation alters lipin 1 activity as at the ER it transforms PA to DAG as a source for TAG synthesis [53]. Importantly, this regulation was conserved in yeast cells [53]. The functionality of lipin 1 relocalization upon Tip60 dependent acetylation in lipid metabolism not only provides an interesting possible link between chapter 2 and 3 of this thesis but also highlights why studying protein relocalization is an important direction in Tip60 research. Until such a time when high-throughput screens for protein localization in human cells are possible, the information we gain in yeast screens, like the one performed in Chapter 2, will provide fundamental information which can be used as a starting point for understanding homologous regulation

in human cells. To this end it will be interesting in the future to determine if Tip60 also regulates mitochondrial structure, glycogen synthesis proteins, or other changes in metabolic protein localization identified in this thesis.

4.1.2 Regulation of PKA by NuA4

Some of the key changes in protein localization and abundance that were identified in our GFP metabolic protein screen were an elongation of the mitochondria and an induction of punctate structures of three glycogen synthesis associated proteins. Both the change in glycogen biosynthesis proteins and the change in mitochondrial proteins upon deletion of *EAF1* were dependent on Bcy1, but even more interestingly, Bcy1 was also one of the original 23 metabolic proteins identified to change localization in our screen. As acetylation on lysine 313 of Bcy1 had previously been proposed [52] we further characterized the change in Bcy1 localization, and the regulation of glycogen and the mitochondria through the use of Bcy1 K313 point mutants. This thesis builds upon previous work which identified protein acetylation as a regulator of the Bcy1-Tpk interaction [52]. Our work suggests that NuA4 regulates PKA activity and Bcy1 localization through Bcy1 K313 acetylation and that this is partially responsible for the regulation of glycogen synthesis and mitochondrial morphology.

PKA activity is a central hub for metabolic control including acting through the Msn2/4 transcription factors [133]. We were therefore intrigued to see that NuA4's regulation of glycogen synthesis was dependent on targets of Msn2/4 and that Msn2 translocates to the nucleus upon deletion of *EAF1,* a common translocation upon stress [132,171,172]. As PKA is the cAMP- dependent cellular kinase, NuA4 dependent regulation of its activity represents modulation of a key metabolic pathway.

4.1.3 NuA4 in lipid metabolism

The final aim of this work was to identify and describe changes in lipid composition dependent on NuA4 activity, specifically detailing a change in ergosterol and ergosteryl ester dynamics in the *eaf1Δ* cell. This work was motivated by parallel work that I co-authored which demonstrates that NuA4

regulates Acetyl-CoA carboxylase 1 (Acc1) activity and localization (Appendix A). Phenotypic changes in Acc1 localization were also found in mutants affecting sphingolipid and very long chain fatty acid metabolism. These links to lipid metabolism motivated us to assess lipid composition of WT and *eaf1Δ* yeast and we found two key changes. First there was an overall reduction in lipid chain lengths in yeast cells deficient for *EAF1*. Second, there was a significant increase in the relative abundance of ergosteryl esters in the *eaf1Δ* cells.

This prompted us to do a deeper assessment into a possible role for the NuA4 complex in the regulation of ergosteryl esters and more broadly ergosterol dynamics. Through our work we found that *eaf1Δ* yeast cells are more sensitive to drugs targeting ergosterol and ergosterol biosynthesis, have increased staining with filipin, contain more ergosterol biosynthesis intermediates, and have more lipid droplets than WT yeast cells. This suggests an increase in both ergosteryl esters and free ergosterol in *eaf1*Δ cells. A further amphotericin B screen to identify molecular mechanisms contributing to increased ergosteryl ester levels in *eaf1*Δ cells identified sixty-one gene deletions which improved *eaf1Δ* growth on amphotericin B and therefore presumably decreased ergosterol content of the cells. From those sixty-one genes 5 top hits, *ERG3, POT1, GAL83, GIP3,* and *AFR1*, were further confirmed to affect *eaf1Δ* yeast sensitivity to other ergosterol inhibitors.

Previous work on NuA4 functions in lipid metabolism had focused on regulation of Kes1 in cell cycle progression and lipid exchange and regulation of Pah1 in TAG synthesis. Interestingly, during the very late stages of this thesis Tip60 (KAT5) was identified to play a role in the lipolysis of lipid droplets in humans through acetylation of the choline kinase, CHKα2 [280]. This aligns well with our work as it further supports our hypothesis that NuA4 affects ergosterol dynamics as well as creating an important link to the human system. This thesis expands this role in lipid metabolism to include ergosterol dynamics in yeast and may have important implications for a similar role of Tip60 in cholesterol dynamics in human disease.

4.1.4 NuA4, a regulator of yeast metabolism

The body of work in this thesis suggests that NuA4 has additional roles in metabolic control within the cell, outside of those previously characterized. Specifically, we found that deleting *EAF1*, to disrupt NuA4 complex structure, led to an elongation of the mitochondria, an increase in glycogen synthesis, and an increase in ergosterol biosynthesis (Figure 4.1). The change in glycogen synthesis was transcriptionally regulated by a relocation of the Msn2/4 transcription factors which in turn are regulated by Tpk (human PKA) activity (Figure 4.1). Interestingly, the mitochondrial elongation was also dependent on Bcy1, the negative regulator of the Tpks, and Bcy1 showed a reduced nuclear localization in the *eaf1Δ* cells. Finally, we identified a NuA4 dependent regulation of ergosterol biosynthesis which was associated with an increased abundance of ergosterol biosynthesis intermediates, increased filipin staining of free ergosterol, and an increased storage of ergosteryl esters in lipid droplets (Figure 4.1). The cumulation of this data adds to the literature knowledge on NuA4 in metabolism and supports a role for NuA4 in regulating diverse metabolic pathways.

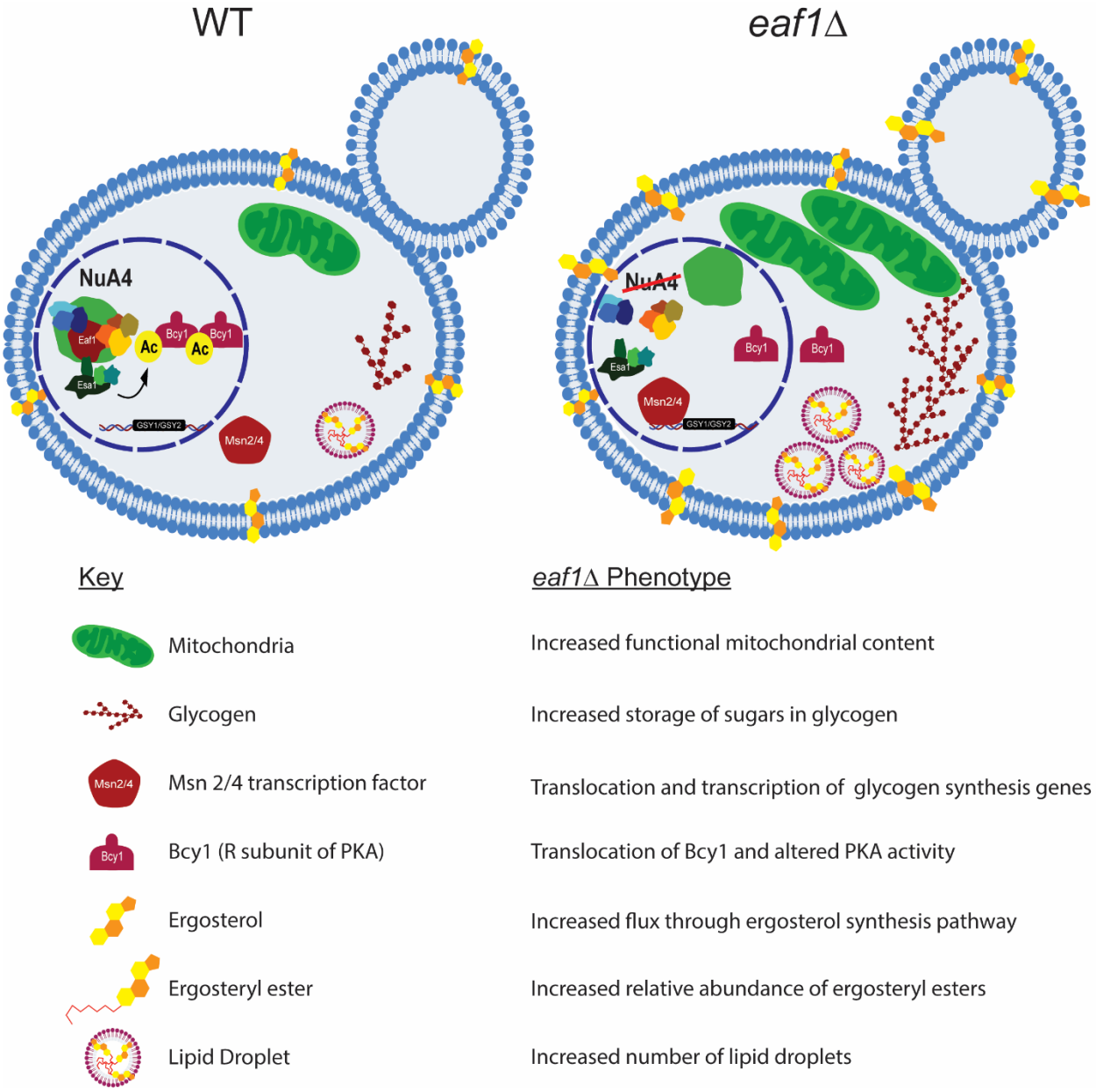

Figure 4.1: Summary of thesis results. Metabolic control by NuA4 is demonstrated in this figure by comparing WT and *eaf1Δ* yeast. Key phenotypes identified in this thesis are shown in the figure and listed on the bottom right.

NuA4 has been previously associated with the stress response pathway [172,180,181], but the addition of this thesis work to the body of knowledge surrounding NuA4 and metabolism supports a possible role in glucose sensing for NuA4. Many of the phenotypes of the *eaf1Δ* and other NuA4 mutants demonstrated in this thesis and the surrounding literature mirror phenotypes associates with changes in glucose

availability. Recent work identified a change in the histone acetylome upon glucose starvation impacting transcription of gluconeogenesis and lipid metabolism genes, but this alteration was dependent on Gcn5 and Rpd3 dependent acetylation regulation [146]. Meanwhile NuA4 may play a role in additional non-histone metabolic control in response to glucose availability. Previous links of NuA4 to glucose sensing include an increased activity of AMPK (Snf1) in NuA4 mutants and an induction of gluconeogenesis [59,60]. In our work we also found many connections. First, PKA is generally activated in high glucose conditions and repressed by galactose [286,287], meanwhile we propose that in our *eaf1Δ*, and NuA4 mutants in general, Bcy1 acetylation is reduced leading to an increased Bcy1-Tpk interaction and reduced PKA (Tpk) activity. Using anti-Phospho-PKA substrate antibodies we found that PKA activity is globally altered in an *eaf1Δ* with a reduction in the phosphorylation of some substrates and an increased phosphorylation of others even in the presence of glucose. Further in glucose starved conditions there was a 30% global reduction in PKA activity in an *eaf1Δ* mutant relative to the WT and the disperse localization of the Bcy1-GFP non-acetylatable mimic (K313R) and Bcy1-GFP in the *eaf1Δ* identified in this thesis appear similar to Bcy1-GFP localization upon glucose deprivation [163,168]. These changes support that NuA4 mutants may impact sensing of the environmental glucose conditions in signalling to PKA and that NuA4 activity may be affected by glucose abundance. Downstream, NuA4 dependent regulation of yeast PKA impacts glycogen storage through translocation and induction of Msn2/Msn4 transcription of glycogen synthesis proteins. The glycogen storage phenotype identified in this thesis is similar to the induction of glycogen storage upon initial starvation of yeast cells, which creates stores that can be degraded once environmental glucose is fully depleted [288]. Other targets of Msn2/Msn4 have also been shown previously to be derepressed in NuA4 mutants [172,180,181] and more recently Msn2 and 4 have been demonstrated to be master regulators of glycolysis [172]. This Msn2/4 derepression and glycogen storage phenotype draws another direct link between NuA4 activity and glucose use. In the future it would be interesting to determine if rates of glycolysis are affected in NuA4 mutants. Our metabolic mitochondrial data showing an increase in oxygen consumption rate (OCR) with the mitochondrial elongation suggests an increase in flux through the oxidative phosphorylation pathway directly downstream of glycolysis which may give

some indication. Unfortunately, while the ratio of glycolysis to oxidative phosphorylation in ATP production can be determined in mammalian cells using the Seahorse extracellular acidification rate (ECAR) technology, this technique is complicated in yeast by fermentation and differences in the effect of inhibitors on the pathway. Novel biosensors may provide information on glycolytic flux in yeast in the future [289]. The mitochondrial elongation phenotype is a bit more of a puzzle as recent work in *Schizosaccharomyces pombe* yeast found that glucose starvation induced mitochondrial fission which was enhanced by low PKA activity. However, the change in mitochondrial length and activity found in our work do still support a change in metabolic sensing [290]. Finally, the regulation of ergosterol has been linked to glucose availability. Recent work showed that acute glucose restriction leads to a relocalization of HMG-CoA proteins, members of the first module of ergosterol biosynthesis, to the nuclear vacuole junction [291]. This starvation induced relocalization is linked to increased flux through the ergosterol biosynthesis pathway similar to what is seen in the *eaf1Δ* cells [291]. Given all these links to glucose sensing, future analysis should delve deeper into investigating whether NuA4 regulates environmental glucose sensing and if the NuA4 mutants are indeed activating survival mechanisms for starvation when glucose is actually abundantly available in the growth environment.

4.2 Techniques in the study of NuA4

Previous to this work, NuA4 function had been probed through transcriptional microarray [67], acetylome profiling [59,153], and genetic interaction screens[79,111] as well as targeted research demonstrating specific roles [53,120]. While some of this work identified metabolism as a target for NuA4 regulation, non-histone targets outside of these studies continued to be identified and research specifically investigating effects on metabolic proteins and lipids had not been performed. Therefore, our work took a combined approach of screening and targeted investigation to uncover additional roles for NuA4 in metabolic control.

In the context of studying NuA4, we use a combination of the *eaf1Δ* mutant and an *esa1-ts* mutant. Benefits of the *eaf1Δ* system are: it is a non-essential deletion mutant which has a significant effect on NuA4 activity, is relatively easy to work with, and Eaf1 is the only member of the NuA4 complex that to date is exclusively shown to function in the NuA4 complex, thereby making research using its deletion specific to NuA4. The fact that Eaf1 is exclusive to the NuA4 complex is important as it can weed out functions by the piccolo NuA4 complex which still function in the *eaf1Δ*. One major drawback of the *eaf1Δ* system is that as an integrated deletion, by the time a phenotype is being assessed, these cells have fully adapted to the mutation. This means that early and direct effects of the disruption of NuA4 activity can be difficult to study in this system and makes cause and effect determinations more difficult. This is where parallel studies with the *esa1-ts* mutant come into play. With this mutant we can assess phenotypes after shifting to a higher temperature on a shorter scale, more similar to the short-term effects of an inhibitor. In experimentation in this thesis, the *esa1-ts* mutant phenocopies the *eaf1Δ* mutant, although generally, with less severe changes relative to the WT. Another set of platforms for NuA4 exploration similar to the temperature sensitive Esa1, are the targeted protein degredation and relocation tools [292]. One such tool is the Esa1 anchor away system [117,293,294]. In the anchor away system Esa1 is tagged with an FRB-tag which upon treatment with rapamycin leads to a depletion of the protein from the nucleus [117,293]. Another tool is the auxin induced degredation (AID) system, where an AID sequence is added to a target protein, in this case Esa1, and the addition of exogenous auxin induces a proteasomal dependent degredation of the target [53,292]. This allows for a timed removal of Esa1 from the cell and therefore timepoint analysis of early effects of Esa1 depletion. These systems provide a way to study function of the Esa1 protein but can also be temperamental to implement and optimize. Indeed, the use of these mutants, especially the anchor away FRB system, may result in unintended consequences such as mistargeting of Esa1 to cytoplasmic targets leading to unintended cellular remodeling. We use the *esa1-ts* system as a secondary confirmation of changes, meanwhile the *eaf1Δ* platform provides a stable study system with many changes in phenotype which are specific to the holo-NuA4 complex and may be more reflective of a Tip60 mutant diseased state.

Pinpointing direct acetylation sites and therefore mechanisms of KAT regulation can be difficult. Our work uses a combination of gene deletions, chemical inhibitions, and point mutations to assess effects of NuA4 activity. Through combining these investigations, we can quickly eliminate pathways which are not involved and narrow in on those which may be affected by NuA4 activity. In terms of studying a specific residue which may be acetylated, one point mutation system that we used to understand possible Bcy1 regulation was substituting the lysine residue of interest for amino acids which mimic an acetylated lysine (Glutamine Q) or mimic a non-acetylatable lysine (Arginine R) (Figure 4.2). With the introduction of CRISPR-Cas9 technology these mutations are more easily created than in the past [225,295]. These acetylation mimicking point mutations are used extensively in the literature and can be a good model to understand how modification of a certain residue may affect protein function, structure, or localization [52,96,116,203] (Figure 4.2). Unfortunately, there are limitations to this model as while the general shape and charge of the Q and R resemble the acetylated and non acetylated state of a lysine residue, there are still differences in the structure which can mean that they do not perfectly phenocopy the acetylation state [134,203] (Figure 4.2). Endogenous expression of these Q/R mimics also create an entirely acetylated or deacetylated population of the target protein while the real stoichiometry of acetylation may affect subpopulations of the target differently as well as interplaying with other post translational modifications [296]. A promising future avenue for explorations of the functions of specific acetylated lysine residues is through the incorporation of noncanonical amino acids into proteins although this technology still has fairly major limitations to its use [203,296,297]. Other available ways to explore specific acetylation sites in the metabolic pathways identified in this thesis in the future would be targeted acetylome profiling through pull downs and mass spectrometry, acetyl-antibody based analysis, or *in vitro* acetyltransferase assays. Future investigations using these techniques may provide more detailed, site specific, mechanistic information for NuA4-dependent regulation of mitochondrial structure, glycogen synthesis, and ergosterol dynamics.

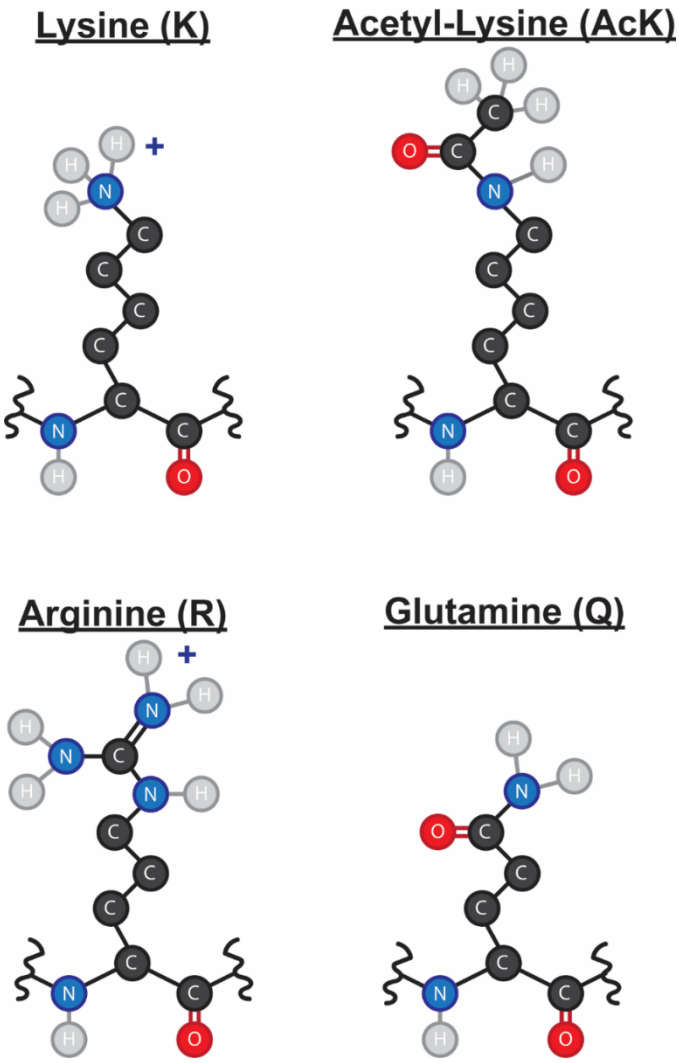

Figure 4.2: Acetylation mimics to study lysine acetylation. Arginine (R.) and Glutamine (Q) are common substitution mutations used to elucidate functions of acetylation at specific lysine residues. Arginine is substituted for lysine to mimic a lysine that cannot be acetylated while glutamine is substituted to mimic a constitutively acetylated lysine residue.

4.3 Implications for NuA4/Tip60 research and human disease

Tip60 deregulation has been linked to complex diseases including cancer and neurodegeneration [61,63,86,96]. Metabolic deregulation is also a common event in these diseases with deregulating cellular metabolism classified as a core hallmark in the recent Hallmarks of Cancer: New Dimensions [298,299]. We are optimistic that the knowledge generated about NuA4 regulation of metabolism in this thesis will be transferrable to human Tip60 functions.

In terms of NuA4 dependent regulation of PKA activity and Bcy1 localization, the work by Filteau and colleagues provides foundational information suggesting this may be conserved to humans [52]. Inhibition of KDACs, overexpression of Tip60, and expression of acetylated mimic RII (the PKA regulator subunit in humans) reduced the formation of the PKA-RII complex in mammalian cells, but no direct testing of this effect on PKA signalling was assessed [52]. Further investigation into if activity of PKA is indeed affected by Tip60 activity could involve knockdown of Tip60 and associated assessment of PKA activity. In addition, these future studies could assess the effect of Tip60 knockdown or overexpression on mitochondrial structure and glycogen storage downstream of potential changes in PKA activity. PKA signalling has been shown to be central to neurodegeneration, metabolic disease, and cancer which our work suggests could also be linked to Tip60 deregulation in these diseases [300–303].

Our work on ergosterol biosynthesis and lipid storage in NuA4 mutants may be of importance to understanding common human diseases associated with cholesterol such as heart disease as well as rare diseases including Niemann Pick Type C disease, a defect in cholesterol storage disease [244,304]. To date, Tip60 has only been tangentially associated with cholesterol through an interaction of Tip60 with cleaved amyloid precursor protein intracellular domain (AICD) affecting LRP1 transcription, which in turn is responsible for cholesterol homeostasis [243]. Meanwhile two NuA4 complex mutants, *eaf1Δ* and *yaf9Δ*, were identified as necessary in a yeast model of Niemann Pick Type C and follow up work demonstrated that HDAC inhibitors were effective at reversing some of the phenotypes of NPC in human cells (46, 47). Our work additionally suggests a potential role for Tip60 in cholesterol biosynthesis and storage through cholesteryl esters. Overall, the implications of future research on the effects of Tip60 on PKA activity, mitochondrial structure, glycogen storage, and cholesterol dynamics may provide further insights into complex human diseases.

Finally, thus far we have focused directly on implications in disease through Tip60 activity in human cells, but roles for NuA4 in pathogenic yeast/fungi may be an additional area of future research with relevance to human and agricultural infection. First, PKA activity contributes to virulence in

pathogenic fungi [305]. Therefore, modulation of PKA activity through acetylation could be used to target infection. Additionally, as previously discussed, ergosterol is a specific target of many current antifungals [230,232,247] . Our work using these antifungal inhibitors and specifically our amphotericin B screen implicates NuA4 in ergosterol regulation in *Saccharomyces cerevisiae*, and as there is high conservation of NuA4 to other fungal organisms, this information may be relevant to NuA4 activity in the drug resistance of fungal pathogens. Indeed, recent work has implicated Tra1, another central member of the NuA4 complex, in pathogenesis traits of *Candida albicans*, the pathogen responsible for most deaths from fungal infection [306]. While transcriptional changes in NuA4 mutants may explain some of the changes in drug resistance, it will be interesting in the future to determine if non-histone targets of NuA4 may also play an important role in fungal infections and the development of drug resistance.

4.4 Conclusions

In this thesis I use a combination of targeted analysis and large-scale yeast screens to characterize novel roles of NuA4 in yeast metabolic control. The combination of these techniques resulted in the identification of changes in protein localization, changes in glycogen storage, a mitochondrial elongation phenotype, altered PKA activity, and changes in ergosterol dynamics in the NuA4 mutant *eaf1Δ* when compared to WT yeast.

Future work on the subject of NuA4 in metabolic control should focus on further characterizing direct mechanisms of NuA4 dependent regulation of PKA and lipid homeostasis. Identification of direct Esa1-dependent acetylation of the identified targets or members of their pathway would strengthen this body of knowledge and deepen our mechanistic understanding of the NuA4 dependent regulation of these metabolic pathways. This could provide additional insight into possible equivalent Tip60 dependent acetylation mechanisms of homologous human acetylation sites which may be deregulated in human disease. Finally, while we show in this thesis that acetylation is important in metabolic control of PKA,

glycogen, mitochondria, and lipid biology, acetylation is a reversible process. Therefore, it is likely that protein deacetylation is also regulating homeostasis in these processes, and it will be interesting to determine which KDAC(s) may be important for opposing NuA4 in metabolic control.

References

1. Choudhary C, Weinert BT, Nishida Y, Verdin E, Mann M. The growing landscape of lysine acetylation links metabolism and cell signalling. Nature Reviews Molecular Cell Biology. 2014;15(8):536–550. http://dx.doi.org/10.1038/nrm3841. doi:10.1038/nrm3841

2. Gil J, Ramírez-Torres A, Encarnación-Guevara S. Lysine acetylation and cancer: A proteomics perspective. Journal of Proteomics. 2017;150:297–309. http://dx.doi.org/10.1016/j.jprot.2016.10.003. doi:10.1016/j.jprot.2016.10.003

3. Morales-Tarré O, Alonso-Bastida R, Arcos-Encarnación B, Pérez-Martínez L, Encarnación-Guevara S. Protein lysine acetylation and its role in different human pathologies: a proteomic approach. Expert Review of Proteomics. 2021;18(11):949–975. https://doi.org/10.1080/14789450.2021.2007766. doi:10.1080/14789450.2021.2007766

4. Weinert BT, Iesmantavicius V, Moustafa T, Schölz C, Wagner SA, Magnes C, Zechner R, Choudhary C. Acetylation dynamics and stoichiometry in S accharomyces cerevisiae. Molecular Systems Biology. 2014;10(1):716. https://onlinelibrary.wiley.com/doi/10.1002/msb.134766. doi:10.1002/msb.134766

5. Drazic A, Myklebust LM, Ree R, Arnesen T. The world of protein acetylation. Biochimica et Biophysica Acta - Proteins and Proteomics. 2016;1864(10):1372–1401. http://dx.doi.org/10.1016/j.bbapap.2016.06.007. doi:10.1016/j.bbapap.2016.06.007

6. Brown JL, Roberts WK. Evidence that approximately eighty per cent of the soluble proteins from Ehrlich ascites cells are Nα acetylated. Journal of Biological Chemistry. 1976;251(4):1009–1014. http://dx.doi.org/10.1016/S0021-9258(17)33793-6. doi:10.1016/s0021-9258(17)33793-6

7. Helsens K, Van Damme P, Degroeve S, Martens L, Arnesen T, Vandekerckhove J, Gevaert K. Bioinformatics analysis of a Saccharomyces cerevisiae N-terminal proteome provides evidence of alternative translation initiation and post-translational N-terminal acetylation. Journal of Proteome Research. 2011;10(8):3578–3589. doi:10.1021/pr2002325

8. Allfrey VG, Faulkner R, Mirsky AE. Acetylation and methylation of histones and their possible role in the regulation of RNA synthesis. Proceedings of the National Academy of Sciences. 1964;51(5):786–794. https://pnas.org/doi/full/10.1073/pnas.51.5.786. doi:10.1073/pnas.51.5.786

9. Verdin E, Ott M. 50 years of protein acetylation: From gene regulation to epigenetics, metabolism and beyond. Nature Reviews Molecular Cell Biology. 2015;16(4):258–264. http://dx.doi.org/10.1038/nrm3931. doi:10.1038/nrm3931

10. Narita T, Weinert BT, Choudhary C. Functions and mechanisms of non-histone protein acetylation. Nature Reviews Molecular Cell Biology. 2019;20(March):156–174. http://dx.doi.org/10.1038/s41580-018-0081-3. doi:10.1038/s41580-018-0081-3

11. Glozak MA, Sengupta N, Zhang X, Seto E. Acetylation and deacetylation of non-histone proteins. Gene. 2005;363(1–2):15–23. doi:10.1016/j.gene.2005.09.010

12. Allis CD, Berger SL, Cote J, Dent S, Jenuwien T, Kouzarides T, Pillus L, Reinberg D, Shi Y, Shiekhattar R, et al. New Nomenclature for Chromatin-Modifying Enzymes. Cell. 2007;131(4):633–636. doi:10.1016/j.cell.2007.10.039

13. Haberland M, Montgomery RL, Olson EN. The many roles of histone deacetylases in development and physiology: Implications for disease and therapy. Nature Reviews Genetics. 2009;10(1):32–42. doi:10.1038/nrg2485

14. Wagner GR, Payne RM. Widespread and enzyme-independent Nε-acetylation and Nε-succinylation

of proteins in the chemical conditions of the mitochondrial matrix. Journal of Biological Chemistry. 2013;288(40):29036–29045. doi:10.1074/jbc.M113.486753

15. Thapa D, Zhang M, Manning JR, Guimarães DA, Stoner MW, O'Doherty RM, Shiva S, Scott I. Acetylation of mitochondrial proteins by GCN5L1 promotes enhanced fatty acid oxidation in the heart. American Journal of Physiology-Heart and Circulatory Physiology. 2017;313(2):H265–H274. doi:10.1152/ajpheart.00752.2016

16. Fan J, Shan C, Kang HB, Elf S, Xie J, Tucker M, Gu TL, Aguiar M, Lonning S, Chen H, et al. Tyr Phosphorylation of PDP1 Toggles Recruitment between ACAT1 and SIRT3 to Regulate the Pyruvate Dehydrogenase Complex. Molecular Cell. 2014;53(4):534–548. doi:10.1016/j.molcel.2013.12.026

17. Baeza J, Smallegan MJ, Denu JM. Mechanisms and Dynamics of Protein Acetylation in Mitochondria. Trends in Biochemical Sciences. 2016;41(3):231–244. https://linkinghub.elsevier.com/retrieve/pii/S096800041500256X. doi:10.1016/j.tibs.2015.12.006

18. Anderson KA, Hirschey MD. Mitochondrial protein acetylation regulates metabolism. Essays In Biochemistry. 2012;52:23–35. http://essays.biochemistry.org/lookup/doi/10.1042/bse0520023. doi:10.1042/bse0520023

19. Lombard DB, Alt FW, Cheng H-L, Bunkenborg J, Streeper RS, Mostoslavsky R, Kim J, Yancopoulos G, Valenzuela D, Murphy A, et al. Mammalian Sir2 Homolog SIRT3 Regulates Global Mitochondrial Lysine Acetylation. Molecular and Cellular Biology. 2007;27(24):8807–8814. doi:10.1128/mcb.01636-07

20. Coffey K, Blackburn TJ, Cook S, Golding BT, Griffin RJ, Hardcastle IR, Hewitt L, Huberman K, McNeill H V., Newell DR, et al. Characterisation of a Tip60 Specific Inhibitor, NU9056, in Prostate Cancer. PLoS ONE. 2012;7(10). doi:10.1371/journal.pone.0045539

21. Zhang R, Erler J, Langowski J. Histone Acetylation Regulates Chromatin Accessibility: Role of H4K16 in Inter-nucleosome Interaction. Biophysical Journal. 2017;112(3):450–459. doi:10.1016/j.bpj.2016.11.015

22. Wilkins BJ, Rall NA, Ostwal Y, Kruitwagen T, Hiragami-Hamada K, Winkler M, Barral Y, Fischle W, Neumann H. A cascade of histone modifications induces chromatin condensation in mitosis. Science. 2014;343(6166):77–80. doi:10.1126/science.1244508

23. Zeng L, Zhang Q, Li S, Plotnikov AN, Walsh MJ, Zhou M-M. Mechanism and regulation of acetylated histone binding by the tandem PHD finger of DPF3b. Nature. 2010;466(7303):258–262. http://www.nature.com/articles/nature09139. doi:10.1038/nature09139

24. Schulze JM, Wang AY, Kobor MS. Reading chromatin: Insights from yeast into yeats domain structure and function. Epigenetics. 2010;5(7):573–577. doi:10.4161/epi.5.7.12856

25. Filippakopoulos P, Picaud S, Mangos M, Keates T, Lambert JP, Barsyte-Lovejoy D, Felletar I, Volkmer R, Müller S, Pawson T, et al. Histone recognition and large-scale structural analysis of the human bromodomain family. Cell. 2012;149(1):214–231. doi:10.1016/j.cell.2012.02.013

26. Dhalluin C, Carlson JE, Zeng L, He C, Aggarwal AK, Zhou MM. Structure and ligand of a histone acetyltransferase bromodomain. Nature. 1999;399(6735):491–496. doi:10.1038/20974

27. Gu W, Roeder RG. Activation of p53 sequence-specific DNA binding by acetylation of the p53 C-terminal domain. Cell. 1997;90(4):595–606. doi:10.1016/S0092-8674(00)80521-8

28. Maruta H, Greer K, Rosenbaum JL. The acetylation of alpha-tubulin and its relationship to the assembly and disassembly of microtubules. Journal of Cell Biology. 1986;103(2):571–579. doi:10.1083/jcb.103.2.571

29. Spange S, Wagner T, Heinzel T, Krämer OH. Acetylation of non-histone proteins modulates cellular signalling at multiple levels. International Journal of Biochemistry and Cell Biology. 2009;41(1):185–198. doi:10.1016/j.biocel.2008.08.027

30. Sun B, Guo S, Tang Q, Li C, Zeng R, Xiong Z, Zhong C, Ding J. Regulation of the histone acetyltransferase activity of hMOF via autoacetylation of Lys274. Cell Research. 2011;21(8):1262–1266. doi:10.1038/cr.2011.105

31. Santos-Rosa H, Valls E, Kouzarides T, Martínez-Balbás M. Mechanisms of P/CAF auto-acetylation. Nucleic Acids Research. 2003;31(15):4285–4292. doi:10.1093/nar/gkg655

32. Ali I, Conrad RJ, Verdin E, Ott M. Lysine Acetylation Goes Global: From Epigenetics to Metabolism and Therapeutics. Chemical Reviews. 2018;118(3):1216–1252. doi:10.1021/acs.chemrev.7b00181

33. Sterner DE, Berger SL. Acetylation of Histones and Transcription-Related Factors. Microbiology and Molecular Biology Reviews. 2000;64(2):435–459. doi:10.1128/mmbr.64.2.435-459.2000

34. Taschner M, Vetter M, Lorentzen E. Atomic resolution structure of human á-tubulin acetyltransferase bound to acetyl-CoA. Proceedings of the National Academy of Sciences of the United States of America. 2012;109(48):19649–19654. doi:10.1073/pnas.1209343109

35. Berndsen CE, Denu JM. Catalysis and substrate selection by histone/protein lysine acetyltransferases. Current Opinion in Structural Biology. 2008;18(6):682–689. doi:10.1016/j.sbi.2008.11.004

36. Ho TCS, Chan AHY, Ganesan A. Thirty Years of HDAC Inhibitors: 2020 Insight and Hindsight. Journal of Medicinal Chemistry. 2020;63(21):12460–12484. doi:10.1021/acs.jmedchem.0c00830

37. Goffeau A, Barrell G, Bussey H, Davis RW, Dujon B, Feldmann H, Galibert F, Hoheisel JD, Jacq C, Johnston M, et al. Life with 6000 genes. Science. 1996;274(5287):546–567. doi:10.1126/science.274.5287.546

38. Nielsen J. Yeast Systems Biology: Model Organism and Cell Factory. Biotechnology Journal. 2019;14(9):1–9. http://dx.doi.org/10.1002/biot.201800421. doi:10.1002/biot.201800421

39. Sarto-Jackson I, Tomaska L. How to bake a brain: yeast as a model neuron. Current Genetics. 2016;62(2):347–370. doi:10.1007/s00294-015-0554-2

40. Picotti P, Clément-Ziza M, Lam H, Campbell DS, Schmidt A, Deutsch EW, Röst H, Sun Z, Rinner O, Reiter L, et al. A complete mass-spectrometric map of the yeast proteome applied to quantitative trait analysis. Nature. 2013;494(7436):266–270. doi:10.1038/nature11835

41. Chong YT, Koh JLY, Friesen H, Duffy SK, Duffy K, Cox MJ, Moses A, Moffat J, Boone C, Andrews BJ. Yeast Proteome Dynamics from Single Cell Imaging and Automated Analysis. Cell. 2015;161(6):1413–24. https://www.ncbi.nlm.nih.gov/pubmed/26046442. doi:10.1016/j.cell.2015.04.051

42. Huh W-KK, Falvo J V, Gerke LC, Carroll AS, Howson RW, Weissman JS, K OE, Ghaemmaghami, S., Huh, K. W, et al. Global analysis of protein localization in budding yeast. Nature. 2003;425(6959):686–691. doi:10.1038/nature02026

43. Giaever G, Chu AM, Ni L, Connelly C, Riles L, Véronneau S, Dow S, Lucau-Danila A, Anderson K, André B, et al. Functional profiling of the Saccharomyces cerevisiae genome. Nature. 2002;418(6896):387–391. http://www.nature.com/articles/nature00935. doi:10.1038/nature00935

44. Giaever G, Nislow C. The yeast deletion collection: A decade of functional genomics. Genetics. 2014;197(2):451–465. doi:10.1534/genetics.114.161620

45. Douglas AC, Smith AM, Sharifpoor S, Yan Z, Durbic T, Heisler LE, Lee AY, Ryan O, Göttert H,

Surendra A, et al. Functional analysis with a barcoder yeast gene overexpression system. G3: Genes, Genomes, Genetics. 2012;2(10):1279–1289. doi:10.1534/g3.112.003400

46. Tong AHY, Evangelista M, Parsons AB, Xu H, Bader GD, Pagé N, Robinson M, Raghibizadeh S, Hogue CW V., Bussey H, et al. Systematic Genetic Analysis with Ordered Arrays of Yeast Deletion Mutants. Science. 2001;294(5550):2364–2368. https://www.ncbi.nlm.nih.gov/pubmed/11743205. doi:10.1126/science.1065810

47. Wagih O, Usaj M, Baryshnikova A, VanderSluis B, Kuzmin E, Costanzo M, Myers CL, Andrews BJ, Boone CM, Parts L. SGAtools: One-stop analysis and visualization of array-based genetic interaction screens. Nucleic acids research. 2013;41(Web Server issue):591–596. doi:10.1093/nar/gkt400

48. Henriksen P, Wagner SA, Weinert BT, Sharma S, Bačinskaja G, Rehman M, Juffer AH, Walther TC, Lisby M, Choudhary C. Proteome-wide Analysis of Lysine Acetylation Suggests its Broad Regulatory Scope in *Saccharomyces cerevisiae*. Molecular & Cellular Proteomics. 2012;11(11):1510–1522. http://www.mcponline.org/lookup/doi/10.1074/mcp.M112.017251. doi:10.1074/mcp.M112.017251

49. Wang L, Mizzen C, Ying C, Candau R, Barlev N, Brownell J, Allis CD, Berger SL. Histone acetyltransferase activity is conserved between yeast and human GCN5 and is required for complementation of growth and transcriptional activation. Molecular and Cellular Biology. 1997;17(1):519–527. doi:10.1128/mcb.17.1.519

50. Brosh RM. Protein Acetylation. 2020. doi:10.32388/w1vy8j

51. Doyon Y, Selleck W, Lane WS, Tan S, Cote J, Côté J. Structural and functional conservation of the NuA4 histone acetyltransferase complex from yeast to humans. Mol Cell Biol. 2004;24(5):1884–1896. http://www.pubmedcentral.nih.gov/articlerender.fcgi?artid=350560&tool=pmcentrez&rendertype=abstract. doi:10.1128/MCB.24.5.1884

52. Filteau M, Diss G, Torres-Quiroz F, Dubé AK, Schraffl A, Bachmann VA, Gagnon-Arsenault I, Chrétien A-È, Steunou A-L, Dionne U, et al. Systematic identification of signal integration by protein kinase A. Proceedings of the National Academy of Sciences. 2015;112(14):4501–4506. http://www.pnas.org/lookup/doi/10.1073/pnas.1409938112. doi:10.1073/pnas.1409938112

53. Li TY, Song L, Sun Y, Li J, Yi C, Lam SM, Xu D, Zhou L, Li X, Yang Y, et al. Tip60-mediated lipin 1 acetylation and ER translocation determine triacylglycerol synthesis rate. Nature Communications. 2018;9(1):1916. http://dx.doi.org/10.1038/s41467-018-04363-w. doi:10.1038/s41467-018-04363-w

54. Downey M. Non-histone protein acetylation by the evolutionarily conserved GCN5 and PCAF acetyltransferases. Biochimica et Biophysica Acta - Gene Regulatory Mechanisms. 2021;1864(2):194608. https://doi.org/10.1016/j.bbagrm.2020.194608. doi:10.1016/j.bbagrm.2020.194608

55. Squatrito M, Gorrini C, Amati B. Tip60 in DNA damage response and growth control: many tricks in one HAT. Trends in Cell Biology. 2006;16(9):433–442. doi:10.1016/j.tcb.2006.07.007

56. Yang XJ, Seto E. The Rpd3/Hda1 family of lysine deacetylases: From bacteria and yeast to mice and men. Nature Reviews Molecular Cell Biology. 2008;9(3):206–218. doi:10.1038/nrm2346

57. Eberharter A, John S, Grant PA, Utley RT, Workman JL. Identification and analysis of yeast nucleosomal histone acetyltransferase complexes. Methods: A Companion to Methods in Enzymology. 1998;15(4):315–321. doi:10.1006/meth.1998.0635

58. Allard S, Utley RT, Savard J, Clarke A, Grant P, Brandl CJ, Pillus L, Workman JL, Cote J, Côté J. NuA4, an essential transcription adaptor/histone H4 acetyltransferase complex containing Esa1p and the ATM-related cofactor Tra1p. EMBO J. 1999;18(18):5108–5119. https://www.ncbi.nlm.nih.gov/pubmed/10487762. doi:10.1093/emboj/18.18.5108

59. Lin Y, Lu J, Zhang J, Walter W, Dang W, Wan J, Tao S, Qian J, Zhao Y, Boeke JD, et al. Protein Acetylation Microarray Reveals that NuA4 Controls Key Metabolic Target Regulating Gluconeogenesis. Cell. 2009;136(6):1073–1084. https://linkinghub.elsevier.com/retrieve/pii/S0092867409000816. doi:10.1016/j.cell.2009.01.033

60. Lu J-Y, Lin Y-Y, Sheu J, Wu J-T, Lee F, Chen Y, Lin M-I, Chiang F, Tai T-Y, Berger SL, et al. Acetylation of Yeast AMPK Controls Intrinsic Aging Independently of Caloric Restriction. Cell. 2011;146(6):969–979. https://www.ncbi.nlm.nih.gov/pubmed/21906795. doi:10.1016/j.cell.2011.07.044

61. Yamada HY. Human Tip60 (NuA4) Complex and Cancer. Colorectal Cancer Biology - From Genes to Tumor. 2012;60:217–240. doi:10.5772/28295

62. Sapountzi V, Logan IR, Robson CN. Cellular functions of TIP60. International Journal of Biochemistry and Cell Biology. 2006;38(9):1496–1509. doi:10.1016/j.biocel.2006.03.003

63. Gehrking KM, Andresen JM, Duvick L, Lough J, Zoghbi HY, Orr HT. Partial loss of Tip60 slows mid-stage neurodegeneration in a spinocerebellar ataxia type 1 (SCA1) mouse model. Human Molecular Genetics. 2011;20(11):2204–2212. doi:10.1093/hmg/ddr108

64. Panikker P, Xu SJ, Zhang H, Sarthi J, Beaver M, Sheth A, Akhter S, Elefant F. Restoring Tip60 HAT/HDAC2 balance in the neurodegenerative brain relieves epigenetic transcriptional repression and reinstates cognition. Journal of Neuroscience. 2018;38(19):4569–4583. doi:10.1523/JNEUROSCI.2840-17.2018

65. Yang P, Xu C, Reece EA, Chen X, Zhong J, Zhan M, Stumpo DJ, Blackshear PJ, Yang P. Tip60- and sirtuin 2-regulated MARCKS acetylation and phosphorylation are required for diabetic embryopathy. Nature Communications. 2019;10(1):1–15. http://dx.doi.org/10.1038/s41467-018-08268-6. doi:10.1038/s41467-018-08268-6

66. Auger A, Galarneau L, Altaf M, Nourani A, Doyon Y, Utley RT, Cronier D, Allard S, Cote J. Eaf1 Is the Platform for NuA4 Molecular Assembly That Evolutionarily Links Chromatin Acetylation to ATP-Dependent Exchange of Histone H2A Variants. Molecular and Cellular Biology. 2008;28(7):2257–2270. http://mcb.asm.org/cgi/doi/10.1128/MCB.01755-07. doi:10.1128/MCB.01755-07

67. Cheng X, Auger A, Altaf M, Drouin S, Paquet E, Utley RT, Robert F, Côté J. Eaf1 links the NuA4 histone acetyltransferase complex to Htz1 incorporation and regulation of purine biosynthesis. Eukaryotic Cell. 2015;14(6):535–544. doi:10.1128/EC.00004-15

68. Chittuluru J, Chaban Y, Monnet-Saksouk J, Carrozza M, Sapountzi V, Selleck W, Huang J, Utley RT, Cramet M, Allard S, et al. Structure and nucleosome interaction of the yeast NuA4 and Piccolo-NuA4 histone acetyltransferase complexes. Nat Struct Mol Bio. 2012;18(11):1196–1203. doi:10.1038/nsmb.2128.Structure

69. Smith ER, Eisen A, Gu W, Sattah M, Pannuti A, Zhou J, Cook RG, Lucchesi JC, Allis CD. ESA1 is a histone acetyltransferase that is essential for growth in yeast. Proceedings of the National Academy of Sciences of the United States of America. 1998;95(7):3561–3565. doi:10.1073/pnas.95.7.3561

70. Wang X, Ahmad S, Zhang Z, Côté J, Cai G. Architecture of the Saccharomyces cerevisiae NuA4/TIP60 complex. Nature Communications. 2018;9(1):1147. http://dx.doi.org/10.1038/s41467-018-03504-5. doi:10.1038/s41467-018-03504-5

71. Boudreault AA, Cronier D, Selleck W, Lacoste N, Utley RT, Allard S, Savard J, Lane WS, Tan S, Cote, et al. Yeast Enhancer of Polycomb defines global Esa1-dependent acetylation of chromatin. Genes and Development. 2003;17(11):1415–1428. doi:10.1101/gad.1056603

72. Selleck W, Fortin I, Sermwittayawong D, Côté J, Tan S. The Saccharomyces cerevisiae Piccolo NuA4

histone acetyltransferase complex requires the Enhancer of Polycomb A domain and chromodomain to acetylate nucleosomes. Molecular and cellular biology. 2005;25(13):5535–42. http://www.pubmedcentral.nih.gov/articlerender.fcgi?artid=1156996&tool=pmcentrez&rendertype=abstract. doi:10.1128/MCB.25.13.5535-5542.2005

73. Cheng X, Côté J. A new companion of elongating RNA polymerase II: TINTIN, an independent sub-module of NuA4/TIP60 for nucleosome transactions. Transcription. 2014;5(5):20–22. doi:10.1080/21541264.2014.995571

74. Sathianathan A, Ravichandran P, Lippi JM, Cohen L, Messina A, Shaju S, Swede MJ, Ginsburg DS. The Eaf3/5/7 subcomplex stimulates NuA4 interaction with methylated histone H3 Lys-36 and RNA polymerase II. Journal of Biological Chemistry. 2016;291(40):21195–21207. doi:10.1074/jbc.M116.718742

75. Knutson BA, Hahn S. Domains of Tra1 Important for Activator Recruitment and Transcription Coactivator Functions of SAGA and NuA4 Complexes. Molecular and Cellular Biology. 2011;31(4):818–831. doi:10.1128/mcb.00687-10

76. Zukin SA, Marunde MR, Popova IK, Soczek KM, Nogales E, Patel AB. Structure and flexibility of the yeast NuA4 histone acetyltransferase complex. eLife. 2022;11(48):1–23. http://www.ncbi.nlm.nih.gov/pubmed/36263929. doi:10.7554/eLife.81400

77. Ji L, Zhao L, Xu K, Gao H, Zhou Y, Kornberg RD, Zhang H. Structure of the NuA4 histone acetyltransferase complex. Proceedings of the National Academy of Sciences. 2022;119(48):2017. https://pnas.org/doi/10.1073/pnas.2214313119. doi:10.1073/pnas.2214313119

78. Qu K, Chen K, Wang H, Li X, Chen Z. Structure of the NuA4 acetyltransferase complex bound to the nucleosome. Nature. 2022;610(7932):569–574. doi:10.1038/s41586-022-05303-x

79. Mitchell L, Lambert J-P, Gerdes M, Al-Madhoun AS, Skerjanc IS, Figeys D, Baetz K. Functional Dissection of the NuA4 Histone Acetyltransferase Reveals Its Role as a Genetic Hub and that Eaf1 Is Essential for Complex Integrity. Molecular and Cellular Biology. 2008;28(7):2244–2256. http://mcb.asm.org/cgi/doi/10.1128/MCB.01653-07. doi:10.1128/MCB.01653-07

80. Dacquay L, Flint A, Butcher J, Salem D, Kennedy M, Kaern M, Stintzi A, Baetz K. NuA4 Lysine Acetyltransferase Complex Contributes to Phospholipid Homeostasis in Saccharomyces cerevisiae. G3 Genes|Genomes|Genetics. 2017;7(6):1799–1809. https://academic.oup.com/g3journal/article/7/6/1799/6029854. doi:10.1534/g3.117.041053

81. Clarke AS, Lowell JE, Jacobson SJ, Pillus L. Esa1p Is an Essential Histone Acetyltransferase Required for Cell Cycle Progression. Molecular and Cellular Biology. 1999;19(4):2515–2526. http://www.ncbi.nlm.nih.gov/cgi-bin/Entrez/referer?http://mcb.asm.org/cgi/content/full/19/4/2515. doi:10.1128/MCB.19.4.2515

82. Mitchell L, Huard S, Cotrut M, Pourhanifeh-Lemeri R, Steunou A-L, Hamza A, Lambert J-P, Zhou H, Ning Z, Basu A, et al. mChIP-KAT-MS, a method to map protein interactions and acetylation sites for lysine acetyltransferases. Proceedings of the National Academy of Sciences. 2013;110(17):E1641–E1650. https://www.ncbi.nlm.nih.gov/pubmed/23572591. doi:10.1073/pnas.1218515110

83. Yamamoto T, Horikoshi M. Novel substrate specificity of the histone acetyltransferase activity of HIV-1-Tat interactive protein Tip60. Journal of Biological Chemistry. 1997;272(49):30595–30598. http://dx.doi.org/10.1074/jbc.272.49.30595. doi:10.1074/jbc.272.49.30595

84. Ghobashi AH, Kamel MA. Tip60 : updates. 2018;2:161–168.

85. Kamine J, Elangovan B, Subramanian T, Coleman D, Chinnadurai G. Identification of a cellular

protein that specifically interacts with the essential cysteine region of the HIV-1 Tat transactivator. Virology. 1996;216(2):357–366. doi:10.1006/viro.1996.0071

86. Li Z, Rasmussen LJ. TIP60 in aging and neurodegeneration. Ageing Research Reviews. 2020;64(October):101195. https://doi.org/10.1016/j.arr.2020.101195. doi:10.1016/j.arr.2020.101195

87. Cheng Z, Ke Y, Ding X, Wang F, Wang H, Ahmed K, Liu Z, Xu Y, Aikhionbare F, Yan H, et al. Functional characterization of TIP60 sumoylation in UV-irradiated DNA damage response. Oncogene. 2008;27(7):931–941. doi:10.1038/sj.onc.1210710

88. Fang X, Lu G, Ha K, Lin H, Du Y, Zuo Q, Fu Y, Zou C, Zhang P. Acetylation of TIP60 at K104 is essential for metabolic stress-induced apoptosis in cells of hepatocellular cancer. Experimental Cell Research. 2017;362(2):279–286. doi:10.1016/j.yexcr.2017.11.028

89. Cheng X, Ma X, Zhu Q, Song D, Ding X, Li L, Jiang X, Wang X, Tian R, Su H, et al. Pacer Is a Mediator of mTORC1 and GSK3-TIP60 Signaling in Regulation of Autophagosome Maturation and Lipid Metabolism. Molecular Cell. 2019;73(4):788-802.e7. doi:10.1016/j.molcel.2018.12.017

90. Charvet C, Wissler M, Brauns-Schubert P, Wang S-J, Tang Y, Sigloch FC, Mellert H, Brandenburg M, Lindner SE, Breit B, et al. Phosphorylation of Tip60 by GSK-3 Determines the Induction of PUMA and Apoptosis by p53. Molecular Cell. 2011;42(5):584–596. https://linkinghub.elsevier.com/retrieve/pii/S1097276511003431. doi:10.1016/j.molcel.2011.03.033

91. Hu Y, Fisher JB, Koprowski S, Mcallister D, Kim M. Homozygus disription of the gene Tip60 causes early embryonic lethality. Dev. Dyn. 2009;238(11):2912–2921. doi:10.1002/dvdy.22110.Homozygous

92. Gorrini C, Squatrito M, Luise C, Syed N, Perna D, Wark L, Martinato F, Sardella D, Verrecchia A, Bennett S, et al. Tip60 is a haplo-insufficient tumour suppressor required for an oncogene-induced DNA damage response. Nature. 2007;448(7157):1063–1067. doi:10.1038/nature06055

93. McGuire A, Casey MC, Shalaby A, Kalinina O, Curran C, Webber M, Callagy G, Holian E, Bourke E, Kerin MJ, et al. Quantifying Tip60 (Kat5) stratifies breast cancer. Scientific Reports. 2019;9(1):1–14. http://dx.doi.org/10.1038/s41598-019-40221-5. doi:10.1038/s41598-019-40221-5

94. Pandey AK, Zhang Y, Zhang S, Li Y, Tucker-Kellogg G, Yang H, Jha S. TIP60-miR-22 axis as a prognostic marker of breast cancer progression. Oncotarget. 2015;6(38):41290–41306. doi:10.18632/oncotarget.5636

95. Tan KN, Avery VM, Carrasco-Pozo C. Metabolic roles of androgen receptor and tip60 in androgen-dependent prostate cancer. International Journal of Molecular Sciences. 2020;21(18):1–16. doi:10.3390/ijms21186622

96. Shiota M, Yokomizo A, Masubuchi D, Tada Y, Inokuchi J, Eto M, Uchiumi T, Fujimoto N, Naito S. Tip60 promotes prostate cancer cell proliferation by translocation of androgen receptor into the nucleus. Prostate. 2010;70(5):540–554. doi:10.1002/pros.21088

97. Su WP, Ho YC, Wu CK, Hsu SH, Shiu JL, Huang JC, Chang S Bin, Chiu WT, Hung JJ, Liu TL, et al. Chronic treatment with cisplatin induces chemoresistance through the TIP60-mediated Fanconi anemia and homologous recombination repair pathways. Scientific Reports. 2017;7(1):1–15. doi:10.1038/s41598-017-04223-5

98. Wang P, Bao H, Zhang XP, Liu F, Wang W. Regulation of Tip60-dependent p53 acetylation in cell fate decision. FEBS Letters. 2019;593(1):13–22. doi:10.1002/1873-3468.13287

99. Ozaki T, Nakagawara A. Role of p53 in cell death and human cancers. Cancers. 2011;3(1):994–1013. doi:10.3390/cancers3010994

100. Pirooznia SK, Sarthi J, Johnson AA, Toth MS, Chiu K, Koduri S, Elefant F. Tip60 HAT activity mediates APP induced lethality and apoptotic cell death in the CNS of a Drosophila Alzheimer's disease model. PLoS ONE. 2012;7(7). doi:10.1371/journal.pone.0041776

101. Beaver M, Bhatnagar A, Panikker P, Zhang H, Snook R, Parmar V, Vijayakumar G, Betini N, Akhter S, Elefant F. Disruption of Tip60 HAT mediated neural histone acetylation homeostasis is an early common event in neurodegenerative diseases. Scientific Reports. 2020;10(1):1–15. https://doi.org/10.1038/s41598-020-75035-3. doi:10.1038/s41598-020-75035-3

102. Lanni C, Racchi M, Memo M, Govoni S, Uberti D. P53 at the crossroads between cancer and neurodegeneration. Free Radical Biology and Medicine. 2012;52(9):1727–1733. http://dx.doi.org/10.1016/j.freeradbiomed.2012.02.034. doi:10.1016/j.freeradbiomed.2012.02.034

103. Humbert J, Salian S, Makrythanasis P, Lemire G, Rousseau J, Ehresmann S, Garcia T, Alasiri R, Bottani A, Hanquinet S, et al. De Novo KAT5 Variants Cause a Syndrome with Recognizable Facial Dysmorphisms, Cerebellar Atrophy, Sleep Disturbance, and Epilepsy. American Journal of Human Genetics. 2020;107(3):564–574. doi:10.1016/j.ajhg.2020.08.002

104. Chen L, Qing W, Yi Z, Lin G, Peng Q, Zhou F. NU9056, a KAT 5 Inhibitor, Treatment Alleviates Brain Dysfunction by Inhibiting NLRP3 Inflammasome Activation, Affecting Gut Microbiota, and Derived Metabolites in LPS-Treated Mice. Frontiers in Nutrition. 2021;8(July):1–16. doi:10.3389/fnut.2021.701760

105. Narkaj K, Stefanelli G, Wahdan M, Azam AB, Ramzan F, Steininger CFD, Walters BJ, Zovkic IB. Blocking H2A.Z incorporation via Tip60 inhibition promotes systems consolidation of fear memory in mice. eNeuro. 2018;5(5). doi:10.1523/ENEURO.0378-18.2018

106. Walden EA, Fong RY, Pham TT, Knill H, Laframboise SJ, Huard S, Harper M-E, Baetz K. Phenomic screen identifies a role for the yeast lysine acetyltransferase NuA4 in the control of Bcy1 subcellular localization, glycogen biosynthesis, and mitochondrial morphology Copenhaver GP, editor. PLOS Genetics. 2020;16(11):e1009220. http://dx.doi.org/10.1371/journal.pgen.1009220. doi:10.1371/journal.pgen.1009220

107. Yang C, Wu J, Zheng YG. Function of the active site lysine autoacetylation in Tip60 catalysis. PLoS ONE. 2012;7(3):1–8. doi:10.1371/journal.pone.0032886

108. Yang C, Wu J, Sinha SH, Neveu JM, Zheng YG. Autoacetylation of the MYST lysine acetyltransferase MOF protein. Journal of Biological Chemistry. 2012;287(42):34917–34926. doi:10.1074/jbc.M112.359356

109. Xu P, Li C, Chen Z, Jiang S, Fan S, Wang J, Dai J, Zhu P, Chen Z. The NuA4 Core Complex Acetylates Nucleosomal Histone H4 through a Double Recognition Mechanism. Molecular Cell. 2016;63(6):965–975. http://dx.doi.org/10.1016/j.molcel.2016.07.024. doi:10.1016/j.molcel.2016.07.024

110. Wang J, Chen J. SIRT1 regulates autoacetylation and histone acetyltransferase activity of TIP60. Journal of Biological Chemistry. 2010;285(15):11458–11464. doi:10.1074/jbc.M109.087585

111. Mitchell L, Lau A, Lambert J-P, Zhou H, Fong Y, Couture J-F, Figeys D, Baetz K. Regulation of Septin Dynamics by the Saccharomyces cerevisiae Lysine Acetyltransferase NuA4 Hardwick KG, editor. PLoS ONE. 2011;6(10):e25336. https://www.ncbi.nlm.nih.gov/pubmed/21984913. doi:10.1371/journal.pone.0025336

112. Lin YY, Qi Y, Lu JY, Pan X, Yuan DS, Zhao Y, Bader JS, Boeke JD. A comprehensive synthetic genetic interaction network governing yeast histone acetylation and deacetylation. Genes and Development. 2008;22(15):2062–2074. doi:10.1101/gad.1679508

113. Bird AW, Yu DY, Pray-Grant MG, Qiu Q, Harmon KE, Megee PC, Grant PA, Smith MM, Christman MF. Acetylation of histone H4 by Esa1 is required for DNA double-strand break repair. Nature. 2002;419(6905):411–415. doi:10.1038/nature01035

114. Altaf M, Auger A, Monnet-Saksouk J, Brodeur J, Piquet S, Cramet M, Bouchard N, Lacoste N, Utley RT, Gaudreau L, et al. NuA4-dependent acetylation of nucleosomal histones H4 and H2A directly stimulates incorporation of H2A.Z by the SWR1 complex. Journal of Biological Chemistry. 2010;285(21):15966–15977. doi:10.1074/jbc.M110.117069

115. Ikura T, Tashiro S, Kakino A, Shima H, Jacob N, Amunugama R, Yoder K, Izumi S, Kuraoka I, Tanaka K, et al. DNA Damage-Dependent Acetylation and Ubiquitination of H2AX Enhances Chromatin Dynamics. Molecular and Cellular Biology. 2007;27(20):7028–7040. doi:10.1128/mcb.00579-07

116. Ahmad S, Côté V, Cheng X, Bourriquen G, Sapountzi V, Altaf M, Côté J. Antagonistic relationship of NuA4 with the non-homologous end-joining machinery at DNA damage sites. PLoS Genetics. 2021;17(9):1–24. doi:10.1371/journal.pgen.1009816

117. Cheng X, Cote VR, Côte J. NuA4 and SAGA acetyltransferase complexes cooperate for repair of DNA breaks by homologous recombination. PLoS Genetics. 2021;17(7):1–19. doi:10.1371/journal.pgen.1009459

118. Hodges AJ, Plummer DA, Wyrick JJ. NuA4 acetyltransferase is required for efficient nucleotide excision repair in yeast. DNA repair. 2019;73(10):91–98. file:///C:/Users/Carla Carolina/Desktop/Artigos para acrescentar na qualificação/The impact of birth weight on cardiovascular disease risk in the.pdf. doi:10.1016/j.dnarep.2018.11.006

119. Renaud-Young M, Lloyd DC, Chatfield-Reed K, George I, Chua G, Cobb J. The NuA4 complex promotes translesion synthesis (TLS)-mediated DNA damage tolerance. Genetics. 2015;199(4):1065–1076. doi:10.1534/genetics.115.174490

120. Ononye OE, Sausen CW, Balakrishnan L, Bochman ML. Lysine acetylation regulates the activity of nuclear Pif1. Journal of Biological Chemistry. 2020;295(46):15482–15497. http://dx.doi.org/10.1074/jbc.RA120.015164. doi:10.1074/jbc.RA120.015164

121. Valdes-Hevia MD, de la Guerra R, Gancedo C. Isolation and characterization of the gene encoding 2,3-oxidosqualene-lanosterol cyclase from Saccharomyces cerevisiae. Proceedings of the National Academy of Sciences. 1989;258(2):313–316. doi:10.1073/pnas.91.15.7370

122. Ashrafi K, Lin SS, Manchester JK, Gordon JI. Sip2p and its partner Snf1p kinase affect aging in S. cerevisiae. Genes and Development. 2000;14(15):1872–1885.

123. Hedbacker K, Carlson M. SNF1/AMPK pathways in yeast. Frontiers in Bioscience. 2008;13(7):2408–2420. doi:10.2741/2854

124. Wilson WA, Hawley SA, Hardie DG. Glucose repression/derepression in budding yeast: SNF1 protein kinase is activated by phosphorylation under derepressing conditions, and this correlates with a high AMP:ATP ratio. Current Biology. 1996;6(11):1426–1434. doi:10.1016/S0960-9822(96)00747-6

125. Toda T, Cameron S, Sass P, Zoller M, Wigler M. Three different genes in S. cerevisiae encode the catalytic subunits of the cAMP-dependent protein kinase. Cell. 1987;50(2):277–287. doi:10.1016/0092-8674(87)90223-6

126. Santangelo GM. Glucose Signaling in Saccharomyces cerevisiae. Microbiology and Molecular Biology Reviews. 2006;70(1):253–282. doi:10.1128/MMBR.70.1.253

127. Toda T, Cameron S, Sass P, Zoller M, Scott JD, McMullen B, Hurwitz M, Krebs EG, Wigler M.

Cloning and characterization of BCY1, a locus encoding a regulatory subunit of the cyclic AMP-dependent protein kinase in Saccharomyces cerevisiae. Molecular and cellular biology. 1987;7(4):1371–7. doi:10.1128/MCB.7.4.1371

128. Scott JD, Pawson T. Cell signaling in space and time: Where proteins come together and when they're apart. Science. 2009;326(5957):1220–1224. doi:10.1126/science.1175668

129. Soulard A, Cremonesi A, Moes S, Schutz F, Jeno P, Hall MN. The Rapamycin-sensitive Phosphoproteome Reveals that TOR Control Protein Kinase A Toward Some But Not All Substrates. Molecular biology of the cell. 2010;21(24):3475–3586. doi:10.1091/mbc.E10

130. Vandamme J, Castermans D, Thevelein JM. Molecular mechanisms of feedback inhibition of protein kinase A on intracellular cAMP accumulation. Cellular Signalling. 2012;24(8):1610–1618. http://dx.doi.org/10.1016/j.cellsig.2012.04.001. doi:10.1016/j.cellsig.2012.04.001

131. Gorner W, Durchschlag E, Martinez-Pastor MT, Estruch F, Ammerer G, Hamilton B, Ruis H, Schuller C. Nuclear localization of the C2H2 zinc finger protein Msn2p is regulated by stress and protein kinase A activity. Genes & Development. 1997;12:586–597. doi:10.1101/gad.12.4.586

132. Martínez-Pastor MT, Marchler G, Schüller C, Marchler-Bauer A, Ruis H, Estruch F. The *Saccharomyces cerevisiae* zinc finger proteins Msn2p and Msn4p are required for transcriptional induction through the stress response element (STRE). The EMBO journal. 1996;15(9):2227–35. http://www.pubmedcentral.nih.gov/articlerender.fcgi?artid=450147&tool=pmcentrez&rendertype=abstract

133. Smith A, Ward MP, Garrett S. Yeast PKA represses Msn2p/Msn4p-dependent gene expression to regulate growth, stress response and glycogen accumulation. EMBO Journal. 1998;17(13):3556–3564. doi:10.1093/emboj/17.13.3556

134. Huang J, Mousley CJ, Dacquay L, Maitra N, Drin G, He C, Ridgway ND, Tripathi A, Kennedy M, Kennedy BK, et al. A Lipid Transfer Protein Signaling Axis Exerts Dual Control of Cell-Cycle and Membrane Trafficking Systems. Developmental Cell. 2018;44(3):378-391.e5. https://doi.org/10.1016/j.devcel.2017.12.026. doi:10.1016/j.devcel.2017.12.026

135. Mousley CJ, Yuan P, Gaur NA, Trettin KD, Nile AH, Deminoff SJ, Dewar BJ, Wolpert M, Macdonald JM, Paul K, et al. A sterol binding protein integrated endosomal lipid metabolism with TOR signalling and nitrogen sensing. Cell. 2012;148(4):702–715. doi:10.1016/j.cell.2011.12.026.A

136. Costanzo M, VanderSluis B, Kock E, ..., Andres B, Boone C. A global interaction network maps a wiring diagram of cellular function. 2016;23(353):6306. doi:10.1245/s10434-015-5063-5.Optimal

137. Douglas LM, Alvarez FJ, McCreary C, Konopka JB. Septin function in yeast model systems and pathogenic fungi. Eukaryotic Cell. 2005;4(9):1503–1512. doi:10.1128/EC.4.9.1503-1512.2005

138. Yi C, Ma M, Ran L, Zheng J, Tong J, Zhu J, Ma C, Sun Y, Zhang S, Feng W, et al. Function and molecular mechanism of acetylation in autophagy regulation. Science Reports. 2012;336(April):474–477. doi:10.1126/science.1216990

139. Lin S-Y, Li TY, Liu Q, Zhang C, Li X, Chen Y, Zhang S-M, Lian G, Liu Q, Ruan K, et al. GSK3-TIP60-ULK1 Signaling Pathway Links Growth Factor Deprivation to Autophagy. Science. 2012;336(6080):477–481. https://www.science.org/doi/10.1126/science.1217032. doi:10.1126/science.1217032

140. Nie T, Yang S, Ma H, Zhang L, Lu F, Tao K, Wang R, Yang R, Huang L, Mao Z, et al. Regulation of ER stress-induced autophagy by GSK3B-TIP60-ULK1 pathway. Cell Death and Disease. 2016;7(12). doi:10.1038/cddis.2016.423

141. Cheng X, Sun Q. RUBCNL/Pacer and RUBCN/Rubicon in regulation of autolysosome formation and lipid metabolism. Autophagy. 2019;15(6):1120–1121. https://doi.org/10.1080/15548627.2019.1596500. doi:10.1080/15548627.2019.1596500

142. Gomar-Alba M, Pozharskaia V, Cichocki B, Schaal C, Kumar A, Jacquel B, Charvin G, Igual JC, Mendoza M. Nuclear pore complex acetylation regulates mRNA export and cell cycle commitment in budding yeast . The EMBO Journal. 2022:1–20. doi:10.15252/embj.2021110271

143. Shi L, Tu BP. Acetyl-CoA and the regulation of metabolism: Mechanisms and consequences. Current Opinion in Cell Biology. 2015;33:125–131. http://dx.doi.org/10.1016/j.ceb.2015.02.003. doi:10.1016/j.ceb.2015.02.003

144. Wellen KE, Thompson CB. A two-way street: Reciprocal regulation of metabolism and signalling. Nature Reviews Molecular Cell Biology. 2012;13(4):270–276. doi:10.1038/nrm3305

145. Hebert AS, Dittenhafer-Reed KE, Yu W, Bailey DJ, Selen ES, Boersma MD, Carson JJ, Tonelli M, Balloon AJ, Higbee AJ, et al. Calorie Restriction and SIRT3 Trigger Global Reprogramming of the Mitochondrial Protein Acetylome. Molecular Cell. 2013;49(1):186–199. doi:10.1016/j.molcel.2012.10.024

146. Hsieh WC, Sutter BM, Ruess H, Barnes SD, Malladi VS, Tu BP. Glucose starvation induces a switch in the histone acetylome for activation of gluconeogenic and fat metabolism genes. Molecular Cell. 2022;82(1):60-74.e5. https://doi.org/10.1016/j.molcel.2021.12.015. doi:10.1016/j.molcel.2021.12.015

147. Menzies KJ, Zhang H, Katsyuba E, Auwerx J. Protein acetylation in metabolism-metabolites and cofactors. Nature Reviews Endocrinology. 2016;12(1):43–60. http://dx.doi.org/10.1038/nrendo.2015.181. doi:10.1038/nrendo.2015.181

148. Hosp F, Lassowskat I, Santoro V, De Vleesschauwer D, Fliegner D, Redestig H, Mann M, Christian S, Hannah MA, Finkemeier I. Lysine acetylation in mitochondria: From inventory to function. Mitochondrion. 2017;33:58–71. http://dx.doi.org/10.1016/j.mito.2016.07.012. doi:10.1016/j.mito.2016.07.012

149. Oanh NTK, Park YY, Cho H. Mitochondria elongation is mediated through SIRT1-mediated MFN1 stabilization. Cellular Signalling. 2017;38(April):67–75. http://dx.doi.org/10.1016/j.cellsig.2017.06.019. doi:10.1016/j.cellsig.2017.06.019

150. Wakil SJ, Abu-Elheiga LA. Fatty acid metabolism: target for metabolic syndrome. Journal of Lipid Research. 2009;50:S138–S143. https://linkinghub.elsevier.com/retrieve/pii/S0022227520306015. doi:10.1194/jlr.R800079-JLR200

151. Pham T, Walden E, Huard S, Pezacki J, Fullerton M, Baetz K. Fine tuning Acetyl-CoA Carboxylase 1 activity through localization: Functional genomics reveal a role for the lysine acetyltransferase NuA4 and sphingolipid metabolism in regulating Acc1 activity and localization. Genetics. 2022;(May). https://doi.org/10.1093/genetics/iyac086. doi:10.1093/genetics/iyac086

152. Choudhary C, Kumar C, Gnad F, Nielsen ML, Rehman M, Walther TC, Olsen J V., Mann M. Lysine Acetylation Targets Protein Complexes and Co-Regulates Major Cellular Functions. Science. 2009;325(5942):834–840. http://www.sciencemag.org/cgi/doi/10.1126/science.1175371. doi:10.1126/science.1175371

153. Downey M, Johnson JR, Davey NE, Newton BW, Johnson TL, Galaang S, Seller CA, Krogan N, Toczyski DP. Acetylome Profiling Reveals Overlap in the Regulation of Diverse Processes by Sirtuins, Gcn5, and Esa1. Molecular & Cellular Proteomics. 2015;14(1):162–176.

https://linkinghub.elsevier.com/retrieve/pii/S1535947620316704. doi:10.1074/mcp.M114.043141

154. Kaluarachchi Duffy S, Friesen H, Baryshnikova A, Lambert J-P, Chong YT, Figeys D, Andrews B. Exploring the Yeast Acetylome Using Functional Genomics. Cell. 2012;149(4):936–948. doi:10.1097/QAI.0b013e318198a619.Relationship

155. Singh BN, Zhang G, Hwa YL, Li J, Dowdy SC, Jiang S. Nonhistone protein acetylation as cancer therapy targets. Expert Rev Anticancer Ther. 2010;10(6):935–954. doi:10.1586/era.10.62.Nonhistone

156. Iyer A, Fairlie DP, Brown L. Lysine acetylation in obesity, diabetes and metabolic disease. Immunology and Cell Biology. 2012;90(1):39–46. http://dx.doi.org/10.1038/icb.2011.99. doi:10.1038/icb.2011.99

157. Zhang Y, Zhou F, Bai M, Liu Y, Zhang L, Zhu Q, Bi Y, Ning G, Zhou L, Wang X. The pivotal role of protein acetylation in linking glucose and fatty acid metabolism to β-cell function. Cell Death and Disease. 2019;10(2). http://dx.doi.org/10.1038/s41419-019-1349-z. doi:10.1038/s41419-019-1349-z

158. Di Martile M, Del Bufalo D, Trisciuoglio D. The multifaceted role of lysine acetylation in cancer: prognostic biomarker and therapeutic target. Oncotarget. 2016;7(34):55789–55810. https://www.oncotarget.com/lookup/doi/10.18632/oncotarget.10048. doi:10.18632/oncotarget.10048

159. Stapleton D, Gao G, Michell BJ, Widmerq J, House M, Wittersq LA. Protein Kinase Non-catalytic Subunits Are Homologs of Snfl Protein Kinase. Journal of biological chemistry. 1994;269(47):29343–29346.

160. Carlson M, Osmond BC, Botstein D. Mutants of yeast defective in sucrose utilization. Genetics. 1981;98(1):25–40.

161. Chevtzoff C, Vallortigara J, Avéret N, Rigoulet M, Devin A. The yeast cAMP protein kinase Tpk3p is involved in the regulation of mitochondrial enzymatic content during growth. Biochimica et Biophysica Acta - Bioenergetics. 2005. doi:10.1016/j.bbabio.2004.10.001

162. Chang-Rung C, Blackstone C, Chang CR, Blackstone C. Cyclic AMP-dependent protein kinase phosphorylation of Drp1 regulates its GTPase activity and mitochondrial morphology. Journal of Biological Chemistry. 2007;282(30):21583–21587. doi:10.1074/jbc.C700083200

163. Griffioen G, Anghileri P, Imre E, Baroni MD, Ruis H. Nutritional control of nucleocytoplasmic localization of cAMP-dependent protein kinase catalytic and regulatory subunits in Saccharomyces cerevisiae. Journal of Biological Chemistry. 2000;275(2):1449–1456. doi:10.1074/jbc.275.2.1449

164. Ould Amer Y, Hebert-Chatelain E. Mitochondrial cAMP-PKA signaling: What do we really know? Biochimica et Biophysica Acta - Bioenergetics. 2018;1859(9):868–877. http://dx.doi.org/10.1016/j.bbabio.2018.04.005. doi:10.1016/j.bbabio.2018.04.005

165. Canaves JM, Taylor SS. Classification and phylogenetic analysis of the cAMP-dependent protein kinase regulatory subunit family. Journal of Molecular Evolution. 2002;54(1):17–29. doi:10.1007/s00239-001-0013-1

166. Griffioen G, Thevelein JM. Molecular mechanisms controlling the localisation of protein kinase A. Current Genetics. 2002;41(4):199–207. doi:10.1007/s00294-002-0308-9

167. Zhang F, Zhang L, Qi Y, Xu H. Mitochondrial cAMP signaling. Cellular and Molecular Life Sciences. 2016;73(24):4577–4590. doi:10.1007/s00018-016-2282-2

168. Griffioen G, Branduardi P, Ballarini A, Anghileri P, Norbeck J, Baroni MD, Ruis H. Nucleocytoplasmic Distribution of Budding Yeast Protein Kinase A Regulatory Subunit Bcy1 Requires

Zds1 and Is Regulated by Yak1-Dependent Phosphorylation of Its Targeting Domain. Molecular and Cellular Biology. 2001;21(2):511–523. http://mcb.asm.org/cgi/doi/10.1128/MCB.21.2.511-523.2001. doi:10.1128/MCB.21.2.511-523.2001

169. Tudisca V, Recouvreux V, Moreno S, Boy-Marcotte E, Jacquet M, Portela P. Differential localization to cytoplasm, nucleus or P-bodies of yeast PKA subunits under different growth conditions. European Journal of Cell Biology. 2010;89:339–348. http://dx.doi.org/10.1016/j.ejcb.2009.08.005. doi:10.1016/j.ejcb.2009.08.005

170. Estruch F, Carlson M. Two homologous zinc finger genes identified by multicopy suppression in a SNF1 protein kinase mutant of Saccharomyces cerevisiae. Molecular and Cellular Biology. 1993;13(7):3872–3881. doi:10.1128/mcb.13.7.3872

171. Rajvanshi PK, Arya M, Rajasekharan R. The stress-regulatory transcription factors Msn2 and Msn4 regulate fatty acid oxidation in budding yeast. Journal of Biological Chemistry. 2017;292(45):18628–18643. doi:10.1074/jbc.M117.801704

172. Kuang Z, Pinglay S, Ji H, Boeke JD. Msn2/4 regulate expression of glycolytic enzymes and control transition from quiescence to growth. eLife. 2017;6:1–16. doi:10.7554/eLife.29938

173. Rollins M, Huard S, Morettin A, Takuski J, Pham TT, Fullerton MD, Côté J, Baetz K. Lysine acetyltransferase NuA4 and acetyl-CoA regulate glucose-deprived stress granule formation in Saccharomyces cerevisiae Caudy A, editor. PLOS Genetics. 2017;13(2):e1006626. https://dx.plos.org/10.1371/journal.pgen.1006626. doi:10.1371/journal.pgen.1006626

174. Tong AHY, Boone C. Synthetic Genetic Array Analysis in Saccharomyces cerevisiae. Methods in Molecular Biology. 313(1):171–191.

175. Tong AHY, Lesage G, Bader GD, Ding H, Xu H, Xin X, Young J, Berriz GF, Brost RL, Chang M, et al. Global mapping of the yeast genetic interaction network. Science. 2004;303:808–814.

176. Wayne AW, Peter JR, Manuel M, Edurne B-F, Francisco José M, Gustavo E, Alejandro MV, Javier P-R. Regulation of glycogen metabolism in yeast and bacteria. FEMS Microbiology Reviews. 2010;34(6):952–985. http://dx.doi.org/10.1111/j.1574-6976.2010.00220.x. doi:10.1111/j.1574-6976.2010.00220.x.Regulation

177. Roach PJ, Cao Y, Corbeti CA, Farkas I, Fiol CJ, Flotow H, Graves PR, Hrubey TW, Viskupic E, Zhang W. Glycogen metabolism and signal transduction in mammals and yeast. Advances in Enzyme Regulation. 1991;31:101–120.

178. Adeva-andany MM, González-lucán M, Donapetry-garcía C, Fernández-fernández C, Ameneiros-rodríguez E. Glycogen metabolism in humans. BBA Clinical. 2016;5:85–100. http://dx.doi.org/10.1016/j.bbacli.2016.02.001. doi:10.1016/j.bbacli.2016.02.001

179. Quain DE, Tubb RS. A rapid, simple, adaptable and widely applicable procedure for the determination of glycogen in yeast. Journal of Institute of Brewing. 1983;89:38–40.

180. Enjalbert B, Parrou JL, Teste MA, Francois J. Combinatorial control by the protein kinases PKA, PHO85 and SNF1 of transcriptional induction of the Saccharomyces cerevisiae GSY2 gene at the diauxic shift. Molecular Genetics and Genomics. 2004;271(6):697–708. http://link.springer.com/10.1007/s00438-004-1014-8. doi:10.1007/s00438-004-1014-8

181. Unnikrishnan I, Miller S, Meinke M, LaPorte DC. Multiple positive and negative elements involved in the regulation of expression of GSY1 in Saccharomyces cerevisiae. Journal of Biological Chemistry. 2003;278(29):26450–26457. doi:10.1074/jbc.M211808200

182. Moskvina E, Schüller C, Maurer CTC, Mager WH, Ruis H. A search in the genome of Saccharomyces cerevisiae for genes regulated via stress response elements. Yeast. 1998;14(11):1041–1050. doi:10.1002/(SICI)1097-0061(199808)14:11<1041::AID-YEA296>3.0.CO;2-4

183. Farkas I, Hardy TA, Goeblt MG, Roach PJ. Two Glycogen Synthase Isoforms in Saccharomyces are coded in distict genes that are differentially controlled. The Journal of Biological Chemistry. 1991;(19):15602–15607.

184. Teste MA, Enjalbert B, Parrou JL, François JM. The Saccharomyces cerevisiae YPR184w gene encodes the glycogen debranching enzyme. FEMS Microbiology Letters. 2000;193(1):105–110. doi:10.1016/S0378-1097(00)00468-7

185. François J, Parrou JL. Reserve carbohydrates metabolism in the yeast Saccharomyces cerevisiae. FEMS Microbiology Reviews. 2001;25(1):125–145. doi:10.1016/S0168-6445(00)00059-0

186. Vowinckel J, Hartl J, Butler R, Ralser M. MitoLoc: A method for the simultaneous quantification of mi tochondrial network morphology and membrane potential in single cells. Mitochondrion. 2015;24:77–86. http://dx.doi.org/10.1016/j.mito.2015.07.001. doi:10.1016/j.mito.2015.07.001

187. Giacomello M, Pyakurel A, Glytsou C, Scorrano L. The cell biology of mitochondrial membrane dynamics. Nature Reviews Molecular Cell Biology. 2020:1–21. http://www.nature.com/articles/s41580-020-0210-7. doi:10.1038/s41580-020-0210-7

188. Hanekamp T, Thorsness MK, Rebbapragada I, Fisher EM, Seebart C, Darland MR, Coxbill JA, Updike DL, Thorsness PE. Maintenance of mitochondrial morphology is linked to maintenance of the mitochondrial genome in Saccharomyces cerevisiae. Genetics. 2002;162(3):1147–1156.

189. Bolotin-Fukuhara M. Thirty years of the HAP2/3/4/5 complex. Biochimica et Biophysica Acta - Gene Regulatory Mechanisms. 2017. doi:10.1016/j.bbagrm.2016.10.011

190. Chowanadisai W, Bauerly KA, Tchaparian E, Wong A, Cortopassi GA, Rucker RB. Pyrroloquinoline quinone stimulates mitochondrial biogenesis through cAMP response element-binding protein phosphorylation and increased PGC-1α expression. Journal of Biological Chemistry. 2010;285(1):142–152. doi:10.1074/jbc.M109.030130

191. Vlahakis A, Lopez Muniozguren N, Powers T. Stress-response transcription factors Msn2 and Msn4 couple TORC2-Ypk1 signaling and mitochondrial respiration to ATG8 gene expression and autophagy. Autophagy. 2017;13(11):1804–1812. https://doi.org/10.1080/15548627.2017.1356949. doi:10.1080/15548627.2017.1356949

192. Dai C, Miao D, Li H, Yi C, Huang Y, Li N, Yuan K, Sun C, Xue R, Yu L, et al. Formation of a Snf1-Mec1-Atg1 Module on Mitochondria Governs Energy Deprivation-Induced Autophagy by Regulating Mitochondrial Respiration. Developmental Cell. 2017;41(1):59-71.e4. doi:10.1016/j.devcel.2017.03.007

193. Martinez-Ortiz C, Carrillo-Garmendia A, Correa-Romero BF, Canizal-García M, González-Hernández JC, Regalado-Gonzalez C, Olivares-Marin IK, Madrigal-Perez LA. SNF1 controls the glycolytic flux and mitochondrial respiration. Yeast. 2019;36:487–494. https://onlinelibrary.wiley.com/doi/abs/10.1002/yea.3399. doi:10.1002/yea.3399

194. Herzig D, Eser P, Radtke T, Wenger A, Rusterholz T, Wilhelm M, Achermann P, Arhab A, Jenni OG, Kakebeeke TH, et al. Relation of heart rate and its variability during sleep with age, physical activity, and body composition in young children. Frontiers in Physiology. 2017;8:1–12. doi:10.3389/fphys.2017.00109

195. Suhm T, Kaimal JM, Dawitz H, Peselj C, Masser AE, Hanzén S, Ambrožič M, Smialowska A,

Björck ML, Brzezinski P, et al. Mitochondrial Translation Efficiency Controls Cytoplasmic Protein Homeostasis. Cell Metabolism. 2018;27(6):1309-1322.e6. doi:10.1016/j.cmet.2018.04.011

196. Zhou W, Chen KH, Cao W, Zeng J, Liao H, Zhao L, Guo X. Mutation of the protein kinase A phosphorylation site influences the anti-proliferative activity of mitofusin 2. Atherosclerosis. 2010;211(1):216–223. http://dx.doi.org/10.1016/j.atherosclerosis.2010.02.012. doi:10.1016/j.atherosclerosis.2010.02.012

197. Pidoux G, Witczak O, Jarnss E, Myrvold L, Urlaub H, Stokka AJ, Küntziger T, Taskén K. Optic atrophy 1 is an A-kinase anchoring protein on lipid droplets that mediates adrenergic control of lipolysis. EMBO Journal. 2011;30(21):4371–4386. doi:10.1038/emboj.2011.365

198. Cribbs JT, Strack S. Reversible phosphorylation of Drp1 by cyclic AMP-dependent protein kinase and calcineurin regulates mitochondrial fission and cell death. EMBO Reports. 2007;8(10):939–944. doi:10.1038/sj.embor.7401062

199. Schmidt O, Harbauer AB, Rao S, Eyrich B, Zahedi RP, Stojanovski D, Schönfisch B, Guiard B, Sickmann A, Pfanner N, et al. Regulation of mitochondrial protein import by cytosolic kinases. Cell. 2011;144(2):227–239. doi:10.1016/j.cell.2010.12.015

200. Gerbeth C, Schmidt O, Rao S, Harbauer AB, Mikropoulou D, Opalinska M, Guiard B, Pfanner N, Meisinger C. Glucose-induced regulation of protein import receptor tom22 by cytosolic and mitochondria-bound kinases. Cell Metabolism. 2013;18(4):578–587. doi:10.1016/j.cmet.2013.09.006

201. Lark DS, Reese LR, Ryan TE, Torres MJ, Smith CD, Lin C Te, Neufer PD. Protein kinase A governs oxidative phosphorylation kinetics and oxidant emitting potential at complex I. Frontiers in Physiology. 2015;6:1–11. doi:10.3389/fphys.2015.00332

202. Xie K, Zhu M, Xiang P, Chen X, Kasimumali A, Lu R, Wang Q, Ni Z, Gu L, Pang H. Protein Kinase A/CREB Signaling Prevents Adriamycin-Induced Podocyte Apoptosis via Upregulation of Mitochondrial Respiratory Chain Complexes. Molecular and Cellular Biology. 2018;38(1):1–16.

203. Kamieniarz K, Schneider R. Tools to Tackle Protein Acetylation. Chemistry and Biology. 2009;16(10):1027–1029. http://dx.doi.org/10.1016/j.chembiol.2009.10.002. doi:10.1016/j.chembiol.2009.10.002

204. Brust H, Orzechowski S, Fettke J. Starch and Glycogen Analyses: Methods and Techniques. Biomolecules. 2020;10(7). doi:10.3390/biom10071020

205. Bodvard K, Peeters K, Roger F, Romanov N, Igbaria A, Welkenhuysen N, Palais G, Reiter W, Toledano MB, Käll M, et al. Light-sensing via hydrogen peroxide and a peroxiredoxin. Nature Communications. 2017;8. doi:10.1038/ncomms14791

206. Budhwar R, Lu A, Hirsch JP. Nutrient Control of Yeast PKA Activity Involves Opposing Effects on Phosphorylation of the Bcy1 Regulatory Subunit Lew DJ, editor. Molecular Biology of the Cell. 2010;21(21):3749–3758. https://www.molbiolcell.org/doi/10.1091/mbc.e10-05-0388. doi:10.1091/mbc.e10-05-0388

207. Li Y, Wang Y. Ras protein/cAMP-dependent protein kinase signaling is negatively regulated by a deubiquitinating enzyme, Ubp3, in yeast. Journal of Biological Chemistry. 2013;288(16):11358–11365. doi:10.1074/jbc.M112.449751

208. Lindstrom KC, Vary JC, Parthun MR, Delrow J, Tsukiyama T. Isw1 Functions in Parallel with the NuA4 and Swr1 Complexes in Stress-Induced Gene Repression. Molecular and Cellular Biology. 2006;26(16):6117–6129. http://mcb.asm.org/cgi/doi/10.1128/MCB.00642-06. doi:10.1128/MCB.00642-06

209. Yu R, Liu T, Ning C, Tan F, Jin SB, Lendahl U, Zhao J, Nistér M. The phosphorylation status of Ser-637 in dynamin-related protein 1 (Drp1) does not determine Drp1 recruitment to mitochondria. Journal of Biological Chemistry. 2019;294(46):17262–17277. doi:10.1074/jbc.RA119.008202

210. Kim YY, Um JH, Yoon JH, Lee DY, Lee YJ, Kim DH, Park JI, Yun J. p53 regulates mitochondrial dynamics by inhibiting Drp1 translocation into mitochondria during cellular senescence. FASEB Journal. 2020;34(2):2451–2464. doi:10.1096/fj.201901747RR

211. Akabane S, Uno M, Tani N, Shimazaki S, Ebara N, Kato H, Kosako H, Oka T. PKA Regulates PINK1 Stability and Parkin Recruitment to Damaged Mitochondria through Phosphorylation of MIC60. Molecular Cell. 2016;62(3):371–384. http://dx.doi.org/10.1016/j.molcel.2016.03.037. doi:10.1016/j.molcel.2016.03.037

212. Bouchez C, Devin A. Mitochondrial Biogenesis and Mitochondrial Reactive Oxygen Species (ROS): A Complex Relationship Regulated by the cAMP/PKA Signaling Pathway. Cells. 2019;8(4):287. doi:10.3390/cells8040287

213. Fernandez-Marcos PJ, Auwerx J. Regulation of PGC-1α, a nodal regulator of mitochondrial biogenesis. The American Journal of Clinical Nutrition. 2011;93(4):884S-890S. https://academic.oup.com/ajcn/article/93/4/884S/4597813. doi:10.3945/ajcn.110.001917

214. Moujalled D, Weston R, Anderton H, Ninnis R, Goel P, Coley A, Huang DC, Wu L, Strasser A, Puthalakath H. Cyclic-AMP-dependent protein kinase A regulates apoptosis by stabilizing the BH3-only protein Bim. EMBO Reports. 2011;12(1):77–83. doi:10.1038/embor.2010.190

215. Lizcano JM, Morrice N, Cohen P. Regulation of BAD by cAMP-dependent protein kinase is mediated via phosphorylation of a novel site, Ser155. Biochemical Journal. 2000;349(2):547–557. doi:10.1042/0264-6021:3490547

216. Harada H, Becknell B, Wilm M, Mann M, Jun-shen Huang L, Taylor SS, Scott JD, Korsmeyer SJ. Phosphorylation and Inactivation of BAD by Mitochondria-Anchored Protein Kinase A tissues and the maintenance of normal tissue homeosta- sis. In order for cells to avoid a suicidal fate, they must receive cues from their extracellular environment (Raff. Molecular Cell. 1999;3:413–422.

217. Langeberg LK, Scott JD. A-kinase-anchoring proteins. Journal of Cell Science. 2005;118(15):3217–3220. doi:10.1242/jcs.02416

218. Galello F, Moreno S, Rossi S. Interacting proteins of protein kinase A regulatory subunit in Saccharomyces cerevisiae. Journal of Proteomics. 2014;109:261–275. http://dx.doi.org/10.1016/j.jprot.2014.07.008. doi:10.1016/j.jprot.2014.07.008

219. Longtine MS, Mckenzie III A, Demarini DJ, Shah NG, Wach A, Brachat A, Philippsen P, Pringle JR. Additional modules for versatile and economical PCR-based gene deletion and modification in Saccharomyces cerevisiae. Yeast. 1998;14(10):953–961. https://onlinelibrary.wiley.com/doi/10.1002/(SICI)1097-0061(199807)14:10%3C953::AID-YEA293%3E3.0.CO;2-U. doi:10.1002/(SICI)1097-0061(199807)14:10<953::AID-YEA293>3.0.CO;2-U

220. Koh JLY, Chong YT, Friesen H, Moses A, Boone C, Andrews BJ, Moffat J. CYCLoPs: A comprehensive database constructed from automated analysis of protein abundance and subcellular localization patterns in Saccharomyces cerevisiae. G3: Genes, Genomes, Genetics. 2015;5(6):1223–1232. doi:10.1534/g3.115.017830

221. Romanauska A, Köhler A. The Inner Nuclear Membrane Is a Metabolically Active Territory that Generates Nuclear Lipid Droplets. Cell. 2018;174(3):700-715.e18. doi:10.1016/j.cell.2018.05.047

222. Hardy TA, Roach PJ. Control of yeast glycogen synthase-2 by COOH-terminal phosphorylation.

Journal of Biological Chemistry. 1993;268(32):23799–23805.

223. Mollica JP, Oakhill JS, Lamb GD, Murphy RM. Are genuine changes in protein expression being overlooked? Reassessing Western blotting. Analytical Biochemistry. 2009;386(2):270–275. doi:10.1016/j.ab.2008.12.029

224. Yao W, King DA, Beckwith SL, Gowans GJ, Yen K, Zhou C, Morrison AJ. The INO80 Complex Requires the Arp5-Ies6 Subcomplex for Chromatin-Remodeling and Metabolic Regulation. Molecular and Cellular Biology. 2016;36(6):979–991. doi:10.1128/MCB.00801-15

225. DiCarlo JE, Norville JE, Mali P, Rios X, Aach J, Church GM. Genome engineering in Saccharomyces cerevisiae using CRISPR-Cas systems. Nucleic Acids Research. 2013;41(7):4336–4343. https://academic.oup.com/nar/article/41/7/4336/1075252. doi:10.1093/nar/gkt135

226. Judes G, Dubois L, Rifaï K, Idrissou M, Mishellany F, Pajon A, Besse S, Daures M, Degoul F, Bignon YJ, et al. TIP60: An actor in acetylation of H3K4 and tumor development in breast cancer. Epigenomics. 2018;10(11):1415–1430. doi:10.2217/epi-2018-0004

227. Grillitsch K, Connerth M, Köfeler H, Arrey TN, Rietschel B, Wagner B, Karas M, Daum G. Lipid particles/droplets of the yeast Saccharomyces cerevisiae revisited: Lipidome meets Proteome. Biochimica et Biophysica Acta - Molecular and Cell Biology of Lipids. 2011;1811(12):1165–1176. http://dx.doi.org/10.1016/j.bbalip.2011.07.015. doi:10.1016/j.bbalip.2011.07.015

228. Radulovic M, Knittelfelder O, Cristobal-Sarramian A, Kolb D, Wolinski H, Kohlwein SD. The emergence of lipid droplets in yeast: Current status and experimental approaches. Current Genetics. 2013;59(4):231–242. doi:10.1007/s00294-013-0407-9

229. Jordá T, Puig S. Regulation of Ergosterol Biosynthesis in Saccharomyces cerevisiae. Genes. 2020;11(7):795. https://www.mdpi.com/2073-4425/11/7/795. doi:10.3390/genes11070795

230. Bhattacharya S, Esquivel BD, White TC. Overexpression or Deletion of Ergosterol Biosynthesis Genes Alters Doubling Time, Response to Stress Agents, and Drug Susceptibility in Saccharomyces cerevisiae Lorenz M, editor. mBio. 2018;9(4):1–14. https://journals.asm.org/doi/10.1128/mBio.01291-18. doi:10.1128/mBio.01291-18

231. Hu Z, He B, Ma L, Sun Y, Niu Y, Zeng B. Recent Advances in Ergosterol Biosynthesis and Regulation Mechanisms in Saccharomyces cerevisiae. Indian Journal of Microbiology. 2017;57(3):270–277. http://link.springer.com/10.1007/s12088-017-0657-1. doi:10.1007/s12088-017-0657-1

232. Liu JF, Xia JJ, Nie KL, Wang F, Deng L. Outline of the biosynthesis and regulation of ergosterol in yeast. World Journal of Microbiology and Biotechnology. 2019;35(7):1–8. https://doi.org/10.1007/s11274-019-2673-2. doi:10.1007/s11274-019-2673-2

233. Yang H, Bard M, Bruner DA, Gleeson A, Deckelbaum RJ, Aljinovic G, Pohl TM, Rothstein R, Sturley SL. Sterol Esterification in Yeast: A Two-Gene Process. Science. 1996;272(5266):1353–1356. https://www.science.org/doi/10.1126/science.272.5266.1353. doi:10.1126/science.272.5266.1353

234. Zavrel M, Hoot SJ, White TC. Comparison of sterol import under aerobic and anaerobic conditions in three fungal species, Candida albicans, Candida glabrata, and Saccharomyces cerevisiae. Eukaryotic Cell. 2013;12(5):725–738. doi:10.1128/EC.00345-12

235. Rine J, Vik A. Upc2p and Ecm22p, Dual Regulators of Sterol Biosynthesis in. Society. 2001;21(19):6395–6405. doi:10.1128/MCB.21.19.6395

236. Hampton RY, Bhakta H. Ubiquitin-mediated regulation of 3-hydroxy-3-methylglutaryl-CoA reductase. Proceedings of the National Academy of Sciences of the United States of America.

1997;94(24):12944–12948. doi:10.1073/pnas.94.24.12944

237. Foresti O, Ruggiano A, Hannibal-Bach HK, Ejsing CS, Carvalho P. Sterol homeostasis requires regulated degradation of squalene monooxygenase by the ubiquitin ligase Doa10/Teb4. eLife. 2013;2013(2):1–17. doi:10.7554/eLife.00953

238. Lan Q, Li Y, Wang F, Li Z, Gao Y, Lu H, Wang Y, Zhao Z, Deng Z, He F, et al. Deubiquitinase Ubp3 enhances the proteasomal degradation of key enzymes in sterol homeostasis. Journal of Biological Chemistry. 2021;296:100348. https://doi.org/10.1016/j.jbc.2021.100348. doi:10.1016/j.jbc.2021.100348

239. Shobayashi M, Mitsueda S, Ago M, Fujii T, Iwashita K, Iefuji H. Effects of culture conditions on ergosterol biosynthesis by Saccharomyces cerevisiae. Bioscience, biotechnology, and biochemistry. 2005;69(12):2381–8. https://academic.oup.com/bbb/article/69/12/2381-2388/5953398. doi:10.1271/bbb.69.2381

240. Shang F, Wen S, Wang X, Tan T. High-cell-density fermentation for ergosterol production by Saccharomyces cerevisiae. Journal of Bioscience and Bioengineering. 2006;101(1):38–41. doi:10.1263/jbb.101.38

241. Shakoury-Elizeh M, Protchenko O, Berger A, Cox J, Gable K, Dunn TM, Prinz WA, Bard M, Philpott CC. Metabolic Response to Iron Deficiency in Saccharomyces cerevisiae. Journal of Biological Chemistry. 2010;285(19):14823–14833. http://dx.doi.org/10.1074/jbc.M109.091710. doi:10.1074/jbc.M109.091710

242. Leber R, Landl K, Zinser E, Ahorn H, Spök A, Kohlwein SD, Turnowsky F, Daum G. Dual localization of squalene epoxidase, Erg1p, in yeast reflects a relationship between the endoplasmic reticulum and lipid particles. Molecular Biology of the Cell. 1998;9(2):375–386. doi:10.1091/mbc.9.2.375

243. Liu Q, Zerbinatti C V., Zhang J, Hoe H-S, Wang B, Cole SL, Herz J, Muglia L, Bu G. Amyloid Precursor Protein Regulates Brain Apolipoprotein E and Cholesterol Metabolism through Lipoprotein Receptor LRP1. Neuron. 2007;56(1):66–78. https://linkinghub.elsevier.com/retrieve/pii/S0896627307006204. doi:10.1016/j.neuron.2007.08.008

244. Munkacsi AB, Chen FW, Brinkman MA, Higaki K, Gutiérrez GD, Chaudhari J, Layer J V., Tong A, Bard M, Boone C, et al. An “exacerbate-reverse” strategy in yeast identifies histone deacetylase inhibition as a correction for cholesterol and sphingolipid transport defects in human niemann-pick type C disease. Journal of Biological Chemistry. 2011;286(27):23842–23851. doi:10.1074/jbc.M111.227645

245. Pipalia NH, Cosner CC, Huang A, Chatterjee A, Bourbon P, Farley N, Helquist P, Wiest O, Maxfield FR. Histone deacetylase inhibitor treatment dramatically reduces cholesterol accumulation in Niemann-Pick type C1 mutant human fibroblasts. Proceedings of the National Academy of Sciences. 2011;108(14):5620–5625. http://www.pnas.org/cgi/doi/10.1073/pnas.1014890108. doi:10.1073/pnas.1014890108

246. Bligh EG, Dyer WJ. A rapid method of total lipid extraction and purification. Canadian Journal of Biochemistry and Physiology. 1959;37(8):911–917.

247. Müller C, Binder U, Bracher F, Giera M. Antifungal drug testing by combining minimal inhibitory concentration testing with target identification by gas chromatography-mass spectrometry. Nature Protocols. 2017;12(5):947–963. doi:10.1038/nprot.2017.005

248. Pluskal T, Castillo S, Villar-Briones A, Orešič M. MZmine 2: Modular framework for processing, visualizing, and analyzing mass spectrometry-based molecular profile data. BMC Bioinformatics. 2010;11. doi:10.1186/1471-2105-11-395

249. Myers OD, Sumner SJ, Li S, Barnes S, Du X. One Step Forward for Reducing False Positive and False Negative Compound Identifications from Mass Spectrometry Metabolomics Data: New Algorithms for Constructing Extracted Ion Chromatograms and Detecting Chromatographic Peaks. Analytical Chemistry. 2017;89(17):8696–8703. doi:10.1021/acs.analchem.7b00947

250. Mi H, Ebert D, Muruganujan A, Mills C, Albou LP, Mushayamaha T, Thomas PD. PANTHER version 16: A revised family classification, tree-based classification tool, enhancer regions and extensive API. Nucleic Acids Research. 2021;49(D1):D394–D403. doi:10.1093/nar/gkaa1106

251. Maere S, Heymans K, Kuiper M. BiNGO: A Cytoscape plugin to assess overrepresentation of Gene Ontology categories in Biological Networks. Bioinformatics. 2005;21(16):3448–3449. doi:10.1093/bioinformatics/bti551

252. Shannon P, Markiel A, Owen Ozier, Nitin S. Baliga JTW, Ramage D, Nada Amin, Schwikowski B, Ideker T. Cytoscape: A Software Environment for Integrated Models. Genome Research. 2003;13(22):426. http://ci.nii.ac.jp/naid/110001910481/. doi:10.1101/gr.1239303.metabolite

253. Hartmann DO, Shimizu K, Rothkegel M, Petkovic M, Ferraz R, Petrovski Ž, Branco LC, Canongia Lopes JN, Silva Pereira C. Tailoring amphotericin B as an ionic liquid: an upfront strategy to potentiate the biological activity of antifungal drugs. RSC Advances. 2021;11(24):14441–14452. http://xlink.rsc.org/?DOI=D1RA00234A. doi:10.1039/D1RA00234A

254. Moosa MYS, Alangaden GJ, Manavathu E, Chandrasekar PH. Resistance to amphotericin B does not emerge during treatment for invasive aspergillosis. Journal of Antimicrobial Chemotherapy. 2002;49(1):209–213. doi:10.1093/jac/49.1.209

255. Lorenz RT, Parks LW. Effects of lovastatin (mevinolin) on sterol levels and on activity of azoles in Saccharomyces cerevisiae. Antimicrobial Agents and Chemotherapy. 1990;34(9):1660–1665. doi:10.1128/AAC.34.9.1660

256. Szomek M, Reinholdt P, Petersen D, Caci A, Kongsted J, Wüstner D. Direct observation of nystatin binding to the plasma membrane of living cells. Biochimica et Biophysica Acta - Biomembranes. 2021;1863(2):183528. https://doi.org/10.1016/j.bbamem.2020.183528. doi:10.1016/j.bbamem.2020.183528

257. Ruckenstuhl C, Lang S, Poschenel A, Eidenberger A, Baral PK, Kohút P, Hapala I, Gruber K, Turnowsky F. Characterization of squalene epoxidase of Saccharomyces cerevisiae by applying terbinafine-sensitive variants. Antimicrobial Agents and Chemotherapy. 2007;51(1):275–284. doi:10.1128/AAC.00988-06

258. Berkow EL, Lockhart SR. Fluconazole resistance in Candida species: A current perspective. Infection and Drug Resistance. 2017;10:237–245. doi:10.2147/IDR.S118892

259. Serhan G, Stack CM, Perrone GG, Morton CO. The polyene antifungals, amphotericin B and nystatin, cause cell death in Saccharomyces cerevisiae by a distinct mechanism to amphibian-derived antimicrobial peptides. Annals of Clinical Microbiology and Antimicrobials. 2014;13(1):18–21. doi:10.1186/1476-0711-13-18

260. Gray KC, Palacios DS, Dailey I, Endo MM, Uno BE, Wilcock BC, Burke MD. Amphotericin primarily kills yeast by simply binding ergosterol. Proceedings of the National Academy of Sciences of the United States of America. 2012;109(7):2234–2239. doi:10.1073/pnas.1117280109

261. Falcón-González JM, Jiménez-Domínguez G, Ortega-Blake I, Carrillo-Tripp M. Multi-Phase Solvation Model for Biological Membranes: Molecular Action Mechanism of Amphotericin B. Journal of Chemical Theory and Computation. 2017;13(7):3388–3397. doi:10.1021/acs.jctc.7b00337

262. Mesa-Arango AC, Scorzoni L, Zaragoza O. It only takes one to do many jobs: Amphotericin B as antifungal and immunomodulatory drug. Frontiers in Microbiology. 2012;3(AUG):1–10. doi:10.3389/fmicb.2012.00286

263. Young LY, Hull CM, Heitman J. Disruption of ergosterol biosynthesis confers resistance to amphotericin B in Candida lusitaniae. Antimicrobial Agents and Chemotherapy. 2003;47(9):2717–2724. https://journals.asm.org/doi/10.1128/AAC.47.9.2717-2724.2003. doi:10.1128/AAC.47.9.2717-2724.2003

264. Van Leeuwen MR, Smant W, de Boer W, Dijksterhuis J. Filipin is a reliable in situ marker of ergosterol in the plasma membrane of germinating conidia (spores) of Penicillium discolor and stains intensively at the site of germ tube formation. Journal of Microbiological Methods. 2008;74(2–3):64–73. https://linkinghub.elsevier.com/retrieve/pii/S0167701208001073. doi:10.1016/j.mimet.2008.04.001

265. Qiu B, Simon M. BODIPY 493/503 Staining of Neutral Lipid Droplets for Microscopy and Quantification by Flow Cytometry. Bio-Protocol. 2016;6(17):1–6. doi:10.21769/bioprotoc.1912

266. Wolinski H, Bredies K, Kohlwein SD. Quantitative Imaging of Lipid Metabolism in Yeast: From 4D Analysis to High Content Screens of Mutant Libraries. Elsevier Inc.; 2012. http://dx.doi.org/10.1016/B978-0-12-386487-1.00016-X. doi:10.1016/B978-0-12-386487-1.00016-X

267. Choi JW, Da Silva NA. Improving polyketide and fatty acid synthesis by engineering of the yeast acetyl-CoA carboxylase. Journal of Biotechnology. 2014;187:56–59. http://dx.doi.org/10.1016/j.jbiotec.2014.07.430. doi:10.1016/j.jbiotec.2014.07.430

268. Vincent O, Carlson M. Gal83 mediates the interaction of the Snf1 kinase complex with the transcription activator Sip4. EMBO Journal. 1999;18(23):6672–6681. doi:10.1093/emboj/18.23.6672

269. Ludin K, Jiang R, Carlson M. Glucose-regulated interaction of a regulatory subunit of protein phosphatase 1 with the Snf1 protein kinase in Saccharomyces cerevisiae. Proceedings of the National Academy of Sciences of the United States of America. 1998;95(11):6245–6250. doi:10.1073/pnas.95.11.6245

270. Lum PY, Armour CD, Stepaniants SB, Cavet G, Wolf MK, Butler JS, Hinshaw JC, Garnier P, Prestwich GD, Leonardson A, et al. Discovering Modes of Action for Therapeutic Compounds Using a Genome-Wide Screen of Yeast Heterozygotes. Cell. 2004;116(1):121–137. doi:10.1016/S0092-8674(03)01035-3

271. Huang Z, Chen K, Zhang J, Li Y, Wang H, Cui D, Tang J, Liu Y, Shi X, Li W, et al. A Functional Variomics Tool for Discovering Drug-Resistance Genes and Drug Targets. Cell Reports. 2013;3(2):577–585. http://dx.doi.org/10.1016/j.celrep.2013.01.019. doi:10.1016/j.celrep.2013.01.019

272. Parsons AB, Lopez A, Givoni IE, Williams DE, Gray CA, Porter J, Chua G, Sopko R, Brost RL, Ho CH, et al. Exploring the Mode-of-Action of Bioactive Compounds by Chemical-Genetic Profiling in Yeast. Cell. 2006;126(3):611–625. doi:10.1016/j.cell.2006.06.040

273. Kornblatt JA, Rudney H. Two Forms of Acetoacetyl Coenzyme A Thiolase in Yeast. Journal of Biological Chemistry. 1971;246(14):4424–4430. http://dx.doi.org/10.1016/S0021-9258(18)62029-0. doi:10.1016/s0021-9258(18)62029-0

274. Mathieu M, Modis Y, Zeelen JP, Engel CK, Abagyan RA, Ahlberg A, Rasmussen B, Lamzin VS, Kunau WH, Wierenga RK. The 1.8 Å crystal structure of the dimeric peroxisomal 3-ketoacyl-CoA thiolase of Saccharomyces cerevisiae: Implications for substrate binding and reaction mechanism. Journal of Molecular Biology. 1997;273(3):714–728. doi:10.1006/jmbi.1997.1331

275. Byrne KP, Wolfe KH. The Yeast Gene Order Browser: Combining curated homology and syntenic context reveals gene fate in polyploid species. Genome Research. 2005;15(10):1456–1461.

doi:10.1101/gr.3672305

276. Yang X, Jiang R, Carlson M. A family of proteins containing a conserved domain that mediates interaction with the yeast SNF1 protein kinase complex. EMBO Journal. 1994;13(24):5878–5886. doi:10.1002/j.1460-2075.1994.tb06933.x

277. Hedbacker K, Carlson M. Regulation of the nucleocytoplasmic distribution of Snf1-Gal83 protein kinase. Eukaryotic Cell. 2006;5(12):1950–1956. doi:10.1128/EC.00256-06

278. Vincent O, Townley R, Kuchin S, Carlson M. Subcellular localization of the Snf1 kinase is regulated by specific ␥ subunits and a novel glucose signaling mechanism. 2001:1104–1114. doi:10.1101/gad.879301.quired

279. Zhang J, Olsson L, Nielsen J. The β-subunits of the Snf1 kinase in Saccharomyces cerevisiae, Gal83 and Sip2, but not Sip1, are redundant in glucose derepression and regulation of sterol biosynthesis. Molecular Microbiology. 2010;77(2):371–383. doi:10.1111/j.1365-2958.2010.07209.x

280. Liu R, Lee JH, Li J, Yu R, Tan L, Xia Y, Zheng Y, Bian XL, Lorenzi PL, Chen Q, et al. Choline kinase alpha 2 acts as a protein kinase to promote lipolysis of lipid droplets. Molecular Cell. 2022;81(13):2722-2735.e9. https://doi.org/10.1016/j.molcel.2021.05.005. doi:10.1016/j.molcel.2021.05.005

281. Beh CT, Cool L, Phillips J, Rine J. Overlapping functions of the yeast oxysterol-binding protein homologues. Genetics. 2001;157(3):1117–1140. doi:10.1093/genetics/157.3.1117

282. Sokolov SS, Trushina NI, Severin FF, Knorre DA. Ergosterol Turnover in Yeast: An Interplay between Biosynthesis and Transport. Biochemistry (Moscow). 2019;84(4):346–357. http://link.springer.com/10.1134/S0006297919040023. doi:10.1134/S0006297919040023

283. McClure JJ, Li X, Chou CJ. Advances and Challenges of HDAC Inhibitors in Cancer Therapeutics. 1st ed. Elsevier Inc.; 2018. http://dx.doi.org/10.1016/bs.acr.2018.02.006. doi:10.1016/bs.acr.2018.02.006

284. Yeung CHL, Sahin N, Andrews B. Phenomics approaches to understand genetic networks and gene function in yeast. Biochemical Society Transactions. 2022;50(2):713–721. doi:10.1042/BST20210285

285. Legube G, Linares LK, Tyteca S, Caron C, Scheffner M, Chevillard-Briet M, Trouche D. Role of the histone acetyl transferase Tip60 in the p53 pathway. Journal of Biological Chemistry. 2004;279(43):44825–44833. doi:10.1074/jbc.M407478200

286. Tamaki H. Glucose-stimulated cAMP-protein kinase a pathway in yeast Saccharomyces cerevisiae. Journal of Bioscience and Bioengineering. 2007;104(4):245–250. doi:10.1263/jbb.104.245

287. Conrad M, Schothorst J, Kankipati HN, Van Zeebroeck G, Rubio-Texeira M, Thevelein JM. Nutrient sensing and signaling in the yeast Saccharomyces cerevisiae. FEMS Microbiology Reviews. 2014;38(2):254–299. doi:10.1111/1574-6976.12065

288. Enjalbert B, Parrou JL, Vincent O, Franc J, Durand G. Mitochondrial respiratory mutants of Saccharomyces cerevisiae accumulate glycogen and readily mobilize it in a glucose-depleted medium. 2000:2685–2694.

289. Monteiro F, Hubmann G, Takhaveev V, Vedelaar SR, Norder J, Hekelaar J, Saldida J, Litsios A, Wijma HJ, Schmidt A, et al. Measuring glycolytic flux in single yeast cells with an orthogonal synthetic biosensor. 2019:1–20. doi:10.15252/msb.20199071

290. Zheng F, Jia B, Dong F, Liu L, Rasul F, He J, Fu C. cro Glucose starvation induces mitochondrial fragmentation depending on the dynamin GTPase Dnm1 / Drp1 in fission. 2019;294(10):17725–17734.

doi:10.1074/jbc.RA119.010185

291. Rogers S, Hariri H, Wood NE, Speer NO, Henne WM. Glucose restriction drives spatial reorganization of mevalonate metabolism. eLife. 2021;10:1–23. https://elifesciences.org/articles/62591. doi:10.7554/eLife.62591

292. Prozzillo Y, Fattorini G, Santopietro MV, Suglia L, Ruggiero A, Ferreri D, Messina G. Targeted Protein Degradation Tools : Overview and Future Perspectives. 2020:1–15.

293. Haruki H, Nishikawa J, Laemmli UK. Technique The Anchor-Away Technique : Rapid , Conditional Establishment of Yeast Mutant Phenotypes. 2008:925–932. doi:10.1016/j.molcel.2008.07.020

294. Bruzzone MJ, Grünberg S, Kubik S, Zentner GE, Shore D. Distinct patterns of histone acetyltransferase and Mediator deployment at yeast protein-coding genes. 2018:1252–1265. doi:10.1101/gad.312173.118.4

295. Reider Apel A, D'Espaux L, Wehrs M, Sachs D, Li RA, Tong GJ, Garber M, Nnadi O, Zhuang W, Hillson NJ, et al. A Cas9-based toolkit to program gene expression in Saccharomyces cerevisiae. Nucleic Acids Research. 2017;45(1):496–508. doi:10.1093/nar/gkw1023

296. Christensen DG, Baumgartner JT, Xie X, Jew KM, Basisty N, Schilling B, Kuhn ML, Wolfe AJ. Mechanisms, detection, and relevance of protein acetylation in prokaryotes. mBio. 2019;10(2):1–20. doi:10.1128/mBio.02708-18

297. Wiltschi B. Incorporation of non-canonical amino acids into proteins in yeast. Fungal Genetics and Biology. 2016;89:137–156. http://dx.doi.org/10.1016/j.fgb.2016.02.002. doi:10.1016/j.fgb.2016.02.002

298. Hanahan D. Hallmarks of Cancer: New Dimensions. Cancer Discovery. 2022;12(1):31–46. doi:10.1158/2159-8290.CD-21-1059

299. Hanahan D, Weinberg RA. Hallmarks of cancer: The next generation. Cell. 2011;144(5):646–674. http://dx.doi.org/10.1016/j.cell.2011.02.013. doi:10.1016/j.cell.2011.02.013

300. Yang J, Zhang X, Yi L, Yang L, Wang WE, Zeng C, Mi M, Chen X. Hepatic PKA inhibition accelerates the lipid accumulation in liver. Nutrition and Metabolism. 2019;16(1):1–14. doi:10.1186/s12986-019-0400-5

301. London E, Stratakis CA. The regulation of PKA signaling in obesity and in the maintenance of metabolic health. Pharmacology and Therapeutics. 2022;237:108113. https://doi.org/10.1016/j.pharmthera.2022.108113. doi:10.1016/j.pharmthera.2022.108113

302. Zhang Z, Shen Q, Wu X, Zhang D, Xing D. Activation of PKA/SIRT1 signaling pathway by photobiomodulation therapy reduces Aβ levels in Alzheimer's disease models. Aging Cell. 2020;19(1):1–15. doi:10.1111/acel.13054

303. Banerjee T Das, Reihl K, Swain M, Torres M, Dagda RK. Mitochondrial PKA Is Neuroprotective in a Cell Culture Model of Alzheimer's Disease. Molecular Neurobiology. 2021;58(7):3071–3083. doi:10.1007/s12035-021-02333-w

304. Korber M, Klein I, Daum G, Vilaça R, Silva E, Nadais A, Teixeira V, Matmati N, Hannun YA, Clara M, et al. Steryl ester synthesis, storage and hydrolysis: A contribution to sterol homeostasis. Biochimica et Biophysica Acta - Molecular and Cell Biology of Lipids. 2017;1862(12):1534–1545. http://dx.doi.org/10.1016/j.bbalip.2017.09.002. doi:10.1016/j.bbalip.2017.09.002

305. Fuller KK, Rhodes JC. Protein kinase A and fungal virulence. Virulence. 2012;3(2):109–121. http://www.tandfonline.com/doi/abs/10.4161/viru.19396. doi:10.4161/viru.19396

306. Razzaq I, Berg MD, Jiang Y, Genereaux J, Uthayakumar D, Kim GH, Agyare-Tabbi M, Halder V, Brandl CJ, Lajoie P, et al. The SAGA and NuA4 component Tra1 regulates Candida albicans drug resistance and pathogenesis. Genetics. 2021;219(2). doi:10.1093/genetics/iyab131

307. Mashima T, Seimiya H, Tsuruo T. De novo fatty-acid synthesis and related pathways as molecular targets for cancer therapy. British Journal of Cancer. 2009;100(100):1369–1372. doi:10.1038/sj.bjc.6605007

308. Currie E, Schulze A, Zechner R, Walther TC, Farese R V. Cellular Fatty Acid Metabolism and Cancer. Cell Metabolism. 2013;18(2):153–161. https://linkinghub.elsevier.com/retrieve/pii/S1550413113002076. doi:10.1016/j.cmet.2013.05.017

309. Fullerton MD, Galic S, Marcinko K, Sikkema S, Pulinilkunnil T, Chen Z-P, O'Neill HM, Ford RJ, Palanivel R, O'Brien M, et al. Single phosphorylation sites in Acc1 and Acc2 regulate lipid homeostasis and the insulin-sensitizing effects of metformin. Nature Medicine. 2013;19(12):1649–1654. https://www.nature.com/articles/nm.3372. doi:10.1038/nm.3372

310. Rios Garcia M, Steinbauer B, Srivastava K, Singhal M, Mattijssen F, Maida A, Christian S, Hess-Stumpp H, Augustin HG, Müller-Decker K, et al. Acetyl-CoA Carboxylase 1-Dependent Protein Acetylation Controls Breast Cancer Metastasis and Recurrence. Cell Metabolism. 2017;26(6):842-855.e5. https://linkinghub.elsevier.com/retrieve/pii/S1550413117305703. doi:10.1016/j.cmet.2017.09.018

311. Engin A. Non-Alcoholic Fatty Liver Disease. In: Adv Exp Med Biol. Vol. 960. 2017/06/07. 2017. p. 443–467. http://link.springer.com/10.1007/978-3-319-48382-5_19. doi:10.1007/978-3-319-48382-5_19

312. Tehlivets O, Scheuringer K, Kohlwein SD. Fatty acid synthesis and elongation in yeast. Biochimica et Biophysica Acta - Molecular and Cell Biology of Lipids. 2007;1771(3):255–270. https://linkinghub.elsevier.com/retrieve/pii/S1388198106001995. doi:10.1016/j.bbalip.2006.07.004

313. Witters LA, Watts TD. Yeast acetyl-CoA carboxylase: In vitro phosphorylation by mammalian and yeast protein kinases. Biochemical and Biophysical Research Communications. 1990;169(2):369–376. https://linkinghub.elsevier.com/retrieve/pii/0006291X9090341J. doi:10.1016/0006-291X(90)90341-J

314. Nielsen J. Systems biology of lipid metabolism: From yeast to human. FEBS Letters. 2009;583(24):3905–3913. http://dx.doi.org/10.1016/j.febslet.2009.10.054. doi:10.1016/j.febslet.2009.10.054

315. Kim J, Kwon J, Kim M, Do J, Lee D, Han H. Low-dielectric-constant polyimide aerogel composite films with low water uptake. Polymer Journal. 2016;48(7):829–834. http://www.nature.com/articles/pj201637. doi:10.1038/pj.2016.37

316. Brownsey RW, Boone AN, Elliott JE, Kulpa JE, Lee WM. Regulation of acetyl-CoA carboxylase. Biochemical Society Transactions. 2006;34(2):223. http://www.biochemsoctrans.org/bst/034/bst0340223.htm. doi:10.1042/BST20060223

317. Chirala SS, Zhong Q, Huang W, Al-Feel W. Analysis of FAS3/ACC regulatory region of Saccharomyces cerevisiae : identification of a functional UAS INO and sequences responsible for fatty acid mediated repression. Nucleic Acids Research. 1994;22(3):412–418. https://academic.oup.com/nar/article-lookup/doi/10.1093/nar/22.3.412. doi:10.1093/nar/22.3.412

318. Carman GM, Han G-S. Regulation of Phospholipid Synthesis in the Yeast Saccharomyces cerevisiae. Annual Review of Biochemistry. 2011;80(1):859–883. http://www.annualreviews.org/doi/10.1146/annurev-biochem-060409-092229. doi:10.1146/annurev-biochem-060409-092229

319. Blank HM, Perez R, He C, Maitra N, Metz R, Hill J, Lin Y, Johnson CD, Bankaitis VA, Kennedy

BK, et al. Translational control of lipogenic enzymes in the cell cycle of synchronous, growing yeast cells. The EMBO Journal. 2017;36(4):487–502. https://onlinelibrary.wiley.com/doi/10.15252/embj.201695050. doi:10.15252/embj.201695050

320. Winder WW, Wilson HA, Hardie DG, Rasmussen BB, Hutber CA, Call GB, Clayton RD, Conley LM, Yoon S, Zhou B. Phosphorylation of rat muscle acetyl-CoA carboxylase by AMP-activated protein kinase and protein kinase A. Journal of Applied Physiology. 1997;82(1):219–225. https://www.ncbi.nlm.nih.gov/pubmed/9029219. doi:10.1152/jappl.1997.82.1.219

321. Woods A, Munday MR, Scott J, Yang X, Carlson M, Carling D. Yeast SNF1 is functionally related to mammalian AMP-activated protein kinase and regulates acetyl-CoA carboxylase in vivo. Journal of Biological Chemistry. 1994;269(30):19509–19515. https://www.ncbi.nlm.nih.gov/pubmed/7913470. doi:10.1016/S0021-9258(17)32198-1

322. Hofbauer HF, Schopf FH, Schleifer H, Knittelfelder OL, Pieber B, Rechberger GN, Wolinski H, Gaspar ML, Kappe CO, Stadlmann J, et al. Regulation of Gene Expression through a Transcriptional Repressor that Senses Acyl-Chain Length in Membrane Phospholipids. Developmental Cell. 2014;29(6):729–739. https://www.ncbi.nlm.nih.gov/pubmed/24960695. doi:10.1016/j.devcel.2014.04.025

323. Schneiter R, Hitomi M, Ivessa AS, Fasch E V, Kohlwein SD, Tartakoff AM. A yeast acetyl coenzyme A carboxylase mutant links very-long-chain fatty acid synthesis to the structure and function of the nuclear membrane-pore complex. Molecular and Cellular Biology. 1996;16(12):7161–7172. https://journals.asm.org/doi/10.1128/MCB.16.12.7161. doi:10.1128/MCB.16.12.7161

324. Schneiter R, Guerra CE, Lampl M, Tatzer V, Zellnig G, Klein HL, Kohlwein SD. A Novel Cold-Sensitive Allele of the Rate-Limiting Enzyme of Fatty Acid Synthesis, Acetyl Coenzyme A Carboxylase, Affects the Morphology of the Yeast Vacuole through Acylation of Vac8p. Molecular and Cellular Biology. 2000;20(9):2984–2995. https://journals.asm.org/doi/10.1128/MCB.20.9.2984-2995.2000. doi:10.1128/MCB.20.9.2984-2995.2000

325. Hunkeler M, Hagmann A, Stuttfeld E, Chami M, Guri Y, Stahlberg H, Maier T. Structural basis for regulation of human acetyl-CoA carboxylase. Nature. 2018;558(7710):470–474. http://dx.doi.org/10.1038/s41586-018-0201-4. doi:10.1038/s41586-018-0201-4

326. Kamiryo T, Parthasarathy S, Numa S. Evidence that acyl coenzyme A synthetase activity is required for repression of yeast acetyl coenzyme A carboxylase by exogenous fatty acids. Proceedings of the National Academy of Sciences of the United States of America. 1976;73(2):386–90. http://www.ncbi.nlm.nih.gov/pubmed/1754. doi:10.1073/pnas.73.2.386

327. Shirra MK, Patton-Vogt J, Ulrich A, Liuta-Tehlivets O, Kohlwein SD, Henry SA, Arndt KM. Inhibition of acetyl coenzyme A carboxylase activity restores expression of the INO1 gene in a snf1 mutant strain of Saccharomyces cerevisiae. Molecular and cellular biology. 2001;21(17):5710–22. http://www.ncbi.nlm.nih.gov/pubmed/11486011. doi:10.1128/MCB.21.17.5710-5722.2001

328. Ogiwara H, Tanabe T, Nikawa J, Numa S. Inhibition of rat-liver acetyl-coenzyme-A carboxylase by palmitoyl-coenzyme A. Formation of equimolar enzyme-inhibitor complex. European journal of biochemistry. 1978;89(1):33–41. https://www.ncbi.nlm.nih.gov/pubmed/29756. doi:10.1111/j.1432-1033.1978.tb20893.x

329. Nikawa J, Tanabe T, Ogiwara H, Shiba T, Numa S. Inhibitory effects of long-chain acyl coenzyme a analogues on rat liver acetyl coenzyme a carboxylase. FEBS Letters. 1979;102(2):223–226. http://doi.wiley.com/10.1016/0014-5793%2879%2980675-4. doi:10.1016/0014-5793(79)80005-8

330. Pinkosky SL, Scott JW, Desjardins EM, Smith BK, Day EA, Ford RJ, Langendorf CG, Ling NXY, Nero TL, Loh K, et al. Long-chain fatty acyl-CoA esters regulate metabolism via allosteric control of

AMPK β1 isoforms. Nature Metabolism. 2020;2(9):873–881. http://www.nature.com/articles/s42255-020-0245-2. doi:10.1038/s42255-020-0245-2

331. Gerth K, Bedorf N, Irschik H, Höfle G, Reichenbach H. The soraphens: a family of novel antifungal compounds from Sorangium cellulosum (Myxobacteria). I. Soraphen A1 alpha: fermentation, isolation, biological properties. The Journal of antibiotics. 1994;47(1):23–31. https://www.ncbi.nlm.nih.gov/pubmed/8119858. doi:10.7164/antibiotics.47.23

332. Naini A, Sasse F, Brönstrup M. The intriguing chemistry and biology of soraphens. Natural Product Reports. 2019;36(10):1394–1411. http://xlink.rsc.org/?DOI=C9NP00008A. doi:10.1039/c9np00008a

333. Vahlensieck HF, Pridzun L, Reichenbach H, Hinnen A. Identification of the yeast ACC1 gene product (acetyl-CoA carboxylase) as the target of the polyketide fungicide soraphen A. Current Genetics. 1994;25(2):95–100. http://link.springer.com/10.1007/BF00309532. doi:10.1007/BF00309532

334. Bozaquel-Morais BL, Madeira JB, Venâncio TM, Pacheco-Rosa T, Masuda CA, Montero-Lomeli M. A Chemogenomic Screen Reveals Novel Snf1p/AMPK Independent Regulators of Acetyl-CoA Carboxylase Polymenis M, editor. PLOS ONE. 2017;12(1):e0169682. https://www.ncbi.nlm.nih.gov/pubmed/28076367. doi:10.1371/journal.pone.0169682

335. Krogan NJ, Baetz K, Keogh M-C, Datta N, Sawa C, Kwok TCY, Thompson NJ, Davey MG, Pootoolal J, Hughes TR, et al. Regulation of chromosome stability by the histone H2A variant Htz1, the Swr1 chromatin remodeling complex, and the histone acetyltransferase NuA4. Proceedings of the National Academy of Sciences. 2004;101(37):13513–13518. http://www.pnas.org/cgi/doi/10.1073/pnas.0601796103. doi:10.1073/pnas.0405753101

336. Han G-S, Wu W-I, Carman GM. The Saccharomyces cerevisiae Lipin Homolog Is a Mg2+-dependent Phosphatidate Phosphatase Enzyme*. Journal of Biological Chemistry. 2006;281(14):9210–9218. https://linkinghub.elsevier.com/retrieve/pii/S0021925819564535. doi:10.1074/jbc.M600425200

337. Brown JAL, Bourke E, Eriksson LA, Kerin MJ. Targeting cancer using KAT inhibitors to mimic lethal knockouts. Biochemical Society Transactions. 2016;44(4):979–986. http://biochemsoctrans.org/cgi/doi/10.1042/BST20160081. doi:10.1042/BST20160081

338. Fiorentino F, Mai A, Rotili D. Lysine Acetyltransferase Inhibitors From Natural Sources. Frontiers in Pharmacology. 2020;11(August):1–15. https://www.frontiersin.org/article/10.3389/fphar.2020.01243/full. doi:10.3389/fphar.2020.01243

339. Wenzel SC, Williamson RM, Grünanger C, Xu J, Gerth K, Martinez RA, Moss SJ, Carroll BJ, Grond S, Unkefer CJ, et al. On the Biosynthetic Origin of Methoxymalonyl-Acyl Carrier Protein, the Substrate for Incorporation of "Glycolate" Units into Ansamitocin and Soraphen A. Journal of the American Chemical Society. 2006;128(44):14325–14336. https://pubs.acs.org/doi/10.1021/ja064408t. doi:10.1021/ja064408t

340. Fernandez-Ricaud L, Kourtchenko O, Zackrisson M, Warringer J, Blomberg A. PRECOG: a tool for automated extraction and visualization of fitness components in microbial growth phenomics. BMC Bioinformatics. 2016;17(1):249. http://dx.doi.org/10.1186/s12859-016-1134-2. doi:10.1186/s12859-016-1134-2

341. Trinkle-Mulcahy L. Resolving protein interactions and complexes by affinity purification followed by label-based quantitative mass spectrometry. PROTEOMICS. 2012;12(10):1623–1638. https://onlinelibrary.wiley.com/doi/10.1002/pmic.201100438. doi:10.1002/pmic.201100438

342. Styles EB, Founk KJ, Zamparo LA, Sing TL, Altintas D, Ribeyre C, Ribaud V, Rougemont J, Mayhew D, Costanzo M, et al. Exploring Quantitative Yeast Phenomics with Single-Cell Analysis of

DNA Damage Foci. Cell Systems. 2016;3(3):264-277.e10. http://dx.doi.org/10.1016/j.cels.2016.08.008. doi:10.1016/j.cels.2016.08.008

343. Lynen F. Yeast fatty acid synthase. In: Methods in Enzymology. Vol. 14. 1969. p. 17–33. https://linkinghub.elsevier.com/retrieve/pii/S0076687969140057. doi:10.1016/S0076-6879(69)14005-7

344. Matias AC, Marinho HS, Cyrne L, Herrero E, Antunes F. Biphasic modulation of fatty acid synthase by hydrogen peroxide in Saccharomyces cerevisiae. Archives of Biochemistry and Biophysics. 2011;515(1–2):107–111. http://dx.doi.org/10.1016/j.abb.2011.08.009. doi:10.1016/j.abb.2011.08.009

345. Ejsing CS, Sampaio JL, Surendranath V, Duchoslav E, Ekroos K, Klemm RW, Simons K, Shevchenko A. Global analysis of the yeast lipidome by quantitative shotgun mass spectrometry. Proceedings of the National Academy of Sciences. 2009;106(7):2136–2141. https://pnas.org/doi/full/10.1073/pnas.0811700106. doi:10.1073/pnas.0811700106

346. Klose C, Surma MA, Gerl MJ, Meyenhofer F, Shevchenko A, Simons K. Flexibility of a Eukaryotic Lipidome – Insights from Yeast Lipidomics Polymenis M, editor. PLoS ONE. 2012;7(4):e35063. https://dx.plos.org/10.1371/journal.pone.0035063. doi:10.1371/journal.pone.0035063

347. Surma MA, Herzog R, Vasilj A, Klose C, Christinat N, Morin-Rivron D, Simons K, Masoodi M, Sampaio JL. An automated shotgun lipidomics platform for high throughput, comprehensive, and quantitative analysis of blood plasma intact lipids. European Journal of Lipid Science and Technology. 2015;117(10):1540–1549. https://onlinelibrary.wiley.com/doi/10.1002/ejlt.201500145. doi:10.1002/ejlt.201500145

348. Herzog R, Schuhmann K, Schwudke D, Sampaio JL, Bornstein SR, Schroeder M, Shevchenko A. LipidXplorer: A Software for Consensual Cross-Platform Lipidomics Brennan L, editor. PLoS ONE. 2012;7(1):e29851. https://dx.plos.org/10.1371/journal.pone.0029851. doi:10.1371/journal.pone.0029851

349. Herzog R, Schwudke D, Schuhmann K, Sampaio JL, Bornstein SR, Schroeder M, Shevchenko A. A novel informatics concept for high-throughput shotgun lipidomics based on the molecular fragmentation query language. Genome Biology. 2011;12(1):R8. http://genomebiology.biomedcentral.com/articles/10.1186/gb-2011-12-1-r8. doi:10.1186/gb-2011-12-1-r8

350. Al-Feel W, Chirala SS, Wakil SJ. Cloning of the yeast FAS3 gene and primary structure of yeast acetyl-CoA carboxylase. Proceedings of the National Academy of Sciences. 1992;89(10):4534–4538. https://www.ncbi.nlm.nih.gov/pubmed/1350093. doi:10.1073/pnas.89.10.4534

351. Hasslacher M, Ivessa AS, Paltauf F, Kohlwein SD. Acetyl-CoA carboxylase from yeast is an essential enzyme and is regulated by factors that control phospholipid metabolism. The Journal of biological chemistry. 1993;268(15):10946–52. https://www.ncbi.nlm.nih.gov/pubmed/8098706

352. Wei J, Tong L. Crystal structure of the 500-kDa yeast acetyl-CoA carboxylase holoenzyme dimer. Nature. 2015;526(7575):723–727. http://link.springer.com/10.1007/BF00309532. doi:10.1038/nature15375

353. Madsen CT, Sylvestersen KB, Young C, Larsen SC, Poulsen JW, Andersen MA, Palmqvist EA, Hey-Mogensen M, Jensen PB, Treebak JT, et al. Biotin starvation causes mitochondrial protein hyperacetylation and partial rescue by the SIRT3-like deacetylase Hst4p. Nature Communications. 2015;6(1):7726. http://dx.doi.org/10.1038/ncomms8726. doi:10.1038/ncomms8726

354. Wolinski H, Natter K, Kohlwein SD. The fidgety yeast: focus on high-resolution live yeast cell microscopy. Methods in molecular biology (Clifton, N.J.). 2009;548:75–99. https://www.ncbi.nlm.nih.gov/pubmed/19521820. doi:10.1007/978-1-59745-540-4_5

355. Breker M, Gymrek M, Schuldiner M. A novel single-cell screening platform reveals proteome

plasticity during yeast stress responses. Journal of Cell Biology. 2013;200(6):839–850. https://www.ncbi.nlm.nih.gov/pubmed/23509072. doi:10.1083/jcb.201301120

356. Breker M, Gymrek M, Moldavski O, Schuldiner M. LoQAtE—Localization and Quantitation ATlas of the yeast proteomE. A new tool for multiparametric dissection of single-protein behavior in response to biological perturbations in yeast. Nucleic Acids Research. 2014;42(D1):D726–D730. https://www.ncbi.nlm.nih.gov/pubmed/24150937. doi:10.1093/nar/gkt933

357. Celenza JL, Eng FJ, Carlson M. Molecular analysis of the SNF4 gene of Saccharomyces cerevisiae: evidence for physical association of the SNF4 protein with the SNF1 protein kinase. Molecular and Cellular Biology. 1989;9(11):5045–5054. https://journals.asm.org/doi/10.1128/mcb.9.11.5045-5054.1989. doi:10.1128/mcb.9.11.5045-5054.1989

358. Erdbrügger P, Fröhlich F. The role of very long chain fatty acids in yeast physiology and human diseases. Biological Chemistry. 2020;402(1):25–38. https://www.degruyter.com/document/doi/10.1515/hsz-2020-0234/html. doi:10.1515/hsz-2020-0234

359. Gable K, Slife H, Bacikova D, Monaghan E, Dunn TM. Tsc3p Is an 80-Amino Acid Protein Associated with Serine Palmitoyltransferase and Required for Optimal Enzyme Activity. Journal of Biological Chemistry. 2000;275(11):7597–7603. http://dx.doi.org/10.1074/jbc.275.11.7597. doi:10.1074/jbc.275.11.7597

360. Hoepfner D, Helliwell SB, Sadlish H, Schuierer S, Filipuzzi I, Brachat S, Bhullar B, Plikat U, Abraham Y, Altorfer M, et al. High-resolution chemical dissection of a model eukaryote reveals targets, pathways and gene functions. Microbiological Research. 2014;169(2–3):107–120. https://www.ncbi.nlm.nih.gov/pubmed/24360837. doi:10.1016/j.micres.2013.11.004

361. Randez-Gil F, Prieto JA, Rodríguez-Puchades A, Casas J, Sentandreu V, Estruch F. Myriocin-induced adaptive laboratory evolution of an industrial strain of Saccharomyces cerevisiae reveals its potential to remodel lipid composition and heat tolerance. Microbial Biotechnology. 2020;13(4):1066–1081. https://onlinelibrary.wiley.com/doi/10.1111/1751-7915.13555. doi:10.1111/1751-7915.13555

362. Schjerling CK, Hummel R, Hansen JK, Børsting C, Mikkelsen JM, Kristiansen K, Knudsen J. Disruption of the Gene Encoding the Acyl-CoA-binding Protein ( ) Perturbs Acyl-CoA Metabolism in. Journal of Biological Chemistry. 1996;271(37):22514–22521. https://linkinghub.elsevier.com/retrieve/pii/S0021925819617849. doi:10.1074/jbc.271.37.22514

363. Han G, Gable K, Kohlwein SD, Beaudoin F, Napier JA, Dunn TM. The Saccharomyces cerevisiae YBR159w Gene Encodes the 3-Ketoreductase of the Microsomal Fatty Acid Elongase. Journal of Biological Chemistry. 2002;277(38):35440–35449. https://linkinghub.elsevier.com/retrieve/pii/S0021925818367814. doi:10.1074/jbc.M205620200

364. Sütterlin C, Doering TL, Schimmöller F, Schröder S, Riezman H. Specific requirements for the ER to Golgi transport of GPI-anchored proteins in yeast. Journal of cell science. 1997;110 (Pt 2(21):2703–14. http://www.ncbi.nlm.nih.gov/pubmed/9427388. doi:10.1242/jcs.110.21.2703

365. Miyake Y, Kozutsumi Y, Nakamura S, Fujita T, Kawasaki T. Serine Palmitoyltransferase Is the Primary Target of a Sphingosine-like Immunosuppressant, ISP-1/Myriocin. Biochemical and Biophysical Research Communications. 1995;211(2):396–403. https://www.ncbi.nlm.nih.gov/pubmed/7794249. doi:10.1006/bbrc.1995.1827

366. Vance D, Goldberg I, Mitsuhashi O, Bloch K, Ōmura S, Nomura S. Inhibition of fatty acid synthetases by the antibiotic cerulenin. Biochemical and Biophysical Research Communications. 1972;48(3):649–656. https://linkinghub.elsevier.com/retrieve/pii/0006291X7290397X. doi:10.1016/0006-

291X(72)90397-X

367. Bao X, Koorengevel MC, Groot Koerkamp MJA, Homavar A, Weijn A, Crielaard S, Renne MF, Lorent JH, Geerts WJ, Surma MA, et al. Shortening of membrane lipid acyl chains compensates for phosphatidylcholine deficiency in choline-auxotroph yeast. The EMBO Journal. 2021;40(20):1–26. https://onlinelibrary.wiley.com/doi/10.15252/embj.2021107966. doi:10.15252/embj.2021107966

368. Meredith MJ, Lane MD. Acetyl-CoA carboxylase. Evidence for polymeric filament to protomer transition in the intact avian liver cell. Journal of Biological Chemistry. 1978;253(10):3381–3383. http://dx.doi.org/10.1016/S0021-9258(17)34809-3. doi:10.1016/S0021-9258(17)34809-3

369. Mackall JC, Lane MD, Leonard KR, Pendergast M, Kleinschmidt AK. Subunit size and paracrystal structure of avian liver acetyl-CoA carboxylase. Journal of Molecular Biology. 1978;123(4):595–606. https://linkinghub.elsevier.com/retrieve/pii/0022283678902085. doi:10.1016/0022-2836(78)90208-5

370. Beaty NB, Lane MD. The polymerization of acetyl-CoA carboxylase. Journal of Biological Chemistry. 1983;258(21):13051–13055. http://dx.doi.org/10.1016/S0021-9258(17)44078-6. doi:10.1016/S0021-9258(17)44078-6

371. Ivessa AS, Schneiter R, Kohlwein SD. Yeast acetyl-CoA carboxylase is associated with the cytoplasmic surface of the endoplasmic reticulum. European journal of cell biology. 1997;74(4):399–406. http://www.ncbi.nlm.nih.gov/pubmed/9438137

372. Noree C, Begovich K, Samilo D, Broyer R, Monfort E, Wilhelm JE. A quantitative screen for metabolic enzyme structures reveals patterns of assembly across the yeast metabolic network Blanchoin L, editor. Molecular Biology of the Cell. 2019;30(21):2721–2736. https://www.molbiolcell.org/doi/10.1091/mbc.E19-04-0224. doi:10.1091/mbc.E19-04-0224

373. Gross AS, Zimmermann A, Pendl T, Schroeder S, Schoenlechner H, Knittelfelder O, Lamplmayr L, Santiso A, Aufschnaiter A, Waltenstorfer D, et al. Acetyl-CoA carboxylase 1–dependent lipogenesis promotes autophagy downstream of AMPK. Journal of Biological Chemistry. 2019;294(32):12020–12039. https://linkinghub.elsevier.com/retrieve/pii/S002192582030154X. doi:10.1074/jbc.RA118.007020

Appendices

Appendix A: Co-First Author Paper (Acc1 regulation by NuA4)

Fine tuning Acetyl-CoA Carboxylase 1 activity through localization: Functional genomics reveal a role for the lysine acetyltransferase NuA4 and sphingolipid metabolism in regulating Acc1 activity and localization.

Trang Pham[#,1,2], Elizabeth Walden[#,1,2], Sylvain Huard[1,2], John Pezacki[1,3], Morgan D. Fullerton[2], Kristin Baetz[1,2,4,*]

[1]Ottawa Institute of Systems Biology, uOttawa, Ottawa, K1H 8M5 Canada

[2]Department of Biochemistry, Microbiology and Immunology, Faculty of Medicine, uOttawa, Ottawa, K1H 8M5 Canada

[3] Department of Chemistry and Biomolecular Sciences, Faculty of Science, uOttawa, Ottawa K1N6N5 Canada

[4] Department of Biological Sciences, Faculty of Science, University of Calgary, Calgary T2N 1N4, Canada

[#] co-first authors

[*] Corresponding author: Department of Biological Sciences, Faculty of Science, University of Calgary, Calgary T2N 1N4, Canada. E-mail: kristin.baetz@ucalgary.ca

Keywords: NuA4, Lysine acetylation, Acc1, Protein localization, Protein aggregation, Fatty acids, *Saccharomyces cerevisiae*

Abstract:

Acetyl-CoA Carboxylase 1 (Acc1) catalyzes the conversion of acetyl-CoA to malonyl-CoA, the committed step of *de novo* fatty acid synthesis. As a master-regulator of lipid synthesis, Acc1 has been proposed to be a therapeutic target for numerous metabolic diseases. We have shown that Acc1 activity is reduced in the absence of the lysine acetyltransferase NuA4 in *Saccharomyces cerevisiae*. This change in Acc1 activity is correlated with a change in localization. In wild-type cells Acc1 is localized throughout the cytoplasm in small punctate and rod-like structures. However, in NuA4 mutants, Acc1 localization becomes diffuse. To uncover mechanisms regulating Acc1 localization we performed a microscopy screen to identify other deletion mutants that impact Acc1 localization and then measured Acc1 activity in these mutants through chemical genetics and biochemical assays. Three phenotypes were identified. Mutants with hyper-active Acc1 form one or two rod-like structures centrally within the cytoplasm, mutants with mid-low Acc1 activity displayed diffuse Acc1, while the mutants with the lowest Acc1 activity (hypomorphs) formed thick rod-like Acc1 structures at the periphery of the cell. All the Acc1 hypomorphic mutants were implicated in sphingolipid metabolism or very-long chain fatty acid elongation and in common, their deletion causes an accumulation of palmitoyl-CoA. Through exogenous lipid treatments, enzyme inhibitors and genetics, we determined that increasing palmitoyl-CoA levels inhibits Acc1 activity and remodels Acc1 localization. Together this study suggests yeast cells have developed a dynamic feed-back mechanism in which downstream products of Acc1 can fine-tune the rate of fatty acid synthesis.

Introduction:

Fatty acids are a key building block of life and while they are taken up from human diet, they can also be synthesized *de novo* in the cell [307]. In the highly proliferative conditions of cancer, changes in cellular energetics is a hallmark, and *de novo* lipogenesis provides lipids for membrane formation allowing for proliferation [299,307]. In fact, regulation and therapeutic targeting of fatty acid availability has been proposed to limit cancer cell growth [307,308]. As a key pathway in lipid metabolism, *de novo* fatty acid synthesis is also relevant to obesity and non-alcoholic fatty liver disease [309–311]. Acetyl-CoA carboxylase (ACC) converts acetyl-CoA into malonyl-CoA creating the committed precursor for fatty acid synthetase to produce long chain fatty acids (Figure 5.1A) [150]. The process is conserved across many forms of life ranging from humans to fungi including *Saccharomyces cerevisiae* [312–314]. In *S. cerevisiae* there are two ACC proteins: Acc1, which functions in the cytoplasm, and Hfa1, which functions in the mitochondria [312,315].

As the enzyme catalyzing the initial and committed step of *de novo* lipid synthesis (lipogenesis), Acc1 activity is highly regulated by multiple mechanisms [313,316]. First, Acc1 is regulated at the transcriptional level through the Ino2/Ino4 transcriptional activator complex and the Opi1 repressor [317] and *ACC1* mRNA is upregulated when phosphatidic acid (PA) levels are high [318]. In addition, Acc1 protein levels are also regulated at the translational level, peaking at G2/M during the cell cycle which is controlled by an upstream open reading frame (uORF) and plays a role in response to nutrient availability, as mutation of the uORF increased expression of Acc1 in a poor carbon source, 3% glycerol [319]. This is not driven by changes in the abundance of *ACC1* mRNA but by increases in translation of Acc1 protein [319]. In both mammals and yeast, Acc1 activity is tightly regulated by phosphorylation, largely by the AMP-activated protein kinase, AMPK or Snf1 in yeast [309,313,320,321]. When Snf1/AMPK activity is induced upon low-glucose or starvation conditions, Snf1/AMPK phosphorylation of Acc1 inhibits its activity, resulting in a decrease in fatty acid (FA) synthesis [313,321]. In yeast, the primary Snf1 phosphorylation site on Acc1 is

serine 1157 and under logarithmic growth over 60% of Acc1 protein is phosphorylated at this site suggesting the majority of enzyme is inactive under this condition [322]. In *snf1Δ* cells and in *acc1*^{S1157A} mutant cells, where the Snf1-S1157 phosphorylation site is mutated to mimic the unphosphorylated state, Acc1 activity is hyperactive, resulting in high levels of FA production, accumulation of TAG, and lipid droplets during logarithmic growth [322]. As the first step of FA synthesis, Acc1 also influences FA chain length. In mutants with low Acc1 activity (hypomorphs) or upon inhibition of Acc1, acyl-chain length decreases whereas in mutants with high Acc1 activity (hypermorphs), such as *acc1*^{S1157A}, acyl-chain length increases [322–324].

In addition, many other pathways influence Acc1 activity. In human cells, citrate allosterically activates ACC activity [312,313]. Citrate regulation is also associated with a polymerization of human Acc1 into long filaments where the Acc1 is locked into the active form [325]. Remarkably, downstream products of Acc1 can also negatively impact Acc1 activity forming a negative feed-back loop. In mammalian cells, exogenous palmitoyl-CoA reduces Acc1 activity through an alteration of the Acc1 conformation and disruption of filament structure [325]. Exogenous long-chain fatty acids inhibit Acc1 activity in yeast extracts [326,327] and 16-20 carbon long chain length acyl-CoAs directly inhibit rat liver Acc1 [328,329], though the exact mechanism of inhibition is not known. In addition, VLCFA-CoAs can feedback onto Acc1 activity through allosteric activation of AMPK [330]. Acc1 is also inhibited by Soraphen A (Sor A), a compound discovered from *Sonrangium cellulosum*, a myxobacteria, which was initially used as an antifungal but has branched into similar compounds being used in clinical trials [331–333]. Soraphen A is commonly used as an indirect measurement of Acc1 activity as mutants deficient for Acc1 activity are hypersensitive and mutants with enhanced Acc1 activity (such as Snf1 or *acc1*^{S1157A} mutants) are resistant to Sor A treatment [80,327,334].

Our lab has recently determined that in mutants of the yeast lysine acetyltransferase (KAT) NuA4 complex, Acc1 activity is decreased and intracellular levels of acetyl-CoA are increased [173]. The NuA4 complex is composed of 13 subunits, including the essential catalytic subunit Esa1 [81]. The cellular activity of NuA4 can be modulated through use of the temperature-sensitive allele of *ESA1*, *esa1-L254P* (*esa1-ts*) [81]. NuA4 activity can also be reduced through the deletion of *EAF1*, a key scaffolding protein of the complex, and deletion of another member, *EAF7*, demonstrates phenotypes associated with NuA4 impairment [79,111,173,335]. Though NuA4 was named for its acetylation of Histone H4, it has a growing list of cellular roles and non-histone targets [59,60,112,134]. In fact, roles for NuA4 have been identified for multiple aspects of lipid homeostasis. NuA4 has been implicated in the negative regulation of Snf1 (AMPK) through the acetylation of Sip2, one of the three Snf1 inhibitory subunits [60]. This acetylation increases the interaction of Sip2 with the Snf1 complex, thereby reducing Snf1 activity [60]. Another target of NuA4 acetylation is Kes1/Osh4, a yeast oxysterol binging protein [134]. Acetylation at the K109 site decreases Kes1 lipid exchange activity and a reduction in NuA4 activity led to an enhancement in Kes1 activity [134]. NuA4 has also been implicated in phospholipid homeostasis through the acetylation of phosphatidic acid phosphatase, Pah1, the enzyme which catalyzes the phosphatidic acid to diacylglycerol step of glycerolipid synthesis [53,336]. Finally, NuA4 mutants display decreases in lipid droplet formation [53,80].

Given the central role of Acc1 in metabolism and disease and the increasing use of KAT inhibitors to treat various diseases [158,337,338], we were motivated to uncover the mechanisms by which NuA4 regulates Acc1 activity. Despite the established role of NuA4 in regulating Snf1/AMPK, we determined that NuA4 regulation of Acc1 activity is only partially through Snf1/AMPK. Surprisingly, we found that NuA4 influences the subcellular localization of Acc1, which impacts its enzymatic activity. Extending this discovery, we performed a targeted genetic screen for changes in Acc1-GFP localization and identified additional mutants that impacted Acc1 localization and activity, which suggests that in

yeast, Acc1 localization and activity are linked. Finally, our data implicates NuA4 in the regulation of sphingolipid flux and palmitoyl-CoA levels which in turn can fine-tune Acc1 activity.

Materials and Methods:

Yeast strains and growth conditions

S. cerevisiae strains used in this study are listed in S5.2 Table. Strains were generated by standard mating procedure or PCR-based genetic deletion/epitope tagging as previously described [219]. Point mutation S1157A of Acc1 was introduced into wild-type strain that expressed GFP-tagged Acc1 at its genomic locus by CRISPR-Cas9 method as previously described [225]. All strains were confirmed by genomic PCR or sequencing with specific primers. Deletion strains for Acc1 localization screen were from the Deletion Mutant Array (DMA) collection (GE, catalog no. YSC1053)**.** Yeast were grown in standard YPD medium (1% yeast extract, 2% peptone, 2% dextrose), synthetic complete (SC) or drop-out medium (2% dextrose, 0.67% yeast nitrogen base (YNB) without amino acids, and 0.2% amino acid complete or drop-out mix) at 30^{o}C unless otherwise specified.

Cells were imaged, subjected to specific treatments, or harvested for further investigation in early logarithmic (log) phase (OD_{600} of 0.4-0.5). For treatment with cerulenin (Sigma, Cat#C2389), myristic acid (Sigma, Cat#M3128), palmitic acid (Sigma, Cat#P0500), stearic acid (Sigma, Cat#S4751), ceramide (Tocris, Cat#0744), Soraphen A (Collaboration with John Pezacki and Rolf Muller) [339], and myriocin (Sigma, Cat#M1177), log phase cells were centrifuged at 3000 rpm for 3 min at room temperature and resuspended in media to which the appropriate drug was added to desired concentration immediately prior to use. Brij58 detergent (Sigma, Cat#P5884) was included in the media at a concentration of 0.1% to solubilize cerulenin, fatty acids and ceramide.

Yeast microscopy and image quantification

Yeast strains that express GFP tagged Acc1 were grown in YPD or SC media overnight, diluted to an OD_{600} of 0.1 and cultured at 30°C to early log phase (OD_{600} of 0.4-0.5). Alternatively, early log phase cells were treated with different compound(s) as indicated. For imaging, 50 µl of the culture was added to a well on a SensoPlate™ 96-well black microplate with glass bottom (Greiner Bio-one, Cat# 82050-792) that was pre-treated with concanavalin A (Sigma, Cat# L7647). The plate was then centrifuged at 500 rpm at room temperature for 1 min. Cells adhered to the bottom of the well were washed once with SC media or SC media containing appropriate compound(s) and then resuspended in the same media. A z-stack of 30 fluorescent and brightfield images across 12 µm were captured with CellVoyager™CV1000 disk confocal imaging system equipped with back-illuminated EMCCD camera and 100x objective lens (Olympus Life Science) at room temperature. At least three independent biological replicates for each yeast strain and condition were performed with at least 100 cells/replicate. Cells and Acc1 structures were identified and quantified by Imaris x64 9.1.0 software (Bitplane) using 2 separate algorithms for automatic segmentation. Both algorithms used the green fluorescent channel that depicts Acc1-GFP localization since Acc1 is localized to both the distinct structures and the cytoplasm. To identify and quantify cells, a surface was modeled based on the average size of a yeast cell with a smoothing factor of twice the pixel size and a lower intensity threshold. Smoothing was omitted and the intensity threshold was increased to model the Acc1 structures. The statistical parameters of interest included the number of disconnected objects and intensity sum (for both cells and Acc1 structures), the intensity average and average volume (for Acc1 structures).

Cell lysis and Acc1 purification

Cells harvested from 100 ml culture of OD_{600} 0.4-0.5 were lysed in 1 ml lysis buffer (mChIP buffer (100 mM HEPES pH8.0, 20 mM magnesium acetate, 200 mM sodium acetate, 10 mM EGTA, 0.1

mM EDTA, 10% glycerol) supplemented with mini protease inhibitor cocktail tablet (Roche Cat# 4693159001), 50 mM sodium butyrate (Sigma, Cat#B5887), 50 mM nicotinamide (Sigma, Cat#72340), 5 μM TSA (Sigma, Cat#EPI008), 0.4 μM apicidin (Sigma, Cat#EPI008), 2 μM M344 (Sigma, Cat#EPI008), 1 mM sodium vaproate (Sigma, Cat#EPI008), 1 mM sodium orthovanadate (Sigma, Cat#S6506), 50 mM sodium fluoride (Sigma, Cat#201154) and phosphatase cocktail 2 and 3 (Sigma, Cat#P5726 and P0044, respectively)). To this mix 500 μl glass beads (Fisher Scientific, USA; 35-535) was added and bead beating was performed for a total of ten 1-minute periods with 1-min interval on ice. Crude cell lysates were centrifuged at 1000 rpm for 1 min at 4^{o}C. Protein concentration of the cloudy whole cell extract was determined with Bio-Rad Protein Assay Dye Reagent (Bio-Rad, Cat# 5000006). When indicated, one percent NP40 was included in the lysis buffer to solubilize Acc1 and in that case crude cell lysate was centrifuged at 13,200 rpm for 15 min at 4^{o}C to obtain a clear extract.

For purification of GFP-tagged Acc1, 50 μl of GFP-trap magnetic beads (ChromoTek, Cat#GTM-100) were incubated with the cell extract by rotating end-over-end for 2h at 4^{o}C. If cell extract contains NP40, the beads were washed 3 times with 1 mL mChIP buffer with 1% NP40 followed by a wash with 1 ml mChIP buffer without NP40. Otherwise, if cell extract does not contain NP40, it is omitted from the wash buffer. Washed beads were resuspended in 50 μL mChIP buffer without NP40 and used immediately for Acc1 assay. Equal amounts of sample were also run on a 6% SDS-PAGE gel followed by coomassie staining with simpleblue safestain coomassie (Thermo Fisher Scientific, Cat#LC6060) for normalization of Acc1 activity.

Tandem affinity purification of TAP tagged Acc1 was performed by incubation of the cell extract with 200 μl of IgG magnetic beads prepared as described previously [82] for 2h at 4^{o}C. The beads were washed as described earlier prior to an additional wash with 1 mL elution buffer (50 mM Tris pH 8.0, 1

mM EDTA, 1 mM DTT, 150 mM NaCl and 10% Glycerol). Acc1 was released from the beads by cleavage with 10 U of ScTEV (Thermo Fisher Scientific, Cat#12575015) in 50 µL of elution buffer overnight at 4^{o}C and was used immediately for Acc1 assay and SDS-PAGE as described above.

Acc1 activity assay

The Acc1 assay was performed as previously described [173]. Briefly, equal volumes of bead slurry that contains purified Acc1-GFP were incubated with reaction buffer (50 mM HEPES pH 7.4, 10 mM $MgCl_2$, 1 mM $MnCl_2$, 2 mM DTT, 0.4 mM ATP, 0.075% fatty acid free BSA (Sigma, cat # A7030), 12.5 mM NaHCO3 and 1.5 µCi 14C-$NaHCO_3$ (Perkin Elmer, cat# NEC086H005MC)) by rotating end-over-end. Palmitoyl-CoA was included in the reaction at 10 µM when indicated. The reactions were incubated at room temperature for 90 min, stopped by the addition of 0.6 N HCl and air-dried overnight at 37^{o}C. The radioactivity of the products was determined by scintillation counting of the dried materials. Acc1 activity was normalized to relative protein abundance in the samples as determined by coomassie staining of SDS-PAGE gels. Protein quantification was performed with Image Lab5.2 software.

Yeast growth assay

Yeast growth was quantitatively monitored by the Bioscreen C automated microbiology growth curve analysis system (Growth Curve USA) that measures the optical density at 600 nm (OD_{600}) of micro-cultures on a honeycomb 100-well plate (Growth Curve USA, 9502550). Log phase cells (note: BY4741 background without Acc1 tagging) were seeded in 200 µl YPD media that contain appropriate treatment. The plate was incubated at 30^{o}C with constant shaking at high amplitude and speed and OD_{600} was measured every 15 min for 2 days. The raw OD_{600} readings were processed by Pregcog software [340] to obtain adjusted OD_{600} values that estimate population size. These values were used to generate the growth curves and calculate the growth rates. Growth rate was defined as the slope of the best-fit line when the

natural logarithm of the adjusted OD was graphed versus time between 1 h and the first time point when the adjusted OD_{600} reaches 25% of the maximum OD_{600}. Three biological replicates, each of which has 2-3 technical replicates, were performed. The growth rates of the technical replicates were averaged and these average values of the 3 biological replicates were used for statistical analysis as indicated.

Lipogenesis assay

Lipogenesis assay was performed by pulse labeling early log phase WT and mutant cells grown in YPD medium with 1 μCi/ml ^{3}H-sodium acetate for 1h at 30^{o}C. For drug treatment, log phase cells were centrifuged at 3000 rpm at room temperature for 3 min and resuspended in YPD medium containing 0.1% Brij58 and appropriate drugs. Cells were then cultured for 2h at 30^{o}C before pulse labeling with ^{3}H-sodium acetate as described above. An equal number of cells was collected for harvest for each sample for both protein and lipid extractions. Lipids were extracted using Bligh and Dyer method [246] with some modifications. Radioactively labeled cells were lysed in 300 μl of methanol: chloroform (2:1) and 80 μl glass beads (Fisher Scientific, USA; 35-535) by vortexing for a total of six 1-minute periods with 1-min interval on ice. Lipid was extracted by the sequential addition of 100 μl chloroform and 100 μl water. Following centrifugation at 5000 xg for 4 min at 4^{o}C, the bottom lipid-containing chloroform layer was recovered and subjected to scintillation counting. Lipogenesis was determined as the radioactivity of the extracted lipid normalized to the protein concentration of lysate made from the same number of cells used for lipid extraction. Protein lysate was made by bead beating cells with 100 μl mChIP buffer (100 mM Hepes pH8.0, 20 mM magnesium acetate, 200 mM sodium acetate, 10 mM EGTA, 0.1 mM EDTA, 10% glycerol) supplemented with protease inhibitor cocktail (Sigma; P8215) and 80 μl glass beads. Protein concentrations of the clarified lysates were measured by microBCA kit (Thermo Scientific Cat#23232) or Bio-Rad protein assay dye reagent (Bio-Rad, Cat# 5000006).

SILAC labeling, purification, and LC-MS/MS analysis of Acc1-TAP

Yeast SILAC labeling was performed as previously described [153] with light (K0) or heavy (K6) lysine (Cambridge Isotope Laboratories, Cat#ULM-8766-0.1 / CLM-2247-H-0.1, respectively). The heavy lysine has a mass shift of +6 Da compared to the light one. Wild-type and *esa1-ts* strains that express TAP tagged Acc1 in a *lys2Δ* background were grown at 30°C to near saturation in synthetic lysine drop-out medium (SC-Lys) supplemented with 30 mg/L of either K0 or K6 overnight before being diluted in the same labeling medium and cultured to near saturation again for a second day. Then cells were diluted to an OD_{600} of 0.1 in 200 ml of the same labeling medium and grown at 30°C to an OD_{600} of 0.2-0.25. Yeast culture was shifted to 34°C for 2 h when its OD_{600} reached 0.45-0.55. Cells were harvested by centrifugation at 3000 rpm for 5 min at 4°C. Cells were washed with 2 ml cold water and snap- frozen. Cell lysis and TAP purification of Acc1 was performed using lysis buffer that contained 1% NP40 as described earlier except that after incubation of lysate with IgG beads, beads from the light and heavy samples were combined prior to 4 wash steps with 1 ml of mChIP buffer that contains 1% NP40. Acc1-TAP was eluted from the beads by heating at 65°C in 40 µl of 2% SDS for 10 min twice. Acc1 was reduced by boiling of the combined SDS eluant in 10 mM DTT (Sigma, Cat#D9779) at 100°C for 10 min. Cysteine alkylation was achieved by incubating the reduced samples with fresh 50 mM 2-iodoacetamide (Sigma, Cat#I1149) at room temperature in the dark for 30 min. NP LDS sample buffer (Thermo Fisher Scientific, Cat#NP0007) was added to the sample prior to protein separation on a 3-8% Tris-Acetate NuPAGE gel (Thermo Fisher Scientific, Cat#EA0375BOX) and coomassie staining with simpleblue safestain coomassie (Thermo Fisher Scientific, Cat#LC6060) according to the manufacture instructions. In-gel digestion and peptide recovery were performed as previously described [341]. Acc1 band was excised from the gel, minced into small pieces with a clean sharp scalpel. All washing and extraction steps were done on a shaking platform at room temperature unless otherwise indicated. Gel pieces were washed with 300 µl of liquid chromatography-mass spectrometry (LC-MS) grade water (Thermo Fisher Scientific, Cat# W61) for 15 min. To this 300 µl of LC-MS grade acetonitrile (Thermo Fisher Scientific,

Cat#A9551) was added, and samples were shaken for another 15 min. After removal of the liquid, gel pieces were sequentially washed with 300 µl of 20 mM ammonium biocarbonate (Thermo Fisher Scientific, Cat#A643) and 300 µl of 20 mM Ammonium biocarbonate: acetonitrile (50:50 v/v) for 15 min each. Gel pieces were dehydrated by 100 µl acetonitrile for 5 min and dried in a speedvac. Trypsin digestion was performed with 630 ng of LC-MS grade trypsin (Thermo Fisher Scientific, Cat#PI90058) in 20 mM ammonium biocarbonate at 37^{o}C overnight. Peptide was eluted by addition of an equal volume of acetonitrile and incubation at 30^{o}C for 30 min followed by two extractions with 100 µl of 1% LC-MC grade formic acid (Thermo Fisher Scientific, Cat#A11750) and one with 200 µl of acetonitrile. All peptide extracts were combined and completely dried in a speedvac. Peptides were cleaned up using Pierce C18 spin tips (Thermo Fisher Scientific, Cat#PI84850) and then dried in a speedvac.

Proteomics analysis was performed at the Ottawa Hospital Research Institute Proteomics Core Facility (Ottawa, Canada). LC-MS/MS was performed using a Dionex Ultimate 3000 RLSC nano HPLC (Thermo Scientific) and Orbitrap Fusion Lumos mass spectrometer (Thermo Scientific). Peptide identification and quantification were performed by MaxQuant 1.5.5.1 software using *S. cerevisiae* sequence database from SwissProt (version 2016-03).

Mini Screen for Acc1 localization

The microscopic screen to identify genetic deletions that affect Acc1 localization was performed by combining synthetic genetic array analysis (SGA) and high-throughput imaging according to a method previously described [41,342] with some modifications. An array of 84 Acc1-GFP expressing deletion mutants was created by crossing a mat α Acc1-GFP expressing query strain (*ura3*Δ::natMX *his3Δ1 leuΔ0 ura3Δ0 MET15 can1pr::RPL39pr-tdTomato::CaURA3 can1* Δ*::STE2pr-LEU2 ACC1-GFP-HIS3*) and a set of corresponding mutants obtained from the yeast haploid deletion collection (S5.1 Table) using SGA

method. The deletion mutants chosen were involved in processes that might regulate Acc1 according to the literature and our own observations (i.e., sphingolipid, citrate, glucose metabolism, glucose sensor and signaling pathways).

SGA procedure was performed by ROTOR HDA (Singer Instruments). After sporulation of the diploids resulted from mating of the query strain and the selected gene deletion array, mating type a haploid deletion mutants were selected for by pinning cells on synthetic medium that lacks leucine and arginine but contains 50 µg/ml canavanine, 200 µg/ml G418 and 100 µg/ml nourseothricin (NAT). Subsequent selections were performed 3 times on synthetic medium that lacks leucine, arginine and histidine but contains canavanine, G418 and NAT to select for strains with both gene deletions and Acc1-GFP expression.

The resultant Acc1-GFP expressing deletion mutants were cultured overnight in complete synthetic medium at 25^{o}C in 96 deep well plates. If the OD_{600} of overnight cultures were above 0.6, the cultures were diluted to an OD_{600} of 0.1 and grown at 25^{o}C until OD_{600} reached 0.4-0.6 (early mid log) when cells were imaged. Otherwise, cells were imaged when OD_{600} of overnight culture was 0.4-0.6. Image acquisition and analysis were performed as described in the microscopy section above. Strains that showed abnormal Acc1-GFP localization as compared to that in wild-type strain based on 2 independent imaging experiments were repeated twice more with growing at 30^{o}C instead of 25^{o}C.

FAS activity assay

FAS activity was determined in cell extracts at 25^{o}C as previously described [343,344]. Yeast (note: BY4741 background without Acc1 tagging) were grown to early log phase (OD_{600} of 0.4-0.5) in YPD

medium and 50 OD_{600} of cells was harvested. Cells were lysed in 600 µl lysis buffer (100 mM potassium phosphate buffer pH 7.5 supplemented with mini protease inhibitor cocktail (Roche Cat# 4693159001), 1 mM PMSF, 50 mM sodium butyrate (Sigma, Cat#B5887), 50 mM nicotinamide (Sigma, Cat#72340), 5 µM TSA (Sigma, Cat#EPI008), 0.4 µM apicidin (Sigma, Cat#EPI008), 2 µM M344 (Sigma, Cat#EPI008), 1 mM sodium orthovanadate (Sigma, Cat#S6506), 50 mM sodium fluoride (Sigma, Cat#201154) and phosphatase cocktail 2 and 3 (Sigma, Cat#P5726 and P0044, respectively)) and 500 µl glass beads (Fisher Scientific, USA; 35-535) by bead beating method. Crude cell lysates were centrifuged at 8000 xg for 20 min at 4^{o}C. 100 µl of clarified extracts were added to 900 µl of FAS assay buffer (100 mM potassium phosphate buffer pH 6.5, 2.5 mM EDTA, 10 mM cysteine, 0.3 mg/mL fatty acid free BSA (Sigma, Cat#A7030), 0.06 mM acetyl-CoA (Sigma, Cat#A2056) and 0.15 mM NADPH (Sigma, Cat#N9960)) in a 1 ml cuvette. The blank rate of NADPH oxidation (Ro) was recorded as the rate of decrease in absorbance at 340 nm for 3 min using Ultrospec 2100 Pro spectrophotometer. The reaction was then started by the addition of 10 µl of 7 mM malonyl-CoA (final concentration of 0.07mM) (Sigma, Cat#M4263) and the total rate of NADPH oxidation (Rx) was recorded as described above. The rate of reaction was calculated by subtracting the blank rate from the total rate (Rx-Ro). One milliunit (mU) of enzyme is defined as the amount of enzyme which consumes 1 nmol of malonyl-CoA per minute (corresponding to 2 nmol of NADPH or a change of 0.006 in absorbance at 340nm) under this reaction condition. Specific activity is expressed as milliunit per milligram of protein (mU/mg). Protein concentration of cell extracts was performed using microBCA kit (Thermo Scientific Cat#23232) according to the manufacture instruction.

Lipidomic analysis

To prepare samples for lipidomic analysis, overnight culture of wild-type and *eaf1Δ* cells (note: BY4741 background without Acc1 tagging) were diluted to an OD_{600} of 0.1 in YPD medium and grown at 30^{o}C to early log phase (OD_{600} of 0.4-0.5) before being harvested. For Soraphen A treatment, log phase

wild-type cells were diluted 100 times in YPD medium that contains 0.3 μM SorA and grown for 24h at 30^{o}C. Twenty OD_{600} of yeast cells were harvested by centrifugation at 4000 xg for 3 min at 4^{o}C. Cells were washed once with 10 ml and once with 1 ml of cold milliQ water. Cell pellets were snap-frozen and stored at -80^{o}C. Cells were lysed in 1 ml LC-MS grade water and 500 μl glass beads using a bead beater for a total of ten 1 min beating periods with 1 min chilling interval. Five hundred μl of crude lysate was used for lipid extraction.

Mass spectrometry-based lipid analysis was performed by Lipotype GmbH (Dresden, Germany) as described previously [345,346]. Lipids were extracted using a two-step chloroform/methanol procedure [345]. Samples were spiked with internal lipid standard mixture containing: CDP-DAG 17:0/18:1, ceramide 18:1;2/17:0 (Cer), diacylglycerol 17:0/17:0 (DAG), lyso-phosphatidate 17:0 (LPA), lyso-phosphatidylcholine 12:0 (LPC), lyso-phosphatidylethanolamine 17:1 (LPE), lyso-phosphatidylinositol 17:1 (LPI), lyso-phosphatidylserine 17:1 (LPS), phosphatidate 17:0/14:1 (PA), phosphatidylcholine 17:0/14:1 (PC), phosphatidylethanolamine 17:0/14:1 (PE), phosphatidylglycerol 17:0/14:1 (PG), phosphatidylinositol 17:0/14:1 (PI), phosphatidylserine 17:0/14:1 (PS), ergosteryl ester 13:0 (EE), triacylglycerol 17:0/17:0/17:0 (TAG), inositolphosphorylceramide 44:0;2 (IPC), mannosyl-inositolphosphorylceramide 44:0;2 (MIPC) and mannosyl-di-(inositolphosphoryl)ceramide 44:0;2 (M(IP)2C). After extraction, the organic phase was transferred to an infusion plate and dried in a speed vacuum concentrator. 1st step dry extract was re-suspended in 7.5 mM ammonium acetate in chloroform/methanol/propanol (1:2:4, V: V: V) and 2nd step dry extract in 33% ethanol solution of methylamine in chloroform/methanol (0.003:5:1; V: V: V). All liquid handling steps were performed using Hamilton Robotics STARlet robotic platform with the Anti Droplet Control feature for organic solvents pipetting.

To acquire MS data, samples were analyzed by direct infusion on a QExactive mass spectrometer (Thermo Scientific) equipped with a TriVersa NanoMate ion source (Advion Biosciences). Samples were analyzed in both positive and negative ion modes with a resolution of Rm/z=200=280000 for MS and Rm/z=200=17500 for MSMS experiments, in a single acquisition. MSMS was triggered by an inclusion list encompassing corresponding MS mass ranges scanned in 1 Da increments [347]. Both MS and MSMS data were combined to monitor EE, DAG, and TAG ions as ammonium adducts; PC as an acetate adduct; and CL, PA, PE, PG, PI, and PS as deprotonated anions. MS only was used to monitor LPA, LPE, LPI, LPS, IPC, MIPC, M(IP)2C as deprotonated anions; Cer and LPC as acetate adducts.

Data were analyzed with in-house developed lipid identification software based on LipidXplorer [348,349]. Data post-processing and normalization were performed using an in-house developed data management system. Only lipid identifications with a signal-to-noise ratio >5, and a signal intensity 5-fold higher than in corresponding blank samples were considered for further data analysis. For diacylglycerol and phospholipid classes whose subspecies were quantified (i.e., DAG, PA, PI, PC, PS, PE, and PG), quantities of different individual fatty acids were derived from the quantities of the lipid species. This was then used to determine the percent of total lipids for each class. Additionally, the number if carbon atoms in the hydrocarbon for each lipid class was estimated by calculating the average length of the chain per lipid class. While data was collected for all the above listed lipids, in this paper we show a subset containing the most highly identified species. All Lipotype data is available in S5.3 Table.

Statistical analysis

Statistical analysis was performed with GraphPad Prism 9 software as indicated in the figure legends.

Data Availability Statement

All relevant data are within the manuscript and its Supporting Information files.

Results:

Reduction of Acc1 activity in *eaf1*Δ cells is independent of SNF1/AMPK1.

We had previously shown that Acc1 activity, but not protein levels, are reduced in whole cell extracts from cells in which *EAF1* is deleted [173]. To confirm that the impact of deletion of *EAF1* on Acc1 activity is not an artifact of whole cell extracts, we performed a series of experiments. As Acc1 can serve as a limiting step of FA biosynthesis [317,321,350,351], wild-type (wt) and *eaf1Δ* cells were treated with ^{3}H-labelled acetate and its incorporation into lipids was measured. In agreement with reduced Acc1 activity, deletion of *EAF1* reduces lipogenesis rates (Figure 5.1B). We next performed *in vitro* Acc1 activity assays using Acc1-GFP purified from wild-type and *eaf1*Δ cells and determined that the *in vitro* activity of Acc1-GFP purified from *eaf1*Δ cells was reduced (Figure 5.1C). It is well established that mutants that have decreased Acc1 activity also display increased sensitivity to, or decreased growth rates, upon treatment with the highly specific Acc1 inhibitor Soraphen A [331,333,352]. Therefore, we performed growth rate analysis comparing the impact of Soraphen A treatment on WT and *eaf1*Δ cells. Control and *eaf1Δ* cells had similar growth rates under untreated conditions (DMSO), but while Soraphen A treatment slightly reduced growth in the wt, the growth rate of *eaf1Δ* cells was further reduced, suggesting that *eaf1Δ* cells have less Acc1 activity than WT (Figure 5.1D and 5.1E). This is in agreement with a chemical genomic screen which identified the NuA4 subunit mutant *eaf7*Δ as hypersensitive to Soraphen A [334]. As previous studies have shown that NuA4 inhibits Snf1/AMPK activity [60], a key regulator of Acc1, we next sought to determine if the reduction in Acc1 activity in *eaf1*Δ cells was fully or partially due to increases in Snf1 activity. Therefore, we extended the Soraphen A growth rate studies to *snf1Δ* and *snf1Δ eaf1Δ*

cells. If the decrease in Acc1 activity displayed by *eaf1*Δ cells was only due to increased Snf1 activity, one would predict the *snf1*Δ *eaf1*Δ cells would be resistant to Soraphen A treatment identical to that of *snf1*Δ cells. Instead, *snf1*Δ *eaf1*Δ cells displayed Soraphen A sensitivity similar to wild-type cells, suggesting that deletion of *SNF1* only partially suppresses the decrease of Acc1 activity in *eaf1Δ* cells. Said another way, the hyperactive Acc1 seen in *snf1*Δ cells can be repressed by deletion of *EAF1*, which suggests NuA4 must be modulating Acc1 activity through pathways independent of Snf1. Taken together, our work indicates that NuA4-dependent regulation of Acc1 activity is not solely through Snf1, but that parallel mechanisms occur.

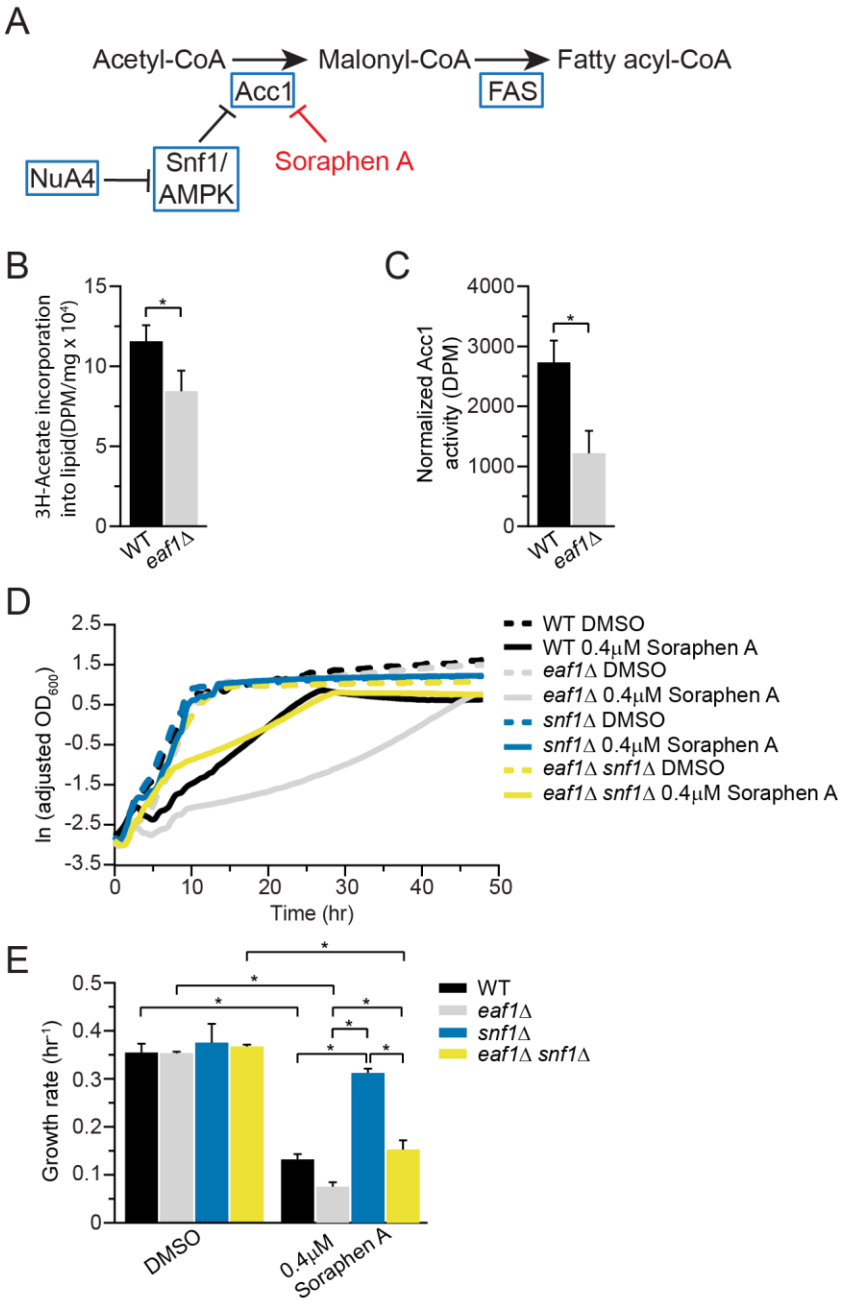

Figure 5.1: NuA4 dependent regulation of Acc1 activity is not solely through Snf1/AMPK1. A) Schematic of *de novo* synthesis pathway of fatty acids. The precursor of fatty acid synthesis is Acetyl-CoA. The essential enzyme Acc1 plays a direct role in regulating fatty acid synthesis. Genetic manipulations of yeast cells (NuA4 mutants) or pharmacological inhibition (Soraphen A) impacting Acc1 activity can attenuate the synthesis of fatty acids. B) Deletion of the NuA4 subunit, *EAF1*, reduces the rate of triglyceride synthesis. Early log phase wild-type (YKB 1079) and *eaf1Δ* (YKB 3333) cells were treated with [^{3}H]-sodium acetate for 1h before harvest and extraction. The lipogenesis rate was obtained by normalizing the incorporation of [^{3}H] into triglycerides from [^{3}H]-acetate precursor to the protein concentration obtained from the same cells. Error bars denote the standard error of the mean (SEM). n=3, * = $p < 0.05$ determined using a two-tailed t-test. C) Acc1 activity is reduced in NuA4 mutant. Wild-type

(YKB 3954) and *eaf1Δ* (YKB 4448) cells expressing endogenously tagged Acc1-GFP were grown to early-log phase at 30°C in YPD. Acc1-GFP was immunoprecipitated and Acc1 activity measured and normalized to Acc1-GFP protein abundance. Error bars denote the standard error of the mean (SEM). n=3, * = $p < 0.05$ determined using a two-tailed t-test. D) *eaf1Δ* cells are sensitive to Soraphen A and *eaf1Δ snf1Δ* cells are more sensitive than *snf1Δ* cells. Wild-type (YKB 1079), *eaf1Δ* (YKB 3333), *snf1Δ* (YKB 3389) and *eaf1Δ snf1Δ* (YKB 3421) cells were grown to early-log phase before being diluted to an OD_{600} of 0.1 in YPD with DMSO control or 0.4 μM Soraphen A in DMSO, and automated growth curve analysis was performed at 30°C for 48 h. E) Growth rates of indicated strains were calculated from logarithmic growth phase of curves in D. Error bars denote the standard error of the mean (SEM). n=3, * = $p < 0.05$ determined using a two-way ANOVA test with a Tukey's multiple comparisons test.

Acc1-GFP localization is modified by NuA4, Snf1, and phosphorylation state of Acc1

We next sought to discover the Snf1-independent pathways through which NuA4 impacts Acc1 activity. As numerous acetylome studies have detected acetylation sites on Acc1 [4,48,353] one possibility is that NuA4 is regulating the activity of Acc1 by direct acetylation. Therefore, we performed SILAC-based quantitative proteomics experiments to identify any Esa1-dependent (catalytic domain of NuA4) acetylation sites on purified Acc1-TAP (S5.1 Fig.). Though numerous acetylations were detected on Acc1, we did not detect any Esa1-dependent sites. We cannot exclude the possibility that there may be NuA4-dependent acetylation sites undetected by this method, but our work suggests that other mechanisms may be contributing to NuA4's regulation of Acc1. As the subcellular localization of Acc1 has been reported to be dynamic in both directed [354] and high throughput studies [41,355] we next asked if NuA4 impacted the localization of Acc1-GFP. Localization of Acc1 was assessed in wild-type and *eaf1Δ* cells expressing Acc1-GFP from its endogenous genomic location. As the localization of Acc1-GFP modulates depending on culture conditions [354], all localization studies were performed using rigorously controlled growth conditions, mid log phase cells (OD_{600} 0.4-0.5) cultured at 30°C in complete media. Further, to facilitate subsequent screens, images were obtained using a high-throughput CV1000 confocal microscope, which has poor brightfield imaging. In wild-type cells Acc1-GFP was found in cytoplasmic punctate structures (Figure 5.2A), similar to what has been previously reported [41,356]. However, in *eaf1Δ* cells the Acc1-GFP signal becomes diffuse throughout the cytoplasm with a significant decrease in the average punctate volume (object volume) (Figure 5.2B). We also assessed the impact of a temperature-

sensitive allele of *ESA1, esa1-L254P* (*esa1-ts*) [81], on Acc1-GFP localization at both a semi-permissive temperature of 25°C and after 2 hours at the non-permissive temperature of 37°C (Figure 5.2C). At both the semi-permissive temperature, where *esa1-ts* activity is partially reduced, and the restrictive temperature of 37°C, we detected a decrease in Acc1-GFP foci and a small but not significant decrease in average object volume (Figure 5.2C and 5.2D).

Our work indicated that the NuA4 complex regulates both the activity and the subcellular localization of Acc1, but we did not know if these were correlated. Therefore we assessed Acc1-GFP localization in strains where Acc1 is hyperactive, *snf1*Δ and *acc1*^{S1157A} [321,322]. Remarkably, in both these strains, Acc1-GFP forms fewer foci, but the average punctate volumes are significantly larger (Figure 5.2A and 5.2B), and 3D reconstruction indicates these structures resemble cylinders or straight thick rods located in the center of the cell (S5.2 Fig). Because of the straight cylinder shape, they appear on 2D images as either round foci or long rods. As *snf1*Δ partially rescues *eaf1*Δ sensitivity to Soraphen A (Figure 5.1), we next assessed Acc1-GFP localization in both *snf1Δ eaf1Δ* and *eaf1Δ acc1*^{S1157A} backgrounds. In both cases, while distinct foci were still formed, they were smaller in average volume, and we detected an increase in overall cytoplasmic localization (Figure 5.2A and 5.2B). These results suggest that the localization of Acc1-GFP is associated with its activity, with large punctate dots forming in the hyperactive form, while the diffuse cytoplasmic pattern is correlated with decreased activity.

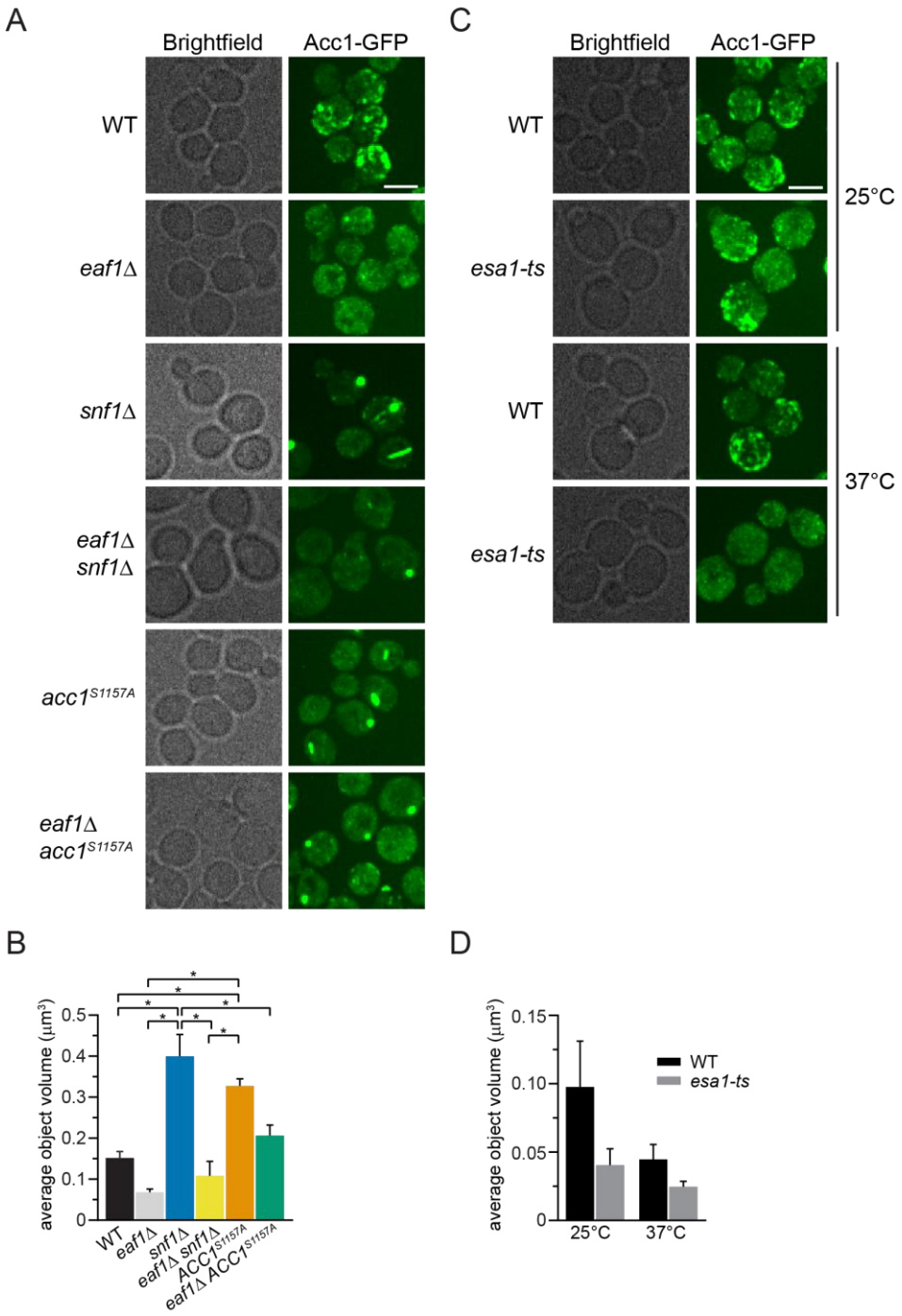

Figure 5.2: NuA4, Snf1, and Acc1 phosphorylation state mutants impact the localization of Acc1-GFP. A) Wild-type (YKB 3954), *eaf1Δ* (YKB 4448), *snf1Δ* (YKB 4348), *eaf1Δ snf1Δ* (YKB 4364), *acc1*^{S1157A} (YKB 4401) and *eaf1Δ acc1*^{S1157A} (YKB 4404) cells expressing endogenously tagged Acc1-GFP were grown to early-log phase at 30°C in YPD and assessed for Acc1-GFP localization. Representative brightfield and fluorescent images are shown. Scale bar: 4 µm. B) The average volume of Acc1-GFP structures in each strain was quantified using IMARIS software. Quantification is the average of three biological replicates, a minimum of 100 cells per replicate were scored. Error bars denote the standard error of the mean (SEM). n=3, * = $p < 0.05$ determined using a one-way ANOVA test with a Tukey's

multiple comparisons test. C) Wild-type (YKB 3954) and *esa1-ts* (YKB 4303) yeast expressing endogenously tagged Acc1-GFP were grown to early-log phase at the permissive temperature of 25°C in YPD. Cells were then diluted to an OD_{600} of 0.2 in YPD and grown at restrictive temperature of 37°C for 2h before Acc1-GFP localization was assessed. Representative brightfield and fluorescent images at 25°C and 37°C are shown. Scale bar: 4 μm. D) The average volume of Acc1-GFP structures in wild-type and *esa1-ts* strains at 25°C and 37°C were quantified using IMARIS software. Quantification is the average of three biological replicates, a minimum of 100 cells per replicate were scored. Error bars denote the standard error of the mean (SEM). n=3, * = $p < 0.05$ determined using a two-way ANOVA test with a Tukey's multiple comparisons test.

Fatty acid elongation cycle and serine palmitoyltransferase contribute to Acc1 activity and localization.

Given the remarkable impact of NuA4 on Acc1 localization, to begin to discern the biological pathways regulating Acc1-GFP localization that NuA4 may be involved in, we performed a high content microscopy screen. We employed synthetic genetic array (SGA) technology [46] to introduce Acc1-GFP into 84 deletion mutants from the BY4741 deletion mutant collection [43]. The deletion mutants selected encoded proteins previously implicated in Acc1 regulation including AMPK signaling, citrate metabolism, fatty acid oxidation, sphingolipid metabolism, glucose signaling, and metabolism (S5.1 Table). Once constructed the Acc1-GFP mutant array strains were imaged and five deletion mutants impacted the localization of Acc1-GFP: *SNF1*, *SNF4*, *ELO2*, *ELO3* and *TSC3* (S5.3 Fig.). While no mutants displayed the diffuse phenotype similar to *eaf1*Δ cells, as expected *snf1*Δ Acc1-GFP cells in the screen displayed large foci similar to what we found in our directed studies with *snf1Δ* Acc1-GFP and $Acc1^{S1157A}$-GFP cells (Figure 5.2A). Large foci were also detected in *snf4Δ* cells which was expected as Snf4 is the regulatory (gamma) subunit of AMPK1/Snf1 and Snf1 activity is reduced in the absence of Snf4 [357]. In contrast, the three other mutants identified in the screen displayed Acc1-GFP localized into thick curved rod-like structures that formed around the periphery of the cell. These Acc1 structures are different in shape and localization from the Acc1-GFP punctate dots seen in *snf1Δ* (Figure 5.3A, 5.3B and S5.3 Fig.). Intriguingly, all three mutants identified are involved in fatty acid elongation and sphingolipid biosynthesis (reviewed in [358] and Figure 5.4A). Elo2 and Elo3 are fatty acid elongases in the very long

chain fatty acid (VLCFA), biosynthesis pathway while Tsc3 is an activator of serine palmitoyltransferase (SPT), which is composed of Lcb1 and Lcb2 [359] . We next assessed the sensitivity of these strains to Soraphen A to determine if these three mutants also potentially had changes in Acc1 activity. Even at 0.1 µM, a concentration that does not impact the growth of wild-type cells, Soraphen A was extremely toxic to *elo2Δ*, *elo3*Δ and *tsc3*Δ cells suggesting they have low levels of Acc1 activity (Figure 5.3C). Our results confirm high throughput Soraphen A chemogenomic screens which identified these mutants as well as work identifying impaired fatty acid elongation in myriocin tolerance adaptation [334,360,361]. A reduction in Acc1 activity upon deletion of *ELO3* was further confirmed using an *in vitro* assay to measure the activity of Acc1 purified from *elo3Δ* cells (Figure 5.3D).

As two of these mutants were implicated in the VLCFA cycle we next directly assessed Acc1-GFP localization in non-essential VLCFA cycle genes that were not included in our screen (Figure 5.4A). Acb1 transports newly synthesized acyl-CoA esters from fatty acid synthesis into the very long chain FA biosynthesis pathway [362], while Ifa38 is a reductase that reduces 3-ketoacyl-CoA to 3-hydroxyacyl-CoA [363]. Like *elo3Δ* and *elo2Δ,* deletion of *ACB1* and *IFA38* caused a thick Acc1-GFP rod formation to occur (Figure 5.4B). Similarly, as the third mutant, *tsc3Δ,* has reduced serine palmitoyltransferase activity, we extended our study to assess Acc1-GFP localization in a temperature sensitive point mutant of *LCB1*, *lcb1-100* , one of two essential catalytic subunits of serine palmitoyltransferase [364]. In parallel we also assessed the effect of myriocin, a serine palmitoyltransferase inhibitor [365], on Acc1-GFP localization and Soraphen A sensitivity. Both conditions resulted in the formation of thick rod structures (Figure 5.4B and C) and myriocin treatment significantly increases the toxicity of Soraphen A, suggesting reduction in serine palmitoyltransferase activity decreases Acc1 activity in cells (Figure 5.4D). Taken together, we have determined that inhibition of VLCFA elongation cycle and serine palmitoyltransferase results in the concentration of Acc1-GFP into thick rod-like structures which is associated with impaired Acc1 activity.

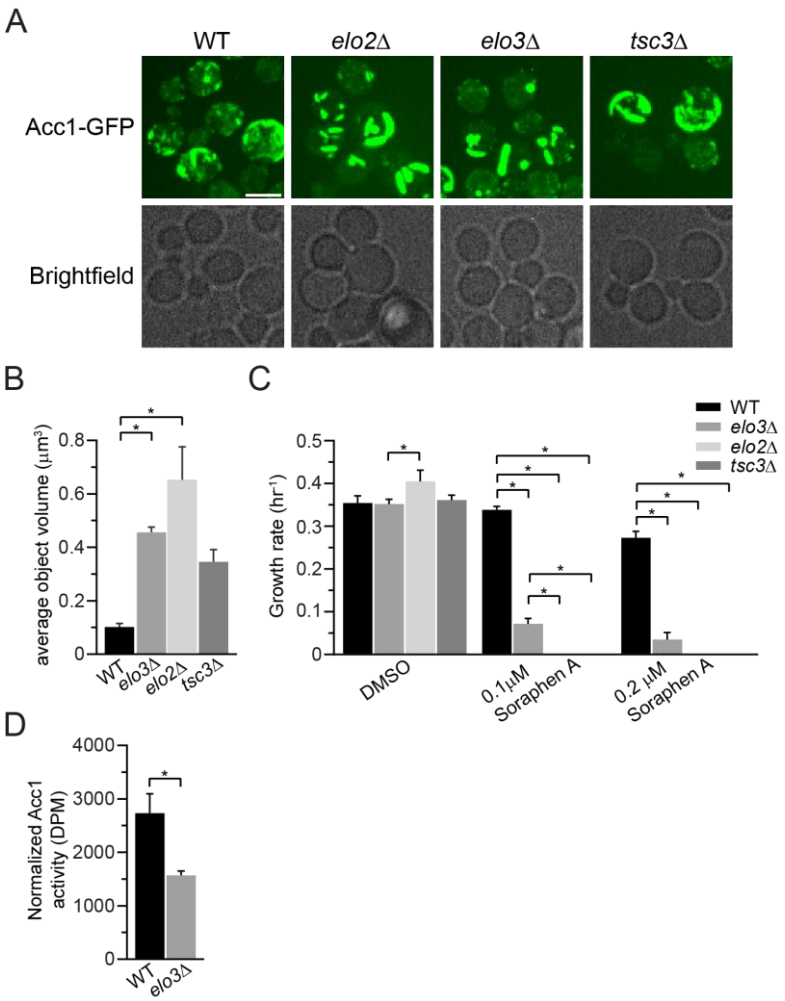

Figure 5.3: Genes from the fatty acid elongation cycle and sphingolipid metabolism impact the localization and the activity of Acc1-GFP. A) Deletion of *ELO2*, *ELO3,* and *TSC3* impact the localization of Acc1-GFP. Wild-type (YKB 3954), *elo2Δ* (YKB 4593), *elo3Δ* (YKB 4594) and *tsc3Δ* (YKB 4599) cells expressing endogenously tagged Acc1-GFP were grown to early-log phase at 30°C in YPD and assessed for Acc1-GFP localization. Representative brightfield and fluorescent images are shown. Scale bar: 4 μm. B) The average volume of Acc1-GFP structures in each strain was quantified using IMARIS software. Quantification is the average of three biological replicates, a minimum of 100 cells per replicate were scored. Error bars denote the standard error of the mean (SEM). n=3, * = $p < 0.05$ determined using a one-way ANOVA test with a Tukey's multiple comparisons test. C) *elo2Δ*, *elo3Δ* and *tsc3Δ* cells display increased sensitivity to Soraphen A. Wild-type (YKB 1079), *elo2Δ* (YKB 3913), *elo3Δ* (YKB 3914) and *tsc3Δ* (YKB 3228) cells were grown to early-log phase before being diluted to an OD_{600} of 0.1 in YPD with DMSO control or 0.1 μM or 0.2 μM Soraphen A in DMSO, and an automated growth curve analysis was performed at 30°C for 48h. Growth rate was calculated from three biological replicates. Error bars denote the standard error of the mean (SEM). n=3, * = $p < 0.05$ determined using a two-way ANOVA test with a Tukey's multiple comparisons test. D) Acc1 activity is reduced in *elo3Δ* cells. Wild-type (YKB 3954) and *elo3Δ* (YKB 4594) cells expressing endogenously tagged Acc1-GFP were grown to early-log phase at 30°C in YPD. Acc1-GFP was immunoprecipitated and Acc1 activity measured and normalized to Acc1-GFP protein abundance. Error bars denote the standard error of the mean (SEM). n=3, * = $p < 0.05$ determined using a two-tailed t-test.

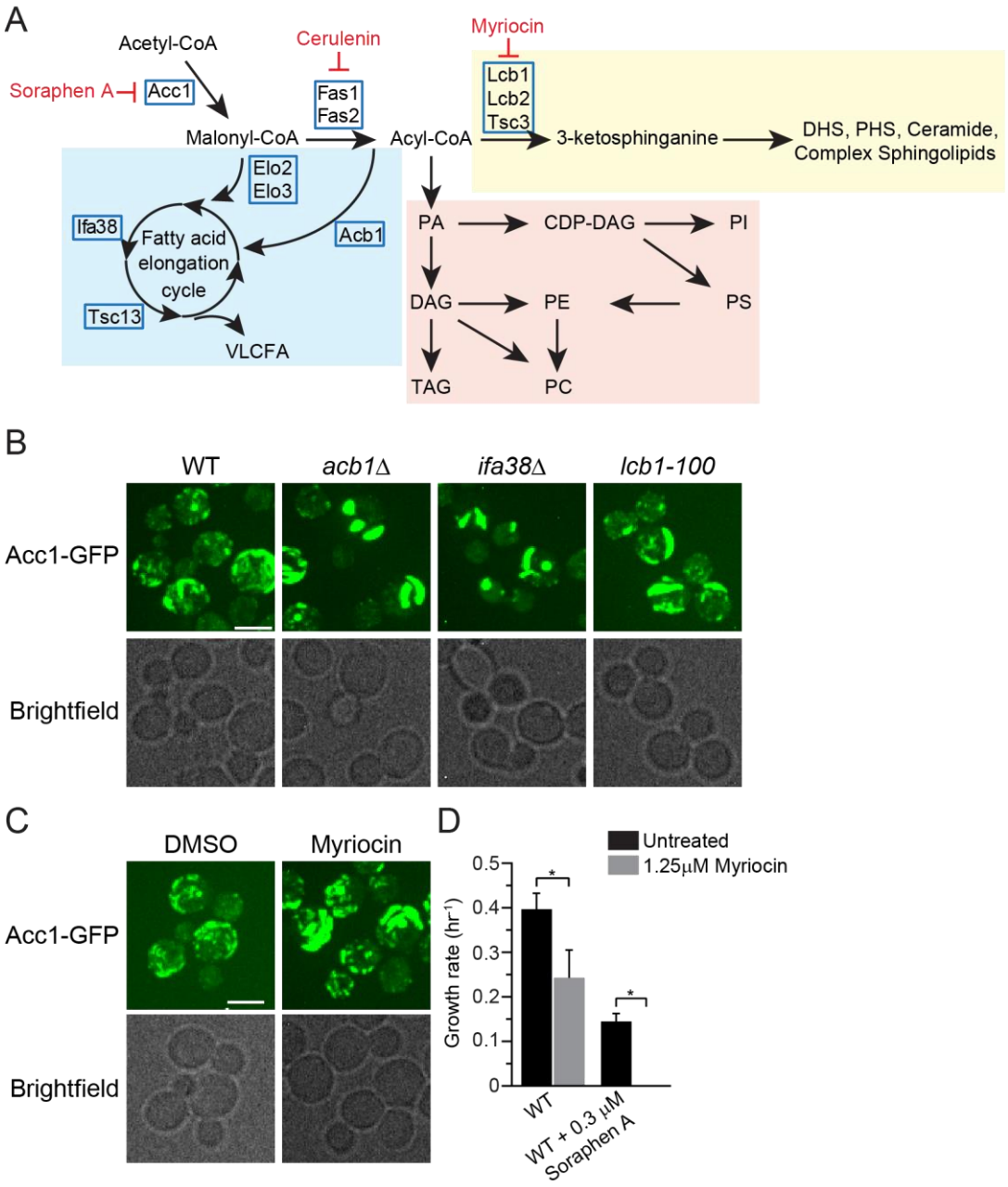

Figure 5.4: Inhibition of the fatty acid elongation cycle and sphingolipid metabolism induce the formation of thick rod-like structures of Acc1-GFP. A) Schematic of the fatty acid elongation and sphingolipid metabolism pathway that includes genes which encode the enzymes within pathway and pharmacological inhibitors Myriocin and Cerulenin. B) *acb1Δ*, *ifa38Δ,* and *lcb1-100* mutants impact the localization of Acc1-GFP. Wild-type (YKB 3954), *acb1Δ* (YKB 4601), *ifa38Δ* (YKB 4629) and *lcb1-100* (YKB 4609) cells expressing endogenously tagged Acc1-GFP were grown to early-log phase at 30°C in YPD and immediately assessed for Acc1-GFP localization within the cells. Representative brightfield and fluorescent images are shown. Scale bar: 4 μm. C) Myriocin, a serine palmitoyltransferase inhibitor, induces the formation of thick rod-like structures of Acc1-GFP. Wild-type (YKB 3954) cells expressing endogenously tagged Acc1-GFP were grown to early-log phase at 30°C in YPD. Cells were then again

diluted to an OD_{600} of 0.1 in YPD with or without 1.25 µM Myriocin, and then grown for 3h at 30°C before imaging Acc1-GFP localization within the cells. Representative brightfield and fluorescent images are shown. Scale bar: 4 µm. D) Myriocin significantly increases the toxicity of Soraphen A. Wild-type (YKB 1079) cells were grown to early-log phase diluted to an OD_{600} of 0.1 in YPD with or without 0.3 µM Soraphen A and/or 1.25 µM Myriocin, automated growth curve analysis was performed at 30°C for 48h and growth rate calculated from three biological replicates. Error bars denote the standard error of the mean (SEM). n=3, * = $p < 0.05$ determined using a two-way ANOVA test with a Sidak's multiple comparisons test.

Palmitic Acid induces Acc1-GFP rod formation and inhibits Acc1 activity.

Remarkably, the mutants that displayed rod-like localization of hypoactive Acc1-GFP, along with myriocin treatment (Figure 5.4), share the common feature that their disruption leads to increased cellular acyl-CoAs such as palmitoyl-CoA. Furthermore, exogenous long-chain fatty acids have been shown to inhibit Acc1 activity in yeast extracts [326,327] and 16-20 carbon long chain length acyl-CoAs directly inhibit rat liver Acc1 [328,329]. Therefore, we next sought to determine if the formation of Acc1-GFP rod-like structures could be driven by an increase in acyl-CoA or fatty acids levels. We first asked if exogenous treatment of cells with myristic acid (C14), palmitic acid (C16) or stearic acid (C18), which are converted to their respective CoA derivatives, impacts Acc1-GFP localization. Brij®58 was used as a vehicle control and had no impact on Acc1-GFP localization, but treatment with myristic acid (C14) and palmitic acid (C16) induced Acc1-GFP rods (Figure 5.5A). In contrast stearic acid (C18) treatment did not induce Acc1-GFP rod formation. In agreement with the correlation that Acc1-GFP rod formation is indicative of decreased Acc1 activity, cells treated with palmitic acid (C16) had an increased sensitivity to Soraphen A compared to untreated or stearic acid (C18) treated cells (Figure 5.5B). A small but significant decrease in the *in vitro* Acc1 activity in the presence of palmitoyl-CoA was also identified (Figure 5.5C). This suggests that chain length of acyl-CoA and downstream FAs and not just concentration impacts Acc1-GFP localization and activity. As increased short (C14 – C16) acyl-CoAs induced Acc1-GFP rods and inhibit Acc1 activity, we next asked whether a decrease in these acyl-CoAs impacts Acc1-GFP localization and activity by treating the cells with cerulenin, an inhibitor of Fatty Acid Synthesis [366]. Surprisingly, we detected diffuse localization of Acc1-GFP upon cerulenin treatment which could be

suppressed by exogenous myristic acid (C14) and palmitic acid (C16), but not stearic acid (C18) (Figure 5.5A). Though the diffuse localization of Acc1-GFP upon cerulenin treatment is reminiscent of *eaf1*Δ cells (Figure 5.2), cerulenin treatment decreased the sensitivity of wild-type cells to Soraphen A treatment (Figure 5.5D). This suggests that inhibiting FAS activity, thereby reducing acyl-CoA synthesis, impacts the localization and enhances the activity of Acc1, which can be reversed by exogenous supply of C14 – C16 fatty acid. Together our work suggests that not only is Acc1 activity negatively regulated by short acyl-CoAs, but that short acyl-CoA chains (C14 – C16) can influence the localization of Acc1-GFP.

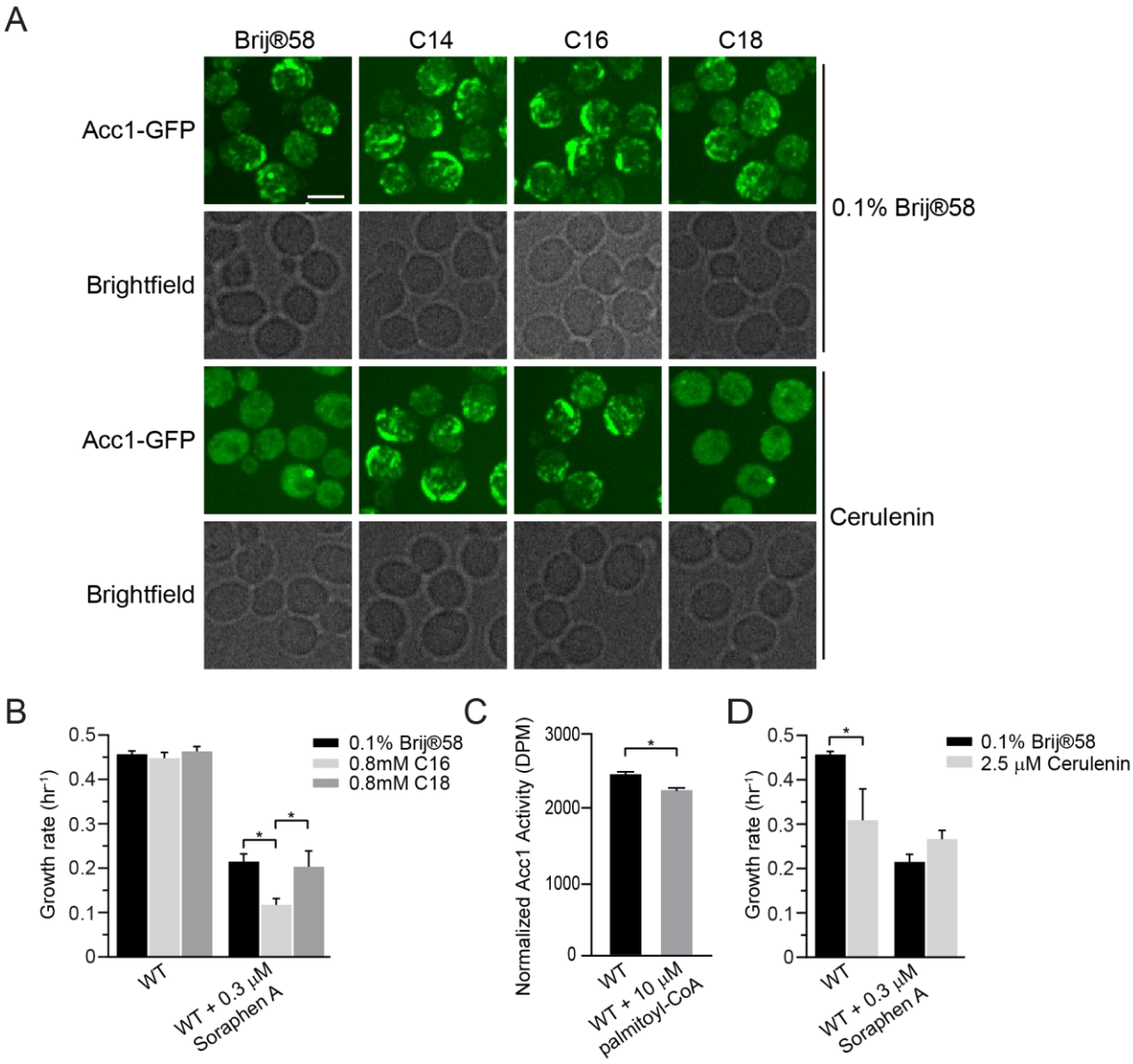

Figure 5.5: Palmitic acid induces the formation of thick rod-like structures of Acc1-GFP and inhibits Acc1 activity. A) Wild-type (YKB 3954) cells expressing endogenously tagged Acc1-GFP were grown to early-log phase before being diluted to an OD_{600} of 0.1 in YPD containing 0.1% Brij®58 with or without 0.8mM myristic acid (C14), 0.8mM palmitic acid (C16) or 0.8mM stearic acid (C18) and/or 40µM Cerulenin, grown for 1h at 30°C and immediately assessed for Acc1-GFP localization. Representative brightfield and fluorescent images are shown. Scale bar: 4 µm. B) Palmitic acid (C16) increases sensitivity of wild-type cells to Soraphen A. Wild-type (YKB 1079) cells were grown to early-log phase at 30°C in YPD. Cells were diluted to an OD_{600} of 0.1 in YPD containing 0.1% Brij®58 with or without 0.3µM Soraphen A and/or 0.8mM palmitic acid (C16) or 0.8mM stearic acid (C18), automated growth curve analysis at 30°C for 48h and growth rate was then calculated from three biological replicates. Error bars denote the standard error of the mean (SEM). n=3, * = $p < 0.05$ determined using a two-way ANOVA test with a Tukey's multiple comparisons test. C) Wild-type (YKB 3954) cells expressing endogenously tagged Acc1-GFP were grown to early-log phase at 30°C in YPD. Acc1-GFP was then immunoprecipitated and incubated with or without 10 µM Palmitoyl-CoA prior to measure it`s specific

activity as described in the Materials and Methods. Acc1-GFP activity was normalized to the relative protein abundance in the sample. Three biological replicates were performed. Error bar indicates the standard error of the mean (SEM). * Denotes statistical significance at a p-Value < 0.05 determined using a t-test. D) Cerulenin dose not increase sensitivity of wild-type cells to Soraphen A. Wild-type (YKB 1079) cells were grown to early-log phase at 30°C in YPD. Cells were diluted to an OD_{600} of 0.1 in YPD containing DMSO with or without 0.3µM Soraphen A and/or 2.5µM Cerulenin, and an automated growth curve analysis was performed at 30°C for 48h and the growth rate was then calculated from three biological replicates. Error bars denote the standard error of the mean (SEM). n=3, * = $p < 0.05$ determined using a two-way ANOVA ‘s test with a Sidak’s multiple comparison’s test.

Cerulenin treatment partially suppresses Soraphen A sensitivity of *eaf1Δ* cells which have elevated FAS activity.

Given the profound impacts of C14 – C16 acyl-CoA and FAS activity on Acc1 localization and activity, we next tested if NuA4 regulates Acc1 via this pathway. First, we assessed FAS activity in *eaf1Δ* cells. In agreement with transcriptome studies which have identified a two- fold induction of *FAS1* and *FAS2* mRNA in *eaf1Δ* background [80], Fas1 and Fas2 protein levels are increased in *eaf1Δ* cells (S5.4 Fig.). FAS activity is also significantly increased nearly 2-fold in *eaf1Δ* cells compared to wild-type cells, which is decreased by Cerulenin treatment to inhibit FAS activity (Figure 5.6A). Further we found that cerulenin treatment to inhibit FAS partially suppressed Soraphen A sensitivity of *eaf1Δ* cells (Figure 5.6B) while exogenous palmitic acid (C16) treatment reduced the growth rate of *eaf1Δ* cells and increased the sensitivity of *eaf1Δ* cells to Soraphen A (Figure 5.6C). The hyper-sensitivity of palmitic acid (C16) treated *eaf1Δ* to Soraphen A is consistent with the formation of large rods structures (Figure 5.6D) previously shown to correlate with reduced Acc1 activity. Interestingly, stearic acid (C18) partially suppressed Soraphen A sensitivity. Together this suggests that despite puzzlingly similar diffuse Acc1-GFP localization in *eaf1Δ* and cerulenin treated cells, elevated FAS activity and its products C14 – C16 acyl-CoAs are indeed contributing to a reduction of Acc1 activity and increased Soraphen A sensitivity in *eaf1Δ* cells in a negative feed-back loop.

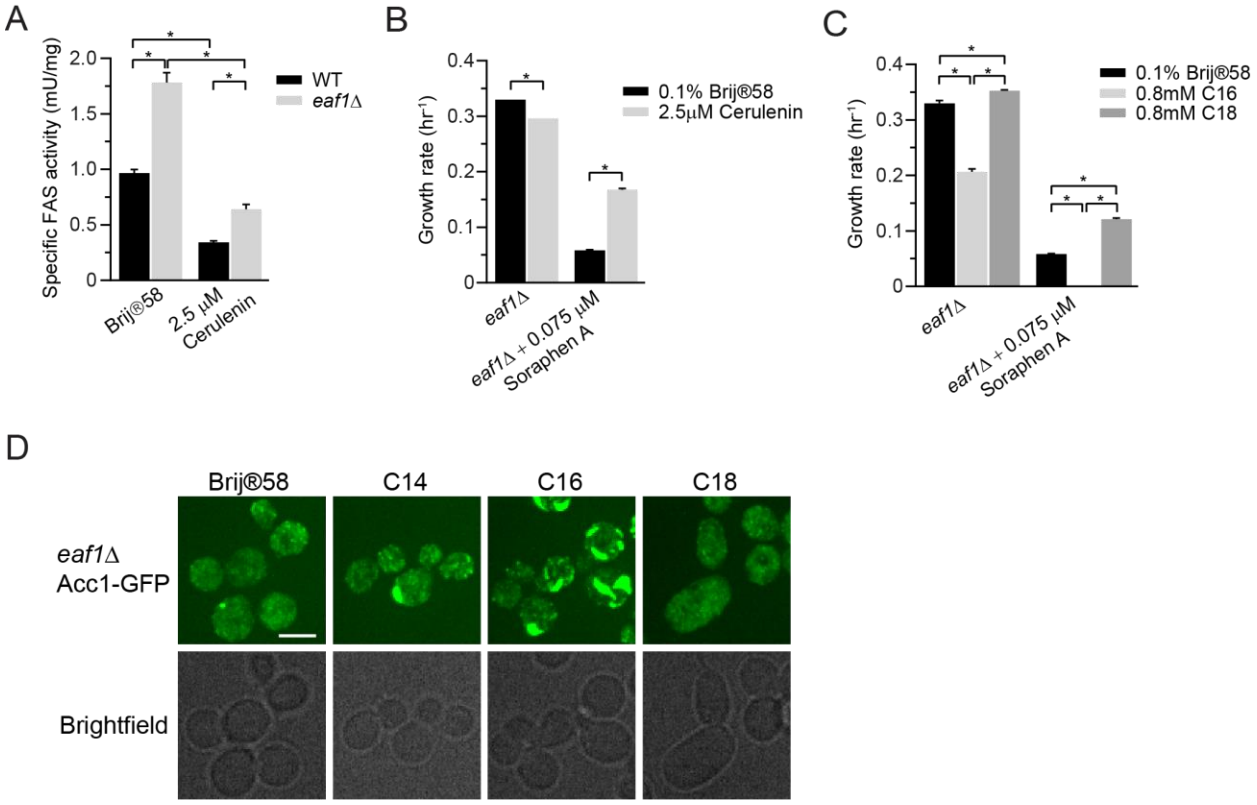

Figure 5.6: Cellular acyl-CoA chain length and FAS activity partially modulates *eaf1Δ* cell sensitivity to Soraphen **A.** A) FAS activity is increased in *eaf1Δ* cells compared to wild-type cells, but Cerulenin inhibits FAS activity in both cells. Wild-type (YKB 1079) and *eaf1Δ* (YKB 3333) were grown to early-log phase at 30°C in YPD. Cells were then again diluted to an OD_{600} of 0.1 in YPD with or without 2.5µM Cerulenin, and then grown for 2h at 30°C. FAS activity assay was performed on the whole cell extracts and was normalized to the relative protein abundance in the sample. Error bars denote the standard error of the mean (SEM). n=3, * = $p < 0.05$ determined using a two-way ANOVA test with a Tukey's multiple comparisons test. B) Cerulenin partially suppresses sensitivity of *eaf1Δ* cells to Soraphen A. *eaf1Δ* (YKB 4448) cells were grown to early-log phase at 30°C in YPD. Cells were then diluted to an OD_{600} of 0.1 in YPD with or without 0.075µM Soraphen A and/or 2.5µM Cerulenin, and an automated growth curve analysis was performed and used to calculate growth rate. Error bars denote the standard error of the mean (SEM). n=3, * = $p < 0.05$ determined using a two-way ANOVA test with a Sidak's multiple comparisons test. C) Palmitic acid (C16) increases sensitivity of *eaf1Δ* cells to Soraphen A. *eaf1Δ* (YKB 4448) cells were grown to early-log phase before being diluted to an OD_{600} of 0.1 in YPD containing 0.1% Brij®58 with or without 0.075µM Soraphen A and/or 0.8mM palmitic acid (C16) or 0.8mM stearic acid (C18), automated growth curve analysis was performed at 30°C for 48h and growth rate was then calculated from three biological replicates. Error bars denote the standard error of the mean (SEM). n=3, * = $p < 0.05$ determined using a two-way ANOVA test with a Sidak's multiple comparison's test. D) Palmitic acid induces the formation of thick rod-like structures of Acc1-GFP in *eaf1Δ* cells. *eaf1Δ* (YKB 4448) cells expressing endogenously tagged Acc1-GFP were grown to early-log phase before being diluted to an OD_{600} of 0.1 in YPD containing 0.1% Brij®58 with or without 0.8 mM myristic acid (C14), 0.8 mM palmitic acid (C16) or 0.8 mM stearic acid (C18) and grown for 2h at 30°C prior to imaging. Representative brightfield and fluorescent images are shown. Scale bar: 4 µm.

Lipids are overall deregulated in NuA4 mutants:

Our data are consistent with the findings of multiple studies that not only is Acc1 regulating acyl-chain length, but that acyl-chain length is directly impacting Acc1 activity through a feedback loop. Hyperactive Acc1 does not significantly change the composition of membrane phospholipids, but leads to an increase in total TAG and a shift towards longer acyl-chain lengths across the glycerolipid classes [322]. Conversely, Acc1 hypomorphs and Soraphen A treated cells also do not dramatically alter most phospholipid composition, but display a shift to shorter average acyl chain length [324,367]. Further, increased FAS activity, which increases cellular concentration of acyl-CoA also directly inhibits Acc1 activity [326,328]. In addition, our work suggests that acyl chain length is also influencing the subcellular localization and activity of Acc1. This negative feed-back seems to partially account for the reduction of Acc1 in the NuA4 mutant *eaf1*Δ. To further characterize the impacts of NuA4 on Acc1 via lipid metabolism in general and through acyl chain length in particular, we performed a shotgun lipidomic analysis to look for overall cellular lipid profile changes in WT, *eaf1Δ,* and Soraphen A treated cells (Figure 5.7 and S5.3 Table). Similar to previous studies, decreasing Acc1 activity through Soraphen A treatment resulted in minor changes in neutral lipid composition of cells, including increased PI and decreases in PC [367] . The limited impact of Soraphen A on PA and even TAG levels, indicate that the cell is able to compensate for overall changes in neutral lipids to maintain homeostasis as previously shown for hyperactive Acc1 mutants [322]. More striking was the common characteristic of a reduction in average number of carbons in the tail chain length for all neutral lipid species in cells treated with Soraphen A (Figure 5.7). Interestingly, while deletion of *EAF1* also did not show broad changes in the composition of the lipotype by lipid class, it also had the trend of decreased average acyl chain length although to a slightly less degree than the Soraphen A treated condition (Figure 5.7). The one significant difference between *eaf1Δ* and Soraphen A treated cells is that the percentage of ergosteryl esters was increased in *eaf1Δ* cells, which suggests NuA4 may be playing a separate role in ergosterol metabolism. Together this work shows that similar to *acc1* hypomorphs, *eaf1Δ* cells display a reduction in acyl chain length.

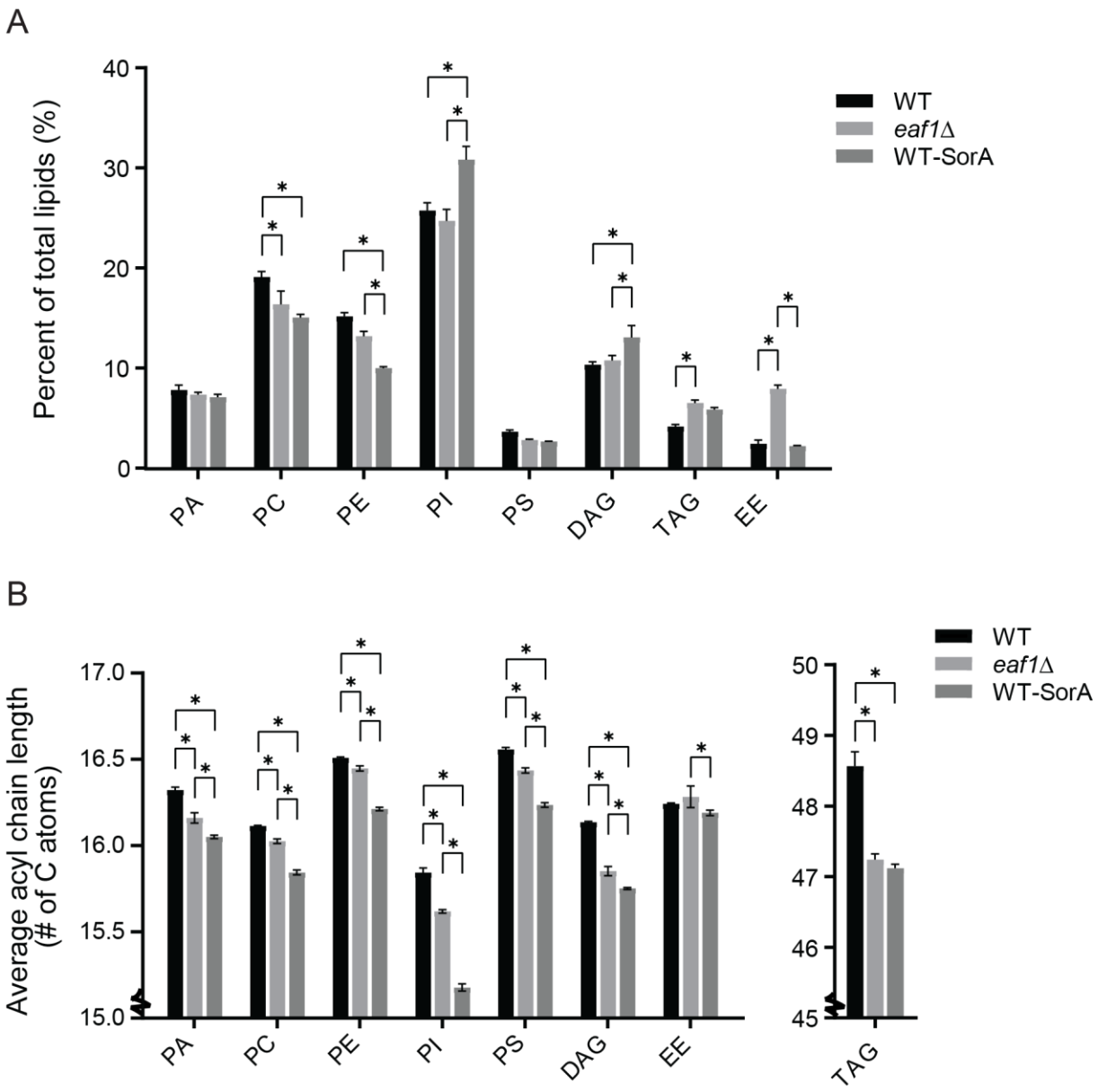

Figure 5.7: Lipidomic analysis of WT and NuA4 mutants**.** The lipid composition of WT, *eaf1Δ*, and Soraphen A treated WT yeast was assessed through lipidomics. WT, *eaf1Δ*, and Soraphen A treated cells were harvested in mid-log and a crude lysate was created through bead beating with water, lipids were then extracted using a chloroform/ methanol procedure and Mass spec analysis was performed by Lipotype GmbH. In this figure are the most prevalent lipids identified: Phosphatidic acid (PA), Phosphatidylcholine (PC), Phosphatidylethanolamine (PE), Phosphatidylinositol (PI), Phosphatidylserine (PS), Diacylglycerol (DAG), Ergosteryl ester (EE), and Triacylglycerol (TAG). A) The composition of lipid classes broken down as a percent of the total lipids. A two-way ANOVA analysis with a Tukey's multiple comparisons test was performed and a * represents an adjusted $p < 0.05$. B) The average acyl chain length for each class of lipid was calculated from the lipidomic data. The Y Axis is broken to zoom in on the data and show the small but significant changes in chain length. A two-way ANOVA analysis with a Tukey's multiple comparisons test was performed and a * represents an adjusted $p < 0.05$.

Discussion:

Through multiple biochemical, chemical, and genetic approaches we confirm that Acc1 activity is reduced upon deletion of *EAF1* and disruption of the NuA4 complex [173] is associated with more diffuse subcellular localization of Acc1-GFP. We determined that in addition to Eaf1, multiple pathways impact Acc1 subcellular localization and activity, including increased palmitoyl-CoA (C16) levels which inhibits Acc1 activity and remodels Acc1 localization. Finally, we found that *eaf1Δ* cells do not have drastic changes in the composition of cellular lipids by class but that they did appear to have reduced overall chain length across fatty acids, which phenocopies Acc1 inhibition through Soraphen A treatment. Therefore, in addition to the well-know Snf1/AMPK signaling pathway, NuA4 regulation of Acc1 may be through a dynamic feed-back mechanism in which altered lipid length can impact Acc1 localization and activity (Figure 5.8A).

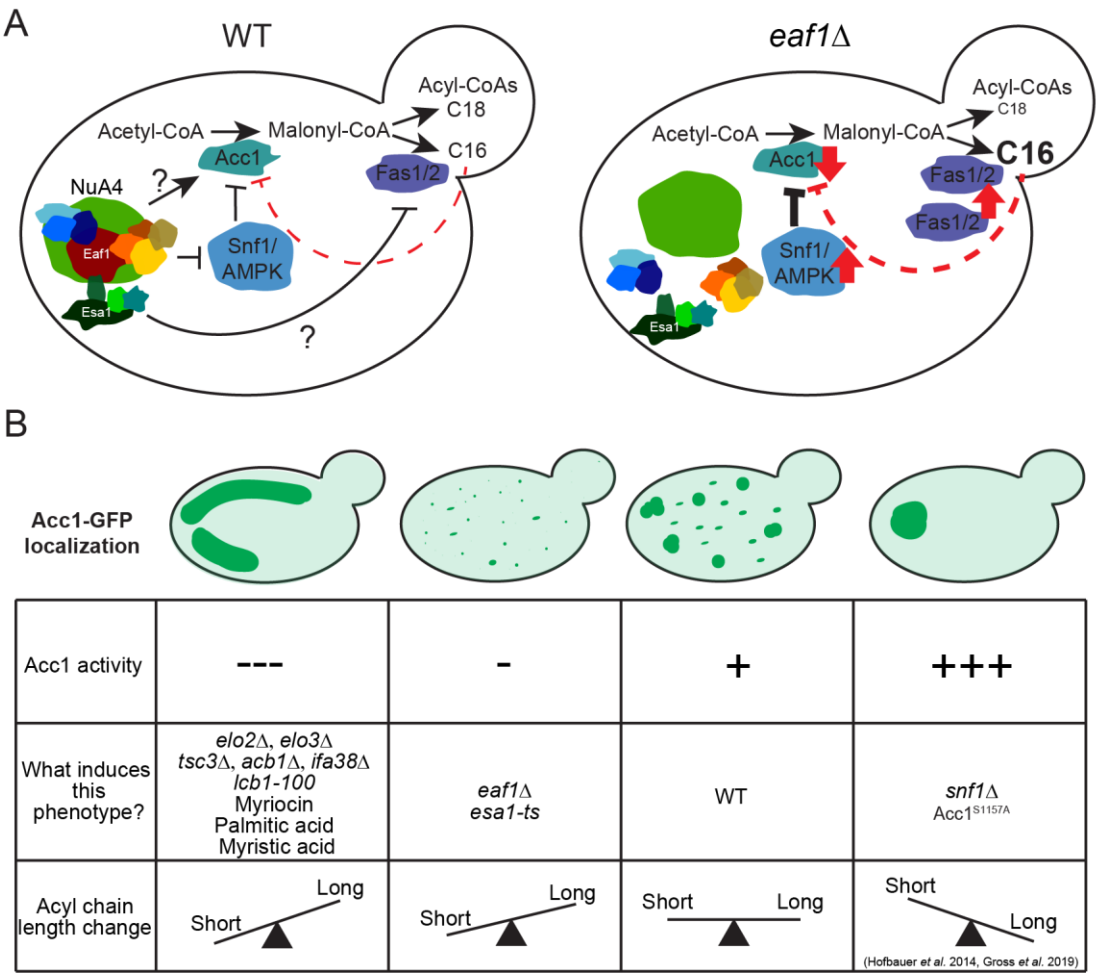

Figure 5.8: Model for NuA4 dependent regulation of Acc1. A) Schematic representing the regulation of Acc1 in WT and *eaf1Δ* yeast by NuA4. B) Four different phonotypes of Acc1-GFP localization were identified in our study. These phenotypes are demonstrated along with a table summarizing the activity of Acc1, causes of the phenotype, and the pattern of acyl-CoA chain length associated with the each of the phenotypes.

Multi-faceted regulation of Acc1 by NuA4

Given the established role of NuA4 in negatively regulating Snf1/AMPK [60], we anticipated that the decrease in Acc1 activity in *eaf1Δ* cells would be solely due to increased inhibition by Snf1/AMPK phosphorylation. If NuA4 was only inhibiting Acc1 due to hyperactive Snf1, we would anticipate that deletion of *SNF1* in an *eaf1Δ* background would result in hyperactive Acc1 and that *snf1Δ* and *snf1Δeaf1Δ* cells would have similar resistance to Soraphen A treatment. Surprisingly, we found this was

not the case and our work suggests that NuA4 is regulating Acc1 through both Snf1-dependent and independent pathways (Figure 5.1). As NuA4 directly regulates other metabolic enzymes [59,60], a likely mechanism for the secondary pathway could be direct acetylation of Acc1. However, though global acetylome studies have identified multiple acetylation sites on Acc1, to date none are attributed to NuA4 [4,48,153,353]. Nor did our SILAC-based proteomic study identify any acetylation sties on Acc1-TAP that are dependent on the catalytic subunit of NuA4, *esa1* (S5.1 Fig.). Though we cannot definitely rule out that NuA4 is regulating the activity of Acc1 through direct acetylation, which would require a systematic mutational analysis of all potential lysine acetylation sites on Acc1 and assessment of activity *in vivo*, our work suggests that NuA4 is likely regulating Acc1 through a more complex mechanism that includes regulation of subcellular localization of Acc1.

Correlation between Acc1 localization and activity

Even as early as the 1970s it was reported that Acetyl-CoA carboxylases from various species form filaments and this polymerization facilitates activation of the enzyme [368–370]. Localization studies of Acc1 in yeast have also indicated that Acc1 can form aggregates. Under logarithmic growth conditions, both indirect immunofluorescence and live GFP imaging have shown that Acc1 is largely diffuse with small punctate structures across the cytoplasm [323,354,371]. More recent studies have shown that Acc1 can form rod like structures in the center of the cell in 19% of cells in log phase and these central rod like filaments increase to 57% cells after 5 days of starvation [372]. Other directed and high content screens have also detected dramatic changes in Acc1 subcellular location upon stress including oxygen deficiency, rapamycin treatment, and DTT treatment [41,354,355]. One screen showed a change from a cytosolic punctate localization to aggregate filament structures similar to those seen in our work upon treatment of Acc1-GFP cells with DTT [355]. However, to our knowledge the diffuse localization of Acc1-GFP that we found in the *eaf1Δ* cells and the Acc1 localization of rod like structures around the periphery of the cell have not yet been documented in yeast.

The association between the changes in localization and activity of Acc1-GFP in each of the mutants was a key finding in our work. We found that in mutants with high Acc1 activity, such as *snf1Δ* and *acc1*^{S1157A} mutants, Acc1-GFP was highly aggregated into a small number of large rod or punctate structures within the centre of the cell (Figure 5.8B). Wild-type levels of Acc1 activity was associated with many punctate structures throughout the cell. Mutants with slightly lowered Acc1 activity, such as our NuA4 mutants displayed decreased aggregation of Acc1 resulting in a more diffuse distribution. Interestingly, our understanding that NuA4 regulation of Acc1 may be independent of Snf1 activity was additionally supported by the fact that the Acc1-GFP aggregates were smaller in the *eaf1Δsnf1Δ* and *eaf1Δ acc1*^{S1157A} mutants than in the *snf1Δ* and acc1^{S1157A} mutants. However, unlike NuA4 mutants, mutants with very low Acc1 activity, such as those involved with sphingolipid metabolism or very-long chain fatty acid elongation, demonstrated Acc1 aggregation into large rod like structures, but these were predominantly visible toward the periphery of the cell (Figure 5.8B). The shape and localization of these inactive Acc1 rods are different from the ones formed by hyperactive Acc1 in *snf1Δ* and *acc1*^{S1157A} mutants.

While in yeast, the correlation of Acc1 activity and localization/aggregation has not previously been explored, recent work by Hunkeler and colleagues obtained cryo electron microscopy structures of human Acc1 filaments which were associated with Acc1 activity. These filaments formed in the presence of citrate (with and without palmitoyl CoA) and the BRCT domains of BRCA1 [325]. Interestingly, these filaments were associated with high and low levels of Acc1 activity respectively, and the high activity of the citrate associated filament was inhibited by the addition of excess palmitoyl-CoA, somewhat mirroring the effects of palmitic acid in our work [325]. However, while we have previously shown that citrate can impact Acc1 activity *in vitro*, an overlay of the yeast Acc1 protein onto the determined human ACC1 filament suggests that the yeast Acc1 is incompatible with the aggregation structures identified by Hunkeler *et. al.* [173,315,325]. Further, while the addition of citrate to Acc1 extracted from *eaf1Δ* yeast did

slightly improve activity, it was well below that of WT, suggesting an alternate mechanism of Acc1 regulation by NuA4 [173]. While our yeast aggregates may not form the filaments documented in the mammalian system, we show the formation of Acc1 aggregates is associated with both low (periphery rods) and high levels (internal large foci) of Acc1 activity and that these structures do appear as separate aggregate phenotypes.

To complicate things, we found that an inhibition of FAS led to a diffuse Acc1 similar to that of the *eaf1Δ* localization, but this treatment seemed to make the cells less sensitive to Soraphen A. This suggests that in contrast to *eaf1Δ*, under FAS inhibition Acc1 activity is increased despite the largely diffuse localization. One possible explanation for this inconsistency is that even though seemingly similar, the diffuse Acc1 can exist in 2 different states or micro-structures that associate with high or low activity, a phenomenon observed with the Acc1 rod like structures and filaments as discussed above. In fact, we did observe the Acc1 structures similar to those in *snf1Δ* and *acc1*^{S1157A} mutants in a few cells under FAS treatment. Our observation raises the possibility that Acc1 localization is highly dynamic and the diffusion of Acc1 structures may represent intermediate states where Acc1 transitions from one type of aggregate to another. Further time-lapse studies using higher imaging resolution may be needed to prove this hypothesis.

The change in localization associated with changes in Acc1 activity in our yeast could have many impacts including impacting protein interactions of Acc1. In fact, a screen which previously identified Acc1 aggregation into rods upon DTT treatment compared the protein interactors of untreated and treated cells and identified 9 new physical interactors proteins of Acc1 upon DTT treatment [355]. However, Noree *et. al*., the authors who identified Acc1 rods under glucose limitation did not identify any aggregating proteins that colocalized with Acc1 structures. While this does not rule out that there are other lower

abundance proteins, lipids, or other compounds present in the Acc1 aggregates, it suggests that the primary protein component of these structures under these conditions is Acc1 [372]. In the future it will be interesting to determine if the different types of aggregates demonstrated in our work, with high and low Acc1 activity and central versus peripheral localization respectively, are associated with different compositions.

Feedback of FAS activity and inhibition of Acc1 through shorter chain acyl-CoAs

After our screen for mutants which affect Acc1-GFP localization highlighted the importance of VLCFA and sphingolipids in maintaining Acc1 localization and activity (Figure 5.3 and 5.4) we asked if acyl-CoA feedback inhibition on Acc1 . [326–329], could be mediated by regulation of Acc 1 subcellular localization.

We found that the effect of the acyl-CoA treatment on Acc1-GFP localization was dependent on the chain length, with the shorter myristic acid (C14) and palmitic acid (C16) inducing rods but not the longer stearic acid (C18) (Figure 5.5 and 5.6). Treatment of cells with C16 also increased their sensitivity to Soraphen A, indicating a decrease in Acc1 activity upon this treatment. The addition of shorter chain length fatty acids having a phenotypic effect aligns well with previous research linking Acc1 activity, FAS activity, and acyl-CoA chain lengths but here we identify an additional change in Acc1 localization [322,361,367,373].

Independent studies by Gross and Hofbauer found that inositol auxotrophy and autophagy defects of the hyperactive mutant $Acc1^{S1157A}$ are phenocopied by adding a longer chain fatty acid, Oleic acid (C18) [322,373]. In fact, exogenous treatment with Oleate was able to partially reverse an autophagy defect

found in Soraphen A treated cells, suggesting that longer chain acyl-CoAs could feed back onto regulation of Acc1 activity [322,373]. Further, the hyperactive Acc1^{S1157A} mutant has an overall shift in lipid content towards longer chain fatty acids with an increase in C18/C16 ratio and an increase in average chain length of fatty acids [322,373]. Similarly, recent work by Bao and colleagues identified a Acc1 hypomorph that allowed growth in the absence of PC [367]. This evolution was associated with a decrease in Acc1 activity and acyl-CoA chain length [367]. Intriguingly, this study also found that a chromosome XV monosomy allowed yeast to grow in the absence of PC [367]. This mutant had apparent increase in FAS activity that was associated with a decrease in acyl-CoA chain length and an inhibition of Acc1 [367]. . In agreement with this finding, our work shows a small but significant decrease in lipid chain length in our *eaf1Δ* cells and in Soraphen A treated cells which coincided with an increase in FAS activity and decrease in Acc1 activity. Additionally, an inhibition of FAS alleviated sensitivity to Soraphen A in both WT and *eaf1Δ* mutant, suggesting that Acc1 activity is increased under FAS inhibition. Intriguingly, the catalytic subunit of NuA4, *ESA1,* is found on chromosome XV, which raises the possibility that the chromosome XV monosomy that suppresses PC-deficiency [367] could partially be through an *ESA1* haploinsufficiency. The decreased Acc1 activity and the reduction in lipid chain length upon deletion of *EAF1* that we report here parallels the increase in chain length in the hyperactive Acc1^{S1157A} by Hofbauer and colleagues as well as the decrease in the in chain length in hypoactive Acc1 conditions by Bao and colleagues [373]. Finally, we were also able to demonstrate that the addition of palmitoyl-CoA decreases Acc1 activity in an *in vitro* assay (Figure 5.5C), thereby suggesting that the decrease in average chain length identified in the *eaf1Δ* may play a role in the indirect regulation of Acc1 activity. The combination of our work with previously published studies suggests that not only does the activity of ACC and FAS impact the production and length of fatty acids but conversely the fatty acid composition, specifically in terms of length, can affect the activity of Acc1 and that this regulation is additionally entangled with the changes in Acc1 localization reported in our study.

Conclusions

Our work demonstrates that NuA4 is required for Acc1 activity and localization, as NuA4 mutants have a decrease in Acc1 activity which is correlated with a diffuse localization of Acc1. We also identify other discrete localizations of Acc1 which are associated with altered activity, specifically for mutants and inhibitors associated with VLCFA and sphingolipid synthesis. The identification of these mutants allowed us to implicate acyl-CoA chain length as an important factor in *EAF1* dependent regulation of Acc1. Though the exact molecular mechanism remain to be determined, our work support that deregulation of lipid length in NuA4 mutants leads to a feed back regulation on Acc1 which is correlated to changes in Acc1 localization. Our observations also highlight the complicated dynamic changes in Acc1 localization in response to cellular acyl-CoA chain length among other signals. The precise mechanism and role of yeast NuA4, and perhaps the homologous human Tip60 complex, in regulating the activity of Acc1 through lipid distributions will be an important exploration in future work.

Acknowledgements

We thank Chloe van Oostende-Triplet from the uOttawa Cell Biology and Image Acquisition Core Facility for her help with the microscopy analysis and the Ottawa Hospital Research Institute Proteomics Core Facility for their mass spectrometry service.

Funding

This work was supported by a grant from the Canadian Institutes of Health Research (CIHR; http://www.cihr-irsc.gc.ca/e/193.html) to KB (MOP-142403) and MDF (PJT-148634). EW was supported by the Natural Sciences and Engineering Research Council (NSERC, https://www.nserc-

crsng.gc.ca/index_eng.asp) Postgraduate Scholarships-Doctoral program and an Ontario Graduate Scholarship.

Conflict of Interest

The authors have no conflicts of interest with regards to this work.

Appendix B: Supplemental Figures and Tables from Manuscripts:

Manuscript 1 Supplements

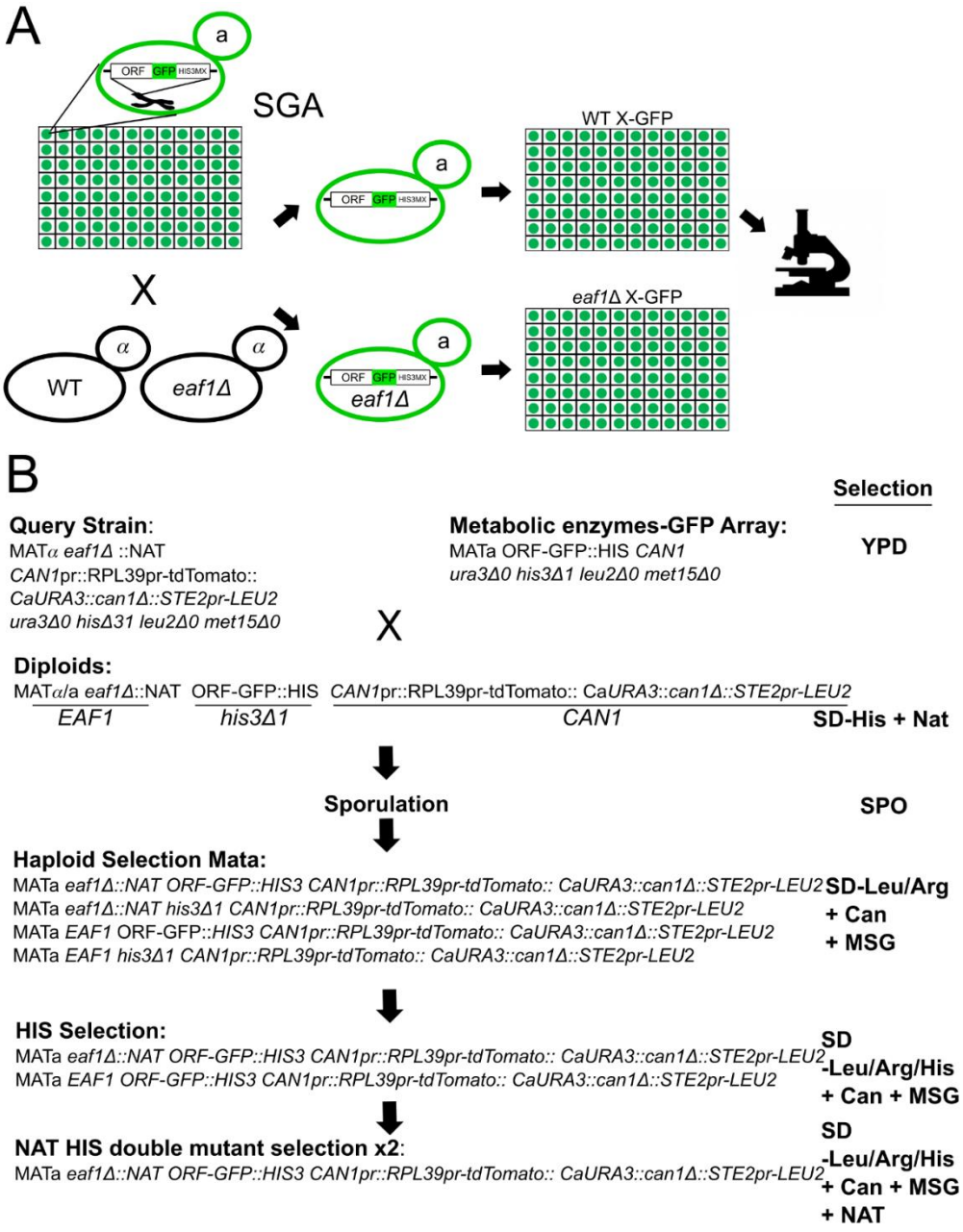

S2.1 Fig. Summary of screen protocol. (A) We selected 407 metabolic genes from the yeast GFP collection where each ORF is tagged with GFP and the *HIS3MX* to create a metabolic protein mini array. This mini array was crossed to WT and *eaf1Δ MAT* alpha query strains and an SGA protocol was followed to create two GFP mini arrays. The protein localization of each metabolic protein was compared between the WT and *eaf1Δ* arrays by high throughput microscopy. (B) A flow chart tracking the strains and markers that were used and produced during our SGA protocol and the selection medias that were used along the way.

S2.1 Table. List of screened strains, top 70 changes, and final 23 changes. Abbreviated. More detailed table available in supplemental of full published paper.

Gene	Change	GFP Intensity Fold Change *eaf1*Δ/WT (From Second_Measurement)
ACO2	Mitochondrial elongation	0.51
ACS2	Nucleus to Cytosol	0.6
ADE3	Cytosol to nucleus	0.84
AIM41	Mitochondrial elongation	0.99
ALD4	Mitochondrial elongation	0.99
ARG5	Mitochondrial elongation	1.11
BCY1	Nucleus to Cytosol	0.92
DUR1	Increased abundance	3.77
FAA3	Cell periphery to cytoplasm	0.94
GBD1	Cytosol to punctate	1.41
GSY1	Cytosol to punctate	1.46
GSY2	Cytosol to punctate	1.62
HEM1	Mitochondrial elongation	0.81
IDH2	Mitochondrial elongation	0.86
ILV6	Mitochondrial elongation	0.6
KGD1	Mitochondrial elongation	1.06
KGD2	Mitochondrial elongation	1.17
LSC1	Mitochondrial elongation	1.16
MIS1	Mitochondrial elongation	1
MSN2	Cytosol to nucleus	1.1
POS5	Mitochondrial elongation	1
RDL2	Mitochondrial elongation	1.02
YDR061W	Mitochondrial elongation	1.39

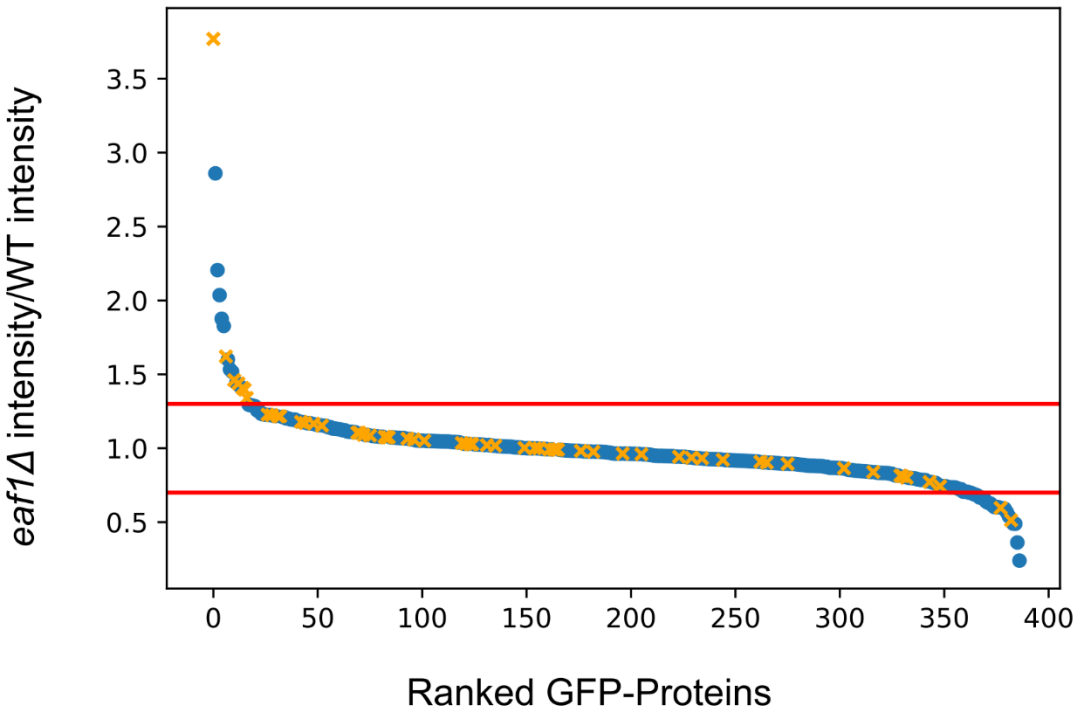

S2.2 Fig. Changes in metabolic protein GFP intensity between and *eaf1Δ* and WT. The mean intensity of GFP signal per cell of each strain was compared between the WT and the *eaf1Δ*. For each GFP-tagged metabolic protein, two field of view images were taken for each the WT and *eaf1Δ* strain using both brightfield and the GFP channel. The *eaf1Δ* average intensity per cell was divided by the paired WT average intensity per cell to give a relative change in GFP signal (*eaf1Δ* cell intensity/WT cell intensity). The relative change was then ranked and plotted using MatPlotLib. Proteins which had a larger than 1.3 or less than 0.7-fold change in were deemed primary hits (outside of the horizontal red lines). All raw intensity measurements and summarized changes with gene names are available in S2. Blue spots are quantifications of the first pass of the screen and orange X points are quantifications of the secondary assessment of primary hits.

S2.2 Table. Classification of the 23 proteins that were confirmed to change between WT and *eaf1*Δ in our GFP screen. A classification of the 23 genes which were identified with high confidence as changing in protein/GFP signal between WT and *eaf1Δ* yeast. Six categories of changes were identified.

Changes in protein/GFP signal classification	**Gene**
Mitochondrial elongation	*ACO2*
	AIM41
	ALD4
	ARG5
	HEM1
	IDH2
	ILV6
	KGD2
	LSC1
	MIS1
	POS5
	RDL2
	YDR061W
	KGD11
Cytosol to punctate	*GBD1*
	GSY1
	GSY2
Nucleus to cytosol	*ACS2*
	BCY1
Cytosol to nucleus	*ADE3*
	MSN2
Cell periphery to cytoplasm	*FAA3*
Increased abundance	*DUR1*

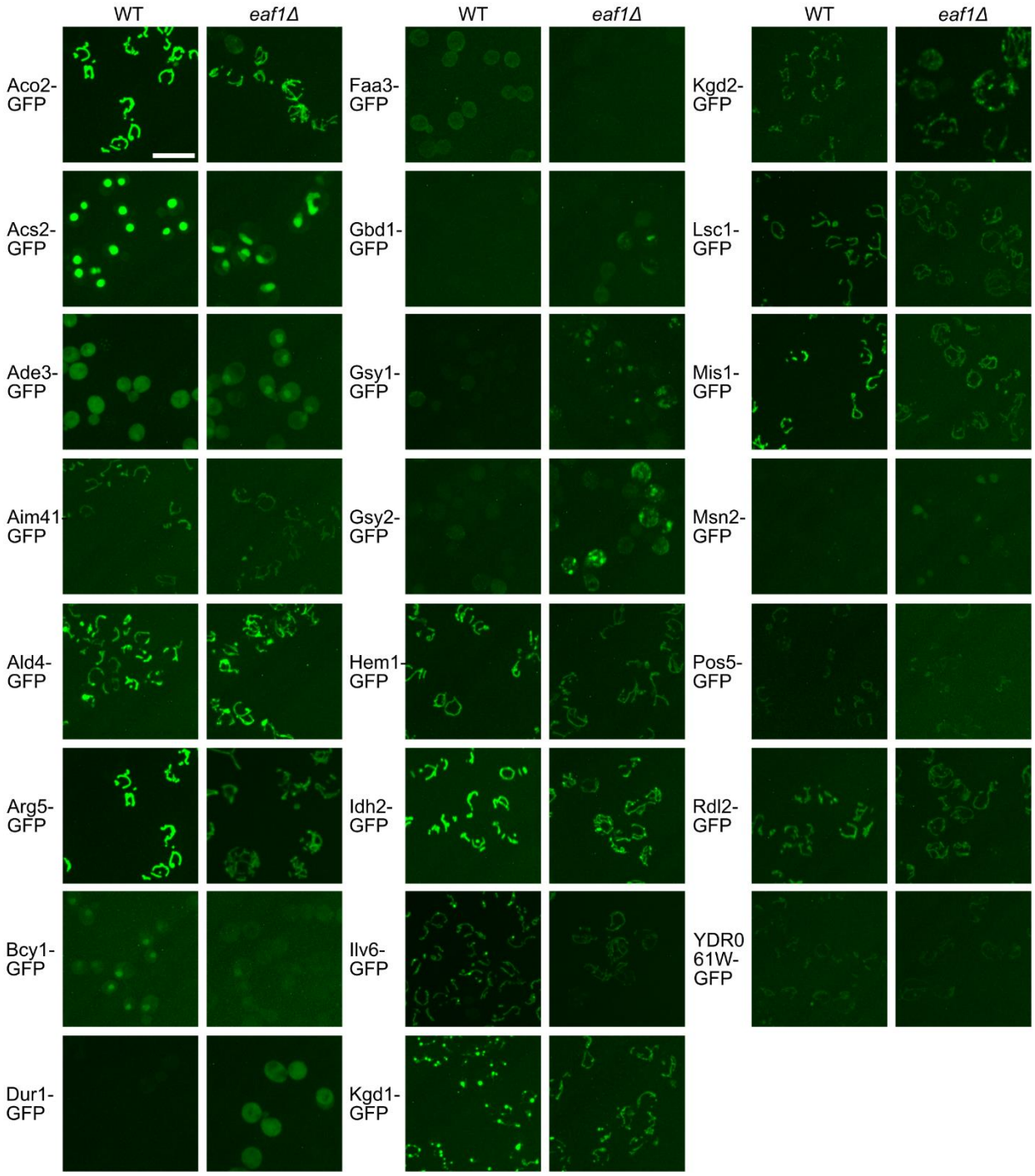

S2.3 Fig. Example images of the 23 proteins that were confirmed to change between WT and *eaf1Δ* in our GFP Screen. Scale bar =10 μm

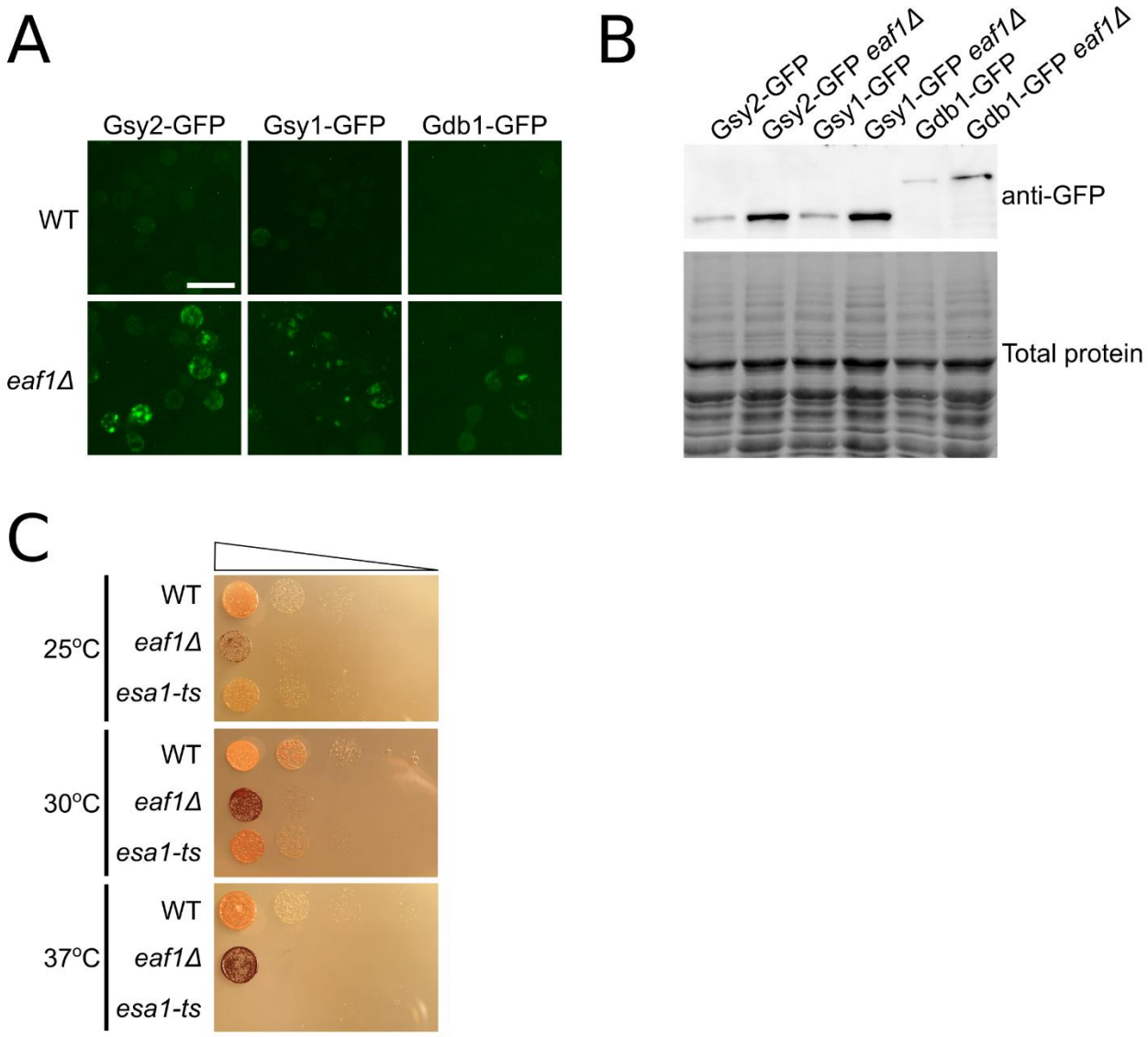

S2.4 Fig. NuA4 plays a role in the regulation of glycogen synthesis. (A) Representative images of WT and *eaf1Δ* cells expressing Gdb1-GFP, Gsy1-GFP and Gsy2-GFP taken from our screen. (Scale bar = 10 μm). (B) Representative western blot of WT or *eaf1Δ* whole cell extracts containing Gsy1-GFP, Gsy2-GFP, and Gdb1-GFP. These show that the abundance of each of these proteins increases in an *eaf1Δ* relative to WT. (C) The glycogen content of WT, *eaf1Δ*, and the temperature sensitive *esa1-ts* mutant were assessed at 3 temperatures using an iodine staining procedure, darker colour is indicative of increased glycogen content. Yeast were spotted onto YPD in 10-fold serial dilutions and grown for 24 h at the designated temperature prior to exposure to iodine crystals. Image is representative of three biological replicates.

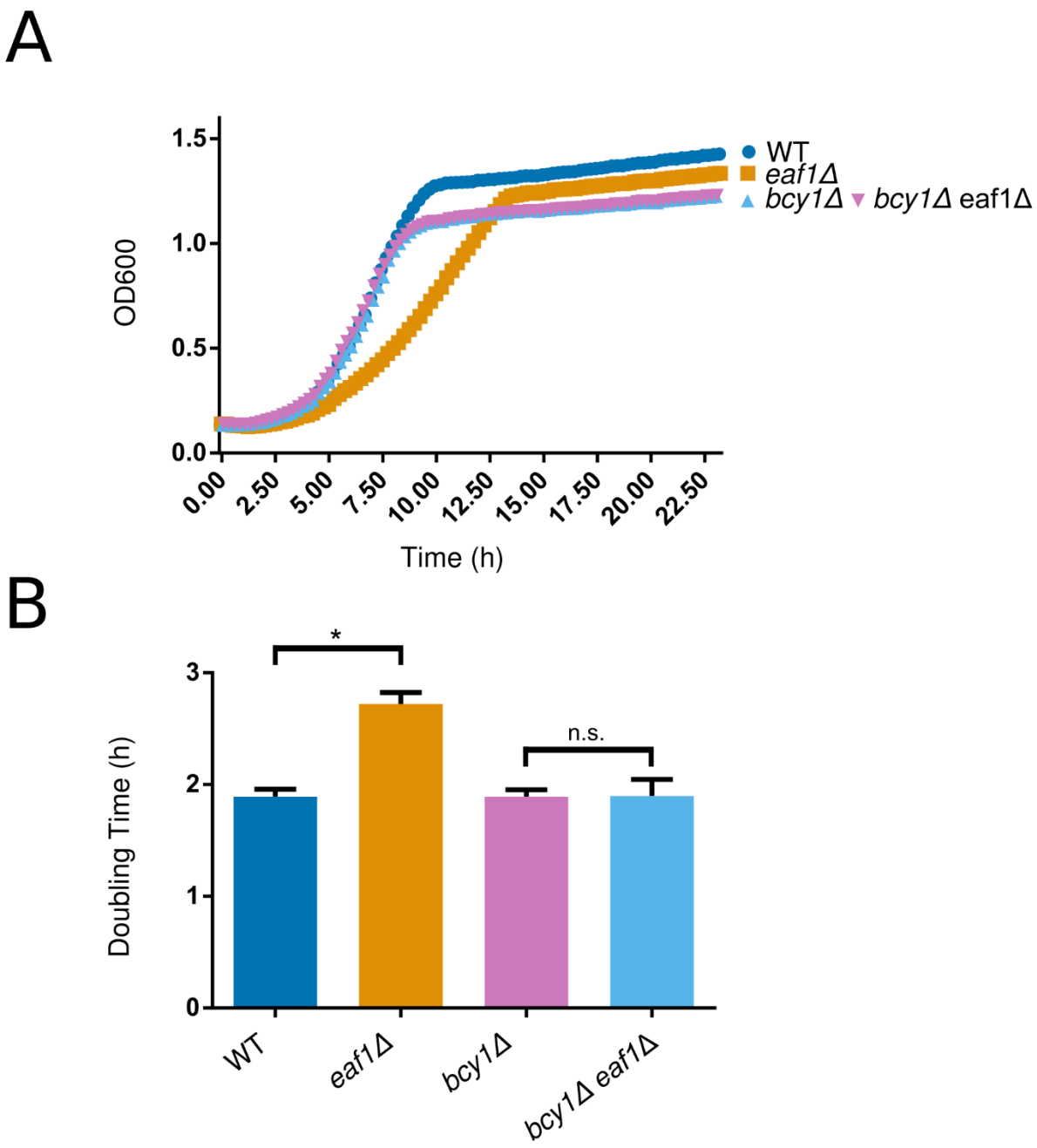

S2.5 Fig. *eaf1Δ* strains have a growth defect which is reversed upon deletion of *BCY1*. (A) Growth curves were produced by measuring OD600 over 24 hours for each of the strains using a BioScreen C plate reader. Three biological replicates were performed of which one representative set is shown here. (B) Doubling time, the number of hours it takes for the yeast culture to double, was calculated using average slope of the log OD growth curve between 3 and 7.5 hours for three biological replicates**.** ANOVA analysis was performed with a Tukey's multiple comparison test comparing pairs of means. *= $p < 0.05$, n.s. = non-significant, relevant significance bars shown.

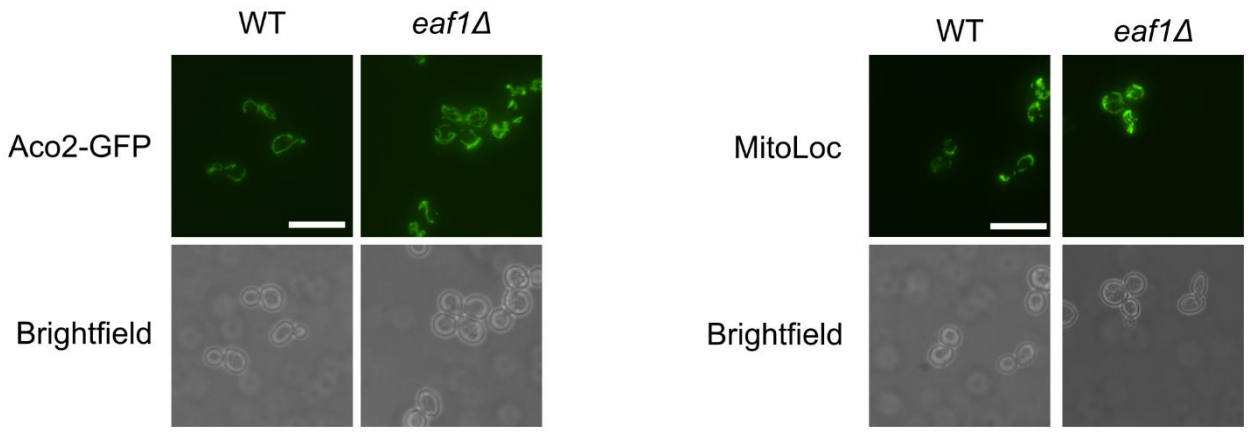

S2.6 Fig. Mitochondrial structure of WT and *eaf1*Δ assessed using Aco2-GFP and MitoLoc**.** Yeast with integrated Aco2-GFP and yeast that contained the MitoLoc Plasmid [186] were prepared to mid-log in YPD for microscopy. Mitochondrial structure was assessed in WT and *eaf1*Δ backgrounds with Aco2-GFP or MitoLoc. Scale bar =10 μm.

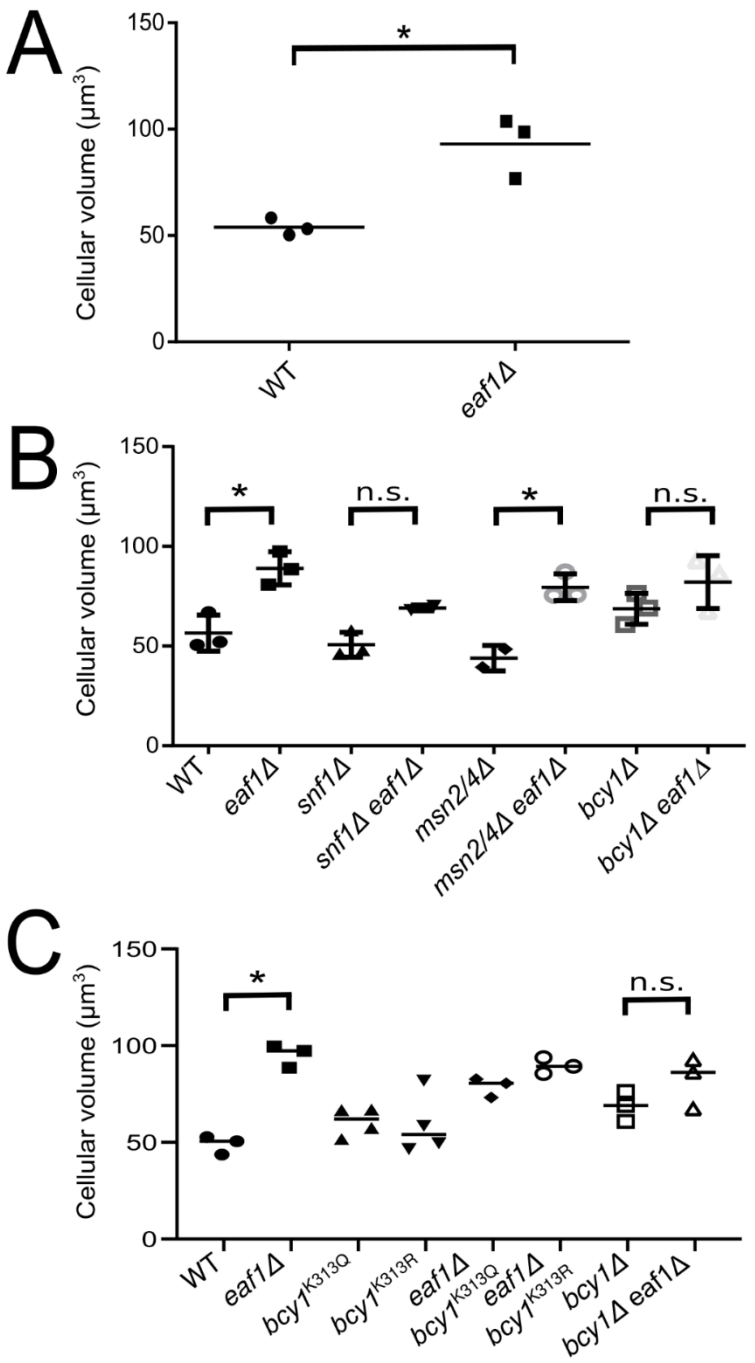

S2.7 Fig. Deletion of *EAF1* affect the size of the cell, measurements of cell size. Cell volume was approximated by taking 2 measurements of cell diameter using ImageJ on scale images, averaging them, and using half that diameter in the $4/3\pi r^3$ formula. This approximates cell volume based on a sphere of the yeast's average diameter. (A) Measurements of cell volume for WT and *eaf1Δ* at 30°C, corresponds with Figure 2.3. (B) Measurements of cell volume for WT and targeted double mutants, corresponds with Figure 2.5. (C) Measurements of cell volume for WT and *bcy1* CRISPR-Cas9 mutants, corresponds with Figure 2.7.

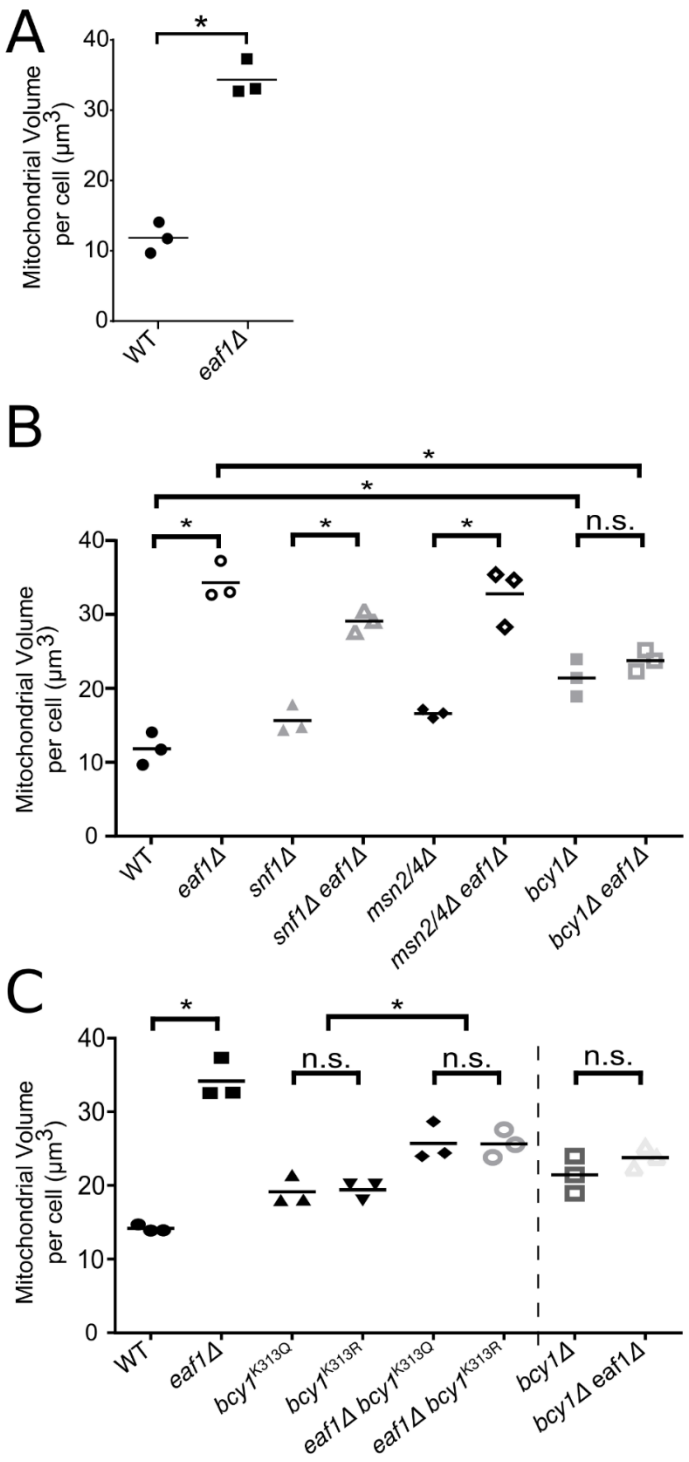

S2.8 Fig. Raw mitochondrial volume measurements. The raw mitochondrial volume of the mitochondria was quantified based on the Cit1-GFP fluorescence and using the MitoMap plugin for ImageJ for 3 biological replicates and at least 50 cells per replicate were analyzed [64]. (A) Raw measurements of mitochondrial volume per cell (μm^3) for WT and *eaf1Δ* at 30°C, corresponds with Figure 2.3. (B) Raw measurements of mitochondrial volume per cell (μm^3) for WT and targeted double mutants, corresponds with Figure 2.5. (C) Raw measurements of mitochondrial volume per cell (μm^3) for WT and *bcy1* CRISPR mutants, corresponds with Figure 2.7.

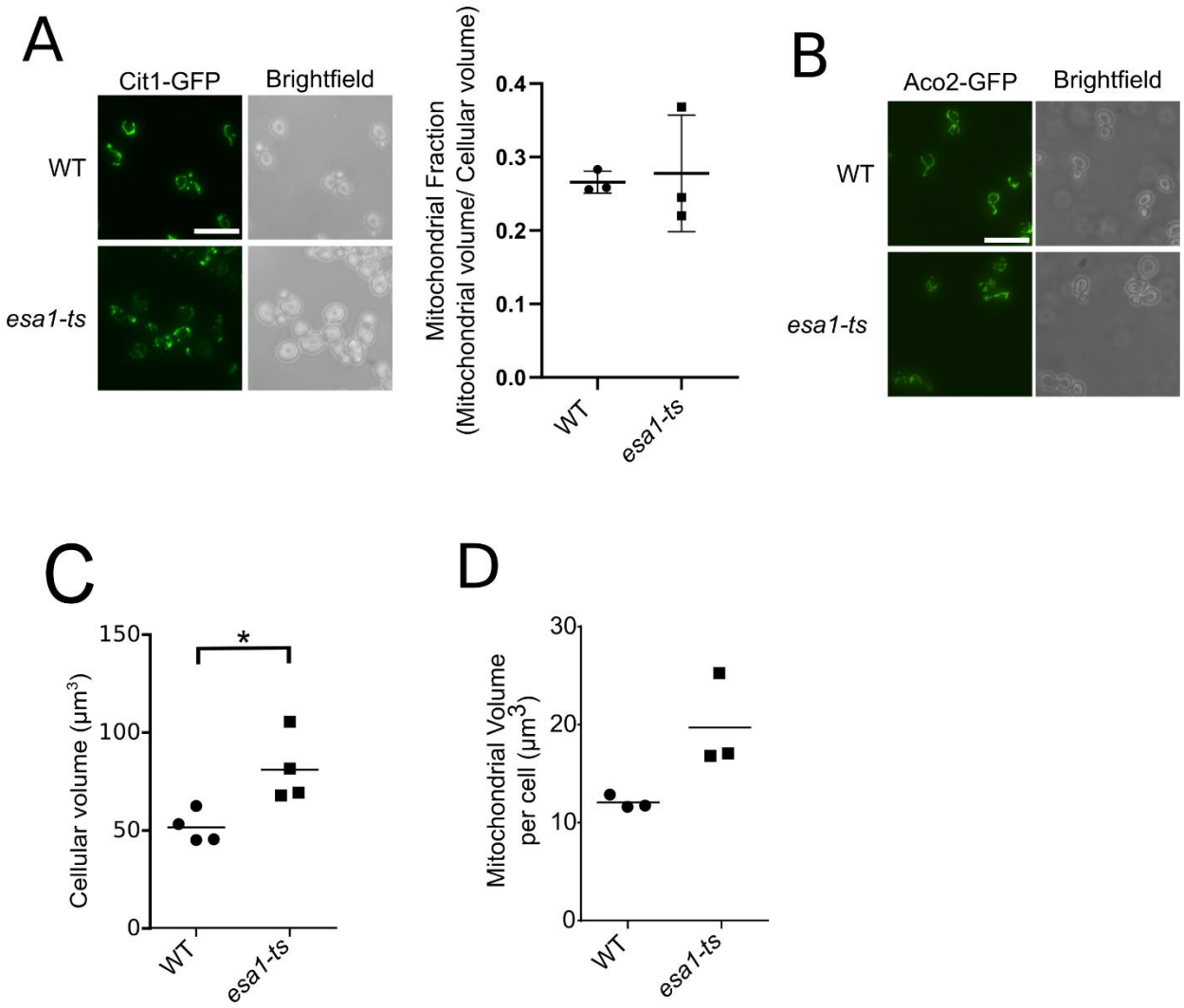

S2.9 Fig. Mitochondrial morphology of the temperature sensitive *ESA1* mutant. (A) The mitochondrial morphology of WT and the *esa1-ts* mutant was assessed after being grown to early log at 25ºC and temperature shifted to 33ºC for 2h with the mitochondrial marker Cit1-GFP. The mitochondrial fraction was quantified based on the Cit1-GFP fluorescence using the MitoMap plugin for ImageJ which was then divided by the average total cellular volume of the strain for 3 independent biological replicates. Images are representative of 3 independent biological replicates and at least 50 cells per replicate were analyzed per replicate for quantification. Scale bar = 10 μm. An unpaired T-test was used to compare groups. (B) WT and *esa1-ts* yeast were grown overnight and in day cultures at 25ºC before being transitioned to the restrictive temperature of 33ºC for 2h. Mitochondrial structure was assessed using Aco2-GFP. (C) Cell volume measurements of temperature shifted WT and *esa1-ts.* Cell volume was approximated by taking 2 measurements of cell diameter using ImageJ on scale images, averaging them, and using half that diameter in the $4/3\pi r^3$ formula. This approximates cell volume based on a sphere of the yeast's average diameter. (D) Raw measurements of mitochondrial volume per cell (μm^3) for WT and *esa1-ts.*

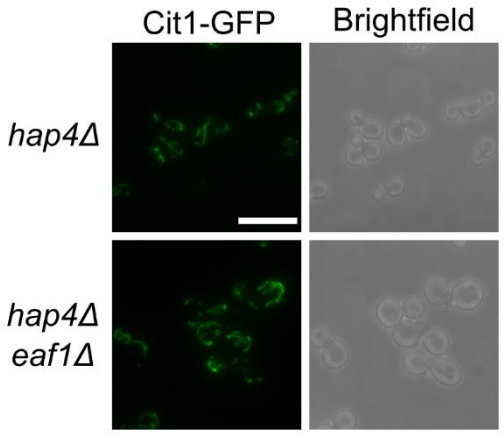

S2.10 Fig. Deletion of *HAP4*, a transcription factor involved in mitochondrial biogenesis, does not reverse the elongation of the mitochondria seen in an *eaf1Δ*. Cit1-GFP was used as a marker of the mitochondrial structure in *hap4*Δ and *eaf1Δ hap4Δ* mutants.

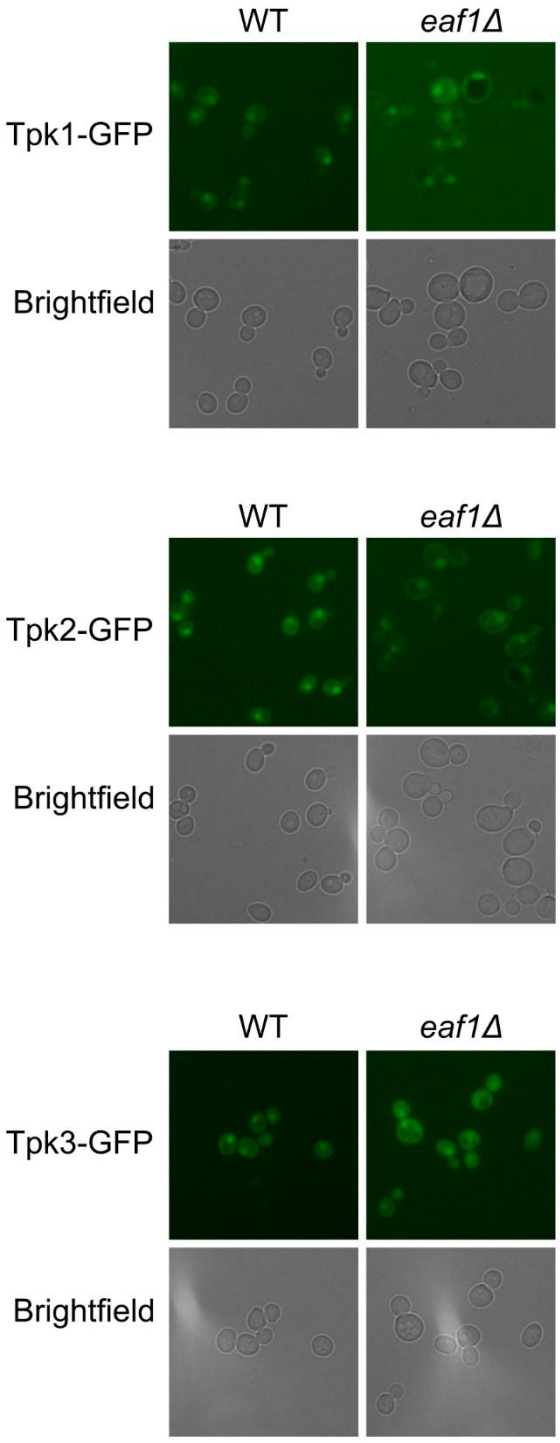

S2.11 Fig. TPK protein localization does not change between the WT and *eaf1Δ*.

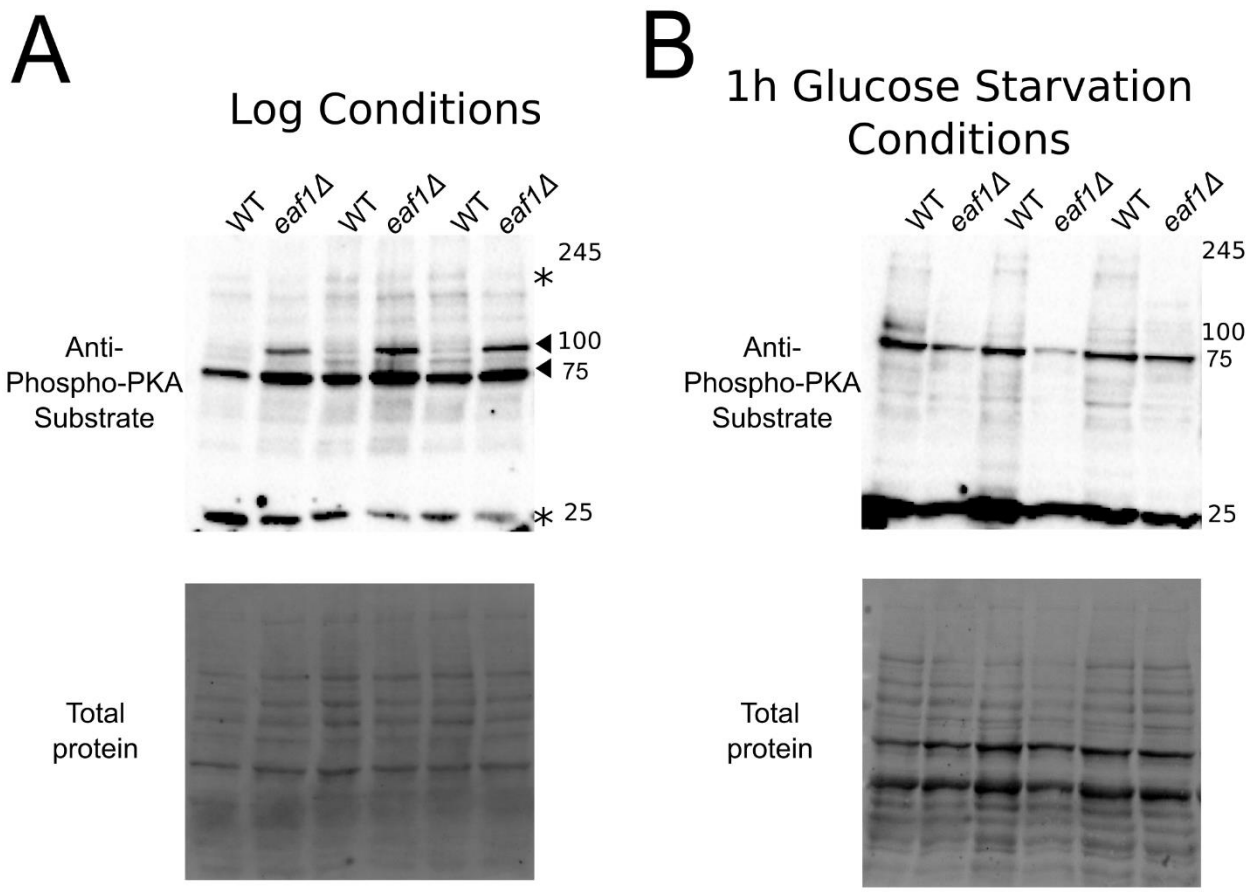

S2.12 Fig. Three replicate western blots showing PKA activity is altered in an *eaf1Δ.* Representative and quantification shown in Figure 2.9. PKA substrate phosphorylation under (A) log growth in glucose rich conditions and (B) Glucose starved conditions was assessed by quantitative western blot analysis using whole cell extracts from WT and *eaf1Δ* strains.

S2.3 Table. List of yeast strains used in this work.

Strain (YKB#)	Genotype	Reference (Where it came from)
YKB1079/BY4741	***MATa*** *his3Δ1 leu2Δ0 met15Δ0 ura3Δ0*	[1]
YKB3333	***MATa*** *his3Δ1 leu2Δ0 met15Δ0 ura3Δ0 eaf1Δ::KAN*	[2]
YKB4803	***MATa*** *his3Δ1 leu2Δ0 met15Δ0 ura3Δ0 eaf1Δ::HYG*	This Study
YKB4586	***MATa*** *esa1Δ::HIS3 esa1ts::URA3 his3Δ1 leu2Δ0 met15Δ0 ura3Δ0*	[3]
YKB4765 YKB4766	***MATa*** *his3Δ1 leu2Δ0 met15Δ0 ura3Δ0 CIT1-GFP::NAT*	This Study
YKB4774 YKB4775	***MATa*** *his3Δ1 leu2Δ0 met15Δ0 ura3Δ0 eaf1Δ::KAN CIT1-GFP::NAT*	This Study
YKB4781 YKB4782	***MATa*** *esa1Δ::HIS3 esa1ts::URA3 CIT1-GFP::NAT his3Δ1 leu2Δ0 met15Δ0 ura3Δ0*	This Study
YKB4814	***MATa*** *his3Δ1 leu2Δ0 met15Δ0 ura3Δ0 bcy1Δ::KAN*	This Study
YKB4871	***MATa*** *his3Δ1 leu2Δ0 met15Δ0 ura3Δ0 bcy1Δ::KAN eaf1Δ::HYG*	This Study
YKB4159	***MATa*** *his3Δ1 leu2Δ0 met15Δ0 ura3Δ0 msn2Δ::HIS msn4Δ::KAN*	This Study
YKB4802	***MATa*** *his3Δ1 leu2Δ0 met15Δ0 ura3Δ0 msn2Δ::HIS msn4Δ::KAN eaf1Δ::HYG*	This Study
YKB3389	***MATa*** *his3Δ1 leu2Δ0 met15Δ0 ura3Δ0 snf1Δ::KAN*	[2]
YKB4801	***MATa*** *his3Δ1 leu2Δ0 met15Δ0 ura3Δ0 snf1Δ::KAN eaf1Δ::HYG*	This Study
YKB4855	***MATa*** *his3Δ1 leu2Δ0 met15Δ0 ura3Δ0 BCY1-GFP::HIS*	[4]
YKB4856	***MATa*** *his3Δ1 leu2Δ0 met15Δ0 ura3Δ0 BCY1-GFP::HIS eaf1Δ::HYG*	This Study
YKB4805	***MATa*** *his3Δ1 leu2Δ0 met15Δ0 ura3Δ0 msn2Δ::HIS msn4Δ::KAN CIT1-GFP::NAT*	This Study
YKB4806	***MATa*** *his3Δ1 leu2Δ0 met15Δ0 ura3Δ0 msn2Δ::HIS msn4Δ::KAN eaf1Δ::HYG CIT1-GFP::NAT*	This Study
YKB4826	***MATa*** *his3Δ1 leu2Δ0 met15Δ0 ura3Δ0 bcy1Δ::KAN CIT1-GFP::NAT*	This Study
YKB4857	***MATa*** *his3Δ1 leu2Δ0 met15Δ0 ura3Δ0 bcy1Δ::KAN eaf1Δ::HYG CIT1-GFP::NAT*	This Study
YKB4812	***MATa*** *his3Δ1 leu2Δ0 met15Δ0 ura3Δ0 snf1Δ::KAN CIT1-GFP::NAT*	This Study
YKB4813	***MATa*** *his3Δ1 leu2Δ0 met15Δ0 ura3Δ0 snf1Δ::KAN CIT1-GFP::NAT eaf1Δ::HYG*	This Study
YKB4503	***MATa*** *his3Δ1 leu2Δ0 met15Δ0 ura3Δ0 GSY2-GFP::HIS*	[4]
YKB4541	***MATa*** *his3Δ1 leu2Δ0 met15Δ0 ura3Δ0 GSY2-GFP::HIS eaf1Δ::NAT*	This Study
YKB4505	***MATa*** *his3Δ1 leu2Δ0 met15Δ0 ura3Δ0 GΔB1-GFP::HIS*	[4]
YKB4542	***MATa*** *his3Δ1 leu2Δ0 met15Δ0 ura3Δ0 GΔB1-GFP::HIS eaf1Δ::NAT*	This Study
YKB4315	***MATα*** *eaf1Δ::NAT CAN1pr:RPL39pr-tdTomato::CaURA3::can1Δ::STE2pr-LEU2 ura3Δ0 his3Δ1 leu2Δ0 met15Δ0*	This Study derived from Brenda Andrews Group [5]

YKB4324	***MATα*** *ura3Δ::NAT CAN1pr:RPL39pr-tdTomato::CaURA3::can1Δ::STE2pr-LEU2 ura3Δ0 his3Δ1 leu2Δ0 met15Δ0*	This Study derived from Brenda Andrews Group [5]
YKB4497	***MATa*** *ura3Δ::NAT CAN1pr::RPL39pr-tdTomato:: CaURA3::can1Δ::STE2pr-LEU2 ura3Δ0 his3Δ1 leu2Δ0 met15Δ0ade2-101 Gsy2-GFP::HIS*	This Study
YKB4498	***MATa*** *eaf1Δ::NAT CAN1pr::RPL39pr-tdTomato:: CaURA3::can1Δ::STE2pr-LEU2 ura3Δ0 his3Δ1 leu2Δ0 met15Δ0ade2-101 Gsy2-GFP::HIS*	This Study
YKB4500	***MATa*** *ura3Δ::NAT CAN1pr::RPL39pr-tdTomato:: CaURA3::can1Δ::STE2pr-LEU2 ura3Δ0 his3Δ1 leu2Δ0 met15Δ0ade2-101 Gsy1-GFP::HIS*	This Study
YKB4501	***MATa*** *eaf1Δ::NAT CAN1pr::RPL39pr-tdTomato:: CaURA3::can1Δ::STE2pr-LEU2 ura3Δ0 his3Δ1 leu2Δ0 met15Δ0ade2-101 Gsy1-GFP::HIS*	This Study
YKB4520	***MATa*** *ura3Δ::NAT CAN1pr::RPL39pr-tdTomato:: CaURA3::can1Δ::STE2pr-LEU2 ura3Δ0 his3Δ1 leu2Δ0 met15Δ0ade2-101 Gdb1-GFP::HIS*	This Study
YKB4521	***MATa*** *eaf1Δ::NAT CAN1pr::RPL39pr-tdTomato:: CaURA3::can1Δ::STE2pr-LEU2 ura3Δ0 his3Δ1 leu2Δ0 met15Δ0ade2-101 Gdb1-GFP::HIS*	This Study
YKB5023	***MATa*** *his3Δ1 leu2Δ0 met15Δ0 ura3Δ0 Gsy2-GFP::NAT*	This Study
YKB5024	***MATa*** *his3Δ1 leu2Δ0 met15Δ0 ura3Δ0 eaf1Δ::HYG Gsy2-GFP::NAT*	This Study
YKB5025	***MATa*** *his3Δ1 leu2Δ0 met15Δ0 ura3Δ0 bcy1Δ::KAN Gsy2-GFP::NAT*	This Study
YKB5026	***MATa*** *his3Δ1 leu2Δ0 met15Δ0 ura3Δ0 bcy1Δ::KAN eaf1Δ::HYG Gsy2-GFP::NAT*	This Study
YKB5027	***MATa*** *his3Δ1 leu2Δ0 met15Δ0 ura3Δ0 msn2Δ::HIS msn4Δ::KAN Gsy2-GFP::NAT*	This Study
YKB5028	***MATa*** *his3Δ1 leu2Δ0 met15Δ0 ura3Δ0 msn2Δ::HIS msn4Δ::KAN eaf1Δ::HYG Gsy2-GFP::NAT*	This Study
YKB4767	***MATa*** *his3Δ1 leu2Δ0 met15Δ0 ura3Δ0 ACO2-GFP::NAT*	This Study
YKB4773	***MATa*** *his3Δ1 leu2Δ0 met15Δ0 ura3Δ0 ACO2-GFP::NAT eaf1Δ::KAN*	This Study
YKB5032	***MATa*** *his3Δ1 leu2Δ0 met15Δ0 ura3Δ0 BCY1-GFP::HIS Bcy1 K313Q*	This Study
YKB5031	***MATa*** *his3Δ1 leu2Δ0 met15Δ0 ura3Δ0 BCY1-GFP::HIS Bcy1 K313R*	This Study
YKB5034	***MATa*** *his3Δ1 leu2Δ0 met15Δ0 ura3Δ0 BCY1-GFP::HIS eaf1Δ::HYG Bcy1 K313Q*	This Study
YKB5033	***MATa*** *his3Δ1 leu2Δ0 met15Δ0 ura3Δ0 BCY1-GFP::HIS eaf1Δ::HYG Bcy1 K313R*	This Study
YKB5030	***MATa*** *his3Δ1 leu2Δ0 met15Δ0 ura3Δ0 CIT1-GFP::NAT Bcy1 K313Q*	This Study
YKB5029	***MATa*** *his3Δ1 leu2Δ0 met15Δ0 ura3Δ0 CIT1-GFP::NAT Bcy1 K313R*	This Study
YKB5037	***MATa*** *his3Δ1 leu2Δ0 met15Δ0 ura3Δ0 eaf1Δ::KAN CIT1-GFP::NAT Bcy1 K313Q*	This Study
YKB5038	***MATa*** *his3Δ1 leu2Δ0 met15Δ0 ura3Δ0 eaf1Δ::KAN CIT1-GFP::NAT Bcy1 K313R*	This Study

S2.4 Table. List of primers used in this work.

Name	OKB REF #	Sequence
TDH3-RT-FW	1329	CTGTCAAGTTGAACAAGGAAACCAC
TDH3-RT-RV	1330	CAACGTGTTCAACCAAGTCGACAA
Gsy2-RT-F3	2256	ACGGTTGCCCAGTATAAAGACC
Gsy2-RT-R3	2257	CACCTTCAATCAGCCACCTC
dsDNA Bcy1K 313R PAM9 FW	2570	TGAAGAGCATGCCAGTTTTGAAGAGTTTGACTACGTACGAtCGTGCCAgACTTGCCG ATGCACTGGATACCAAGATCTACCAGCCGGGTG
dsDNA Bcy1K 313R PAM9 RV	2571	CACCCGGCTGGTAGATCTTGGTATCCAGTGCATCGGCAAGTcTGGCACGaTCGTACG TAGTCAAACTCTTCAAAACTGGCATGCTCTTCA
dsDNA Bcy1K 313Q PAM9 FW	2572	TGAAGAGCATGCCAGTTTTGAAGAGTTTGACTACGTACGAtCGTGCCcAACTTGCCG ATGCACTGGATACCAAGATCTACCAGCCGGGTG
dsDNA Bcy1K 313Q PAM9 RV	2573	CACCCGGCTGGTAGATCTTGGTATCCAGTGCATCGGCAAGTTgGGCACGaTCGTACG TAGTCAAACTCTTCAAAACTGGCATGCTCTTCA
Bcy1 K313 confirmation RV	2574	CCAGTAAACGTTGAAAACCAC
Bcy1 K313 confirmation FW	2575	CTACGTCAACGACAACAAGG
Bcy1 Pam9 gRNA FW	2638	GTGCATCGGCAAGTTTGGCAgTTTTAGAGCTAGAAATAGCAAGTTAAAATAAGGCTA G
Bcy1 Pam9 gRNA RV	2639	TGCCAAACTTGCCGATGCACgatcatttatctttcactgcggagaagtttcgaacgcc
Pam9 gRNA confirm	2640	TGCCAAACTTGCCGATGCAC
Bcy1	2641	GATCTTGGTATCCAGTGCATgTTTTAGAGCTAGAAATAGCAAGTTAAAATAAGGCTA

Pam6 gRNA FW		GTC
Bcy1 Pam6 gRNA RV	2642	ATGCACTGGATACCAAGATCgatcatttatctttcactgcggagaagtttcgaacgccgaaac
dsDNA Bcy1K 313R PAM6 FW	2643	TGAAGAGCATGCCAGTTTTGAAGAGTTTGACTACGTACGACCGTGCCAgACTTGCaG ATGCACTGGATACCAAGATCTACCAGCCGGGTG
dsDNA Bcy1K 313R PAM6 RV	2644	CACCCGGCTGGTAGATCTTGGTATCCAGTGCATCtGCAAGTcTGGCACGGTCGTACGT AGTCAAACTCTTCAAAACTGGCATGCTCTTCA
dsDNA Bcy1K 313Q PAM6 FW	2645	TGAAGAGCATGCCAGTTTTGAAGAGTTTGACTACGTACGACCGTGCCcAACTTGCaG ATGCACTGGATACCAAGATCTACCAGCCGGGTG
dsDNA Bcy1K 313Q PAM6 RV	2646	CACCCGGCTGGTAGATCTTGGTATCCAGTGCATCtGCAAGTTgGGCACGGTCGTACGT AGTCAAACTCTTCAAAACTGGCATGCTCTTCA
PAM6 gRNA confirm ation	2647	ATGCACTGGATACCAAGATC

Manuscript 2 Supplements:

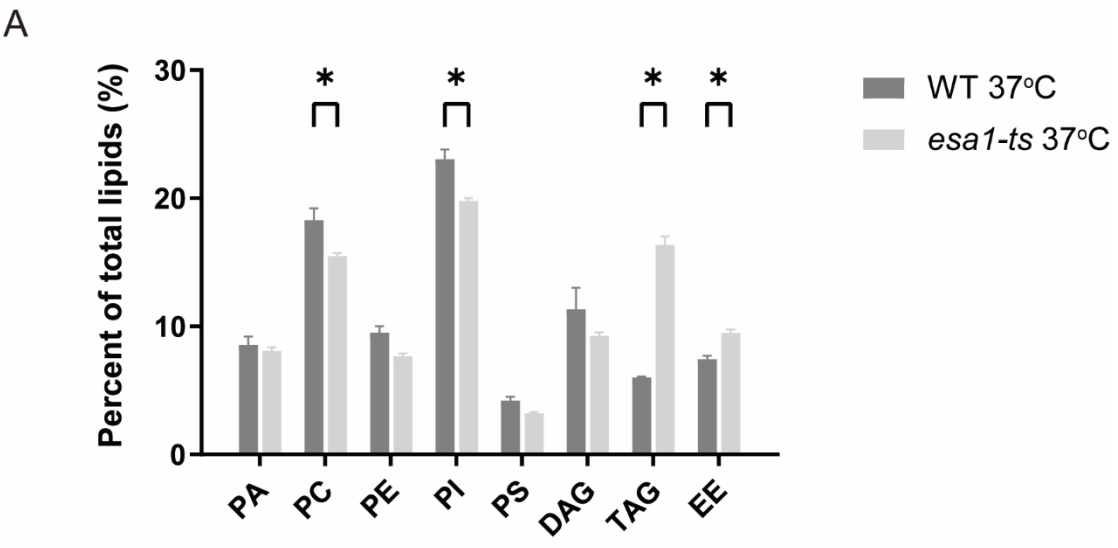

S3.1 Fig: Lipidomic analysis of WT and *esa1-ts* yeast cells. The lipid composition of WT and *esa1-ts* yeast was assessed through lipidomics. WT and *esa1-ts* yeast cells were grown to early log phase before shifting to 37^{o}C for 2 hours. Cells were harvested and a crude lysate was created through bead beating with water, lipids were then extracted using a chloroform/methanol procedure and Mass spec analysis was performed by Lipotype GmbH. In this figure are the most prevalent lipids identified: Phosphatidic acid (PA), Phosphatidylcholine (PC), Phosphatidylethanolamine (PE), Phosphatidylinositol (PI), Phosphatidylserine (PS), Diacylglycerol (DAG), Ergosteryl ester (EE), and Triacylglycerol (TAG). The composition of lipid classes broken down as a percent of the total lipids. A 2-way ANOVA analysis with a Tukey's multiple comparisons test was performed and a * represents an adjusted $p < 0.05$.

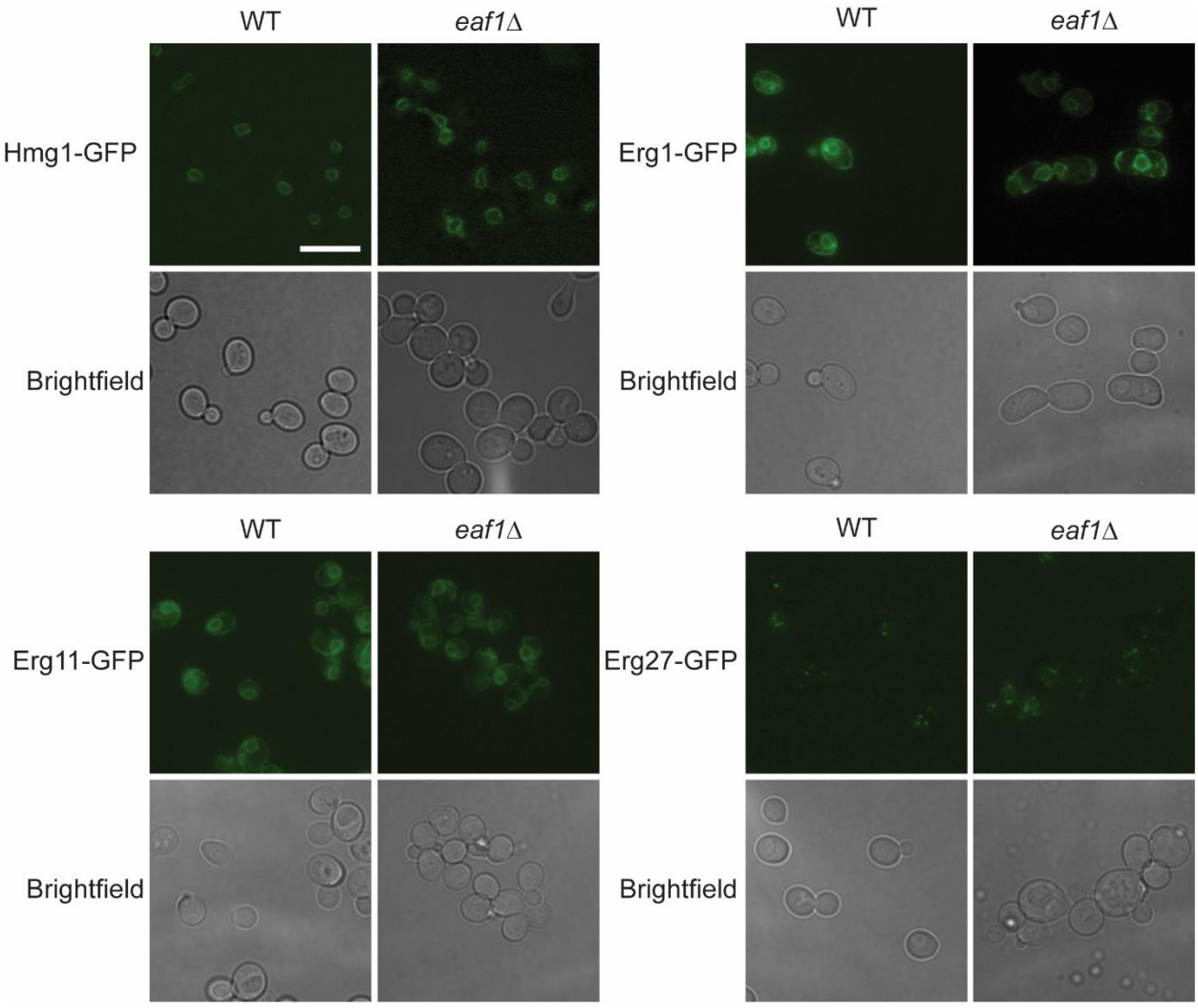

S3.2 Fig: NuA4 dependent regulation of ergosterol is independent of ergosterol biosynthesis protein localization or abundance and Acc1 activity. The localization and abundance of members of the ergosterol biosynthesis pathway was assessed by comparing GFP tagged proteins in the WT and *eaf1Δ* background. Images were taken in mid-log growth in YPD media. Figures are representative of n=3. Scale bar = 10 μm.

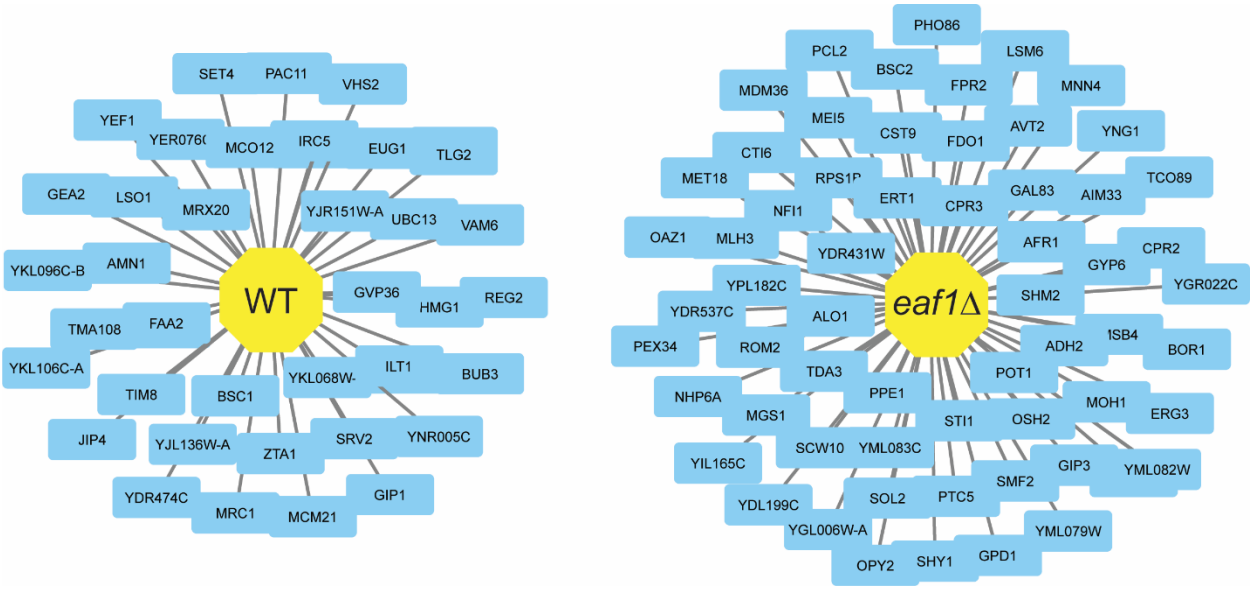

S3.3 Fig: A screen of the deletion mutant array in the WT or *eaf1Δ* background was performed on YPD with and without amphotericin B was performed. Venn diagram style network map showing all hits that were above a threshold of 0.6 for the WT and *eaf1Δ* collections. The WT collection has only a small growth impairment on Amphotericin B while the *eaf1Δ* collection only has a few strains that are able to grow. This resulted in more hits for the AT and no common hits between the two screens. Gene names are also available in S3.2 Table.

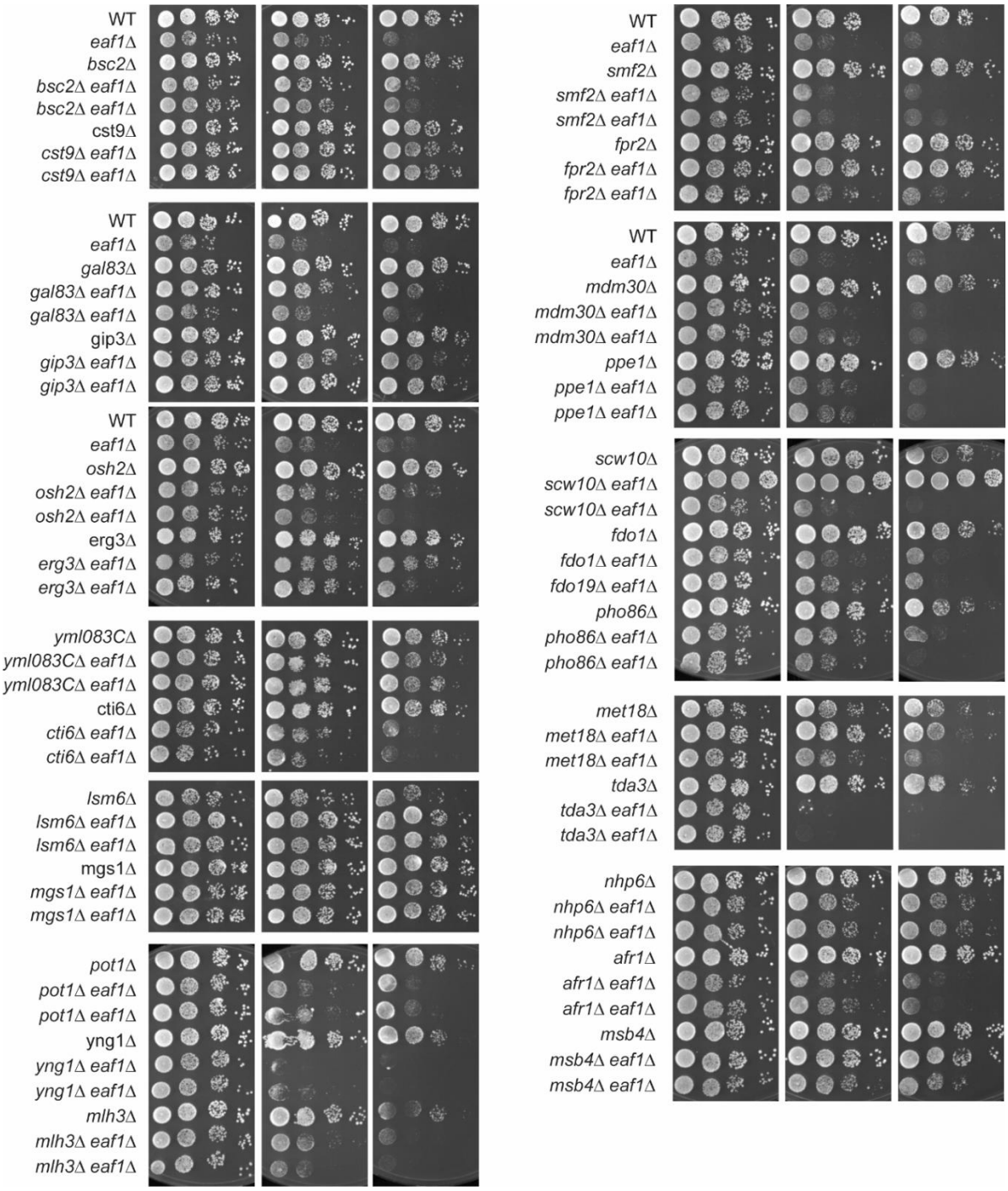

S3.4 Fig: Dot assays of 25 selected tops hits from the screen. Following our initial screen, we followed up with 25 of the top hits of interest by performing dot assays to get a clearer measurement of growth on amphotericin B. The growth of the double mutant was compared to the growth of the single DMA mutant and the *eaf1Δ* as well as to the WT BY4741 strain. These hits were additionally confirmed by PCR analysis of both deletions in the genomic DNA. Yeast were grown to mid log in liquid YPD before being spotted onto solid YPD with or without a series of ergosterol targeting compounds. The strains were spotted in serial dilutions beginning at 0.1 and three 10-fold dilutions from there onto the plates. These spots were then allowed to grow for 48 h and images were taken.

S3.1 Table. List of yeast strains used in this work.

Short Name	Genotype	YKB REF #
WT	***MATa*** *his3Δ1 leu2Δ0 met15Δ0 ura3Δ0*	1079
eaf1Δ: KAN	***MATa*** *his3Δ1 leu2Δ0 met15Δ0 ura3Δ0 eaf1Δ::KAN*	3333
eaf1Δ: HYG	***MATa*** *his3Δ1 leu2Δ0 met15Δ0 ura3Δ0 eaf1Δ::HYG*	4803
erg3Δ	***MATa*** *his3Δ1 leu2Δ0 met15Δ0 ura3Δ0 erg3Δ::KAN*	4875
erg3Δ eaf1Δ	***MATa*** *his3Δ1 leu2Δ0 met15Δ0 ura3Δ0 erg3Δ::KAN eaf1Δ::HYG*	5213
Faa4-GFP	***MATa*** *his3Δ1 leu2Δ0 met15Δ0 ura3Δ0 FAA4-GFP::HIS*	4453
Faa4-GFP *eaf1Δ*	***MATa*** *his3Δ1 leu2Δ0 met15Δ0 ura3Δ0 FAA4-GFP::HIS eaf1Δ::HYG*	4997
esa1-TS	***MATa*** *esa1Δ::HIS3 esa1ts::URA3 his3Δ1 leu2Δ0 met15Δ0 ura3Δ0*	4586
eaf1Δ: *NAT* Query Strain	**MATα** *can1Δ::STE2pr-SP-his5 lyp1Δ his3Δ1 leu2Δ0 ura3Δ0 met15D0 LYS2+ eaf1Δ::NAT*	4887
Erg8-GFP	***MATa*** *his3Δ1 leu2Δ0 met15Δ0 ura3Δ0 ERG8-GFP::HIS*	4950
Erg1-GFP	***MATa*** *his3Δ1 leu2Δ0 met15Δ0 ura3Δ0 ERG1-GFP::HIS*	4949
erg11-GFP	***MATa*** *his3Δ1 leu2Δ0 met15Δ0 ura3Δ0 ERG11-GFP::HIS*	5084
Erg6-GFP	***MATa*** *his3Δ1 leu2Δ0 met15Δ0 ura3Δ0 ERG6-GFP::HIS*	4952
Erg3-GFP	***MATa*** *his3Δ1 leu2Δ0 met15Δ0 ura3Δ0 ERG3-GFP::HIS*	5087
Hmg1-GFP	***MATa*** *his3Δ1 leu2Δ0 met15Δ0 ura3Δ0 HMG1-GFP::HIS*	4947
Hmg2-GFP	***MATa*** *his3Δ1 leu2Δ0 met15Δ0 ura3Δ0 HMG2-GFP::HIS*	4948
Erg19-GFP	***MATa*** *his3Δ1 leu2Δ0 met15Δ0 ura3Δ0 ERG19-GFP::HIS*	5098
Erg5-GFP	***MATa*** *his3Δ1 leu2Δ0 met15Δ0 ura3Δ0 ERG5-GFP::HIS*	5089
Erg4-GFP	***MATa*** *his3Δ1 leu2Δ0 met15Δ0 ura3Δ0 ERG4-GFP::HIS*	5088
Erg27-GFP	***MATa*** *his3Δ1 leu2Δ0 met15Δ0 ura3Δ0 ERG27-GFP::HIS*	5086
Erg26-GFP	***MATa*** *his3Δ1 leu2Δ0 met15Δ0 ura3Δ0 ERG26-GFP::HIS*	5085
Erg7-GFP	***MATa*** *his3Δ1 leu2Δ0 met15Δ0 ura3Δ0 ERG7-GFP::HIS*	5083
Erg9-GFP	***MATa*** *his3Δ1 leu2Δ0 met15Δ0 ura3Δ0 ERG9-GFP::HIS*	5082
Erg12-GFP	***MATa*** *his3Δ1 leu2Δ0 met15Δ0 ura3Δ0 ERG12-GFP::HIS*	5080
Erg10-GFP	***MATa*** *his3Δ1 leu2Δ0 met15Δ0 ura3Δ0 ERG10-GFP::HIS*	5079
Erg24-GFP	***MATa*** *his3Δ1 leu2Δ0 met15Δ0 ura3Δ0 ERG24-GFP::HIS*	4951
Erg25-GFP	***MATa*** *his3Δ1 leu2Δ0 met15Δ0 ura3Δ0 ERG25-GFP::HIS*	5114
Erg8-GFP *eaf1Δ*	***MATa*** *his3Δ1 leu2Δ0 met15Δ0 ura3Δ0 ERG8-GFP::HIS eaf1Δ::HYG*	5000
Erg1-GFP *eaf1Δ*	***MATa*** *his3Δ1 leu2Δ0 met15Δ0 ura3Δ0 ERG1-GFP::HIS eaf1Δ::HYG*	4999
Erg11-GFP *eaf1Δ*	***MATa*** *his3Δ1 leu2Δ0 met15Δ0 ura3Δ0 ERG11-GFP::HIS eaf1Δ::HYG*	4998
Erg6-GFP *eaf1Δ*	***MATa*** *his3Δ1 leu2Δ0 met15Δ0 ura3Δ0 ERG6-GFP::HIS eaf1Δ::HYG*	4996
Erg3-GFP *eaf1Δ*	***MATa*** *his3Δ1 leu2Δ0 met15Δ0 ura3Δ0 ERG3-GFP::HIS eaf1Δ::HYG*	4995
Hmg1-GFP *eaf1Δ*	***MATa*** *his3Δ1 leu2Δ0 met15Δ0 ura3Δ0 HMG1-GFP::HIS eaf1Δ::HYG*	5001
Hmg2-GFP *eaf1Δ*	***MATa*** *his3Δ1 leu2Δ0 met15Δ0 ura3Δ0 HMG2-GFP::HIS eaf1Δ::HYG*	5002
Erg27-GFP *eaf1Δ*	***MATa*** *his3Δ1 leu2Δ0 met15Δ0 ura3Δ0 ERG27-GFP::HIS eaf1Δ::HYG*	5165
Erg7-GFP *eaf1Δ*	***MATa*** *his3Δ1 leu2Δ0 met15Δ0 ura3Δ0 ERG7-GFP::HIS eaf1Δ::HYG*	5166
Erg12-GFP *eaf1Δ*	***MATa*** *his3Δ1 leu2Δ0 met15Δ0 ura3Δ0 ERG12-GFP::HIS eaf1Δ::HYG*	5167
Erg10-GFP *eaf1Δ*	***MATa*** *his3Δ1 leu2Δ0 met15Δ0 ura3Δ0 ERG10-GFP::HIS eaf1Δ::HYG*	5168
Erg24-GFP *eaf1Δ*	***MATa*** *his3Δ1 leu2Δ0 met15Δ0 ura3Δ0 ERG24-GFP::HIS eaf1Δ::HYG*	4958

Erg25-GFP *eaf1Δ*	***MATa*** *his3Δ1 leu2Δ0 met15Δ0 ura3Δ0 ERG25-GFP::HIS eaf1Δ::HYG*	5224
snf1Δ	***MATa*** *his3Δ1 leu2Δ0 met15Δ0 ura3Δ0 snf1Δ::KAN*	3389
snf1Δ eaf1Δ: NAT	***MATa*** *his3Δ1 leu2Δ0 met15Δ0 ura3Δ0 snf1Δ::KAN eaf1Δ::NAT*	3421
snf1Δ eaf1Δ: HYG	***MATa*** *his3Δ1 leu2Δ0 met15Δ0 ura3Δ0 snf1Δ::KAN eaf1Δ::HYG*	4801
fdo1Δ	***MATa*** *his3Δ1 leu2Δ0 met15Δ0 ura3Δ0 fdo1Δ::KAN*	5181
bsc2Δ	***MATa*** *his3Δ1 leu2Δ0 met15Δ0 ura3Δ0 bsc2Δ::KAN*	5182
scw10Δ	***MATa*** *his3Δ1 leu2Δ0 met15Δ0 ura3Δ0 swc10Δ::KAN*	5183
mgs1Δ	***MATa*** *his3Δ1 leu2Δ0 met15Δ0 ura3Δ0 mgs1Δ::KAN*	5184
nhp6aΔ	***MATa*** *his3Δ1 leu2Δ0 met15Δ0 ura3Δ0 nhp6aΔ::KAN*	5185
msb4Δ	***MATa*** *his3Δ1 leu2Δ0 met15Δ0 ura3Δ0 msb4Δ::KAN*	5186
ppe1Δ	***MATa*** *his3Δ1 leu2Δ0 met15Δ0 ura3Δ0 ppe1Δ::KAN*	5187
smf2Δ	***MATa*** *his3Δ1 leu2Δ0 met15Δ0 ura3Δ0 smf2Δ::KAN*	5188
afr1Δ	***MATa*** *his3Δ1 leu2Δ0 met15Δ0 ura3Δ0 afr1Δ::KAN*	5189
mdm36Δ	***MATa*** *his3Δ1 leu2Δ0 met15Δ0 ura3Δ0 mdm36Δ::KAN*	5190
ppr1Δ	***MATa*** *his3Δ1 leu2Δ0 met15Δ0 ura3Δ0 ppr1Δ::KAN*	5191
erg3Δ	***MATa*** *his3Δ1 leu2Δ0 met15Δ0 ura3Δ0 erg3Δ::KAN*	5192
yml083cΔ	***MATa*** *his3Δ1 leu2Δ0 met15Δ0 ura3Δ0 yml083cΔ::KAN*	5193
lsm6Δ	***MATa*** *his3Δ1 leu2Δ0 met15Δ0 ura3Δ0 lsm6Δ::KAN*	5194
cti6Δ	***MATa*** *his3Δ1 leu2Δ0 met15Δ0 ura3Δ0 cti6Δ::KAN*	5195
yng1Δ	***MATa*** *his3Δ1 leu2Δ0 met15Δ0 ura3Δ0 yng1Δ::KAN*	5196
mlh3Δ	***MATa*** *his3Δ1 leu2Δ0 met15Δ0 ura3Δ0 mlh3Δ::KAN*	5197
pot1Δ	***MATa*** *his3Δ1 leu2Δ0 met15Δ0 ura3Δ0 pot1Δ::KAN*	5198
met18Δ	***MATa*** *his3Δ1 leu2Δ0 met15Δ0 ura3Δ0 met18Δ::KAN*	5199
pho86Δ	***MATa*** *his3Δ1 leu2Δ0 met15Δ0 ura3Δ0 pho86Δ::KAN*	5200
tda3Δ	***MATa*** *his3Δ1 leu2Δ0 met15Δ0 ura3Δ0 tda3Δ::KAN*	5201
fdo1Δ eaf1Δ	***MATa*** *his3Δ1 leu2Δ0 met15Δ0 ura3Δ0 fdo1Δ::KAN eaf1Δ::HYG*	5202
bsc2Δ eaf1Δ	***MATa*** *his3Δ1 leu2Δ0 met15Δ0 ura3Δ0 bsc2Δ::KAN eaf1Δ::HYG*	5203
scw10Δ eaf1Δ	***MATa*** *his3Δ1 leu2Δ0 met15Δ0 ura3Δ0 scw10Δ::KAN eaf1Δ::HYG*	5204
mgs1Δ eaf1Δ	***MATa*** *his3Δ1 leu2Δ0 met15Δ0 ura3Δ0 mgs1Δ::KAN eaf1Δ::HYG*	5205
nhp6aΔ eaf1Δ	***MATa*** *his3Δ1 leu2Δ0 met15Δ0 ura3Δ0 nhp6aΔ::KAN eaf1Δ::HYG*	5206
msb4Δ eaf1Δ	***MATa*** *his3Δ1 leu2Δ0 met15Δ0 ura3Δ0 msb4Δ::KAN eaf1Δ::HYG*	5207
ppe1Δ eaf1Δ	***MATa*** *his3Δ1 leu2Δ0 met15Δ0 ura3Δ0 ppe1Δ::KAN eaf1Δ::HYG*	5208
smf2Δ eaf1Δ	***MATa*** *his3Δ1 leu2Δ0 met15Δ0 ura3Δ0 smf2Δ::KAN eaf1Δ::HYG*	5209
afr1Δ eaf1Δ	***MATa*** *his3Δ1 leu2Δ0 met15Δ0 ura3Δ0 afr1Δ::KAN eaf1Δ::HYG*	5210
mdm36Δ eaf1Δ	***MATa*** *his3Δ1 leu2Δ0 met15Δ0 ura3Δ0 mdm36Δ::KAN eaf1Δ::HYG*	5211
fpr1Δ eaf1Δ	***MATa*** *his3Δ1 leu2Δ0 met15Δ0 ura3Δ0 fpr1Δ::KAN eaf1Δ::HYG*	5212
erg3Δ eaf1Δ	***MATa*** *his3Δ1 leu2Δ0 met15Δ0 ura3Δ0 erg3Δ::KAN eaf1Δ::HYG*	5213
yml083cΔ eaf1Δ	***MATa*** *his3Δ1 leu2Δ0 met15Δ0 ura3Δ0 yml083cΔ::KAN eaf1Δ::HYG*	5214
lsm6Δ eaf1Δ	***MATa*** *his3Δ1 leu2Δ0 met15Δ0 ura3Δ0 lsm6Δ::KAN eaf1Δ::HYG*	5215
cti6Δ eaf1Δ	***MATa*** *his3Δ1 leu2Δ0 met15Δ0 ura3Δ0 cti6Δ::KAN eaf1Δ::HYG*	5216
yng1Δ eaf1Δ	***MATa*** *his3Δ1 leu2Δ0 met15Δ0 ura3Δ0 yng1Δ::KAN eaf1Δ::HYG*	5217

mlh3Δ eaf1Δ	***MATa*** *his3Δ1 leu2Δ0 met15Δ0 ura3Δ0 mlh3Δ::KAN eaf1Δ::HYG*	5218
pot1Δ eaf1Δ	***MATa*** *his3Δ1 leu2Δ0 met15Δ0 ura3Δ0 pot1Δ::KAN eaf1Δ::HYG*	5219
met18Δ eaf1Δ	***MATa*** *his3Δ1 leu2Δ0 met15Δ0 ura3Δ0 met18Δ::KAN eaf1Δ::HYG*	5220
pho86Δ eaf1Δ	***MATa*** *his3Δ1 leu2Δ0 met15Δ0 ura3Δ0 pho86Δ::KAN eaf1Δ::HYG*	5221
tda3Δ eaf1Δ	***MATa*** *his3Δ1 leu2Δ0 met15Δ0 ura3Δ0 tda3Δ::KAN eaf1Δ::HYG*	5222
osh2Δ	***MATa*** *his3Δ1 leu2Δ0 met15Δ0 ura3Δ0 osh2Δ::KAN*	5223
gip3Δ	***MATa*** *his3Δ1 leu2Δ0 met15Δ0 ura3Δ0 gip3Δ::KAN*	5224
gal83Δ	***MATa*** *his3Δ1 leu2Δ0 met15Δ0 ura3Δ0 gal83Δ::KAN*	5225
cst9Δ	***MATa*** *his3Δ1 leu2Δ0 met15Δ0 ura3Δ0 cst9Δ::KAN*	5226
osh2Δ eaf1Δ	***MATa*** *his3Δ1 leu2Δ0 met15Δ0 ura3Δ0 osh2Δ::KAN eaf1Δ::HYG*	5227
gip3Δ eaf1Δ	***MATa*** *his3Δ1 leu2Δ0 met15Δ0 ura3Δ0 gip3Δ::KAN eaf1Δ::HYG*	5228
gal83Δ eaf1Δ	***MATa*** *his3Δ1 leu2Δ0 met15Δ0 ura3Δ0 gal83Δ::KAN eaf1Δ::HYG*	5229
cst9Δ eaf1Δ	***MATa*** *his3Δ1 leu2Δ0 met15Δ0 ura3Δ0 cst9Δ::KAN eaf1Δ::HYG*	5230
gip3Δ eaf1Δ	***MATa*** *his3Δ1 leu2Δ0 met15Δ0 ura3Δ0 gip3Δ::KAN eaf1Δ::HYG*	5228
gal83Δ eaf1Δ	***MATa*** *his3Δ1 leu2Δ0 met15Δ0 ura3Δ0 gal83Δ::KAN eaf1Δ::HYG*	5229
cst9Δ eaf1Δ	***MATa*** *his3Δ1 leu2Δ0 met15Δ0 ura3Δ0 cst9Δ::KAN eaf1Δ::HYG*	5230

S3.2 Table. Top hits following confirmation: 25 top hits were selected for follow-up analysis by dot assay an PCR. The score for both the *eaf1Δ* and the WT screen are combined for comparison in this table. More detailed table available in supplemental of full published paper.

Gene	**Full name**	**Systematic Name**	***eaf1D* average score**	**WT average score**
NHP6A	Non-Histone Protein	YPR052C	0.8107675	0.13048
ERG3	ERGosterol biosynthesis	YLR056W	0.801025	0.148515
MET18	METhionine requiring	YIL128W	0.78444	-0.447935
LSM6	Like SM	YDR378C	0.7840325	-0.105245
MGS1	Maintenance of Genome Stability	YNL218W	0.7140125	-0.002355
FPR2	FKBP Proline Rotamase	YDR519W	0.7055425	-0.03337
CST9	Chromosome STability	YLR394W	0.7002525	0.10894
MSB4	Multicopy Suppression of a Budding defect	YOL112W	0.7001275	-0.01767
FDO1	Forkhead one interacting protein involved in DOnor preference	YMR144W	0.69224	-0.05168
GIP3	Glc7 Interacting Protein	YPL137C	0.659945	0.429555
POT1	Peroxisomal Oxoacyl Thiolase	YIL160C	0.661355	0.28212
YML083C		YML083C	0.7493925	0.041935
BSC2	Bypass of Stop Codon	YDR275W	0.85252	0.01652
PHO86	PHOsphate metabolism	YJL117W	0.7259075	0.01676
AFR1	Alpha-Factor Receptor regulator	YDR085C	0.682805	-0.106975
SCW10	Soluble Cell Wall protein	YMR305C	0.678795	-0.02816
OSH2	OxySterol binding protein Homolog	YDL019C	0.598645	0.03015
GAL83	GALactose metabolism	YER027C	0.634675	-0.3094
PPE1	Phosphoprotein Phosphatase methylEsterase	YHR075C	0.768975	0.01678
MDM36	Mitochondrial Distribution and Morphology	YPR083W	0.6757425	-0.06677
MLH3	MutL Homolog	YPL164C	0.6755525	-0.053955
SMF2	Suppressor of Mitochondria import Function	YHR050W	0.6746925	-0.04414
TDA3	Topoisomerase I Damage Affected	YHR009C	0.66744	0.142695
CTI6	Cyc8-Tup1 Interacting protein	YPL181W	0.6300325	0.032475
YNG1	Yeast iNG1 homolog	YOR064C	0.5962275	0.01658

S3.3 Table. % of total lipids (plotted): This is the final n=3 data that was plotted for S3.1 Fig. More detailed table available in supplemental of full published paper.

Lipid class % of total lipids n=3						
Lipid class	**WT-37-1**	**WT-37-2**	**WT-37-3**	**esa1-ts-1**	**esa1-ts-2**	**esa1-ts-3**
PA	9.789647	7.67538	8.253641	8.028775	8.609333	7.616088
PC	16.44503	19.12893	19.31762	15.209	15.99458	15.28554
PE	8.500582	9.852614	10.16948	8.090858	7.599402	7.269273
PI	21.6362	23.16121	24.33012	19.85361	19.34177	20.13809
PS	3.641983	4.594097	4.413453	3.032951	3.15038	3.432986
DAG	14.628	10.16852	9.234632	9.271449	8.824727	9.72787
EE	7.924891	7.418054	6.976059	9.325752	9.141739	10.00898
TAG	5.886813	6.14285	6.023605	15.52354	15.90891	17.68955

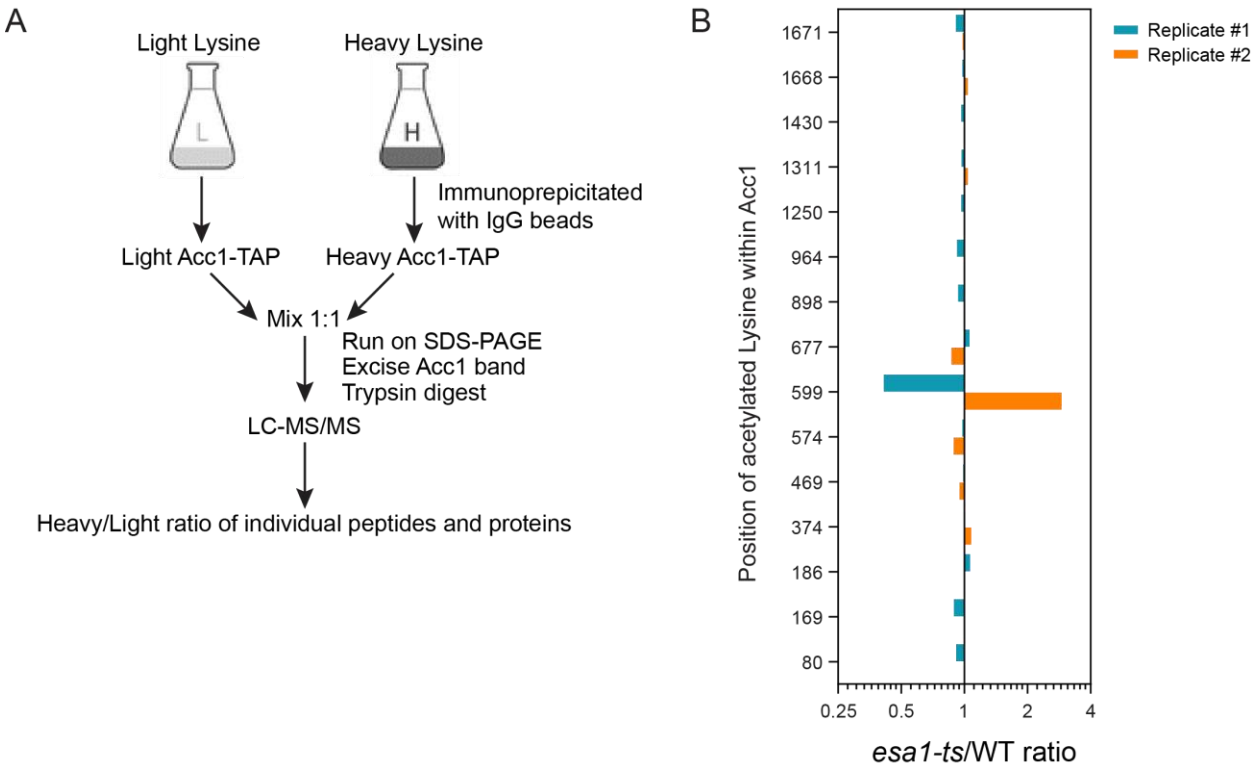

S5.1 Fig: A) Experimental design of the SILAC, a quantitative approach to identify acetylated lysine onto immunopurified Acc1-TAP. To examine potential acetylation of lysine residues, Wild-type (YKB 4305) and *esa1-ts* (YKB 4306) expressing endogenously tagged Acc1-TAP was grown separately in heavy or light labelled lysine as described in the Materials and Methods. The heavy lysine has a mass shift of +6 Da compared to the light lysine. Acc1-TAP was immunopurified prior to digestion with trypsin. Peptides were analyzed by mass spectrometry. B) Data showing the position of the acetylated lysine within Acc1-TAP. Two biological replicates were performed.

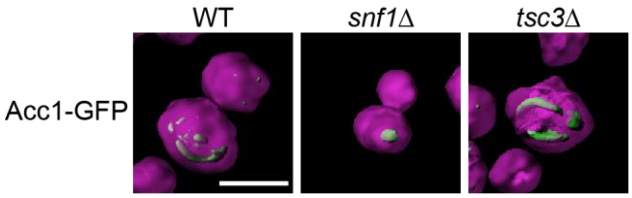

S5.2 Fig: A) Wild-type (YKB 3954), *eaf1Δ* (YKB 4448), *snf1 Δ* (YKB 4348), *tsc3 Δ* (YKB 4599) cells expressing endogenously tagged Acc1-GFP were grown to early-log phase at 30°C in YPD and immediately assessed for Acc1 localization within the cells. 3D reconstruction of the different Acc1-GFP structures being identified was built using Imaris image analysis software. Scale bar: 7µm.

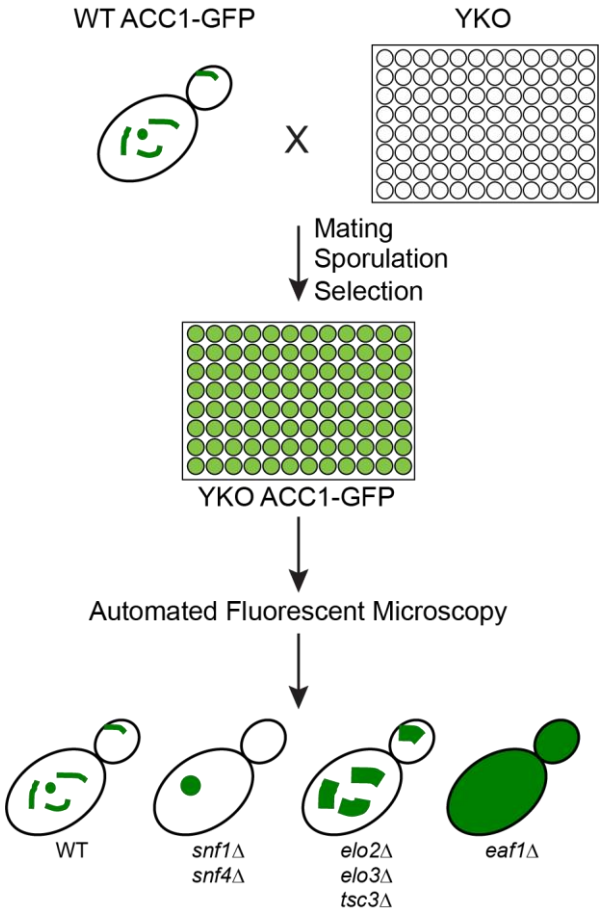

S5.3 Fig: The microscopic screen used to identify genetic deletions that affect Acc1 localization within the cells.

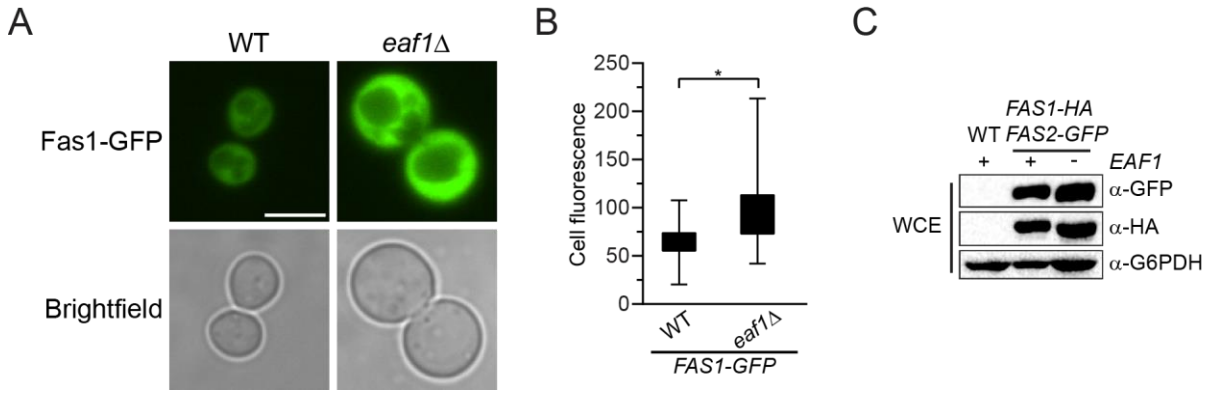

S5.4 Fig: A) Level of Fas1-GFP is increased in *eaf1Δ.* Wild-type (YKB 3983) and *eaf1Δ* (YKB 4051) cells expressing endogenously tagged Fas1-GFP were grown to early-log phase at 30°C in YPD and immediately assessed for Fas1-GFP localization within the cells. Representative brightfield and fluorescent images. Scale bar: 5 μm. B) Mean cell GFP fluorescence was measured. Three biological replicates were performed. Error bar indicates the standard error of the mean (SEM). * Denotes statistical significance at a p-value < 0.05 determined using a t-test. C) Western blot analysis of whole cell extracts looking at levels of Fas2-GFP and Fas1-HA in WT and *eaf1Δ* yeast. G6PDH is used as a loading control. Representative of n=3.

S5.1 Table: List of gene deletions selected for Acc1-GFP mini screen.

Process	Systematic name	Name
AMPK signaling	YDR216W	ADR1
AMPK signaling	YMR280C	CAT8
AMPK signaling	YER027C	GAL83
AMPK signaling	YGL035C	MIG1
AMPK signaling	YDR028C	REG1
AMPK signaling	YER129W	SAK1
AMPK signaling	YDR422C	SIP1
AMPK signaling	YGL208W	SIP2
AMPK signaling	YDL047W	SIT4
AMPK signaling	YDR477W	SNF1
AMPK signaling	YGL115W	SNF4
Citrate metabolism	YNR001C	CIT1
Citrate metabolism	YCR005C	CIT2
Citrate metabolism	YPR001W	CIT3
Citrate metabolism	YBR291C	CTP1
Citrate metabolism	YOL067C	RTG1
Citrate metabolism	YGL252C	RTG2
Fatty acid oxidation	YML042W	CAT2
Fatty acid oxidation	YKR009C	FOX2
Fatty acid oxidation	YGL205W	POX1
Fatty acid oxidation	YPL147W	PXA1
Fatty acid oxidation	YKL188C	PXA2
Glucose signaling and metabolism	YFR019W	FAB1
Glucose signaling and metabolism	YLR081W	GAL2
Glucose signaling and metabolism	YCL040W	GLK1
Glucose signaling and metabolism	YER020W	GPA2
Glucose signaling and metabolism	YOR371C	GPB1
Glucose signaling and metabolism	YAL056W	GPB2
Glucose signaling and metabolism	YDL035C	GPR1
Glucose signaling and metabolism	YJR090C	GRR1
Glucose signaling and metabolism	YFR053C	HXK1
Glucose signaling and metabolism	YGL253W	HXK2
Glucose signaling and metabolism	YHR094C	HXT1
Glucose signaling and metabolism	YFL011W	HXT10
Glucose signaling and metabolism	YIL170W	HXT12
Glucose signaling and metabolism	YMR011W	HXT2
Glucose signaling and metabolism	YDR345C	HXT3
Glucose signaling and metabolism	YHR092C	HXT4
Glucose signaling and metabolism	YHR096C	HXT5
Glucose signaling and metabolism	YJL214W	HXT8
Glucose signaling and metabolism	YOL081W	IRA2
Glucose signaling and metabolism	YDR277C	MTH1
Glucose signaling and metabolism	YGL248W	PDE1

Glucose signaling and metabolism	YOR360C	PDE2
Glucose signaling and metabolism	YGR240C	PFK1
Glucose signaling and metabolism	YMR205C	PFK2
Glucose signaling and metabolism	YOR101W	RAS1
Glucose signaling and metabolism	YNL098C	RAS2
Glucose signaling and metabolism	YKL038W	RGT1
Glucose signaling and metabolism	YDL138W	RGT2
Glucose signaling and metabolism	YHR205W	SCH9
Glucose signaling and metabolism	YLL016W	SDC25
Glucose signaling and metabolism	YDL194W	SNF3
Glucose signaling and metabolism	YOR047C	STD1
Glucose signaling and metabolism	YPL180W	TCO89
Glucose signaling and metabolism	YJR066W	TOR1
Glucose signaling and metabolism	YGL179C	TOS3
Glucose signaling and metabolism	YJL164C	TPK1
Glucose signaling and metabolism	YPL203W	TPK2
Glucose signaling and metabolism	YKL166C	TPK3
Glucose signaling and metabolism	YHR135C	YCK1
Glucose signaling and metabolism	YNL154C	YCK2
Glycerol metabolism	YDL022W	GPD1
Glycerol metabolism	YOL059W	GPD2
Glycerol metabolism	YIL053W	GPP1
Glycerol metabolism	YER062C	GPP2
Glycerol metabolism	YHL032C	GUT1
Glycerol metabolism	YIL155C	GUT2
Sphingolipid metabolism	YJL196C	ELO1
Sphingolipid metabolism	YCR034W	ELO2
Sphingolipid metabolism	YLR372W	ELO3
Sphingolipid metabolism	YML008C	ERG6
Sphingolipid metabolism	YKL008C	LAC1
Sphingolipid metabolism	YHL003C	LAG1
Sphingolipid metabolism	YGR038W	ORM1
Sphingolipid metabolism	YLR350W	ORM2
Sphingolipid metabolism	YPL057C	SUR1
Sphingolipid metabolism	YDR297W	SUR2
Sphingolipid metabolism	YBR058C-A	TSC3
Trehalose metabolism	YJR153W	PGU1
Trehalose metabolism	YBR126C	TPS1
Trehalose metabolism	YDR074W	TPS2
Trehalose metabolism	YMR261C	TPS3
Trehalose metabolism	YML100W	TSL1

S5.2 Table: List of strains used in this study. Note: Strains that express tagged ACC1 (GFP and TAP) were used only when absolutely needed. I.e., for Acc1 purification, microscopy, or western blot. For any other experiments (e.g., flux assay, citrate assay, FAS assay, BioScreen etc.) normal deletion without Acc1 tagging were used.

OKB#	genotype	background	Mat	Note
1079	WT BY4741	*his3Δ1 leu2Δ0 met15Δ0 ura3Δ0*	a	Gift from Kaern Lab
3453	*eaf1Δ::NAT*	*his3Δ1 leu2Δ0 met15Δ0 ura3Δ0*	a	This Study
3333	*eaf1Δ::KAN*	*his3Δ1 leu2Δ0 met15Δ0 ura3Δ0*	a	DMA
3292	*eaf7Δ::KAN*	*his3Δ1 leu2Δ0 met15Δ0 ura3Δ0*	a	DMA
3913	*elo2Δ::KAN*	*his3Δ1 leu2Δ0 met15Δ0 ura3Δ0*	a	DMA?
3914	*elo3Δ::KAN*	*his3Δ1 leu2Δ0 met15Δ0 ura3Δ0*	a	DMA?
1118	WT BY4742	*his3Δ1 leu2Δ0 ura3Δ0 lys2Δ0*	α	Gift from Kaern Lab
3954	*ACC1-GFP::HIS*	*his3Δ1 leu2Δ0 met15Δ0 ura3Δ0*	a	GFP Collection
4448	*eaf1Δ::NAT ACC1-GFP::HIS*	*his3Δ1 leu2Δ0 met15Δ0 ura3Δ0*	a	This Study
4593	*elo2Δ::KAN ACC1-GFP::HIS*	*his3Δ1 leu2Δ0 met15Δ0 ura3Δ0*	a	This Study
4594	*elo3Δ::KAN ACC1-GFP::HIS*	*his3Δ1 leu2Δ0 met15Δ0 ura3Δ0*	a	This Study
4599	*tsc3Δ::KAN ACC1-GFP::HIS*	*his3Δ1 leu2Δ0 met15Δ0 ura3Δ0*	a	This Study
4601	*acb1Δ::KAN ACC1-GFP::HIS*	*his3Δ1 leu2Δ0 met15Δ0 ura3Δ0*	a	This Study
4609	*lcb1-100 ACC1-GFP::HIS*	*his3Δ1 leu2Δ0 met15Δ0 ura3Δ0*	a	This Study
4348	*snf1Δ::KAN ACC1-GFP::HIS*	*his3Δ1 leu2Δ0 met15Δ0 ura3Δ0*	a	This Study
4364	*snf1Δ::KAN eaf1Δ::NAT ACC1-GFP::HIS*	*his3Δ1 leu2Δ0 met15Δ0 ura3Δ0*	a	This Study
4115	*esa1-ts ACC1-GFP::HIS*	*his3-Δ200 leu2-3,112 trp-1Δ1 ura3-52 ade2-101*	a	This Study
4305	*ACC1-TAP::TRP lys2D*	*his3-Δ200(or his3Δ1) leu2-3,1112(or leu2Δ0) ura3-52(or ura3Δ0) trp1-Δ1 lys2Δ0*	a	This Study
4306	*esa1-ts ACC1-TAP::TRP lys2D*	*his3-Δ200(or his3Δ1) leu2-3,1112(or leu2Δ0) ura3-52(or ura3Δ0 trp1-Δ1 lys2Δ0*	a	This Study
4629	*if38Δ::KAN ACC1-GFP::HIS*	*his3Δ1 leu2Δ0 met15Δ0 ura3Δ0*	a	This Study
4675	*if38Δ::KAN*	*his3Δ1 leu2Δ0 met15Δ0 ura3Δ0*	a	This Study
3228	*tsc3Δ::KAN*	*his3Δ1 leu2Δ0 met15Δ0 ura3Δ0*	a	DMA
3389	*snf1Δ::KAN*	*his3Δ1 leu2Δ0 met15Δ0 ura3Δ0*	a	DMA
3421	*snf1Δ::KAN eaf1Δ::NAT*	*his3Δ1 leu2Δ0 met15Δ0 ura3Δ0*	a	This Study
4401	*acc1-S1157A-GFP::HIS*	*his3Δ1 leu2Δ0 met15Δ0 ura3Δ0*	a	This Study
4404	*acc1-S1157A-GFP::HIS eaf1Δ::NAT*	*his3Δ1 leu2Δ0 met15Δ0 ura3Δ0*	a	This Study
4303	*esa1::HIS esa1-L254P::URA ACC1-GFP::HIS*	*his3-Δ200(or his3Δ1) leu2-3,1112(or leu2Δ0) ura3-52(or ura3Δ0) met15Δ0 lys2Δ0*	a	This Study

S5.3 Table: Supplemental lipidomic data. A) % of total lipids (plotted): This is the final n=3 data that was plotted for Figure 5.7A. B) Chain length (plotted): This is the final n=3 data that was plotted for Figure 5.7B. More detailed table available in supplemental of full published paper.

A)

Lipid class % of total lipids n=3									
Lipid Class	**WT-1**	**WT-2**	**WT-3**	***eaf1Δ*-1**	***eaf1Δ*-2**	***eaf1Δ*-3**	**WT-SorA-1**	**WT-SorA-2**	**WT-SorA-3**
PA	8.808319	7.70911	7.168114	7.031555	7.827166	7.387905	7.558414	7.369918	6.587717
PC	20.01251	19.39978	18.10025	14.60633	15.64172	19.06434	15.78081	14.83655	14.75127
PE	14.58784	15.94567	15.16231	12.25293	13.94131	13.55049	10.27827	10.11627	9.799517
PI	24.60282	25.6457	27.22984	27.06281	24.02353	23.27125	30.77518	28.72091	33.24002
PS	3.353745	3.872343	3.941388	2.790846	3.04049	2.838598	2.803309	2.716953	2.743127
DAG	9.877092	10.82778	10.57172	9.903528	11.53552	11.096	11.65613	15.46645	12.31826
EE	3.243952	2.075997	2.236501	8.408973	8.32993	7.299955	2.329182	2.378309	2.125234
TAG	4.62894	4.177691	3.904959	6.210088	7.183463	6.387178	5.697104	5.819516	6.315803

B)

Average lipid chain length n=3									
Lipid Class	**WT-1**	**WT-2**	**WT-3**	***eaf1Δ* - 1**	***eaf1Δ* - 2**	***eaf1Δ* - 3**	**WT-SorA-1**	**WT-SorA-2**	**WT-SorA-3**
PA	16.3509	16.29	16.3249	16.192	16.1002	16.1881	16.0544	16.0651	16.0324
PC	16.1156777	16.118642	16.10738	16.032829	16.044706	15.99936	15.833441	15.873587	15.826992
PE	16.4973591	16.513387	16.51457 6	16.44919	16.473698	16.420069	16.231439	16.198336	16.205667
PI	15.8750093 3	15.791146	15.86516	15.600466	15.624319	15.632443	15.167972	15.217943	15.147217
PS	16.5691214 8	16.534656	16.569431	16.436918	16.4106	16.459957	16.223767	16.221405	16.263213
DAG	16.1428	16.1243	16.1394	15.8893	15.8672	15.7997	15.7398	15.7598	15.7556
EE	16.2362454 5	16.248486	16.24503	16.407432	16.206854	16.235463	16.1592	16.206348	16.20636
TAG	48.5160704 9	48.938487	48.23616 8	47.373889	47.26109	47.08766	47.226271	47.094864	47.042493

Appendix C: Elizabeth Walden CV

Education:

Ph.D. Student in Biochemistry, University of Ottawa (Expected Completion Fall 2022)

- Working under the supervision of Dr. Kristin Baetz I am performing independent research exploring the role of NuA4, a lysine acetyl transferase, in the regulation of metabolism in a yeast model organism system.

Masters of Science in Biochemistry, University of Western Ontario (2017).

- Thesis project on characterizing the role of Ku70 phosphorylation on the DNA damage response pathway under the supervision of Dr. Caroline Schild-Poulter
- Techniques included: expressing, purifying, and characterizing recombinant proteins; polymerase chain reaction (PCR); gel electrophoresis; western blot; immunofluorescent microscopy; flow cytometry; and culturing of *E. coli*, and immortalized cell lines.

Bachelor of Education, Queens University (2015)

- Qualified to teach grades 7-12, specifically in Biology, Chemistry, and General Science.
- Developed communication, organization, and teaching skills, specifically in communicating science to the general population.

Bachelor of Science in Biology and Chemistry, Trent University (2014)

- Honours thesis project on using counterflow centrifugal elutriation to separate stages of the *Giardia lamblia* encystation process under the supervision of Dr. Yee.
- Undergraduate summer researcher student for 3 years in Dr. Yee's lab.

Undergraduate Exchange, University of Dundee Scotland (2013)

- Courses in Molecular Biology, Molecular Physiology, Endocrine, and Neurophysiology.

Awards:

- Ontario Graduate Scholarship (1 year) (2021)
- Best Poster (PhD) (UOttawa Faculty of Medicine Research Day 2020)
- NSERC PGS- D Scholarship (3 years) (2017- 2020)
- Graduate student leadership Award (UOttawa Faculty of Medicine 2019)
- Top Biochemistry Ph.D. Talk (UOttawa BMI Seminar Day 2019)
- Ontario Graduate Scholarship (1 year) (2016-2017)
- NSERC Canada Graduate Scholarship- Masters (1 year) (2015-2016)
- NSERC Undergraduate Student Research Awards (3 years) (2012-2014)
- Trent National Renewable Scholarship (4 years) (2010-2014)
- Robert Annett Scholarship in Biochemistry (1 year) (2013)
- President's Honour Roll (4 years) (2010-2014)

Publications:

Walden, E., Knill H., Sproule, A., Overy, D., and Baetz, K. The lysine acetyltransferase NuA4 in regulation of ergosterol dynamics in *Saccharomyces cerevisiae*. Submitted October 2022 to G3.

Pham, T., * **Walden, E.*,** Huard, S., Pezacki, J., Fullerton, M.D., and Baetz, K. Fine-tuning acetyl-CoA carboxylase 1 activity through localization: functional genomics reveals a role for the lysine acetyltransferase NuA4 and sphingolipid metabolism in regulating Acc1 activity and localization. Genetics. 2022 Jul 30;221(4): iyac086. *Co-First Authors

Mercurio, K., Singh, D., **Walden, E.A**., and Baetz, K. Global analysis of *Saccharomyces cerevisiae* growth in mucin**.** G3. 2021 Oct 19;11(11).

Fletcher, E., Mercurio, K., **Walden, E.A.,** and Baetz, K. A yeast chemogenomic screen identifies pathways that modulate adipic acid toxicity. iScience. 2021 Mar 18;24(4).

Walden, E.A., Fong, R.Y., Pham, T., Knill, H., Laframboise, S.J., Huard, S., Harper, M-E., Baetz, K. Phenomic screen identifies a role for yeast lysine acetyltransferase NuA4 in the control of Bcy1 subcellular localization, glycogen biosynthesis, and mitochondrial morphology. PLOS Genetics. 2020;16(11).

Fell, V.L., **Walden, E.A**., Hoffer, S.M., Rogers, S.R., Aitken, A.S., Salemi, L.M., and Schild-Poulter, C. Ku70 Serine-155 mediates Aurora B inhibition and activation of the DNA damage response. Sci Rep. 2016 Nov 16; 6:37194.

Oral Presentations:

Walden, E.A., Pham, T., Knill, H., and Baetz, K. Characterizing a role for NuA4 in the regulation of ergosterol in yeast. **Canadian Society for Molecular Biosciences Conference (CSMB) (2021).**

Walden, E.A., Fong, R., Pham, T., Huard, S., Knill, H., Harper, M., and Baetz, K. Phenomic screen implicates the yeast lysine acetyltransferase NuA4 in regulation of glycogen synthesis and mitochondrial morphology through the PKA inhibitor Bcy1. **The Allied Genetics Conference (TAGC) (2020).**

Walden, E.A., Fong, R., Pham, T., Huard, S., Knill, H., Harper, M., and Baetz, K. Phenomic screen implicates the yeast lysine acetyltransferase NuA4 in regulation of glycogen synthesis and mitochondrial morphology through the PKA inhibitor Bcy1. **Yeast 2019, Gothenburg Sweden (2019).**

Walden, E.A., Fong, R., Pham, T., Huard, S., Knill, H., Harper, M., and Baetz, K. Phenomic screen implicates the yeast lysine acetyltransferase NuA4 in regulation of glycogen synthesis and mitochondrial morphology through the PKA inhibitor Bcy1. **Canadian Society for Molecular Biosciences Conference, Montreal (2019).**

Walden, E.A., Fong, R., Pham, T., Huard, S., Knill, H., Harper, M., and Baetz, K. Phenomic screen implicates the yeast lysine acetyltransferase NuA4 in regulation of glycogen synthesis and mitochondrial morphology through the PKA inhibitor Bcy1**. Ottawa Institute of Systems Biology, Cornwall (2019).**

Walden, E.A., Fong, R., Pham, T., Huard, S., Knill, H., Harper, M., and Baetz, K. Phenomic screen implicates the yeast lysine acetyltransferase NuA4 in regulation of glycogen synthesis and mitochondrial morphology through the PKA inhibitor Bcy1**. UOttawa Biochemistry Seminar Day, Ottawa (2019).**

Walden, E., and Baetz, K. Characterizing the role of the *Saccharomyces cerevisiae* lysine acetyltransferase NuA4 in yeast mitochondrial dynamics and function. **Ottawa Microorganism Day, Ottawa, Canada (2017).**

Walden, E., Fell, V., and Schild-Poulter, C. 2016. Regulation of cell cycle checkpoints and DNA damage response through Ku70 phosphorylation. **Robarts Research Institute Molecular Medicine Seminar, London, Canada (2016)**.

Poster Presentations:

Walden, E.A., Pham, T., and Baetz, K. Characterizing a role for NuA4 in the regulation of ergosterol in yeast. **American Society for Biochemistry and Molecular Biology (ASBMB) (2021).**

Walden, E.A., Fong, R., Pham, T., Huard, S., Knill, H., Harper, M., and Baetz, K. Phenomic screen implicates the yeast lysine acetyltransferase NuA4 in regulation of glycogen synthesis and mitochondrial morphology through the PKA inhibitor Bcy1. **UOttawa Faculty of Medicine Research Day (2020).**

Walden, E.A., Fong, R., Pham, T., Huard, S., Knill, H., Harper, M., and Baetz, K. Phenomic screen implicates the yeast lysine acetyltransferase NuA4 in regulation of glycogen synthesis and mitochondrial morphology through the PKA inhibitor Bcy1. **Yeast 2019, Gothenburg Sweden (2019).**

Walden, E.A., Fong, R., Pham, T., Huard, S., Knill, H., Harper, M., and Baetz, K. Phenomic screen implicates the yeast lysine acetyltransferase NuA4 in regulation of glycogen synthesis and mitochondrial morphology through the PKA inhibitor Bcy1. **Canadian Cancer Research Conference, Ottawa (2019).**

Walden, E.A., Fong, R., Pham, T., Huard, S., Knill, H., Harper, M., and Baetz, K. Phenomic screen implicates the yeast lysine acetyltransferase NuA4 in regulation of glycogen synthesis and mitochondrial morphology through the PKA inhibitor Bcy1. **UOttawa Faculty of Medicine Research Day, Ottawa (2019).**

Walden, E.A., Fong, R., Pham, T., Huard, S., Knill, H., Harper, M., and Baetz, K. Phenomic screen implicates the lysine acetyltransferase NuA4 in yeast mitochondrial morphology and function. **Yeast Genetics Meeting, Stanford CA (2018).**

Walden, E.A., Fong, R., Pham, T., Huard, S., Knill, H., Harper, M., and Baetz, K. Phenomic screen implicates the lysine acetyltransferase NuA4 in yeast mitochondrial morphology and function. **UOttawa Biochemistry Research Day, Ottawa (2018).**

Walden, E., and Schild-Poulter, C. 2017. Assessing the role of Ku70 vWA domain phosphorylation in the inhibition of Aurora B and activation of the DNA damage response. **Canadian Society for Molecular Biosciences 60th annual conference, Ottawa (2017).**

Walden, E., Fell, V., and Schild-Poulter, C. 2017. Assessing the role of Ku70 vWA domain phosphorylation in the inhibition of Aurora B and activation of the DNA damage response. **Biochemistry Department Annual Research Showcase, London (2017).**

Walden, E., Fell, V., and Schild-Poulter, C. Regulation of DNA Damage signaling through Ku70 phosphorylation. Poster presentation at Cancer Research and Technology Transfer (CaRTT) Oncology Research & Education Day, **London, Canada (2016)**.

Walden, E., Fell, V., and Schild-Poulter, C. Regulation of DNA Damage signaling through Ku70 phosphorylation. **Canadian Symposium on Telomeres & Genome Integrity, Calgary, (2016).**

Walden, E., Fell, V., and Schild-Poulter, C. 2016. Regulation of cell cycle checkpoints and DNA damage response through Ku70 phosphorylation. **Biochemistry Department Annual Research Showcase, London, Canada (2016).**

Horlock-Roberts, K., **Walden, E**., Yee, J. Analysis of cells with unusually high DNA content in the Giardia intestinalis trophozoite cell cycle. **Quebec Molecular Parasitology Meeting, Montreal, (2014).**

Teghtmeyer, M., Brown, J., Drake, D., **Walden, E**., and Yee, J. 2013. Heme proteins in Giardia lamblia. **13th Annual Quebec Molecular Parasitology Meeting, Quebec City, (2013).**

Teaching Qualifications and Experience:

- Mentor of M.Sc. and Undergraduate Laboratory Students (2018-2022)
- Teaching Assistant for 2nd year Biochemistry Introductory Course (2015 and 2016)
- Teaching Assistant for 3rd year Biochemistry Laboratory Course (2016)
- Practicums for Bachelor of Education, focus on students aged 11-17 (2010 – 2015)

Volunteer

- Founding Chair Ottawa Institute of Systems Biology Trainee Committee (2020-2022)
- Volunteering with Let's Talk Science (2015-2021).
    - Honourable Mention, Top 5 for National Volunteer Award 2019
- Executive member of BMI graduate student association (2018-2020)
    - Awarded 2019 Graduate Leadership Award
- Peer mentor in BMI Mentorship Program (2018- Present)
- Departmental communications committee organizing public science outreach (2018-Present)
- CSMB 2020 Conference Organizing Committee
- DEGREE Shadowing Program Mentor (2018)
- Served on National Scholarship Ranking Committee for University of Western Ontario (2016)
- Served on Recruitment Committee, Department of Biochemistry, University of Western Ontario (2015-2016).

Professional Development

- S2BN In Focus: Scientific Communications Workshop (2020)
- See It Be It STEM It Role Model (2020)
- ComSciConCan 2019 science communication conference attendee (2019)
- Zeiss Microscopy Course (2019)
- CRISPR Workshop (2019)
- Created Science Communication Videos on Yeast and Research (2018, 2019)
- Winning Government Job Competitions (2019)
- French course at UOttawa – intermediate level (2017-2019)
- Science advocacy training for CSMB members by Evidence for Democracy (2018)
- Bench, Biz, and Beyond: The Basics of Research Commercialization series participant
- Equity, Inclusion, and the Future of STEM Learning with Let's Talk Science
- Communication course: Community Outreach and Media Relations in the Sciences (2018)
- Participant in the Mentor STEM WISE Leaders Program (Fall 2017)
- Member of Canadian Society for Molecular Biosciences (2017- present)
- Science & Policy: Bridging the Gap. Workshop at UOttawa (2017)
- Explore program - Five-week French-language immersion program (Summer 2017)